

UNIVERSITY OF BIRMINGHAM

Towards the development of surface-confined fluorescence boronic acid-based sensors for saccharide detection

by

Laura Buccoli

A thesis submitted to The University of Birmingham for the degree of DOCTOR OF PHILOSOPHY

School of Chemical Engineering
College of Physical Sciences and Engineering
The University of Birmingham

December 2022

UNIVERSITY OF
BIRMINGHAM

University of Birmingham Research Archive

e-theses repository

This unpublished thesis/dissertation is copyright of the author and/or third parties. The intellectual property rights of the author or third parties in respect of this work are as defined by The Copyright Designs and Patents Act 1988 or as modified by any successor legislation.

Any use made of information contained in this thesis/dissertation must be in accordance with that legislation and must be properly acknowledged. Further distribution or reproduction in any format is prohibited without the permission of the copyright holder.

ABSTRACT

Carbohydrates (saccharides) are among the most abundant organic compounds in nature. Due to their diversity and the ability to conjugate with themselves or other molecules, they create an enormous variety of compounds called glycans in biological settings. Glycans are involved in several physiological events inside the body. The discovery of abnormal concentrations of glycans can be indicative of disease, making their detection useful for early diagnosis and treatment. Therefore, research on glycan sensing systems has become substantial in recent years. One of the more interesting strategies is the use of boronic acids, which have the ability to form complexes with diols. Several boronic acid sensing systems have been designed to improve the sensing efficiency. These include strategies such as supramolecular aggregation, multicomponent covalent assembly, and the use of new materials such as polymer gels, nanoparticles, or quantum dots. Due to the quick response time, low cost, and local observation capabilities, fluorescence techniques have been widely employed in sensing applications. Boronic acids (BAs) are used in conjunction with dyes to modulate the signal upon saccharide binding through fluorescent mechanism as Photoinduced electron transfer (PET), Internal charge transfer (ICT), Forster resonance energy transfer (FRET), or their combination. The performance of the sensor has been demonstrated to be enhanced by its attachment to a solid surface. The effect of the surface is to reduce the matrix interference and bring close each component of the sensing system, as main units or as additional probe strengthening their interaction and so the fluorescence mechanism involved. Moreover, the sensitivity could be improved by incorporating multiple sensors on the surface. Although different materials such as quantum dots, polymers, and hybrid nanogels have been functionalized with BAs, boronic acid-based sensors designed to be surface-confined have not been extensively investigated in research associated with saccharides detection.

The aim of this work was to design fluorescence boronic acid sensing systems to detect sugars that could be immobilized onto solid supports for high-sensitivity saccharide detection. Different boronic acid-based sensing systems with fluorescent capabilities were investigated. In conjunction, the functionalization of silicon wafers and silica nanoparticles was explored as solid supports for the immobilization of the fluorescence systems.

The first sensing system consisted of two single units: phenylboronic acid as a receptor and an anthracene dye as a fluorophore. The anthracene fluorescence was expected to be modulated by a PET mechanism due to the quenching effect associated with the boronic acid. The amine group incorporated was supposed to enhance the affinity with saccharides. The binding with analyte will then suppress this mechanism, amplifying the response. The interaction between units can be strengthened by immobilising the sensor system onto a silica surface, thereby promoting the PET mechanism, and further improving the signal response. However, in contrast to that found in the literature, a fluorescence quenching following the interaction with the boronic acid was not observed. Since it was supposed that PET was not involved in the first designed sensor system, experiments with saccharides have not been performed.

To promote the interaction between the receptor and fluorescent units, the second sensing system involved a pyrene-based sensor with BA unit incorporated into the structure of the fluorophore. To evaluate the affinity towards sugars and the fluorescence response two strategies were investigated: direct connection into the structure of the fluorophore or through an alkyl chain with an amino group as a linker. Moreover, since FRET mechanism can occur at longer distances (10 to 100 Å) compared to PET, it was considered an alternative fluorescent mechanism. Coumarin was selected as a probe to act as acceptor in FRET couple with the pyrene acting as donor. The change in fluorescence intensity caused by saccharide binding would lead to the interaction

between 1-boronic acid pyrene and coumarin, promoting FRET. However, addition of sugar resulted in a minor fluorescence intensity increase, insufficient to cause an efficient interaction between the FRET couple. To produce the sufficient change in fluorescence required to induce FRET, a pyrene-based sensor, involving an alkyl chain with an amino group as a linker with phenylboronic acid receptor, was synthesised using another approach. The fluorescence of this designed sensor was planned to be modulated by ICT mechanism. A noticeable shift in the emission spectra was expected upon sugar binding, enabling FRET via coumarin **9.** Despite multiple attempts, the presence of side reactions and issues with purification meant the designed sensor could not be synthesised successfully. Experiments were therefore conducted with a derivative, which displayed a higher fluorescence intensity increase compared to the previous system. However, evidence in support of an ICT mechanism occurring was not found. It was concluded that the structure of the sensing system required improvement to promote the fluorescence mechanism involved. Focus was also given to a different mechanism as PET or FRET process, which is less affected by matrix composition, in comparison to ICT, aiming to achieve the required fluorescence intensity.

The third system aimed to strengthen the weak interaction between units seen in the previous systems, which resulted in the unsatisfactory fluorescence signals seen. It focused on the structure of the sensor towards the presence of a rigid linker and a quenching group in a strategic position, aiming to achieve a higher sensitivity for saccharide binding. The third system involved a pyrene-based sensor with the boronic acid connected through a piperazine ring. Piperazine acts as both as a linker and a fluorescence quencher due to its amino group, ensuring a PET process is involved. The sensor was also functionalized with an acetylene group to allow for immobilization onto surfaces. The synthesis of final sensors was performed employing a definitive combination and

sequence of reactions. Performed studies with the final system showed a quenching behaviour of the fluorophore, which was thought to be due to the length and rigidity of linker, absent in the previous system. The synthesized compound displayed fluorescence enhancement after sugar addition in the millimolar range. This confirmed that the assumed PET mechanism was involved, and further suppressed to restore the fluorescence abilities of pyrene. The fluorescence intensity change produced by the saccharides binding by PET was then successfully employed to establish the interaction with an alternative probe, attesting to a FRET process.

The systems were planned to be immobilized onto silica surfaces such as silicon wafers or silica nanoparticles. The functionalization of silicon wafers with different silanes was achieved successfully by self-assembled monolayer (SAM) formation. However, there was a considerable degree of inter-chip variation and poor reproducibility. Silica nanoparticles (SiO_2 NPs) were selected as an alternative solid support due to their reported use in sensing applications. The azide group was incorporated in amino-functionalised SiO_2 NPs for future sensor inclusion.

The boronic acid drives the action in this sensing system and the presence of an amino group improves the affinity of boronic acid towards saccharides. Moreover, this interaction was strengthened by employing a linker with a semi-rigid structure such as piperazine. Having an amino group in a strategic position acting as a quencher, strengthened the PET mechanism towards the fluorophore. The fluorescence response achieved following saccharide binding could be employed to establish the interaction with an additional suitable probe, that can act as acceptor or donor to enable a FRET mechanism with final sensor as designed Since the versatility in sensing application and the wide range of techniques available for their characterization, SiO_2 NPs have been selected as solid support for the incorporation of sensing systems. The azide functionalized

surface will enable the immobilisation of the system through click chemistry by acetylene-azide reaction.

Chapter 1: *Introduction*

The chapter provides a basic understanding of glycans and their detection through molecular sensors. It describes the use of boronic acids and fluorescent techniques as functional parts of the sensor mechanism, attending to the fundamental theories that make the system works. As part of it, a review of boronic acid-based fluorescent system is also provided. Furthermore, the properties and advantages of flat or silica nanoparticles surfaces are defined.

Chapter 2: *Techniques*

This chapter gives a general overview of techniques used for analysis and purification of described sensor and characterization of employed surfaces.

Chapter 3: *Assessment of several boronic-based fluorescence systems*

This chapter describes the first sensing systems investigated. The first is composed on (3-((allyl (methyl) amino) methyl) phenyl) boronic acid, acting as receptor and 9-(azidomethyl) anthracene, as a fluorophore unit. Fluorescent experiments were performed to evaluate the PET mechanism involved upon sugar-binding. The second sensing system involved FRET process through the interaction of pyrene-based dye-based boronic acid (donor) and coumarin dye (acceptor). The two strategies proposed to design the boronic acid-based pyrene are described. Fluorescence experiments with pyrene boronic acid were performed to evaluate the fluorescence response upon sugar binding and the interaction with coumarin. Additionally, design of sensor based the second strategies and methods of its synthesis and purification were provided.

Chapter 4: *Fluorescent sensing system based on PET-pyrene boronic acid sensor*

This chapter describes the last undertaken sensing system, based on pyrene-based sensor with the boronic acid connected through a piperazine ring. Preliminary experiments were conducted to verify the supposed PET mechanism involved. The different strategies for synthesis and purification of sensor were discussed. Fluorescence experiments were conducted to assess the fluorescence response upon sugar-binding. Preliminary FRET experiments were performed to evaluate the behaviour of sensor both as donor and acceptor.

Chapter 5: *Surface solid support*

This chapter describes the functionalization and characterization of silica solid substrate selected for the future incorporation of sensor design. SAM formation on silicon wafers surface, the functionalization of silica nanoparticles and their characterization are described.

Chapter 6: *Experimental*

This chapter describes the experimental procedures employed during the investigation performed in this thesis.

Chapter 7: *Conclusion and future work*

The main conclusion, possible improvements and future work are provided.

Appendixes

They contain additional data obtained during the investigation performed in this thesis.

ACKNOWLEDGEMENTS

Firstly, I would like to thank my supervisor, Professor Paula M. Mendes, for her support and guidance during my Ph.D. course. I also would like to thank my second supervisor Dirk-Peter Herten for his guidance in important steps of research. A big thank you to Dr. Marcos Fernandez-Villamarin for having taught me, always support me, and helped in this challenging moment.

A thank you to all the members of the Mendes Group, from the older to the newest that who have shared with me this experience: Dr. Giuseppe Di Palma, Dr. France Allabush, Dr. Kamlesh Patel, Dr. Joshua Norman,Dr.Yazmin Tagger, Dr.Setareh Vafaei, Dr Seyed Tabaei, Dr. Craig Ward, Dr. Nasim Mahmoodi, Dr. Joshua Simon Gibson, Laura Brooks, Pushpa Patel, Dario Bazzoli, Miguel Alena Rodriguez, Charlie Keene, Daniel Carroll, Hannah Williamson, Sohail Vasim Ghani, Daniel Kgautlhe. I believe that I would not have been able to arrive until the end without their help.

I would thank also to the University and mainly the beautiful city of Birmingham and all the people that I have met during this journey, with their advice, support but mainly friendship- James, Bernardo, Ana, Anna, Ioannis, Daniele B, Daniele R, Clarissa, Micheal, Andrea Patricia, Chiara, Federica, Christos, and the list could be continued. I feel grateful to have had the possibility to know each of them.

A special thank you go to one of my closest friends-Barbara and Gianluca have taught me what real friendship is, become my model of life, and never left me alone. They have made these years unforgettable. Another thank you is for Lucrezia; she has been literally the person that let me carry on and reminds me to not stop to breathe. You know.

I wish to thank friends that supported me from Italy and are always present for me - Alessandra for being so special and Francesco, one of the reasons why I decided to start the Ph.D.

Finally, thank you to my so close and beautiful family. My parents, my brothers Michele who more than all can understand what means this journey and Carlo, and my person, my sister Beatrice.

TABLE OF CONTENTS

ABSTRACT **3**

ACKNOWLEDGEMENTS **9**

1 CHAPTER 1: INTRODUCTION **19**

1.1 Saccharides 19

1.2 Molecular recognition 24

1.2.1 Sensor Performance Parameters 25

1.3 Boronic acids 27

1.4 The importance of boronic acid 29

1.4.1 Interaction with diols 30

1.5 Fluorescence technique 36

1.5.1 Fluorescence signal transduction mechanism 40

1.6 Solid substrates 48

1.6.1 Self-assembled monolayers (SAMs) 48

1.6.2 Nanoparticles 55

1.7 Boronic acid-based fluorescent sensing systems 57

1.8 Boronic acid-functionalized surfaces for saccharides sensing 68

1.9 Summary 72

1.10 Aims of this work 73

2 CHAPTER 2: TECHNIQUES 77

2.1 Spectroscopic Techniques 77

2.1.1 UV–Vis spectroscopy (UV-Vis) 77

2.1.2 IR spectroscopy 79

2.1.3 Fluorescence spectroscopy 81

2.2 Organic chemistry techniques: analysis, separation, and purification 81

2.2.1 Nuclear Magnetic Resonance (NMR) Spectroscopy 81

2.2.2 Mass spectrometers (MS) 84

2.2.3 Thin layer chromatography TLC 85

2.2.4 Liquid chromatography (LC) and high-performance liquid chromatography (HPLC) 86

2.2.5 Liquid chromatography-mass spectrometry 88

2.3 Solid substrate analysis and characterization 89

2.3.1 Contact angle 89

2.3.2 Ellipsometry 91

2.3.3 Dynamic light scattering (DLS) 92

2.3.4 Zeta potential 95

2.3.5 Thermogravimetric analysis (TGA) 96

3 CHAPTER 3: ASSESSMENT OF SEVERAL BORONIC-BASED FLUORESCENCE SYSTEMS 98

3.1 PET fluorescent sensing system based on phenylboronic acid and anthracene 98

3.2 Fluorescence-based sensing system: design and fluorescence experiments 101

3.3 FRET fluorescent sensing system: pyrene boronic-acid based sensor and coumarin probe 108

3.3.1 Sensor **6**: fluorescence experiments 111

3.3.2 Sensor 7: design and fluorescence experiments 122

3.4 Summary and outlook 142

4 CHAPTER 4: FLUORESCENT SENSING SYSTEM BASED ON PET-PYRENE BORONIC ACID SENSOR 145

4.1 Introduction 145

4.2 Sensor 13: design 148

4.3 Synthesis and purification 151

4.4 Fluorescence experiments 192

4.5 Summary and outlook 238

5 CHAPTER 5: SURFACE SOLID SUPPORTS 241

5.1 SAM formation on silicon wafer surfaces 241

5.2 SiO_2 NPs characterization 254

5.3 Functionalization and characterization 256

5.4 Summary and outlook 266

6 CHAPTER 6: EXPERIMENTAL METHODS 268

6.1 Fluorescent sensing system 268

6.1.1 Material and methods 268

6.1.2 Optical Spectroscopy experiments 278

6.2 Silica solid substrate 282

6.2.1 Materials and methods 282

6.2.2 SAMs formation 283

6.2.3 Functionalization of silica nanoparticles 284

7 CHAPTER 7: CONCLUSION AND FUTURE WORK 286

APPENDIX I: CHEMICAL STRUCTURES 291

APPENDIX II: ELLIPSOMETRY & CONTACT ANGLE DATA 300

APPENDIX III: NMR, IR & MASS SPECTRA 304

APPENDIX IV: FLUORESCENCE SPECTRA 318

BIBLIOGRAPHY 322

LIST OF DEFINITIONS AND ABBREVIATIONS

a. u	Arbitrary Unit
ADV	Advancing contact angle
APTES	(3-aminopropyl) trimethoxysilane
APTMS	(3-aminopropyl) trimethoxysilane
AU	Absorbance units
BA	Boronic acid
BINAP	(2,2′-bis(triphenylphosphine)-1,1′-binaphthyl)
B-N	Boron-nitrogen
Boc	Tert-Butoxycarbonyl protecting group
$CDCl_3$	Deuterated chloroform
COSY	Correlated Spectroscopy
CuAAC	Copper (I)-catalysed azide-alkyne cycloaddition
DAD	Diode array detection
DCM	Dichloromethane
DLS	Dynamic light scattering
DMF	Dymethylformamide
DMSO	Dimethyl sulfoxide
EDC	Ethyl-3-(3-dimethylaminopropyl) carbodiimide
Em	emission
ESI	Electrospray ionisation
Et_2O	Diethyl ether
Et_3N	Triethylamine
EtOAc	Ethyl acetate
EtOH	Ethanol
Ex	Excitation

FRET	Forster resonance energy transfer
FTIR	Fourier transform infrared
H	Enthalpy
h	Planck constant
HEPES	(4-(2-hydroxyethyl)-1-piperazineethanesulfonic acid)
Hex	Hexane
HFIP	1,1,3,3,3-Hexafluoro-2-propanol
HOMO	Highest occupied molecule orbital
HPLC	High Performance Liquid Chromatography
HSQC	Heteronuclear single quantum Correlation
I	Nuclear spin quantum number
ICT	Internal charge transfer
IR	Infrared
IUPAC	International union of pure and applied chemistry
J	Coupling constant
K	Binding constant
Kd	Dissociation constant
Keq	Equilibrium constant
LC	Liquid Chromatography
LE	Locally excited state
LOD	Limit of detection
LOQ	Limit of quantification
LS	Light scattering
LUMO	Lowest un-occupied molecule orbital
m/z	Mass to charge ratio
MeCN	Acetonitrile
MeOH	Methanol

MPTMS	(3-mercaptopropyl) trimethoxysilane
MS	Mass Spectrometry
n	Stoichiometry of binding, number of binding sites
NHS	N-hydroxy succinimide
NMR	Nuclear Magnetic Resonance
PB	Phosphate buffer
PBA	Phenylboronic acid/Pyrene boronic acid
PET	Photo-induced electron transfer
ppm	Parts per million
Q	Quencher
REC	Receding contact angle
Rf	Retention factor
RT	Room temperature, Retention time
SAM	Self-assembled monolayer
SDS	Sodium dodecyl sulfate
Si	Silicon
SiO_2 Np	Silica nanoparticles
SiO_2	Silicon oxide
SLS	Static light scattering
T	Transmittance
TBAF	Tetra-n-butylammonium fluoride
TEM	Transmission electron microscopy
TFA	Trifluoroacetic acid
TGA	Thermogravimetric analysis
THF	Tetrahydrofuran
TICT	Twisted intramolecular charge transfer
TLC	Thin layer chromatography

TMS	Trimethylsilyl
TOF	Time of flight
UV/vis	Ultraviolet/ visible
γ	Gyromagnetic ratio
δ	Chemical shift
λ	Wavelength
μ	magnetic moment
ν	Frequency
Φ	Quantum yield

CHAPTER 1: INTRODUCTION

This chapter provides a description of glycans and their detection by molecular sensors. Glycans are the name given to carbohydrates ranging from their most simple structure, monosaccharides, to a more complex oligosaccharide. Since glycans are involved in several physiological events, the effective and efficient detection of glycans, their derivatives, and the recognition of abnormal concentrations can lead to the early diagnosis of disease and the development of treatments.

Research on simple saccharide identification systems has become substantial in recent years. Saccharides are an example of polyhydroxy compounds in which the stereochemistry of a single hydroxyl group may represent the only difference between the chemical structures of saccharides. Due to the ability of boronic acid to bind diols, they are widely employed as receptor units in molecular sensors for saccharides. Fluorescence techniques are widely used in sensing applications, and fluorescence quenching processes are a commonly used transducer mechanism. Sensing performance can be improved by the inclusion of solid supports. For example, flat surfaces and silica nanoparticles have been widely exploited as they do not affect the fluorescence properties of the sensor components. In this chapter, boronic acid-based fluorescence sensing systems are reviewed, with a focus on the different signal units used, choice of fluorescence mechanism and whether a solid support is included.

1.1 Saccharides

Saccharides, commonly known as carbohydrates, are among the most abundant organic compounds in nature. They are divided as monosaccharide, disaccharide, oligosaccharide and polysaccharide. Saccharides are defined as polyhydroxy compounds with carbonyl groups. Monosaccharide refers to the simple sugars that cannot be hydrolysed into the simpler compound,

involving a single polyhydroxy aldehyde or ketone unit. They are defined by the number of carbon atoms and the configuration of hydroxyl groups around the chiral carbon. The configuration D and L represent the position of the second last hydroxyl group in a carbohydrate, as evidenced in Figure 1.1, towards the right side in D and to the left side in L. The structural diversity increases with the increasing length of the carbon chain, adding more stereo centres and thus more stereoisomers. One source of the structural complexity of monosaccharides is their ability to form ring structures in an aqueous solution. This occurs by reaction between the carbonyl group and hydroxyl group along the chain through the formation of an intramolecular hemiacetal. The two structures, linear and cyclic, are in dynamic equilibrium in solution (Figure 1.1).

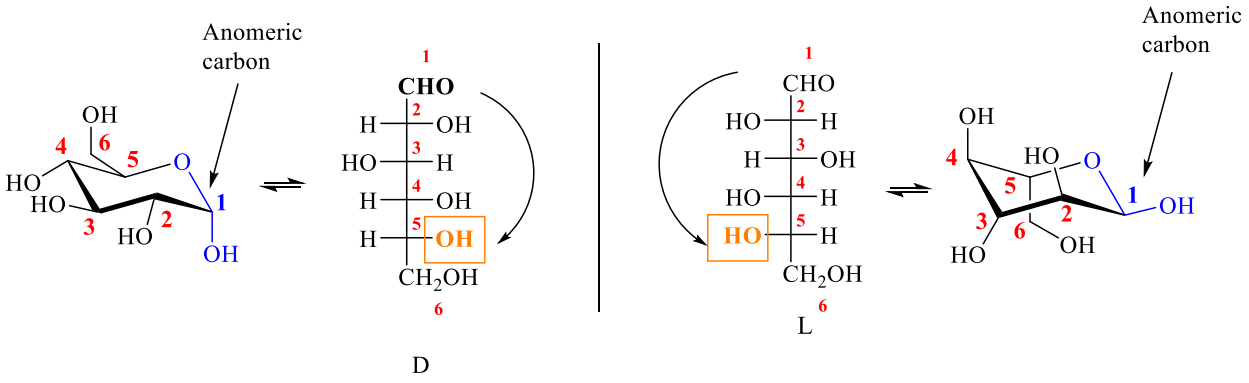


Figure 1.1. *Linear and cyclic structures of α-D- and α-L-glucopyranoses in dynamic equilibrium in solution*

The cleavage of the hemiacetal ring allows interconversion between the two cyclic forms via acyclic intermediate and inversion of configuration at the anomeric centre, equilibrating the two enantiomers. This process is called mutarotation, and the distribution frequency depends on each monosaccharide. For example, fructose is a 6-carbon polyhydroxy ketone that exists in aqueous solution as an equilibrium mixture between two cyclic structures, furanose and pyranose respectively five and six members, each one producing two stereoisomers referred to as α and β

(Figure 1.2). The respective form of fructose is the tautomer's β-D-fructopyranose, β-D-fructofuranose, α-D-fructofuranose and α-D-fructopyranose in equilibrium with keto-D-fructose (the noncyclic form). The distribution between the tautomer depends on several factors however in normal "aqueous" conditions, pyranose: furanose ratio is around 1:3 as 70 % fructopyranose and 22% fructofuranose.[1-3]

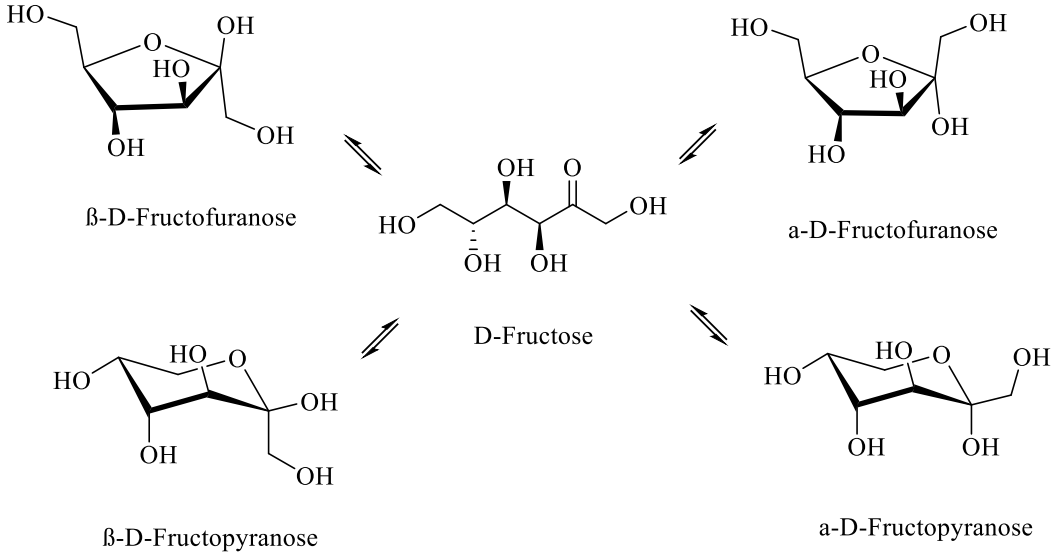


Figure 1.2. *Linear structure of D-fructose (middle) and equilibrium mixture of the two cyclic structures, furanose and pyranose and their tautomer α and β: β-D-fructopyranose, β-D-fructofuranose, α-D-fructofuranose and α-D-fructopyranose.*

Simple monosaccharides can conjugate between them through the formation of glycosidic linkage. The reaction occurs between the hemiacetal or hemiketal group of a saccharide and a hydroxyl group of some compound. In the same way, trisaccharide contain three sugars through glycosidic bonds, with tetrasaccharides, pentasaccharides, etc following this pattern. Compounds containing a low number of monosaccharide units are commonly referred to as oligosaccharides. Conversely, polysaccharides are denoted to those who possess a large number of monosaccharide units, usually more than 10 units (Figure 1.3).[4]

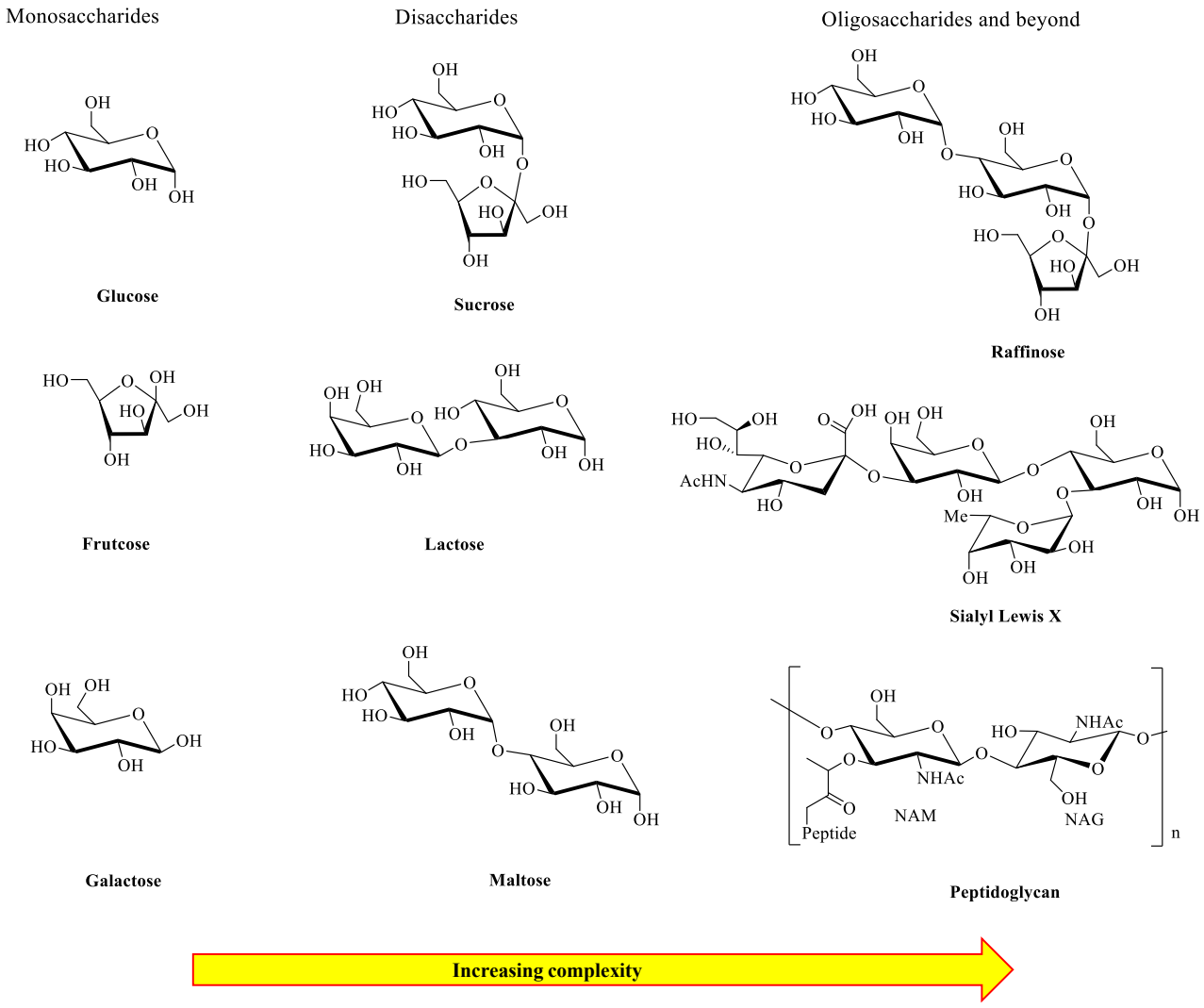


Figure 1.3. *The increasing complexity of saccharides as higher-order structures are formed from simple saccharides.*

The term glycan refers to polysaccharides or oligosaccharides normally linked to several biological molecules to form glycoproteins, glycolipids, and peptidoglycans. They belong to one of the fundamental macromolecule classes of lipids, proteins, and nucleic acids. The core difference of glycans from these classes is the glycosidic linkage, formed between the hemiketal group of a saccharide (or molecule derived) and a hydroxyl group. The nature of the linkage defines the structural properties and biological function. Glycans are characterized by the characteristic

sequence and nature of the monosaccharide constituents linked together by chemical bonds. Therefore, the possible presence of carbohydrate units, configuration and position following glycosylation reaction offer a further differentiation method. [5-9]

Simple monosaccharides and complex oligosaccharides perform a wide range of roles. Glucose is the main energy source and can be polymerized to glucan for energy storage. Complex oligosaccharides, involving different saccharide monomers are used for the cell recognition event. Some saccharides, such as ribose, are very important for the storage of genetic information whilst aminoglycosides, amino-modified sugars, play are potent antimicrobials and are used in bacterial infection treatment.[10] The natural diversity of the constituents, the variability of the glycosidic bond and the possibility of conjunction with other molecules, involve the glycans in several physiological events inside the body. Furthermore, they are involved in the adhesion of microorganisms to host cells, tumour growth and metastasis. Therefore, the effective and efficient detection of glycans, their derivatives and the recognition of abnormal concentrations play an important role in the diagnosis of disease and subsequent treatment management. Specifically, saccharides and their glycoconjugates regulate tumour proliferation and invasion since certain structures are overexpressed on the surface of pathogens and malignant cells. They can therefore be used as biomarkers for a wide range of diseases and their early detection. [4, 11, 12]

Since the monosaccharides are the precursor for the formation of glycans, the research on simple monosaccharide identification systems has progressed in recent years. The spatial and chemical complexities of saccharides represent a challenge for the development of efficient sensors with high selectivity. The recognition of individual saccharides is challenging in a biological and physiological environment, where solvent, temperature and pH can affect sensor performance. Glucose is the most abundant carbohydrate in the blood, with concentrations in the range of 3.5-

5.5 mM. Other simple sugars such as D-Fructose, which is found at a concentration lower than 0.1 mM, are markedly less abundant, making detection difficult.[13, 14] Consequently molecular sensors have been widely investigated to solve this challenge, achieving both qualitative and quantitative detection of saccharides.

1.2 Molecular recognition

Molecular recognition techniques are usually based on specific interactions between two or more molecules through noncovalent bonding such as hydrogen bonding, metal coordination, hydrophobic forces, Van der Waals forces, π-π interaction, halogen bonding and electrostatic and/or electromagnetic effects.[15] However, covalent interactions have been found to provide strong affinity and improved selectivity due to the functional group's intrinsic preference towards a specific analyte. According to the IUPAC definition, a chemical sensor is a device that transforms chemical information into an analytically useful signal.[16] The chemical information may derive from a change of physical property of the system following the interaction with analyte. Sensors are comprised of two basic functional units: a receptor, and a transducer, sometimes divided by a spacer, to obtain the desired response. Additionally, sensor molecules can be immobilised onto planar surfaces for efficient sensor operation changes, such as faster response times and higher sensitivity[17] The receptor or recognition unit specifically and selectively interacts with the target analyte. This interaction transforms the chemical information into a form of energy that can be measured by the transducer and further converted into a useful analytical signal. Physical measurements of absorbance refractive index, conductivity, temperature and mass change have been employed as analytical signals.[16]

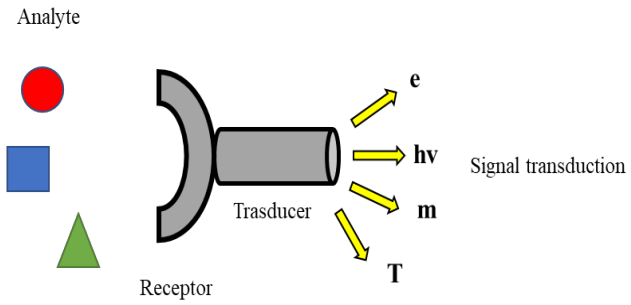


Figure 1.4. *Schematic illustration of chemical sensor components (receptor and transducer) and the different types of signal transduction following the interaction with analyte: electrochemical (e), optical (hv), mass (m) and calorimetric (T).*

1.2.1 Sensor Performance Parameters

The performance of diagnostic sensors can be reported regarding certain parameters, making performance easily comparable between different sensors. Limit of detection (LOD) is defined as the lowest detectable concentration of an analyte whilst limit of quantification (LOQ) refers to this concentration at an acceptable uncertainty. This concentration must produce a detectable signal, which can be distinguished from the blank or the background signal. Selectivity and LOD define capability and limitations, and thus the potential application of sensors. The sensitivity S is defined as the slope of the calibration curve of analytical signal X versus concentration C.[18]

$$S = \frac{dX}{dC} \approx \frac{\Delta X}{\Delta C} \qquad \text{Equation 1-1}$$

The higher the sensitivity, the lower the LOD. LOD and LOQ can be expressed as a function of S, and σ_B, the standard deviation of a set of blank signals in several measurements without an analyte.

$$LOD = \frac{3\sigma_B}{S} \qquad \text{Equation 1-2}$$

$$LOQ = \frac{5\sigma_B}{S}$$ Equation 1-3

The selectivity of a sensor is its capacity to respond preferentially to the analyte of interest i.e., preferential detection of a saccharide over other species within a sample. However as mentioned previously, the high structural similarity between saccharides poses a major challenge to their selective detection. Usually, the affinity- based sensors are not operative for the whole range of concentration from moles to single molecules. In the case of reversible binding, the response of the sensor increases with target concentration until the sensor receptor sites become saturated, reaching the highest limit where a plateau in signal occurs.

In a generic recognition process, the interaction occurs between the analyte (A) and the receptor (R) to give the complex P.

$$A + R \leftrightarrows P$$ Equation 1-4

The kinetics of complex formation is expressed by the rate constant k_1 and the dissociation of the complex by rate constant k_2. The equilibrium dissociation constant K_D can be characterized by a ratio between these constant k_1 and the dissociation constant of the complex k_2, as represented in the equation 1.5.

$$K_D = \frac{k_1}{k_2} = \frac{[P]}{[A]\,[R]}$$ Equation 1-5

K_D represents the affinity of the recognition receptor for the analyte, and it can be represented in terms of the concentration of analyte in the sample. The affinity of a sensor reflects its sensitivity and selectivity towards a specific analyte. To determine the stability constants, different analytical

approaches are used, such as graphic method, ratiometric or calorimetric measurements, or some other specific approach depending on the sensor's mechanism of action.[19, 20]

Chemical sensors are commonly classified according to the principle which the transducer operates such as electrochemical, mass sensitive devices, thermometric devices or paramagnetic devices. Optical sensors are based on optical phenomena resulting from interaction of the analyte with a reporter. They are classified depending on optical properties such as particle size-dependent light scattering, optothermal effect by measurement of thermal effects, or reflectance such as luminescence and fluorescence.

The binding affinity of specific analytes to some compounds commonly used as receptors in molecular recognition are widely known and reported in the literature. In the case of sugars, one of the more interesting compounds for molecular recognition are boronic acids (BA) derivatives, due to the boric acid abilities to form a complex with diols with a hydroxyl group.[21, 22]

1.3 Boronic acids

Boronic acids belong to the family of organoboron compounds which contain one C-B bond (Figure 1.5). They include a tricoordinate boron atom with two hydroxyl groups and an organic substituent. Boronic acid and boranes possess more organic substituents compared to boric acid, which has a fully oxygenated boron centre with three hydroxyl groups.

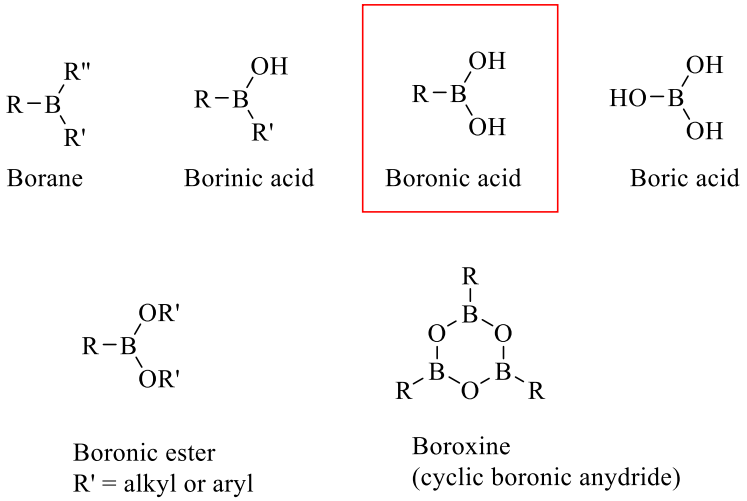


Figure 1.5. *Organoboron compounds containing C-B bond. Boronic acid is highlighted.*

Boron as an element is notably more electropositive compared to carbon and hydrogen therefore the boron centre is left electron deficient in the formation of covalent bonds. Boronic acid shows a trigonal planar geometry with a central boron atom hybridized sp^2 and an R-B-R bond angle of 120°. Due to only six valence electrons and a resulting deficiency of two electrons, the tricoordinate boron atom keeps a vacant p orbital perpendicular to the plane of the molecule (Figure 1.6).[23]

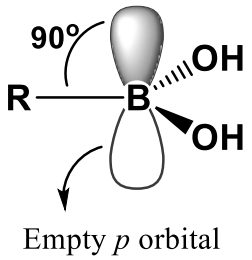


Figure 1.6. *Boronic acid structure with the representation of empty p orbital perpendicular to the plane of the molecule.*

The presence of this vacant p orbital explains Lewis' acid behaviour and their ability to react with electron-rich species, forming species (adducts) by reaction with Lewis' base, that have lone-pair

electrons available to donate. The interaction with water involves a dynamic equilibrium in which the boronic acid hybridisation is converted to a tetrahedral sp^3 boronate, with the release of a hydronium ion (H^+).



Figure 1.7. *Formation of borate anion and hydronium ion by ionization of boronic acid with water.*

When boronic acids possess strong electron-withdrawing substituents that can stabilise the resulting boronate anion, the acidity of the boronic acid increases. Conversely, sterically hindered groups, such as ortho substituents, decrease the Lewis acidity.[24-26]

1.4 The importance of boronic acid

Due to its high stability and easy handling, boronic acid have been widely employed as a building block for a diverse range of chemical syntheses, acting both as a catalyst and reagent. In addition, due to its generally low toxicity and its solubility in water, boronic acid has been used as a biochemical tool for various purposes including signal pathway interference,[27] enzyme inhibition[28] and as a cell delivery system.[29] The Lewis acidic nature of boron has also led to the development of anion receptors and sensors.[30] Thanks to its strong interaction with diols, boronic acid moieties are widely used as receptors in sensing amino acids, α-hydroxyl acids and alcohols, as well as cyanide and fluoride. They play a crucial role in carbohydrate chemistry and glycobiology, mainly in analysis, separation, protection, and activation. The most used is the complexation with diols, allowing for application in glycan analysis, and recognition of cell-surface carbohydrate biomarkers and glycoproteins.[29, 31-33]

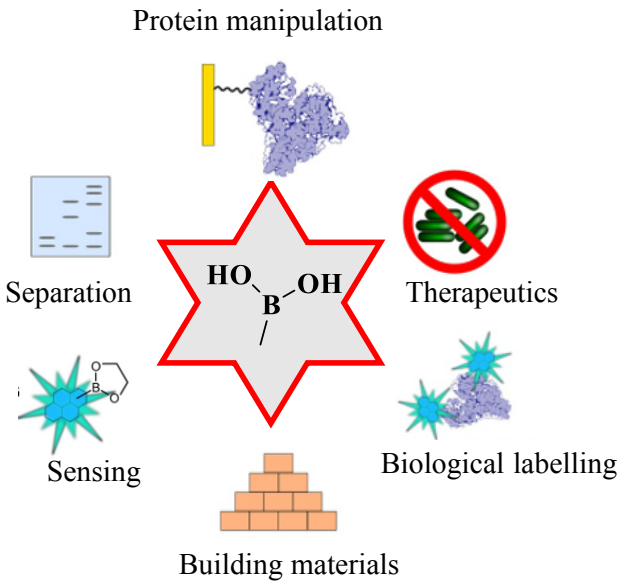


Figure 1.8. *Diverse usage and application of boronic acid. Image adapted from reference [32].*

Due to the similar behaviour of lectins, carbohydrate-binding proteins, boronic acid-based sensors are defined as boronolectins.[34] Compared to lectins, boronic acid is smaller and can be incorporated easily into a wide range of chemical synthesis, and into nanoscale detection systems. Additionally, due to the simpler structure, the boronic acid groups can provide a more specific and suitable chemical group to facilitate the synthesis of sensor platforms. The incorporation of boronic acid onto solid planar surfaces or nanoparticles allows the production of sensors with amplified binding signal and increased sensitivity.[35] Synthetic chemo sensors, and boronic acid-based sensor are considered a valuable choice for saccharide binding.

1.4.1 Interaction with diols

The ability of boronic acids to form complexes in solution with hydroxyl groups in favourable 1,2 and 1,3 configurations has been known since 1900.[36] Moreover, the method has been employed for the determination of the structure of pyranose and furanose forms of glucose.[37] In 1959, Lorand and Edward gave the first quantitative examination into the interaction of boronic acids and polyols

in water.[38] They conducted a series of experiments between phenylboronic acids and a range of polyols. The pH was adjusted to have an equal equilibrium of phenylboronic acid in its neutral and anionic form, which is referred to as the pKa. By examining the equilibrium between the trivalent neutral form and the anionic tetrahedral species of the boron, they confirmed the ability of boronic acid to act as Lewis' acid and its tetrahedral coordination upon interaction with a basic molecule. A boronic ester forms by the interaction of boronic acid sp^2 with a Lewis base, forming a covalent bond with tetrahedral sp^3 geometry. Boronic acids can exist in two different hybrid forms sp^2 (A) or sp^3, of which the tetrahedral hybridization more preferably forms an ester (B), as shown in the Figure 1.9. The equilibrium constant of esterification Ka acid depends on the pKa of both an acid, a diol, and on structural factors. $K_{eq\text{-}trig}$ represents the equilibrium constant between A and diol to form the species D. $K_{eq\text{-}tet}$ refers to the second equilibrium, which involves the process between sp^3 hybridized borate anions **B** to borate ester anions **C** (Figure 1.9). As Wang et al. showed, $K_{eq\text{-}tet}$ can be measured by the pH drop method while the third general combination constant $K_{eq\text{-}trig}$ can be measured by spectroscopy.[39, 40]

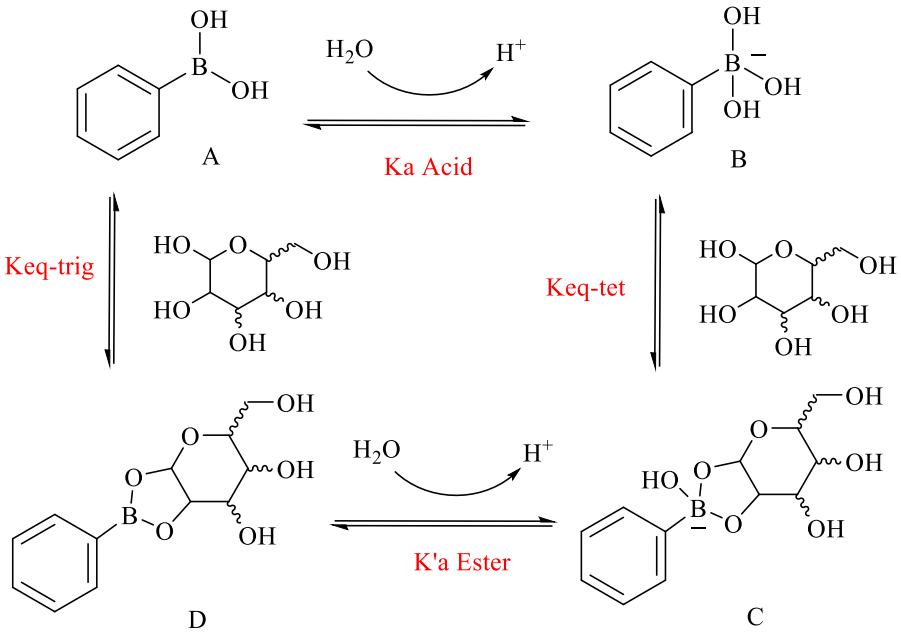


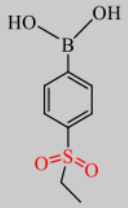
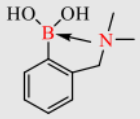
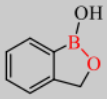
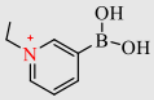
Figure 1.9. *Transformation of boronic acid to boronic ester. Image adapted from reference [39].*

The process of formation of a cyclic boronic ester from a boronic acid anion is faster than that of a neutral boronic acid. The equilibrium constants demonstrated that the formation of a complex with monosaccharide is more favourable at high pH where the boronate ions predominate. The favourable binding at high pH was attributed to release of angle stain upon formation of hydroxyboronate complexes of 1,2-diols. This results from rehybridization of boron from sp^2 to sp^3. [38, 39, 41, 42]

Therefore, greater electronegativity of substituents promotes higher stability of the transition state and the product. The substituent has the effect of delocalising the negative charge on boron in the reaction, increasing acidity of boronic acid, stabilizing transition state and anionic product thereby increasing the stability constant. The optimal binding depends on the pKa of the boronic acid and diol, as well as pH.[43] For the application of boronic acid in saccharide detection, the formation of the saccharide complex is important that occurs efficiently at physiological pH (7.4). To enable

this formation at desired pH, the pKa of the boronic acid should be < 7. However, most of the phenylboronic acid (PBA) are weak acids with a pKa of 8.8, meaning that a basic environment is required to form complexes. Consequently, strategies exploiting boronic acid derivates with lower acidity are essential. Different types of boronic acid can be employed to reach low binding pH, as summarized in the Table 1.1.

Table 1.1. *Types of boronic acids derivative, providing low binding pH.*

Boronic acid Type			pKa
a	Electron withdrawing groups		7.0
b	Intramolecular B-N coordination "Wulff- type"		5.5
c	Intramolecular B-O coordination "improved Wulff-type"		5.0
d	Heterocyclic groups		4.5

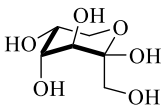
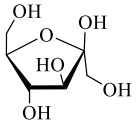
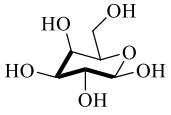
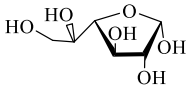
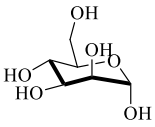
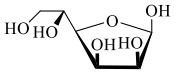
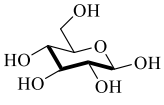
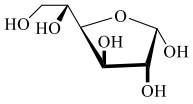
The electron density of the phenyl ring, and thus of the boron atom, can be changed by the introduction of acidic substituents. Nitro, sulfonyl, fluoro, and carbonyl as substituents can increase the acidity of boronic acids due to their strong withdrawing inductive effect (Table 1.1a). In the case of an *ortho* position, the properties of boronic acid are influenced by inductive and

coupling effects due to steric effect between the interaction with diols. Wulff-type boronic acid (Table 1.1b) involves intramolecular tetracoordinate B-N or B-O bonds which promote the formation of tetragonal boronate anion (sp^3).[44] The stability of this state remains under neutral or basic conditions, facilitating boronate esterification with cis diols. The existence of a dative nitrogen-boron was studied for the first time in 1862, with the discovery of a complex between ammonia and trimethyl borane.[45, 46] Wulff has demonstrated how the incorporation of an amine adjacent to the boronic acid brings a tetrahedral sp^3 boron at neutral or weak basic pH.[47] It has been observed that the boron- nitrogen interaction decreases the pKa of the boronic acid from 9 to 5, while the pKa of a tertiary ammonium increases from 9 to 12. Furthermore, with the formation of boronate ester, the Lewis acidity of the boron increases, making the boron-nitrogen interaction stronger. Moreover, the substituents of both nitrogen and boron affect the strength of the N-B bond. Electron withdrawing groups increase the Lewis acidity of the boron atom, while electron-donating groups increase the basicity of nitrogen. Improved Wulff-type boronic acids (Table 1.1c), known as benzoboroxoles, involve an intramolecular tricoordinate bond. In comparison with "Wulff-type PBA", they show a similar pKa but an improved water solubility.[44, 48] Finally, the presence of the heteroatom in the ring results in a low binding pH in the heterocyclic boronic acids (d).[49]

The reversible covalent interaction between boronic acids and cis 1,2 or 1,3 diols has been proven to enable their detection in the range of mM or sub-mM. The binding affinity of PBA usually follows the order fructose> galactose> mannose and glucose.[50] The higher selectivity for fructose is due to its high abundance in solution in the form of a syn-periplanar pair of hydroxyl groups available for boronic acid-binding. Moreover, solvent type, pH and the temperature of the medium influence the configuration composition.[51, 52] The single boronic acid prefers to bind with the five-

membered furanose to decrease the ring tension in the boronic ester generated. The binding constant of phenylboronic acid with fructose is 4370 M^{-1}, that exists in the reactive furanose only as 25 % of dissolved fructose. The glucofuranose form is present only as 0.14 % and the resulting binding for glucose is 110 M^{-1}.[53] Table 1.2 reports proportions of the most abundant and reactive species of monosaccharides dissolved in water and the corresponding binding constant between monosaccharides and PBA. To enhance the saccharides' affinity, multi-boronic acid-based sensors have been developed to promote the multivalency of binding sites.[54-56]

Table 1.2. *The proportions of the most abundant and reactive species of monosaccharides dissolved in water and the corresponding binding constant between monosaccharides and PBA.*[53]

Saccharide	**Configuration**	**Binding constants (K)**
Fructose	 β-D-Fructopyranose 61 %  β-D-Fructofuranose 25 %	4370 M^{-1}
Galactose	 β-D-Galactopyranose 64 %  α-D-Galactofuranose 2.5 %	276 M^{-1}
Mannose	 α -D-Mannopyranose 65.5 %  β-D-Mannofuranose 0.3 %	172 M^{-1}
Glucose	 β-D-Glucopyranose 65 %  α -D-Glucofuranose 0.14 %	110 M^{-1}

Boronic acids act as receptors, but a transducer mechanism such as fluorescence is also required to fabricate a molecular sensor.

1.5 Fluorescence technique

Compared to other transduction methods, optical sensing, and particularly fluorescence-based methods, are one of the most employed mechanisms. This is due to the main advantages of quick response time, low cost and local observation capabilities. Fluorescent sensors, chemosensors or fluorescent probes report the presence of a selective target or a mixture of species by modulation of their fluorescence properties. Fluorescence-based sensing presents several applications in analytical chemistry, clinical biochemistry, medicine, and the environment, due to the wide range of detectable species: cations, anions, neutral molecules and gases.[57-59] Fluorescence is a form of luminescence that involves the emission of light by a molecule or material (fluorophore) after electronic excitation by light irradiation. By absorbing light, a fluorophore is excited from the lowest vibration level in its ground state (S_0) to higher excited state (S_1 or S_2) (Figure 1.10). Fluorescence emission has a lower energy compared to that absorbed due to a non-radiative decay process that can occur between return in the ground state. Internal conversion that is the rapid transition to a lower state, solvent effect, excited-state reactions, complex formation, and energy transfer are process that can cause an energy lost. The Jablonski diagram below shows electronic levels and the possible transitions between singlet states (Figure 1.10). These processes are responsible for dissipating a smaller or bigger portion of the excitation energy, resulting in a spectral shift between the absorbed radiation and the emitted.

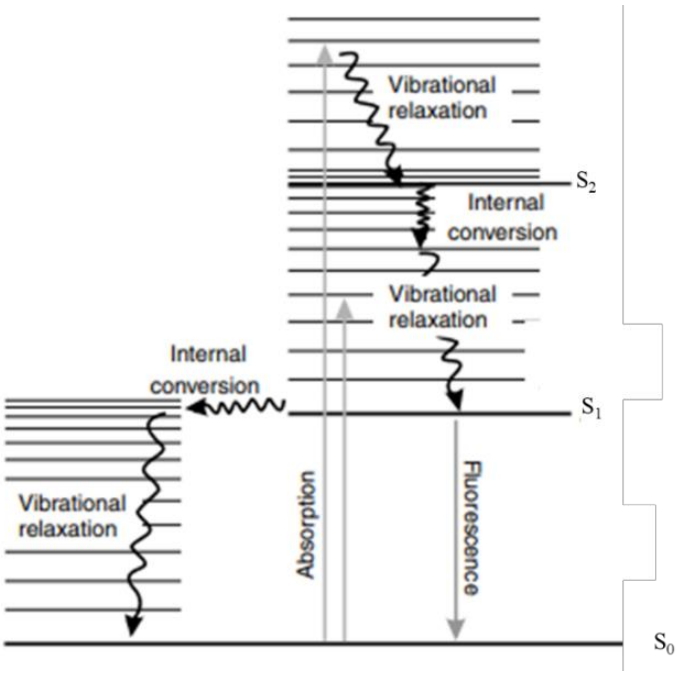


Figure 1.10. *Jablonski diagram. Image adapted from reference [60].*

Fluorescent-based sensing employed in molecular recognition involves the main component as described in section 1.2, and a signalling unit, such as fluorophore. The receptor unit can be part of the π-system of the fluorophore, allowing interaction with an analyte. Otherwise, it can be covalently linked with the fluorophores, acting as a signalling unit whilst being electronically independent. In this case, the receptor molecules are synthesized and then attached to a fluorophore acting as a sensitive probe. The two units are directly connected through a chemical bond or a linker and/or a spacer. This allows the modulation of photophysical properties of the fluorophore in response to target recognition, acting as a communication mechanism whilst helping to control the space orientation of units of the system. Fluorescence wavelength and lifetime have been used as measurable outputs however intensity is the most common detectable response used for direct target recognition, due to the simplicity in instrumentation and measurements, and the highest absolute sensitivity.[61]

In fluorescence intensity measurements, the proper selection of excitation and emission wavelengths is important. A shift to longer wavelengths in the fluorescence spectrum compared to the absorption spectrum is defined as the Stokes shift. It is commonly expressed as the difference between the two maxima. Since usually the fluorescence spectrum matches the absorption spectrum, the absorption maxima are selected as excitation wavelengths. To avoid complication due to light scattering, excitation and emission wavelengths should be separated with a resulting larger Stokes shift. Some artefacts can be affected by the fluorescence spectrum and need to be distinguished. The Raman scattering bands, common in any solvent, overlap the fluorescence spectrum and can be recognized by a shift, changing the excitation wavelength (Figure 1.11). This may produce complications if the fluorescence intensity of the dye selected is very low.

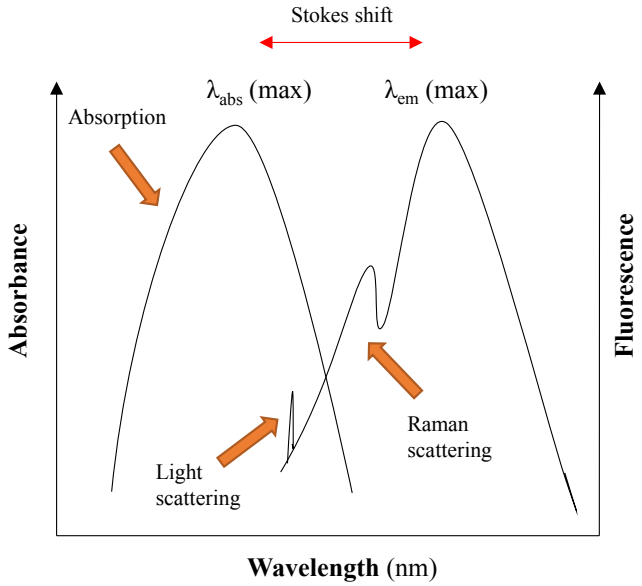


Figure 1.11. *Typical absorption and fluorescence emission spectra. Representation of Stokes shift and some artefacts as light and Raman scattering.*

Signalling unit

Organic dyes are widely used as signalling units due to their high availability, low price, and versatility. The main properties of fluorescent dyes are high molar absorbance and quantum yield (Φ),[62] which represents the ratio of the number of photons emitted as fluorescence to the number of all absorbed photons. Quantum yield is commonly measured using the relative[63] or absolute method.[64] In the relative quantum yield method, Φ of the sample of interest is calculated by comparing its photoluminescence emission with a standard with known quantum yield. Conversely, the absolute method does not need any reference, instead employing an integrating sphere to capture all light emitted by the sample. Quantum yield is determined by comparing the number of emitted photons and the absorbed ones. The optimal excitation is important to achieve the highest brightness and emission wavelength, and thus to gain the best sensitivity. A large Stokes shift reduces the effects of light scattering and could be useful in homo-FRET, that is excitation energy transfer between the same dye molecules. The high photostability of dyes means less degradation after a number of excitation-emission cycles. Solubility, and reactivity in the system should also be considered as factors in designing the sensor. The presence of some groups in the structure can cause fluorescence intensity variation, for example, the presence of heavy atoms as substituents (internal heavy atom effect) that decrease the fluorescence of the dye due to an intersystem crossing process.[65] This effect is minor when the fluorescence quantum yield is large and, the de-excitation by fluorescence emission dominates. Overall, electron-donating groups promote an increase of molar absorption coefficient and a shift in absorption and fluorescence spectra. Fluorescence sensing is based on the change of one or more fluorescence characteristics of a fluorophore upon interaction with an analyte through different fluorescence signal transduction mechanism.

1.5.1 Fluorescence signal transduction mechanism

The changes of fluorescence characteristic can result from an alteration of the ground state of the fluorophore or by an excited state process by an analyte such as electron transfer, charge transfer, energy transfer and excimer or exciplex formation or disappearance. Similar to the collision with heavy atoms or with paramagnetic species, all these reactions involve a one-step deactivation of the excited state, called quenching, meaning a decrease of fluorescence intensity. It occurs by a decrease of population in the excited state or by a decrease in the fluorescence quantum yield. There are different ways in which intermolecular process involving the excited state of sample (M*) and the quencher (Q) compete with the typical de-excitation to the ground state (M). The probability of interaction rises at higher concentrations of Q. When Q is not at large excess and there is not possibility of interaction between M^* and Q during the excited state lifetime, quenching cannot occur. In this case, quenching only occurs if there is a significant interaction at longer distances, such as long-range non-radiative energy transfer. The formation of an excimer (excited dimer), self-quenching with formation of product MM^*, is caused by an equal concentration between Q and M. The characteristic emission band arising from excimer/exciplex formation can be employed in sensing applications.[61, 62, 66]

1.5.1.1 Excimer/exciplex formation or disappearance

Dyes can be involved in their excited state in a collision between an identical unexcited molecule or with another unexcited molecule (electron acceptor or donor), forming excimers or exciplexes respectively. The result is a broad fluorescence band shifted to a lower energy compared to the characteristic fluorophore emission. The concentration of the species, temperature, viscosity, and solvent properties influence the formation of excimers and exciplex. Usually, the fluorescence emission band of an excimer is located at wavelengths higher than that of the monomer. Molecules

such as pyrene, anthracene, and fluorene, owing a high electron density and planar structures, are more susceptible to intermolecular assembling and, thus to excimer/exciplex formation as well.

1.5.1.2 Photoinduced electron transfer (PET)

PET involves the promotion of electron transfer from a donor (D) to an acceptor (A) molecule. The molecule that absorbs light is in the excited state. The singlet or triplet state represents the fluorophore whereas the other molecule involved is referred to as the quencher. The process requires a wavefunction overlap between the donor and the acceptor, which is only possible at short distances, typically 10 Å. Sensors based on PET are in the format of fluorophores-spacer-receptor (Figure 1.12). The linker or spacer has the function to connect the fluorophore with the receptor, which has a non-bonding electron pair, isolating the terminal functional units of the sensor.[67-69]

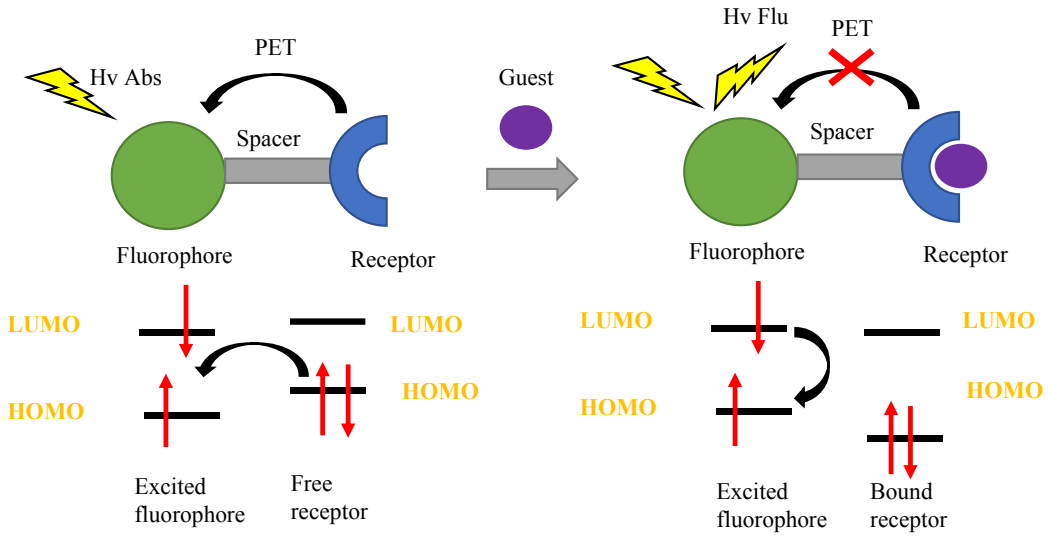


Figure 1.12. *Schematic PET mechanism between fluorophore and receptor.*

In the absence of analyte, after the excitation of the fluorophores an intramolecular electron transfer occurs between the highest occupied molecular orbital (HOMO) of the receptor and

excited fluorophore. This results in the quenching of the probe fluorescence (Figure 1.12left). When analyte is bound, the energy of the HOMO of the receptor becomes lower than that of the fluorophore. In this way, the PET process can occur, restoring fluorescence (Figure 1.12right). The direction of electron transfer is determined by the oxidation and reduction potential of the ground and excited state. Indeed, the process can be predicted using the Rehm Weller equation if the redox potentials of fluorophore and quencher are known.[70]

$$\Delta G = E(D^+/D) \ - E(\ A^+/A^-) - \Delta G_{00} \ - \frac{e^2}{\varepsilon d} \qquad \text{Equation 1-6}$$

Where $E(D^+/D)$ and $E(\ A^+/A^-)$ refers to the oxidation and reduction process:

$$A_P + e \ \rightarrow \ A_P^- \qquad \text{Equation 1-7}$$

$$D_P^+ + e \ \rightarrow \ D_P \qquad \text{Equation 1-8}$$

ΔG_{00} is the energy of the transition of the fluorophore ($S_0 \rightarrow S_1$), which can be either of donor or acceptor. The last term of the equation is the columbic attraction energy (*e*) between ion pairs following the electron transfer reaction, the dielectric constant of the solvent (ε) and the distance between the charges (d).

1.5.1.3 Intramolecular Charge transfer (ICT)

Intramolecular charge transfer is observed when organic dyes contain both an electron-donating group (often a dialkylamino group) and an electron withdrawing group, that acts as an acceptor. If these groups are located on opposite sides of the molecule, charge transfer from the donor to the acceptor occurs. This results in the establishment of a strong dipole which depends on the microenvironment of the fluorophore, such as solvent polarity. The guest interaction with the

receptor linked to the fluorophore alters the strength of the dipole, resulting in intensity changes and a spectral shift. (Figure 1.13),.[61]

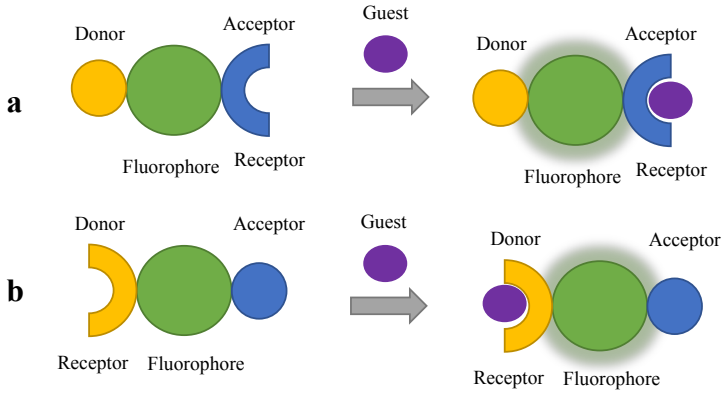


Figure 1.13. *Schematic representation of ICT mechanism, with consequent red (a) or blue (b) shift in the emission spectra.*

The change in the medium system causes the formation of a locally excited state (LE) which can be the precursor of ICT. Commonly, there is only a simple decay in low polar solvents, or a direct excitation to CT at high temperature or medium polarity. The ICT emission can be accomplished by changing the planarity between electron-donor and acceptor fragments, determining twisted intramolecular charge transfer (TICT) state (Figure 1.14). It produces the maximum charge separation between the groups and is stabilized by solvent environments.[71, 72]

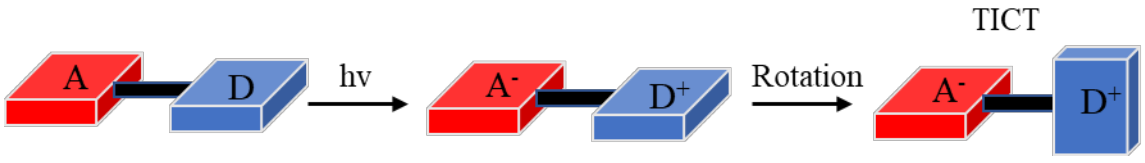


Figure 1.14*. Representation of twisted intramolecular charge transfer (TICT) state.*

PET is the most general photophysical mechanism employed due to its ease of use. Despite ICT probes displaying clear fluorescence band shifts in the binding processes, the presence of suitable electron and acceptor groups is required to establish a high dipole moment. Moreover, fluorescence properties are subjected to quenching in highly polar media.[73, 74]

1.5.1.4 Fluorescence resonance transfer (FRET)

FRET is a distance-dependent photophysical process, collision-free, described by Förster in the 1940s. Comparing to the previous mechanism, FRET involves transferring energy from an excited donor (D) to a suitable acceptor (A), through long-range dipole-dipole. The overlap between the emission spectrum of the donor and the excitation spectrum of the acceptor is required for a suitable energy coupling between the two compounds. The proximity of donor and acceptor, within a distance from 10 to 100 Å and appropriate relative orientation of the dipole vectors promote the efficiency of the process. The Jablonski Diagram shows the excitation of the donor and its consequent relaxation (Figure 1.15). FRET ensues with energy transfer to the acceptor, with consequent emission of photons.[75-78] The binding event produces a conformational change or relative orientation of the paired motif, allowing detection through resulting fluorescence modulation.

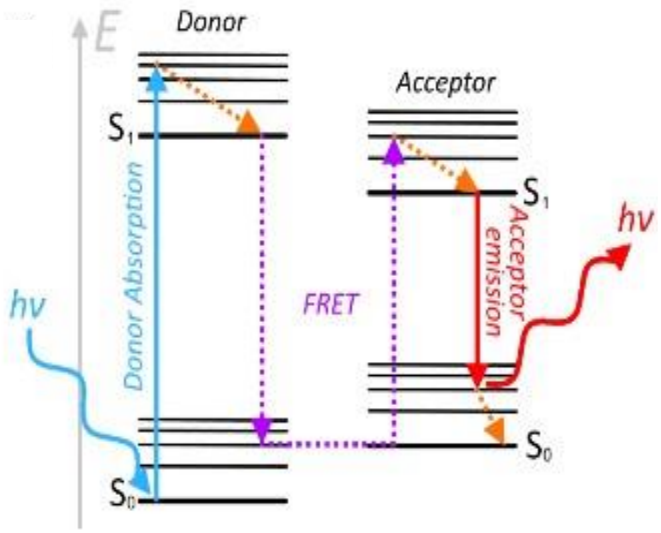


Figure 1.15. *Schematic representation of FRET mechanism. Image reproduced from reference [76].*

The rate of energy transfer (k_T) is given by:

$$k_T(r) = \frac{1}{\tau_D} \left(\frac{R_0}{r}\right)^6 \qquad \text{Equation 1-9}$$

τ_D is the donor lifetime in the absence of acceptor, r is the distance between the two centres of donor and acceptor. R_0 is called Förster distance and describes the distance at which FRET is 50 % efficient. The rate of energy transfer depends also on the relative orientation of the donor and acceptor dipoles, defined by the orientation factor κ^2, and on the sixth exponentiation of the distance, existing between them. The transfer efficiency (E) can be calculated from the lifetimes or using the relative fluorescence intensity of the donor when the donor is present (F_{DA}) or absent (F_D).

$$E = 1 - \frac{F_{DA}}{F_D}$$ Equation 1-10

$$E = 1 - \frac{\tau_{DA}}{\tau_D}$$ Equation 1-11

FRET "antenna" and surplus effect

The efficiency of FRET can be amplified without a real change in molecular distance but by increasing the probability of FRET occurring through a multi-acceptors system. FRET "antenna" and surplus effect are two approaches proposed to explain the mechanism (Figure 1.16). The first is called "antenna" because it increases the sensitivity of the response. The multiple acceptors can be considered as a new virtual acceptor that allows a higher transfer rate, increasing the probability that an excited donor finds an acceptor partner before de-excitation. This leads to a rise in rate and efficiency of transfer. In contrast with the theoretical kinetic model, measured FRET efficiencies for the single pairs do not add and the sum will not be equal to the measured FRET efficiency of both acceptors.[78, 79] FRET surplus has been described by Koushik et al., who observed an exceeded compressive FRET transfer rate in a multi-acceptor system.[80] In their experiments, FRET can be explained by the statistical nature of the distribution of dipole orientation for two competing FRET reactions. The sum of both rates represents an equal chance for each acceptor to establish FRET upon each excitation donor event. The average relative dipole orientation factor κ^2 for a single donor-to-acceptor FRET transition is assumed to be 2/3. In the presence of multiple acceptors, the acceptor with the most favourable relative dipole orientation to the donor will determine the probability to select it for energy transfer. This selection brings to an increase of the relative dipole orientation, more than 2/3 for a single pair, causing an additional increase in the FRET rate. They also observed that the probability that an individual donor interacts with an acceptor does not increase with an increasing number of donor dyes. The part of donor molecules that lose the

absorbed energy through FRET does not change and the transfer efficiency remains the same. There are no present disadvantages to having multiple donors because donor excitation is faster and two excited donors do not compete for the same acceptor.

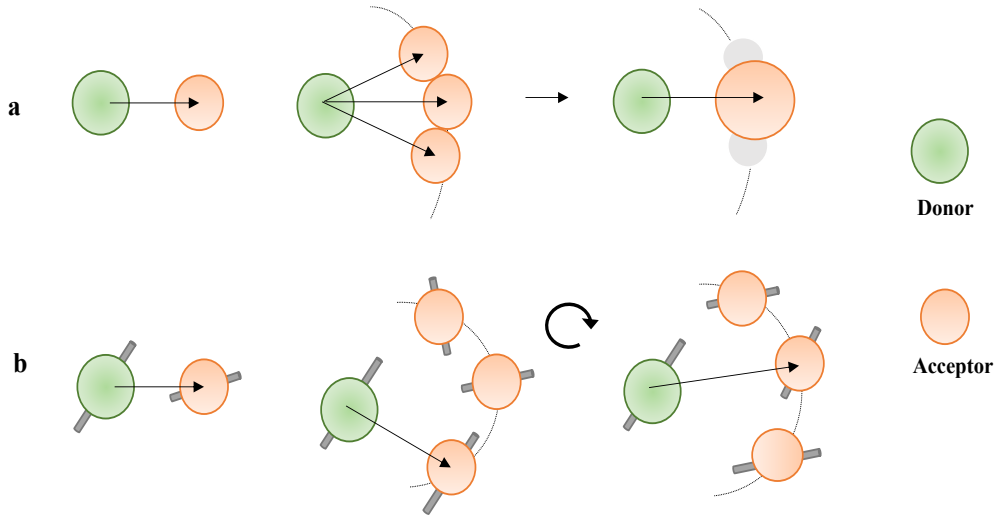


Figure 1.16. *FRET "antenna" (a) and surplus effect (b) with multiple acceptors per donor. Image adapted from reference [79].*

Solid support

The performance of molecular sensors, including sensitivity, faster response or signal intensity brightness of fluorescence-based systems can be improved by their attachment to flat or porous surfaces, or by the incorporation onto polymeric and silica nanoparticles (NP). Macromolecules, NP, and supramolecular structures can be used as passive support surfaces so that individual sensors cannot freely diffuse in solution and mix with other sensors. Surface immobilization therefore ensures the communication between the components of the fluorescent system by their spatial closeness but can allow spatial separation of sensors with different targets, enabling multiplexed sensing.[81]

1.6 Solid substrates

The immobilization of fluorescence systems on solid surfaces offers advantages in terms of reversibility and reproducibility.[82-84] Among the different types of solid supports available for the attachment of fluorescent systems, silicon-based surfaces are widely used due to their high chemical and thermal stability, as well as their relative inertia to their surrounding environment.[85-87]

Silicon or silicon oxide (Si/SiO_2) substrates are commonly used as solid supports for fluorescence systems due to their transparent and photophysical inert properties. Moreover, the high stability, reusability and ease of fabrication have seen the employment of self-assembled monolayers (SAM) of fluorophores to obtain thin-film sensors. Thus, silicon surfaces are ideal substrates to generate fluorescent films. They can form stable, ordered monolayers with reactive terminal groups which can be later modified with selected fluorophores. Due to recent developments in nanoparticle technology, silica-based NP are often used due to their excellent stability, recyclability, biocompatibility, and low toxicity. They are characterized by good optical permeability and stability without influencing the photophysical properties of the fluorophore.[83, 86, 88] Dye doped silica NP allow an enhancement of fluorescence signal, increased sensitivity, prolonged detection time and better reproducibility.[89-91]

1.6.1 Self-assembled monolayers (SAMs)

SAMs result from a spontaneous molecular organization on different surfaces such as metal, glass, or silica. They allow the formation of film sensors with high stability, high ordering, and high surface diversity. SAMs can be formed from a variety of active self-molecules on different

surfaces. One of the most common systems used is alkyl silanes on SiO_2, which allow the generation of a chemically and physically stable, covalently attached film.[92-94]

SAMs are composed of an end group (or head), that bind to the surface, a backbone (or spacer) responsible for the molecular ordering and a terminal group (Figure 1.17).

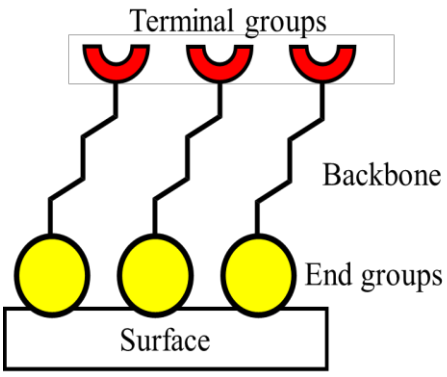


Figure 1.17. *Scheme representing a component of SAM: terminal group, backbone, and end group.*

The terminal functional group defines the properties of the surface, and it can be established by deposition of self-assembling molecules with a modified end group or by chemical transformation of the terminal group to further SAM formation. Furthermore, an alkyl chain[95] or an aromatic ring[96] is usually used as a spacer which has a role in the packing/ ordering of the molecules on the surface.

The head groups provide the site of reaction with a strong affinity to a particular substrate. They consist of a silicon atom tetrahedrally bound first with three similar functional groups, and then to a functional group. The most commonly used due to their high reactivity are trichlorosilane (-$SiCl_3$), trimethoxysilane (-Si (OCH_3)$_3$) or triethoxysilane (-Si(OCH_2CH_3)$_3$.[93] Upon contact with an activated surface, the silane is subjected to hydrolysis to produce silanol, needed for inorganic surface coupling. The first reaction is the condensation or silane coupling in which the silane

network interacts with the inorganic substrate through hydrogen bonding. Water is produced during the formation of the covalent link and needs to be removed by heat or vacuum to promote the condensation and a stable siloxane linkage (Figure 1.18). A monolayer form when each silane is coupled directly to the substrate via a siloxane bond. The silane coupling agent with specific functional and reactive groups can be used to promote the link between inorganic substrates and biomolecules.[97-99]

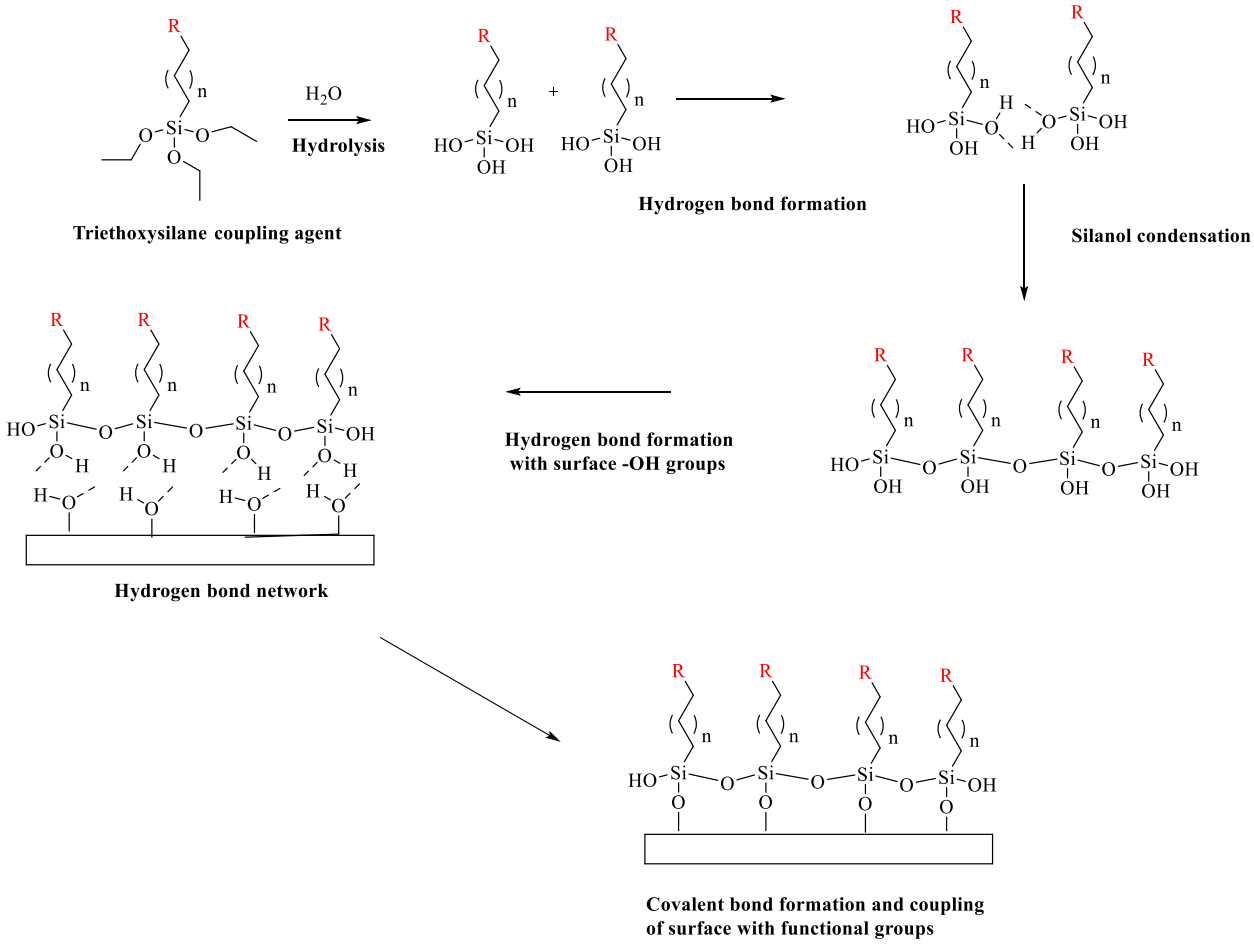


Figure 1.18. *The reactions involved with the coupling of an organo silane compound to an inorganic surface containing available OH (silanization reaction).*

SAM deposition

The formation of SAMs involves the chemical adsorption of self-assembling molecules onto the surface and their further organization through intermolecular interactions. When the molecules have reacted with all accessible reactive groups on the surface, the SAM formation stops. The length of the self-assembling molecule and the angle relative to the surface determine the thickness of a closely packed and ordered SAM.

The deposition of an organo-silane SAM with functional or reactive groups such as hydroxyl, amino, aldehyde, epoxy, thiol, carboxylate, and alkyl groups are used to directly functionalize the surface with such selected groups. This allows further reactions such as click chemistry, Diels Alder reaction and nucleophilic substitution, and the conjugation of biomolecules to inorganic substrates to be performed. Amino functionalized surfaces are widely used, enabling the immobilization of different kinds of molecules, such as enzymes or antibodies, fluorescence molecules or organic dyes.[99-101]

3-Aminopropyl trimethoxysilane (APTMS) and (3-aminopropyl) trimethoxysilane (APTES) are the most popular, inexpensive, and commercially available reagents used for amine surface treatment (Figure 1.19). APTMS is the most reactive, and the reaction can be conducted in a non-aqueous system, avoiding hydrolysis and polycondensation reactions. Indeed, a large amount of water brings excessive polymerization and the formation of a multilayer film.

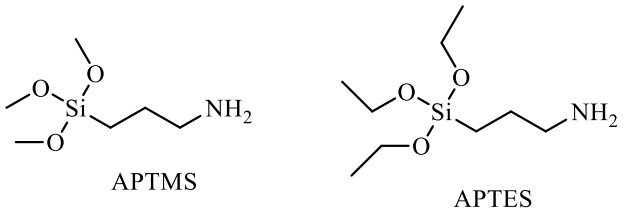


Figure 1.19. *Structures of (3-aminopropyl) trimethoxysilane (APTMS) and (3-aminopropyl) triethoxysilane (APTES).*

Due to the tendency of uncontrolled polymerisation of amino alkoxysilane in solution, it is not easy to have a sufficiently high content of primary amines on the surface and reach a homogeneous amine modification.[102] Water content, type of surfactant, concentration of the solution, temperature and choice of solvent are all parameters that influence the quality of SAMs and could hinder the formation of a well-defined monolayer. [103-106] The effect of concentration has been investigated by Ito *et al.*, who observed an incomplete monolayer formation with a low concentration of silane, whereas a more concentrated solution brings less ordered films.[107] Chen and Smith compared commercially available short and long-chained amino alkoxysilane. They detected a loss of the amine functionality on silica surfaces over time, due to its ability for coordination. The primary amine in the propyl position tends to coordinate with silicon atoms intramolecularly, with further cleavage by hydrolysis, or by the formation of a five-membered cyclical intermediate (Figure 1.20a). N-(6-aminohexyl) aminomethyltriethoxysilane derived surfaces were resistant to hydrolysis and able to produce stable amine-functionalized silica surfaces thanks to the longer chain length (Figure 1.20b). In this case, the intramolecular coordination with atoms is not possible, thus the amine functionality on silica remains longer. [108] However, it has been observed that long alkyl chain carbons produce less ordered films and make the surface less suitable for sensor fabrication. [109]

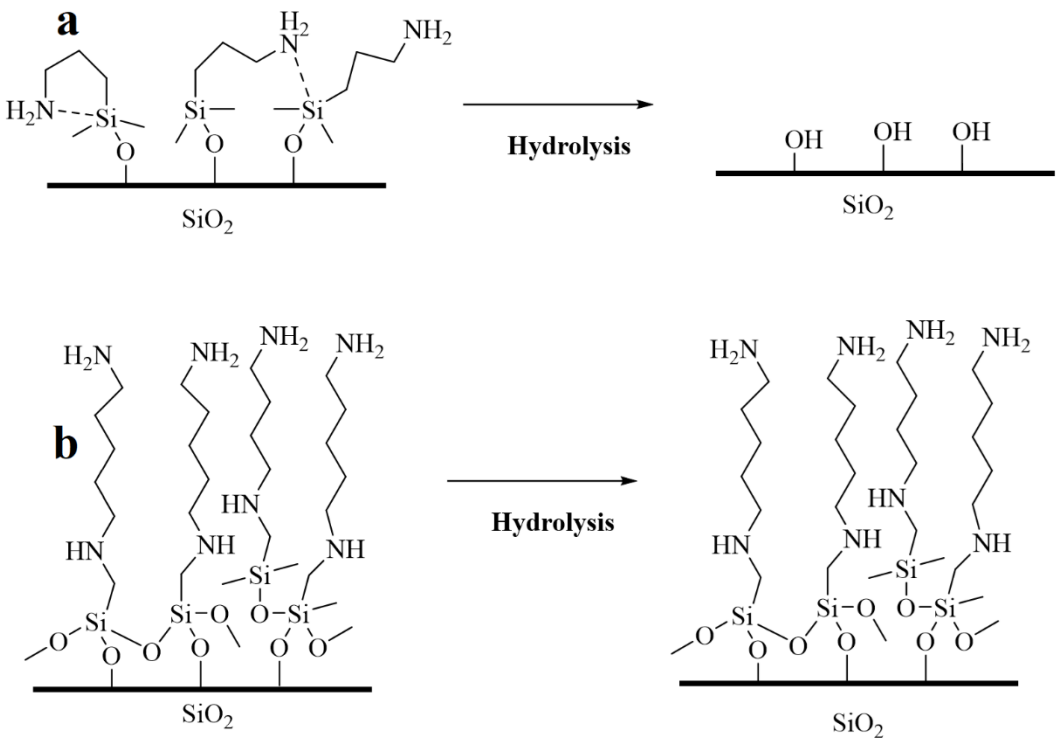


Figure 1.20. *Modification of SiO_2 surface with APTMS (**a**) compared to N-(6-aminohexyl) aminomethyltriethoxysilane (**b**).*

The deposition of SAMs can be conducted through liquid deposition by an intramolecular interaction between the surface and the solution containing adsorbing molecular species. Whilst this allows the reaction to occur, it requires a large amount of solvent and does not offer precise control over SAM formation, affecting reproducibility and quality. Occasionally, it leads to microstructural defects such as pinholes or aggregates at the surface which make the surfaces difficult to characterize properly. Haller *et al.* have proposed a vapour-phase alternative, showing a well-defined APTMS-SAM with the use of a vapour 5 wt.% solution of APTES in toluene. This technique involves the volatilization of silane coupling agents through an enclosed chamber under heat or vacuum. The substrate is placed within the chamber in a way that allows the vapour phase to access all the functionalisation area. This method is commonly employed with silane which is

difficult to suspend in solution. To let the whole modification occur uniformly, the substrates are placed in a rack within the chamber.[110, 111] This reduces the amount of organo silane needed and allows more control of deposition conditions for better-quality SAM formation.[112]

1.6.1.1 Fluorescent film sensor

The sensors are prepared by immobilizing the fluorescent reporter subunits on solid surfaces. The chemical monolayer assemblies of fluorophore on solid surfaces via SAM technique leads to the high stability, high ordering, and high surface diversity (Figure 1.21). Moreover, the generated thin film layer provides a fast response in detection on the analyte. The fluorescent film sensor consists of a spacer, that needs to connect the other two typical building units, as fluorophore and substrate. The efficiency of the system depends on the nature of the fluorophore and the choice of substrate. Small organic dyes with high quantum yield are mostly chosen, due to their small molecular size and ease of derivatization. Flat oxidised silicon surfaces are ideal substrates, due to their easy and versatile functionalization by the formation of SAM. Moreover, SiO_2 glass substrates are light transparent and photo-physically inert. The preparation of fluorescent film sensors can be achieved in two approaches. The first involves the pre-functionalization of the surface with functional terminals, used to attach the fluorophore. The second strategy consists of the formation of SAMs of alkyl silanes on SiO_2, followed by the functionalization of the terminal group to allow bonding with fluorophore derivatives. For both methods, the fluorophores are located at the end of the functional films and exposed to the analyte.[88, 93]

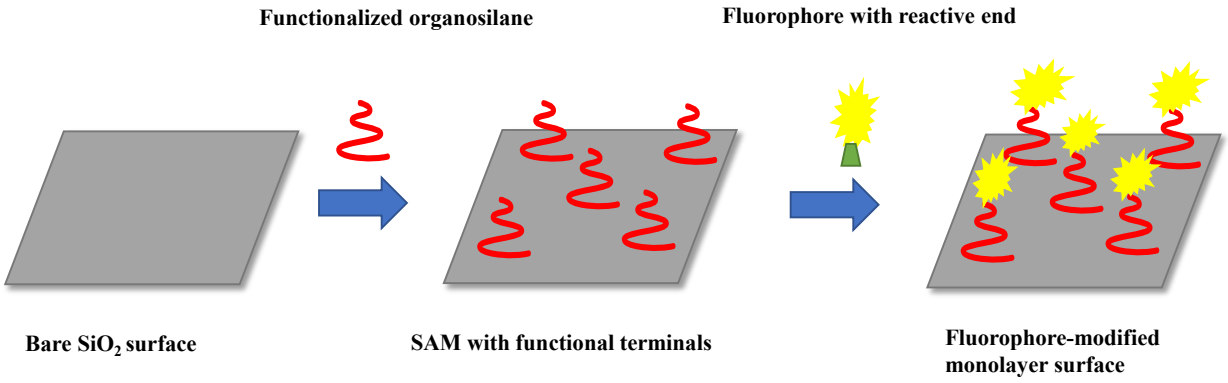


Figure 1.21. *Schematic representation of the formation of fluorophore modified monolayer surface. Image adapted from reference [88].*

1.6.2 Nanoparticles

As mentioned previously, silica-based NP are often used due to their excellent stability, recyclability, biocompatibility, and low toxicity. They consist of siloxane (-Si-O-Si-O) structures, with high concentrations of silanol (Si-OH) groups on the surface, produced by Stober process or microemulsion. Due to their biocompatibility, low toxicity, thermal stability, easy synthetic route, large-scale synthetic availability and water stability, silica-based NP are promising substrates for biological use. Modification makes the surfaces suitable platforms for biomedical imaging, detection, therapeutic delivery, monitoring, and resection therapy. Surface modification methods help to improve the colloidal stability of NP in biological systems, to reduce toxicity and aggregation and to increase circulation time. The functionalization of the surface with groups such as amines, carboxylates, epoxides, and thiols allow for further reactions. This enables NPs to act as a scaffold for the grafting of desired ligands through conjugation chemistry, such as carbodiimide, disulphide-coupling or succinyl ester hydrolysis chemistry.[90, 111]

SiO_2 NPs can be synthesized directly to contain functional groups or by attachment of an additional layer of linker molecules with functional groups once NP have been formed (post-coating). The

modification of SiO_2 NPs can be done similarly to flat SiO_2 substrates, employing the formation of functional silane SAM. For example, the reaction between silica particles with 3-aminopropylthoxysilane (APTES) leads to the coating of the surface with primary amino groups. Usually, the reaction is catalysed by heat or with a partially aqueous system to provide the alkoxy groups (Figure 1.22).[87]

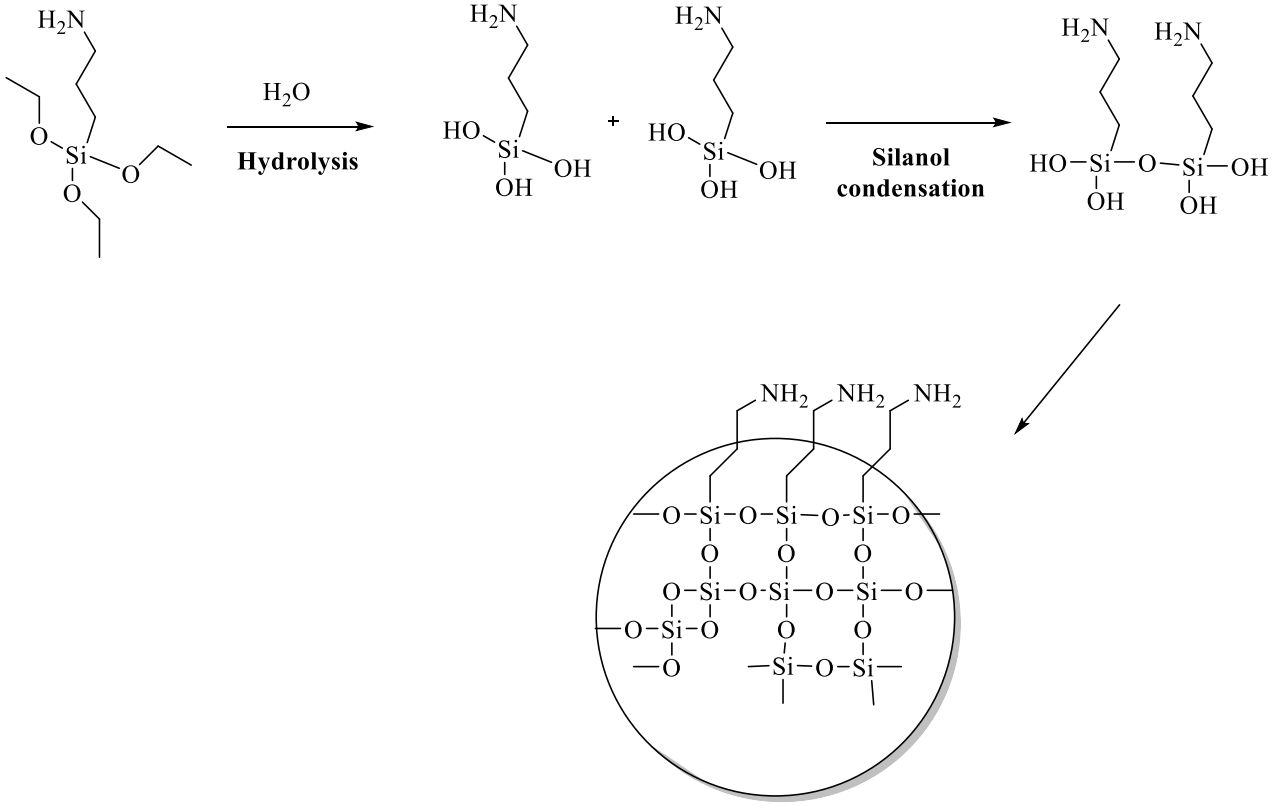


Figure 1.22. *Functionalization of silica particles by reaction with APTES.*

1.6.2.1 Fluorescent silica particles

Fluorescent nanoprobes are developed by combining organic fluorescent probes into nanoparticles. Due to the binding with more organic probes, the resulting NP enable multiple analyte detection and provide a stronger fluorescence response compared to single organic fluorophores. NP probes also have increased selectivity and better reproducibility. Dye molecules can be incorporated by physical entrapment during synthesis or by covalent attachment. The second strategy is preferred because it minimises dye leakage from the NP over time.[111] Since silica does not absorb visible light and it is possible to dye doping the silica matrix, SiO_2NPs show photophysical properties similar to the chromophores used to functionalize them. The use of fluorescent NP in sensors, maximises the brightness and enhances the sensitivity, due to the higher number and concentration of dyes incorporated. However, some of them have low brightness and too many fluorophores densely packed can reduce fluorescence intensity due to self-quenching.[111, 113] This effect can be attributed to FRET, aggregation of fluorophores and inner filter effects. Homo-FRET occurs when two of the same dyes are close to each other. Hertz et al. explained how choosing fluorophores with large Stokes shift can help to overcome this problem.[113, 114]

Over the years, surface confined strategies have been employed in the design of novel boronic acid-based sensing systems. Moreover, different structures, multi-receptor systems and combined fluorescence signal transduction mechanisms have been exploited to improve the sensing performance.

1.7 Boronic acid-based fluorescent sensing systems

Because of the binding capacity of boronic acids with diol-containing compounds, boronic acid-based sensors have been widely investigated for saccharide detection. Furthermore, fluorescent

techniques have been commonly used to design the sensing system. Several boronic acid-based sensing systems have been developed with the purpose to improve the sensitivity, selectivity, and fluorescence signal efficiency. Over the years, the strategies adopted to design the sensing system have become more sophisticated, ranging from unimolecular sensors [4] to two or more component sensing moieties,[52] or by incorporating boronic acid onto the surface of functionalized nanomaterials or alternative materials. [115, 116] Although examples of fluorescence boronic acid-based sensors are widely reported and discussed, an overview of the system reported led to the investigation into the key properties needed for an efficient fluorescence response. Additionally, the advantages offered by a solid surface allow further improvement of the final performance.

The choice of the signalling unit and fluorescence mechanism boronic acid sensing system are two key properties which are paramount to achieve the desire response. Anthracene, pyrene, and naphthalene have been widely used as probes in fluorescent sensors due to their higher quantum yields. ICT, PET, and FRET are the most common fluorescence mechanisms employed. [3, 117]

ICT based sensors

In ICT-based fluorescent sensors, the boronic acid acts as an electron acceptor in the neutral form. Upon the binding with saccharides, the boronic acid group changes to its anion form and stops acting as an electron acceptor, bringing a noticeable emission band shift. The first fluorescent sensor for saccharides was reported by Czarnik in 1992.[118] The sensor involved a boronic acid fragment directly connected to anthracene (Figure 1.23 left). Upon the binding with sugars, a decrease of fluorescence emission by 30 % was observed. This change was attributed to the change of hybridisation of boronic acid to the neutral sp^2 to the anionic sp^3 of boronate, which displayed a smaller intensity of fluorescence emission. The system was tested at pH 7.4, as intermediate value between the two pKa values, respectively 8.8 for 2-anthrylboronic acid and 5.9 for its

complex with sugar. The addition of saccharide forms a boronic ester, increasing the acidity of boronic species below the pH, which results in a decrease of observed fluorescence. The isomer 9-anthrylboronic acid was also examined, displaying a smaller change in fluorescence emission which was attributed to unfavourable peri-interaction in 9-position. [118]



Figure 1.23. *First fluorescence ICT sensors for saccharides: anthrylboronic acid(left) and isomer (right).*

In 1995, the Shinkai group developed four sensors with a stilbene core, which promote the fluorescence process due to a large conjugated π system of electrons, enabling ICT to occur. [119] Four compounds were analysed, evaluating both electron donating groups as hydrogen (**a**), methoxy (**b**), and amino (**d**)and withdrawing groups, as nitrile (**c**)as shown in (Figure 1.24). A pH increase brought a blue shift in the emission spectra and an increase in intensity in the presence of sugars. It is attributed to the lack of electron-withdrawing properties of boron in its anionic form. The fluorescence response was verified by increasing the pH and by addition of saccharide, observing two different behaviours according to the different effects of electro-donating and electron-withdrawing substituents. The emission spectra of **b** and **d** improved with the change from neutral to anionic form of boronic acid by increasing the pH, due to the loss of electron-withdrawing effect. The addition of saccharide brings a blue shift and an increase in intensity. In contrast, a red shift and a decrease in the emission intensity was observed for **c**, upon binding with sugar.

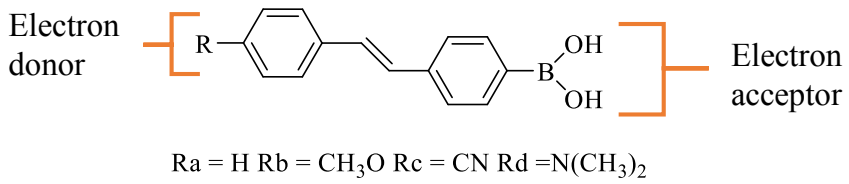


Figure 1.24. *First fluorescence ICT sensor with an evaluation of different groups attached.*

For most boronic acid-based sensors, the formation of boronic ester upon binding with sugars is slow at physiological pH. The addition of a suitable substituent promotes the phenylboronic acid in the binding with diol species. The most efficient is the placement of the basic aminomethyl group on *ortho* position, lowering the pKa of the proximal boronic acid due to its electron-withdrawing nature and a field effect from the ammonium ion. The equilibrium has been shifted to the charged boronate form, promoting a fast ligand exchange. It has been proposed that the presence of a weak dative bond between boron atom and amine, and the modulation of N-B bond strength can increase the fluorescence response upon saccharide binding. Bosh *et al.* developed an aniline based sensor, employing ICT, as reported in Figure 1.25.[117] Upon the addition of saccharides, the B-N bond strength reduces to form the boronate species **b**, emitting at 362 nm when excited at 274 nm. Different fluorescence properties of the two sensors are attributed to two different states of the aniline fluorophore: locally excited (LE) and twisted internal charge transfer (TICT). When the ion pair is coordinated with the boron and perpendicular to the π system the species shows TICT state as species **a**. Oppositely, species **b** in which the nitrogen ion pair is free to conjugate with the π-system, shows the band associates with LE state.[41, 120]

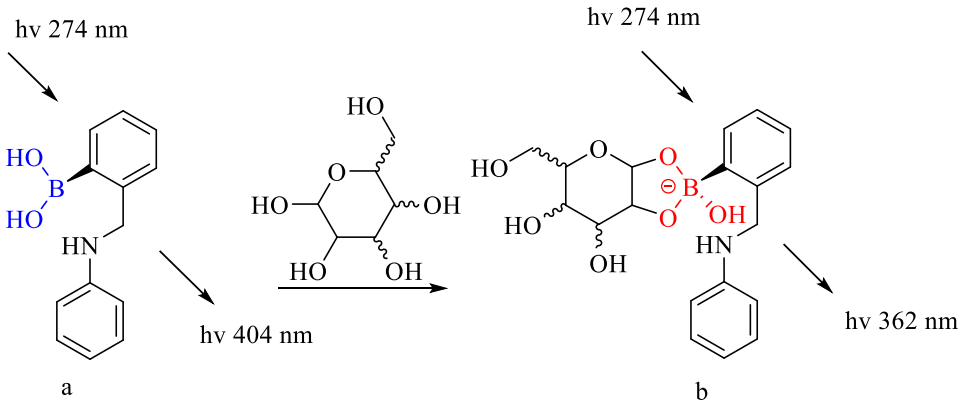


Figure 1.25. *ICT process occurring in aniline-based sensor. Change of fluorescence properties upon saccharide binding, due to conversion from locally excited state LE (a) to twisted internal charge transfer TICT (b).*

PET based sensors

In 1994, Shinkai and co-workers showed the first example of (o-(aminomethyl) phenyl) boronic acid saccharide sensor-based PET (Figure 1.26).[121] The emission of anthracene is supposed to be quenched via PET mechanism by the nitrogen electron pair, not strongly coordinated to boron. The binding with sugars strengthens the N-B Lewis interaction between the amine lone pair and the boron with higher acidity. As a result, the quenching effect is reduced, and the fluorescence of the probe is restored. The system is mainly selective for D-fructose (Ka= 1000 M^{-1}) over D-Glucose and other relevant saccharides.

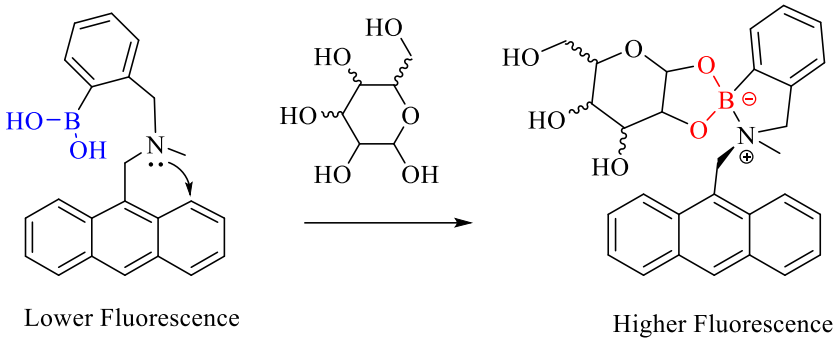


***Figure 1.26**. Boronic acid-based sensor involving the amino group, based PET mechanism proposed by Shinkai and co-workers.[121] Higher fluorescence upon saccharide detection, due to suppression of PET process.*

Furthermore, sensors involving a nitrogen lone pair in the PET process were developed, supporting this theory. The actual role of the ortho-aminomethyl group has been widely analysed. The group of Wang demonstrated, through density functional theory calculations, that the N-B bond strength upon ester formation was not significant to produce a change in PET quenching. Alternatively, a "pKa switch" or hydrolysis/solvolysis" theory was also proposed. The mechanism was proposed involving a switch between B-N interaction to a solvent insertion followed diol binding.[122, 123]

Recently, studies proposed disaggregation rather than PET as an explanation of fluorescence response. Anslyn and co-workers observed that in 2:1 water/MeOH solution with NaCl which does exists as a ground state aggregate, forming excimers upon irradiation. It was found that several stimuli such as irradiation, sonication or fructose addition produce the same increase in fluorescence emission and a decrease in excimer emission. It has been observed that in solvents in which the sensor is completely soluble, such as MeOH solution, there was no aggregate-state excimer, and the addition of fructose did not produce any fluorescence change. They concluded that the fluorescence turn-on has been achieved mainly by solvation properties generated by the saccharides. Moreover, the same fluorescence response in presence of fructose, has been observed

to analogue of the sensor that does not contain a boronic acid, despite having no functional group to bind sugars. The results support the theory of disaggregation as cause of fluorescence modulation observed.[124]

Figure 1.27 summarizes the different theories previously proposed to explain the role of B-N in fluorescence properties. Xiaolong Sun *et al.* conducted several experiments with different probes highly water-soluble, to remove disaggregation issues to create a unifying theory to explain the emission turn-on of ortho-aminomethylphenylboronic acids. They demonstrated that the PET or pKa switch mechanism was not supported because both boronic acid and boronate esters are mainly solvent inserted. Thus, the switch proposed cannot occur. Moreover, it has been verified that the sensors were not aggregated, in contrast with the theory of disaggregation. The emission turn-on of the sensor upon saccharide binding has been justified with "a loose bolt effect" internal conversion. They observed how in MeOH no fluorescence response upon fructose binding, due to an exchange of the group $-B(OH)_2$ to $-B(OMe)_2$. After excitation, the fluorophore acts as an energy donor, while the –OH rotors of $–B(OH)_2$ work as energy acceptors. The internal conversion is suppressed with the replacement of hydroxyl groups with fructose or methyl groups from methanol. The mechanism proposed represent a valid explanation of fluorescence response observed ortho-aminomethylphenylboronic acid-based fluorescence sensors. [125]

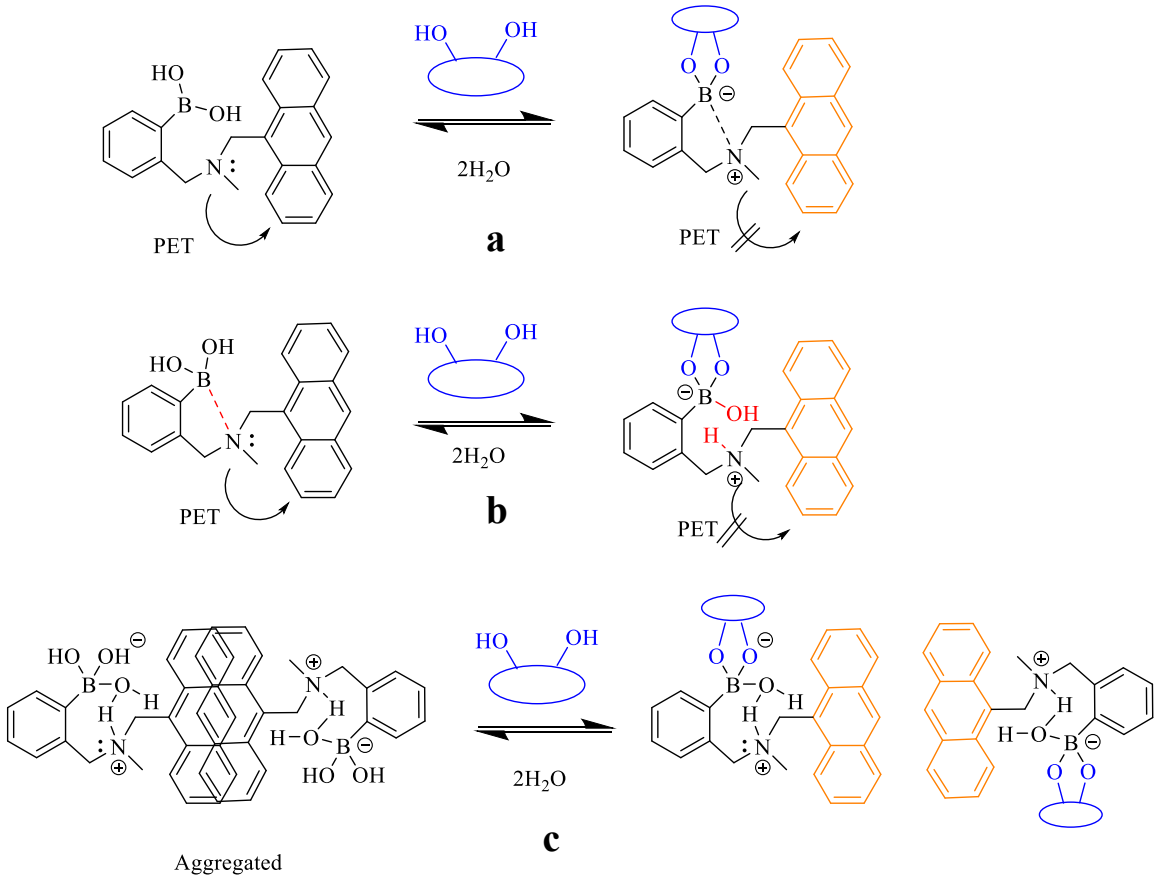


Figure 1.27. *Different proposed mechanisms t explain emission turn on (a) change in the strength of an N−B bonding interaction upon sugar binding; (b) breaking of an N−B bond and insertion of Solvent upon sugar Binding, and (c) aggregation and disaggregation with solvent insertion.*

Alternative dye based fluorescent sensors

The use of polyarene molecules often requires the addition of an organic solvent as co-solvent due to their lower solubility in water. To promote the application of boronic acid-based sensors in the biological system, naphthylamide has been often used as a fluorophore due to its absorption and emission in the visible region and its ease of modification (Figure 1.28a). Mori et al. synthesized a phenylboronic acid derivative of 1,8-napthalimide linked by a flexible aliphatic chain with an appended amino group.[126] Due to the low fluorescence enhancement observed upon addition of

fructose (approx. 3-fold), later studies conducted by the group of Qian improved the structure of sensor. They included a more rigid and bulky piperazine instead of aliphatic amine to strengthen the interaction between boronic acid and amino group.[127] The enhancement of 50-fold upon D-fructose addition has been attributed to a PET process, which is possibly endorsed by TICT process caused through piperazine structure. [128]

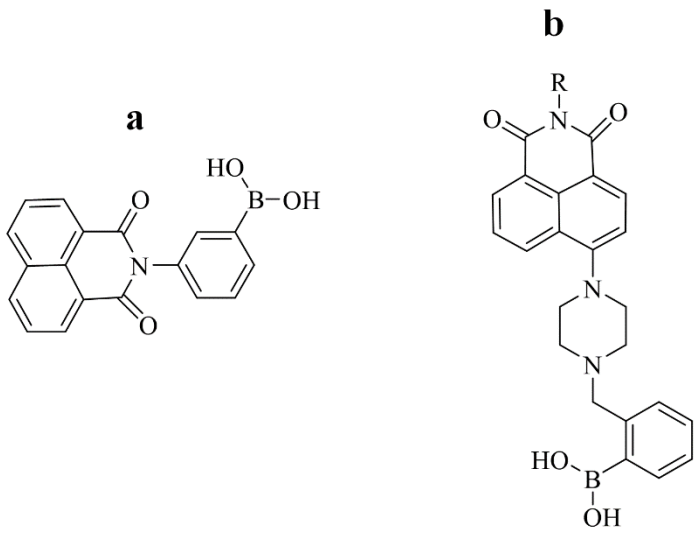
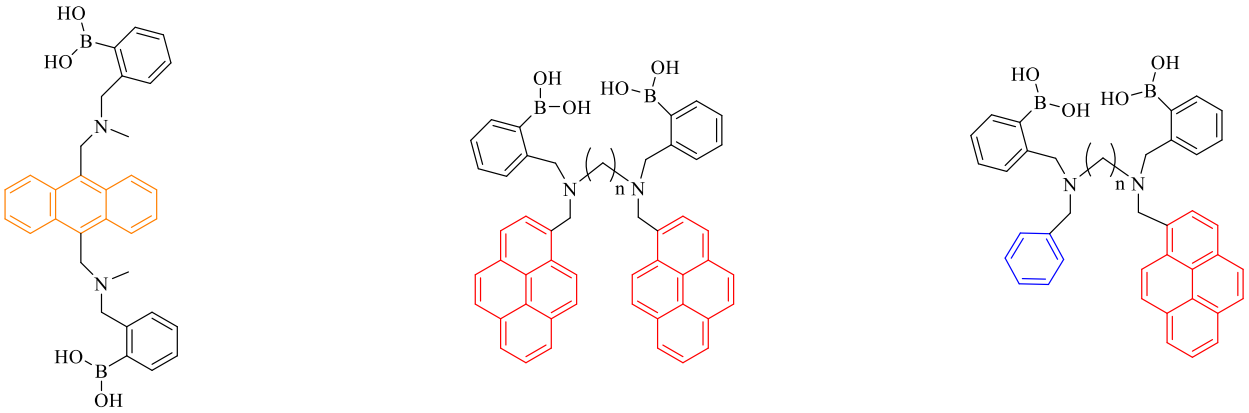


Figure 1.28. *Example of 1,8-napthalimide based sensor (a) and improved structure with piperazine ring (b).*

Di-/multi-boronic acid sensors for saccharides

The selective binding towards some sugars depends on structural characteristics. The system must be modified to include more selective recognition elements to increase the affinity and selectivity of glucose. The group of Shinkai reported one of the first systems which involved two appropriately spaced boronic acids (Figure 1.29a). [129] The spacing and the orientation of the two boronic acids enabled the binding of two diols, and so enhancement of the fluorescence response upon glucose binding, over other monosaccharides. Later, glucose sensors were developed,

employing a longer spacer to link two fluorescence sensors and a different fluorophore which had been demonstrated to affect the selectivity. Since the low fluorescence response observed in **b,**[130]due to the self-quenching effect by the same pyrene probe, asymmetrical diboronic acid (**c**) [131] has been developed (Figure 1.29b and c).



a **b** **c**

Figure 1.29. *Example of sensing system with more selective recognition boronic units to increase binding affinity and selectivity to glucose (a). Improvement of the length of linker (b) and use of different asymmetric probes (c).*

FRET bases sensors

Using polyaryl systems, James *et al* prepared a FRET saccharide sensor with two different fluorophores (Figure 1.30).[132] The system was based on phenanthrene as the donor and pyrene as the acceptor separated by hexamethylene as linker. The emission wavelength of the donor at 369 nm and the excitation of pyrene (acceptor) at 342 nm, were suitable to achieve spectra overlap, enabling FRET mechanism. The system conjugate with D-glucose was irradiated at the excitation wavelength of the donor, observing the highest fluorescence response at 397 nm (3.9 times). The

binding with D-glucose was observed to be stronger than that of other saccharides, serving as a selective glucose sensor.

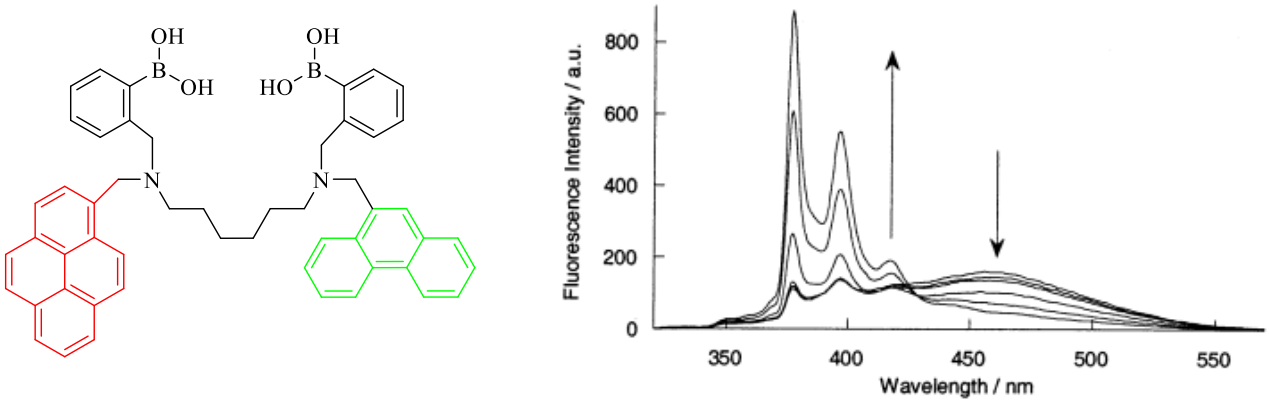


Figure 1.30. *FRET-based system developed by James and co-workers (left) Fluorescence spectral change of sensor with different concentrations of D-glucose. Image adapted from reference [132].*

Fluorescent sensor-based FRET requires suitable spatial positions of the boronic acids involved and some strict requirements regarding emission and excitation properties of the sensor involved. However, FRET can be used a method to enhance sensitivity and selectivity. Moreover, it has been widely used in boronic acid sensors, further supporting its use in this work.

An example is reported by Chaicham *et al*.[133] They reported a FRET-based sensing system for catecholamine detection. The system involved two different fluorescent sensors where a suitable catecholamine act as a guest linker between boronic acid and aldehyde, inducing a FRET mechanism (Figure 1.31). The ability of the sensor to differentiate structurally similar catecholamines through a FRET on/off process was demonstrated.

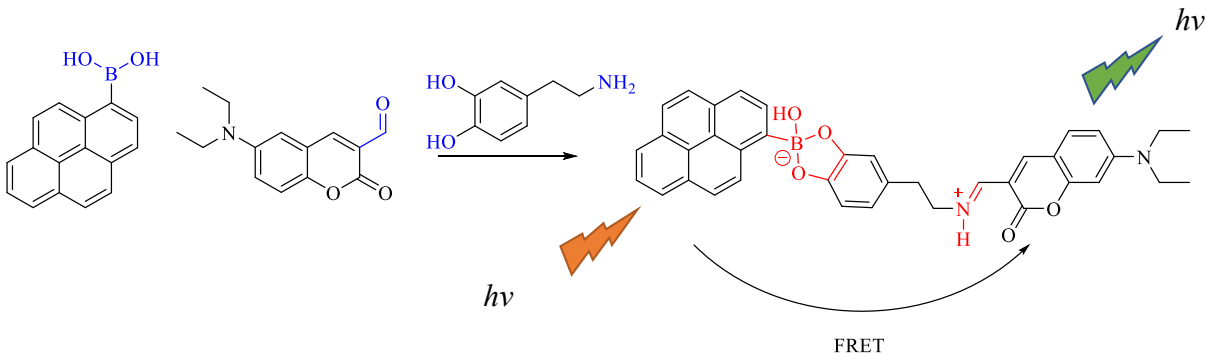


Figure 1.31. *FRET based system for catecholamine detection. Image reproduced from reference [133].*

1.8 Boronic acid-functionalized surfaces for saccharides sensing

In recent years, innovative systems have been developed by functionalization of BA in different materials such as quantum dots,[134] carbon nanotubes,[135] nanofibers,[136] or graphene oxide.[137] Also, functional polymers,[138] hybrid nanogels,[139, 140] or molecularly imprinted polymers[141] though BA modification is emerging as a strategy in sensing systems development. The incorporation of boronic acid into the polymer matrix, or onto the nanoparticles or nano sensors' surface enhances the binding towards analytes, reducing the matrix interference since the recognition processes take place in the solid-liquid interface. Moreover, it is possible to develop multivalent boronic acid, by incorporating multiple sensors, enhancing the sensitivity towards analyte. The controllability of the size and shape of nanoparticles /sensors and their inherent properties confer tailorable characteristics to the final developed sensor system that can improve performance.

Recently, hydrogels have been widely used due to their high biocompatibility, flexibility and mechanical properties that facilitate the incorporation of boronic acid moieties. Cai et al synthesized a multifunctional hybrid nanogel with 3-acrylamidophenyl boronic acid copolymerized with ethyl aminoethyl methacrylic (p(APBA-b-LAMA)) for high selectivity glucose detection.[142] The improvements of hydrogel with PBA for smart glucose response delivery

systems, enable their application in the treatments of diabetes. Alternative systems have been developed by functionalization of BA in different materials such as quantum dots, carbon nanotubes, nanofibers, or graphene oxide. For example, in 2010, Zhou and co-workers reported phenylboronic acid-functionalised cadmium telluride (CdTe)/ zinc telluride (ZnTe)/ zinc sulfide (ZnS) quantum dots (PBA-QDs) for selective detection of glucose (Figure 1.32) [143] They observed a fluorescence quenching of about 67 % upon the addition of 20 mM glucose, verifying the high sensitivity towards it.

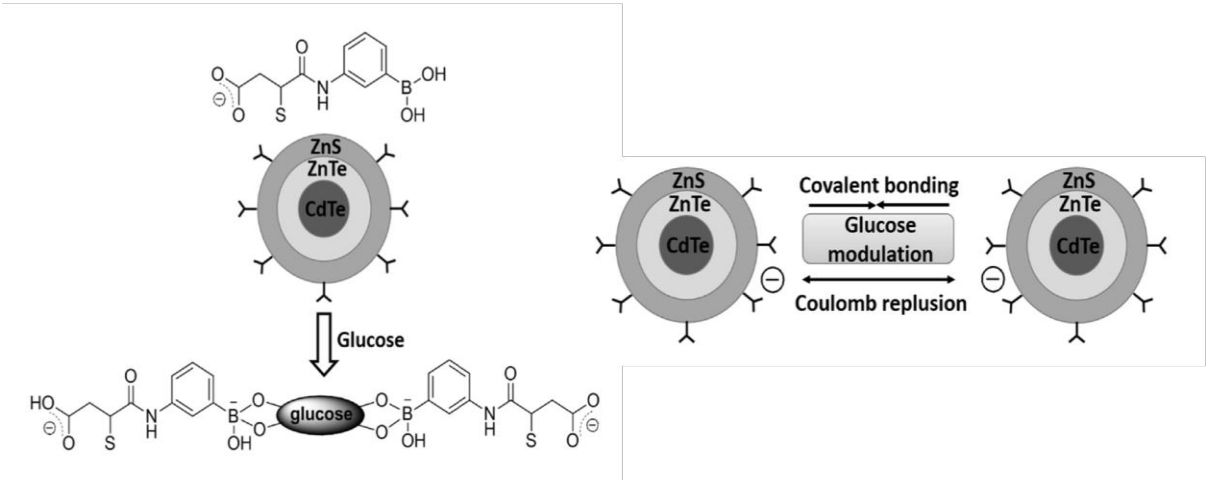


Figure 1.32. *Glucose induced assembly of PBA modified QDs. Image reproduced from reference [143].*

Boronic acid-modified glass-surface was engaged to fabricate a covalent carbohydrate microarray.[144] The system was proved to be able to immobilize several carbohydrates of different sizes, and thus employed to identify carbohydrate-protein interactions (Figure 1.33).

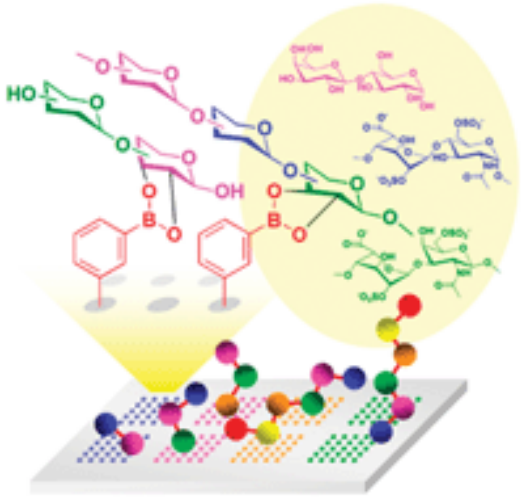


Figure 1.33. *Fabrication of carbohydrate microarray. Image reproduced from reference [144].*

James et al developed a FRET-based sensing system for saccharides by using Avidin microspheres as a substrate. [145] They detected as the decreasing fluorescence intensity of a biotinylated boronic ester in the presence of a quencher involving a diol. Once added, the fructose competes with the quencher for the binding site, replacing it and allowing restoration of the fluorescence (Figure 1.34).

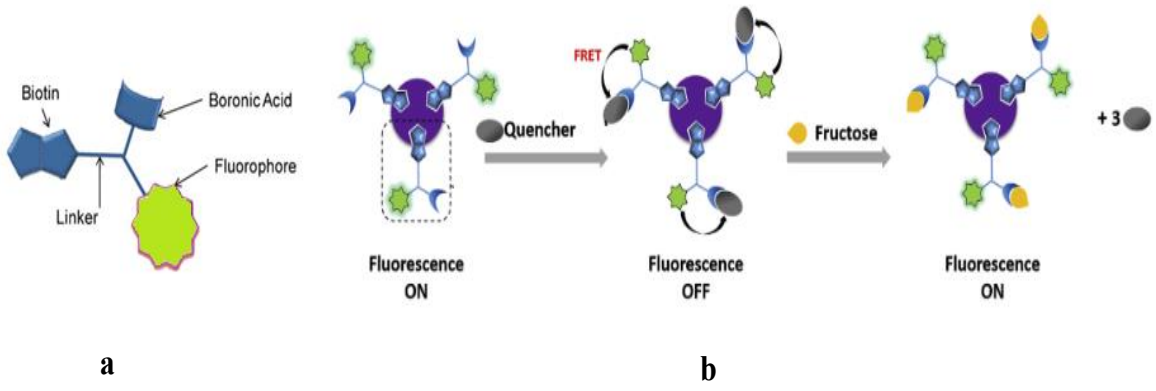


Figure 1.34. *Boronic acid-fluorophore conjugate, (a) FRET-based fructose sensing on a microsphere (b). Image reproduced from reference [145].*

Different and innovative materials have been employed in the recent years, however the development of self-assembled simple boronic acid-based sensors to confined to solid substrates remains unexplored. The surface can be employed to enhance the sensitivity and efficiency of a simple boronic acid-based sensor. Qian and co-workers improved the performance of their previous designed 1-8 naphthene-based system (Figure 1.28b), through its incorporation onto the surface of silica nanoparticles (Figure 1.35). [146] They observed that the length of the linker does not significantly affect the spectral response, while a particle size of 100 nm, compared to smaller sizes, showed a significant response toward fructose and sorbitol.

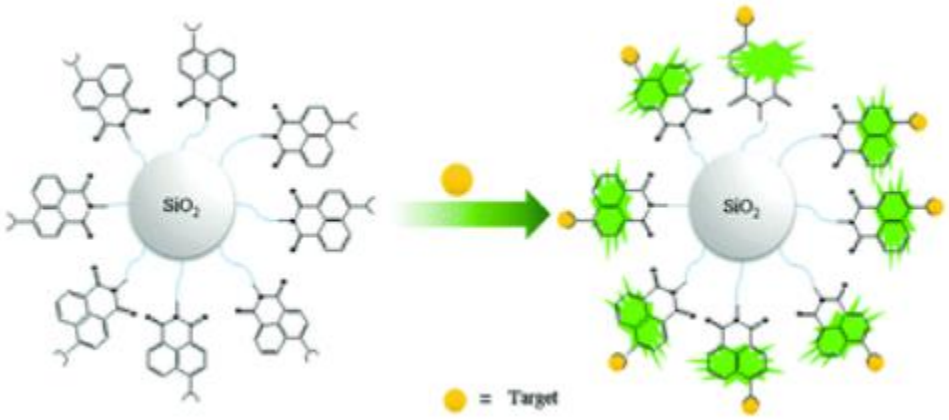


Figure 1.35. *Incorporation of multi sensor into silica nanoparticles surface. Image reproduced from reference [146].*

Due to the several advantages of chemical and thermal stability, biocompatibility, and functionalisation versatility, silica-based surfaces represent a powerful support for the development of advanced sensing systems Moreover, the transparent and photophysical inert properties of silicon substrates promote the fluorescence signal of the sensor, making additional fluorescent processes possible.

An initial investigation of the structure, single units, and fluorescent mechanism involved will allow the development of a high-sensitivity fluorescent boronic acid-based system. Incorporation onto a surface will allow further adjustment of the system's properties and improve the efficiency of saccharide detection.

1.9 Summary

Because of the natural diversity of the constituents, the variability of the glycosidic bond, and the ability of conjugate with other molecules, glycans are involved in several physiological events inside the body. The effective and efficient detection of glycans, their derivatives, and the recognition of abnormal concentrations can lead to the early diagnosis of diseases and the development of treatments. Therefore, research into simple saccharide identification systems has become pertinent in recent years. As previously mentioned, a molecular sensor is formed of a receptor and a transducer. Since boronic acids can bind to polyhydroxy compounds, such as saccharides, they are widely employed as receptor units in sensing applications. The presence of specific groups, such as amino, its suitable position, and the structure of boronic acid derivatives, can promote the interaction with diols in terms of selectivity and sensitivity. With boronic acid acting as the receptor unit, a transducer mechanism is also required. Due to advantages such as higher sensitivity, selectivity, response time, low cost, and local observation, fluorescence is the most used traducer mechanism for modulating the signal upon saccharide binding. Different types of signalling units and signal transduction (PET, ICT, or FRET) can be employed. Several boronic acid-based sensing systems have been developed with the purpose to improve sensitivity, selectivity, and fluorescence signal efficiency. The performance of the sensor has been demonstrated to enable to increase in its attachment to a solid surface. The effect of the surface is to reduce the matrix interference and bring close the system units strengthening their interaction

and so the fluorescence mechanism involved. The strategies adopted to design the sensing system range from unimolecular sensors to two or more component sensing moieties or incorporating boronic acid onto the surface of functionalized nanomaterials or alternative materials. Although different materials such as quantum dots, polymers, and hybrid nanogels have been functionalized with BA, boronic acid-based sensors designed to be surface-confined have not been extensively investigated in saccharides detection research.

1.10 Aims of this work

The aim of this work is to design fluorescence boronic acid sensing systems with the capability to be immobilized onto solid supports. The project will contribute to the research of high sensitivity sensor for saccharide detection. Each system is based on boronic acid as the receptor unit and a fluorophore that provides a fluorescence intensity change modulated by a fluorescence mechanism. The system is planned to be immobilized onto a silica surface, aiming to strengthen the interaction between the units involved and thus the performance of the system. Different boronic acid-based sensing systems were explored, with investigation into the structure of the units involved, their connection and the employed fluorescence mechanism.

The first sensing system consists of two single units: phenylboronic acid as a receptor and an anthracene dye as a fluorophore. The fluorescence mechanism selected to modulate the response upon sugar binding is PET, as shown in Figure 1.36. The incorporation of the units onto the surface works to strengthen the interaction between the two units and promote the PET mechanism involved.

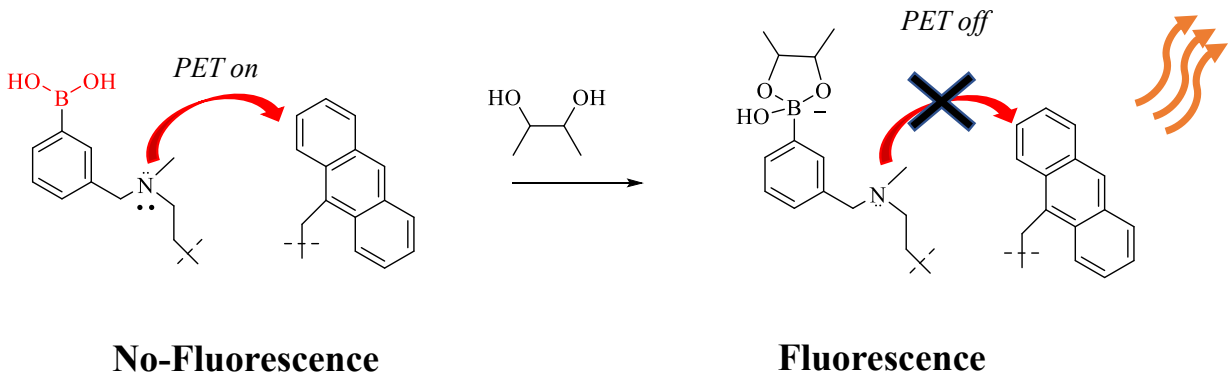


Figure 1.36. *Representative scheme of first sensing system: PET system based on phenylboronic acid and anthracene.*

The second sensing system involved a pyrene-based sensor with BA unit incorporated into the structure of the fluorophore. The boronic acid moiety is connected to the fluorophore directly (**a**) or through an alkyl chain with an amino group as a linker (**b**), as shown in Figure 1.37. The system aims to enhance the performance of the sensing system employing FRET mechanism, by interaction between BA-based sensor acting as donor and coumarin dye as acceptor. In the first strategy (**a**) the fluorescence response of BA based sensor achieved upon saccharide binding enables the interaction with coumarin and thus FRET mechanism. In strategy **b**, the fluorescence response is modulated by ICT mechanism, where the shift in the emission spectra upon sugar binding enables FRET with coumarin.

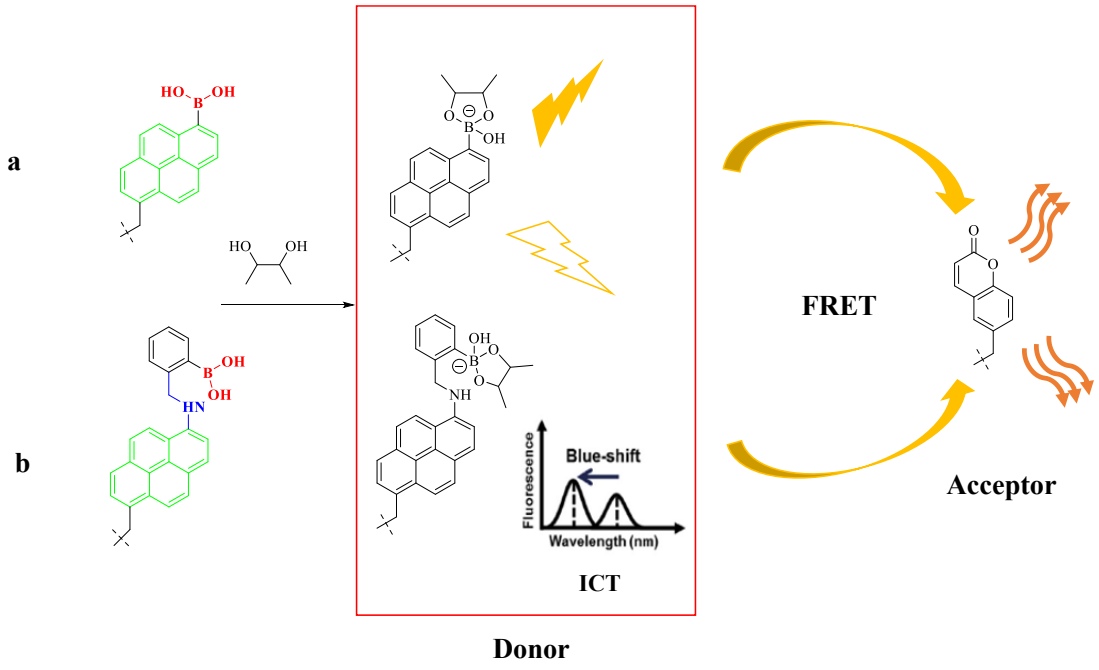


Figure 1.37. *Representative scheme of second sensing system by different strategies:* ***a****) direct connection of BA (red) with fluorophore (green),* ***b****) connection through a linker (blue). FRET system between pyrene boronic-acid based sensor following fluorescence response (a) and ICT mechanism (b) as donor and coumarin probe as acceptor.*

The final system involves a pyrene-based sensor with the boronic acid connected through a piperazine ring modulated by a PET mechanism. The fluorescence response produced by saccharide binding by PET is employed to establish an interaction with an additional probe. The fluorescence performance of the system is then improved through FRET mechanism (Figure 1.38).

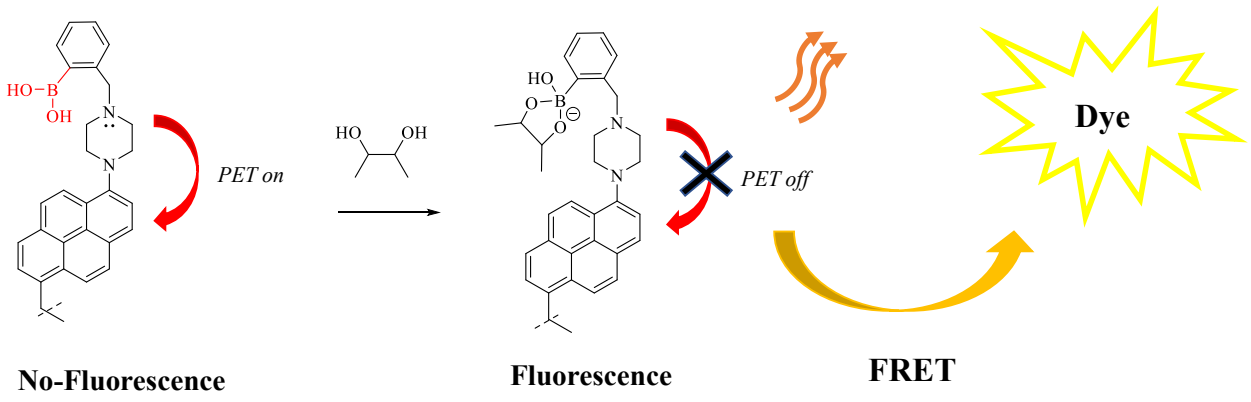


Figure 1.38. *Schematic representation of third sensing system: combination of PET-pyrene boronic-acid sensor and FRET.*

The binding abilities of the sensor towards saccharides are assessed by fluorescence measurements. Experiments at different pH, range of sugar concentration and different saccharides are performed to evaluate the binding condition, sensitivity, and selectivity of three different sensing systems.

The properties and functionalization methods of silicon wafers and silica nanoparticles are explored to evaluate their use as solid supports for the immobilization of the fluorescence systems. The units involved in the sensing system are planned to be modified to promote further reaction on the surface via functional groups. Alkene, azide and alkyne groups are explored to enable immobilisation onto the surface through radical addition (alkene group) or click chemistry reaction by azide-alkyne cycloaddition.

CHAPTER 2: TECHNIQUES

2.1 Spectroscopic Techniques

Spectroscopy refers to those techniques that employ the electromagnetic radiation to interact with a sample. These techniques can be classified depending on the frequency of radiation employed, which determine the object of study, or their complexity. For example, simple techniques, such as absorption, obtain qualitative and quantitative data from the intensity of adsorbed light in function of wavelength; while other more complex techniques, such as Circular dichroism, that can offer more deep structural information.[147]

Table 2.1. *Examples of spectroscopic techniques.*

ELECTROMAGNETIC RADIATION	SPECTROSCOPIC TECHNIQUE
X-ray	X-ray photoelectron spectroscopy
Ultraviolet–visible	UV-Vis spectroscopy Fluorescence spectroscopy Circular dichroism
Infrared	IR spectroscopy Raman spectroscopy
Microwave	Rotational spectroscopy

For the purpose of this project, UV-Vis, Fluorescence, and IR spectroscopy are described here.

2.1.1 UV–Vis spectroscopy (UV-Vis)

UV–Vis spectroscopy is a widely used analytical technique, for qualitative and quantitative analysis, that employs radiation of frequencies in the ultraviolet and visible regions of the electromagnetic spectrum. This kind of radiation interact mainly with the highest occupied orbitals

from molecules and atoms, giving basic structural information. The adsorption spectrum is measured by recording the intensity of radiation that passes through a sample. The wavelengths that are absorbed are those interacting with the sample, represented in the spectrum as an absorption peak. For organic molecules, those peaks are correlated with some specific type of bonds and, therefore, may be employed as support for the identification of functional groups. Basic aromatic molecules absorb in the ultraviolet part of the spectra and more extended conjugated molecules have more redshifted absorption, potentially reaching near infrared wavelengths. However, it also can help to determine the molecule concentration, thanks to Beer-Lambert law. This law defines the direct proportion between the concentration of absorbing species in the solution and the intensity of light absorbed[147] as seen in this equation:

$$A = Log_{10}\left(\frac{I_0}{I}\right) = \varepsilon CL \qquad \text{Equation 2-1}$$

Where A is the measured absorbance, dimensionless but reported in Absorbance units (AU) (reference), is the logarithmic ratio between I_0, the intensity of incident light on the sample, and I, the intensity of transmitted light from the sample. This value gives quantifiable information about light absorbed at a selected wavelength and is directly proportional to the concentration of sample *C*. The other two parameter in this equation are *L*, the optical path length and ε (extinction coefficient), an intrinsical property of the molecule at specific temperature, pressure and solvent.

Another common parameter is the transmittance (*T*), defined as ratio between intensity of light after (*I*) and before (I_0) passing through a sample. It is expressed as percentage (T%) and correlated with absorbance by the following expression:

$$T = \frac{I}{I_0} = 10^{-A} \qquad \text{Equation 2-2}$$

Basic UV-Vis absorbance measurements are performed in UV-Vis spectrophotometer, an apparatus composed of a light source, a sample holder, a monochromator to separate the different wavelengths of light, and a detector. A combination of lamps as light source is required to cover all UV-Vis range. Tungsten filament lamp, deuterium or xenon arc lamp are ones of the most common. Some kind of light-detecting device, such as a photomultiplier tube, a photodiode, or a photodiode array, is used as detector unit. More complex instruments are available, such as double beam spectrophotometer, which splits the incident light in two beams and allows to measure a reference at the same time as the sample. Moreover, it can be used as a detector unit for high-performance liquid chromatography (HPLC) techniques for analytical or preparative applications.[148]

2.1.2 IR spectroscopy

IR absorption spectroscopy refers to the interaction of infrared radiation (wavelengths from 700 nm to 1 mm) with a sample. In this wavelength region, the light induces vibrational changes in covalent bonds of atoms or groups of atoms, thus can be employed for their characterization. Rotation and vibration motions are characteristic of organic molecules and can be employed for their characterization. Furthermore, there are different vibrational modes corresponding to the relative movement of 2 atoms such as bond stretching or 3 atoms: angle twisting, wagging, etc. The frequency and amount of absorbed radiation is different for each vibration mode, being the stretching frequencies higher, and corresponding peaks more intense than others. The same tendency can be observed with the increase of the number of bonds, triple bonds higher than single ones, and for lighter atoms, heavier atoms have smaller stretching frequencies than hydrogen. Additionally, they are dependent on molecular symmetry and spectroscopic selection rules, such as changes in dipole moment.[148, 149]

The region from 500 to 1500 cm^{-1} of infrared spectra is called the fingerprint region, because many different peaks appear and very complex to analyse. Nevertheless, some interesting peaks appear in this region such as C-O stretching (1160-1080) or Si-O stretching (950-810). The region from 1500 to 4000 cm^{-1} is clearer and is related to the stretching vibration of diatomic units, resulting in strong characteristic peak. In this region appear peaks such as C–H stretching (3300-2800), N-H/O-H (3650-3300), C=O stretching (1600-1400) or azides (2200-2100).[150]

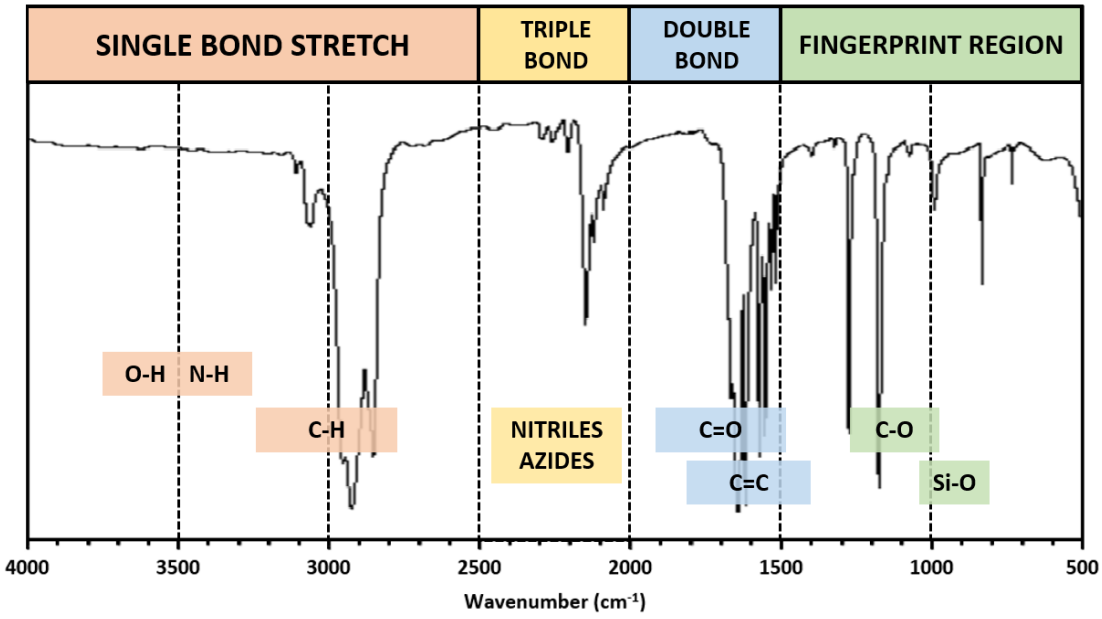


Figure 2.1. *Regions of the infrared spectrum and specific wavelength of common functional groups.*

Infrared spectra are traditionally plotted in graphs of infrared light transmittance versus wavenumber, the inverse of the wavelength, expressed in cm^{-1}. Infrared spectrophotometers were originally very similar in design to UV-Vis spectrophotometers, but new Fourier transform infrared (FTIR) spectrophotometers were developed allowing fast response, high sensitivity and precise measurements. This equipment employs an interferometer as an infrared source, using only

radiation of one singular wavelength, then transmitted light is processed using a Fourier transform to obtain a typical infrared spectrum.[151]

2.1.3 Fluorescence spectroscopy

Since the objective of this work is to develop fluorescence-based sensor, fluorescent techniques are already described in detail in section 1.5.

2.2 Organic chemistry techniques: analysis, separation, and purification

Nuclear Magnetic Resonance (NMR) spectrometry, mass spectrometry (MS) and liquid Chromatography (LC-MS), and thin layer chromatography (TLC) are common techniques of analysis in organic chemistry. Chromatographic column and HPLC are employed as separation and purification methods.

2.2.1 Nuclear Magnetic Resonance (NMR) Spectroscopy

NMR spectroscopy is an advanced characterization technique used to determine the molecular structure at the atomic level of the sample. NMR is based on the interaction between atom nuclei and an external applied radiofrequency radiation. Nuclear spin, an intrinsic property of protons and neutrons, is modified due to this interaction leading to an exchange of energy that is later emitted back, revealing information about its structure.

The overall spin number (I), defined as the number of unpaired protons and neutrons, is directly related to the magnetic moment μ and determines NMR susceptibility. Nuclei with even number of protons and neutrons, such as ^{12}C, ^{16}O, has a zero magnetic moment ($\mu = 0$) and therefore is NMR inactive; while other nuclei with non-zero magnetic moment ($\mu \neq 0$), such as ^{1}H, ^{13}C, ^{11}B, are NMR active. Following the application of an external magnetic field (B_0), the magnetic dipoles

of these nuclei distribute along the axis of the applied field in different states, which number S is defined by the following equation.

$$S = 2I + 1 \qquad \text{Equation 2-3}$$

Thus, for an atom with a single proton, spin number I will be 1/2 and the nuclei can assume two different orientations to the applied magnetic field. The magnetic moment of the lower energy +1/2 state is aligned with the external field, while that of the higher energy -1/2 spin state is opposed to the external field. The energy difference between the two states depends on the applied magnetic field, the Planck constant and from the magnetogyric ratio (γ), defined by the nucleus types.

$$\Delta E = \gamma\, h/2\pi Bo \qquad \text{Equation 2-4}$$

The excitation of nuclei will lead to a spin inversion, which occurs when is applied an electromagnetic radiation of frequency *v* correspondent to the energy difference. After excitation, the nuclei relax emitting energy as radiofrequency, which produces a characteristic signal called free induction decay (FID) and is registered by the detector. The FID is then processed by Fourier transformation to produce the NMR spectrum. The NMR spectrum presents the resonant frequencies for each nucleus displayed as a signal after transformation into a chemical shift (δ) reported in ppm. The chemical shift is defined by the frequency (Hz) of the nucleus, (*v*i), the frequency of a reference (νR), and the frequency of the instrument in MHz (v_0).[152]

$$\delta = (vi - vR)/v0 \qquad \text{Equation 2-5}$$

The chemical environments where the nuclei are present describes the shielding to which it is subjected and thus affects the resonant frequency of a specific nucleus and, as consequence, the chemical shift. If a nucleus possesses electrons near, it is subjected to a magnetic field opposed to

B_0, reducing the effective magnetic field seen by the nucleus, and a lower resonance frequency. For higher electron densities, the chemical shift is smaller because the shielding is greater, and the signal is shifted to a higher field. In the opposite way, nuclei less shielded provide larger δ shifts.

Signal multiplicity, coupling constant (J) and signal integral are other key parameters for the interpretation of NMR spectra. Thus, the multiplicity gives information on the number of NMR-active nuclei that are within a certain distance (usually 3-bond away from a given nuclei). For example, the signal multiplicity in 1H NMR spectrum is equivalent to the number of neighbouring protons, plus one. A signal that appears as a doublet suggests the presence of one hydrogen on the adjacent atom; the resonance will be split into two peaks of equal size. The integrated area of a peak gives another important piece of information, as is directly proportional to the total number of protons producing the signal. Other atoms, such as 13C NMR, are also commonly employed in the identification of organic molecules. However, it is a lesser abundant isotope ^{13}C active isotope that is used in NMR, is less abundant than ^{12}C making its sensitivity much lower than 1H NMR. Consequently, 13C NMR analysis requires more concentrated samples.

2-D experiments can also be performed to provide additional information on the molecular structure, such as COrrelated SpectroscopY (COSY) and Heteronuclear Single Quantum Correlation (HSQC) employed in this work. COSY refers to the ^{1}H-^{1}H correlation spectroscopy and displays the correlation between H nuclei separated by a maximum of 3 bonds. The correlation between protons is displayed as cross peaks in the 2-D spectra. $^{1}H^{13}C$, HSQC is similar and is used to observe the correlation of protons attached to a specific carbon.[153]

2.2.2 Mass spectrometers (MS)

MS is an analytic tool that measures the mass/charge ratio (m/z) of one or more molecules present in a sample. It is used to calculate the exact molecular weight of sample components, enabling the identification of unknown compounds, structure determination and elucidation of the chemical properties of molecules.

MS consists of an ionisation source, a mass analyser and an ion detector. A sample is vaporized and subjected to ionization, that can also include fragmentation. The ionization of small molecules provides charged ions that are absorbed from the sample by an extraction system. The ions are enhanced through an electric /magnetic field into the mass analyser that separates them depending on their masses. The separated fragments are measured by the detector that calculates their m/z and their relative abundance. The generated ions are very reactive and short lived, so their formation and manipulation have to be conducted in a vacuum.[154]

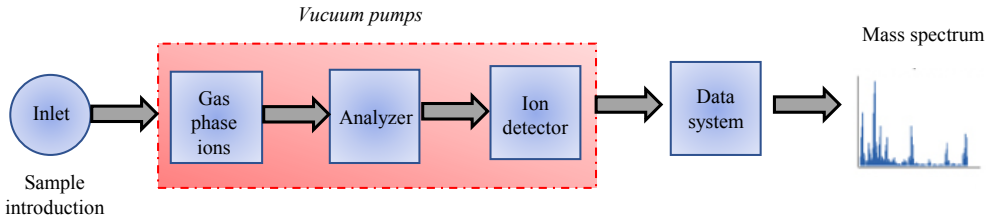


Figure 2.2. *Schematic scheme of mass spectrometer MS.*

Different techniques of ionization can be applied, depending on the chemical and physical properties of the sample. The sample can be introduced directly or in the case of mixtures, through an intermediary chromatographic device (gas chromatography, liquid chromatography, etc). Electro impact and/or chemical ionization are employed for non-thermolabile samples, while electrospray (ESI) and matrix assisted laser desorption (MALDI) are employed as soft ionization

for more sensitive compounds. The ionization process via ESI forms positive or negative ions depending on the sign of the applied electrical field. The achieved m/z values usually correspond to the mass of analyte plus a proton [M + H] or deprotonated in negative mode [M -H]. Common mass analysers include an electrostatic-magnet (EB), ion trap (IT), quadrupole (Q) and time of flight (TOF).[155]

A mass spectrum refers to the plot of the m/z ratio of the ions present in the sample versus their abundance. Ions provide information about the nature and the structure of their precursor molecule. Molecular ions, if present, appear as the highest value of m/z ratio and give the molecular mass of the compound. The fragmentation pattern can give useful information about the structure of molecular ions. However, it is not always possible to explain the origin of all the fragments if the structure is unknown. Mass spectra can also identify elements with different isotopes that show characteristic patterns, such as compounds containing Br, Cl, or B. Chlorine atoms possess the most abundant isotopes ^{35}Cl and ^{37}Cl, and the peak heights reflect the relative proportion between them (3:1). In the same way, bromine shows two peaks in the same ratio, corresponding to its two isotopes. Although MS is considered a destructive technique, it is widely employed because it requires very little amounts of material for analysis (~1 μg). [156]

2.2.3 Thin layer chromatography TLC

TLC is an example of analytical chromatography widely used in synthetic chemistry to monitor the progression of a reaction or identify compounds. It is employed to optimize the solvent system for further separation through column chromatography. Compared to column, TLC requires only a small quantity of compound, and is an easy and quick technique. The separation is achieved by the different affinity of analytes towards the stationary and mobile phase. A TLC plate, involving a sheet of glass, metal plastic coated with a thin layer of solid adsorbed (silica or alumina) refers

to the stationary phase. A small amount of mixture to analytes is spotted close to the bottom of the plate. The TLC plate is placed in a developing chamber with a thin layer of solvent with which is in contact with the bottom of the plate. This liquid, or the eluent, is the mobile phase, and it causes the analyte to slowly rise up the TLC plate by capillary action. Following complete elution, the plate is removed, and the separated components are visualized. Since most organic compounds are colourless, a UV lamp is employed for the visualisation on the plates. Furthermore, several permanent or semi-permanent methods exist which allow the determination of specific functional groups contained within the molecule. Some of TLC stains used are reported in the table below.[157]

***Table 2.2**. List of some TLC employed, compounds visualized and colours.*

TLC staining	Compounds visualized	Colours
UV-light	Compounds with extended conjugation	Pink on light green background
Ninhydrin	Amino acids, amines	Purple or yellow (2° amine)
Bromocresol Green	Carboxylic acids (pK_a<5)	Yellow spot-on blue background
Iodine	Unsaturated and aromatic compounds	Brown spots
Curcumin[158]	Boronic acid compounds	Red spots

2.2.4 Liquid chromatography (LC) and high-performance liquid chromatography (HPLC)

LC and HPLC are chromatography techniques employed for the separation of complex mixtures.[159] LC relies on gravity for the passage of the mobile phase through the column, while HPLC represents an advanced type of LC, by operating at a higher pressure range of 50-350 bar. The separation is achieved by the different affinities of analytes towards the stationary and mobile phase. Each component is adsorbed and desorbed differentially into the stationary phase, and

eluted through a change of the solvent, composing the mobile phase. Reverse phase chromatography involves a hydrophobic stationary phase (as standard C18 columns) and a polar mobile phase, or eluent, passing through the column. The common eluent involves a gradient or isocratic mixture of water, acetonitrile (MeCN) or methanol (MeOH). Small amounts of acetic acid, formic acid, ammonium hydroxide/ammonia solution, or ammonium acetate can also be used in the mobile phase, to promote the separation and enhance peak resolution.[160] Upon mixture loading into the column, the components are separated depending on their affinities into stationary phase versus mobile phase. Because of the low polarity of the stationary phase, apolar components show higher affinity compared to the polar solvent and they are retained in the column. Depending on the degree of affinity, the components of the mixture are eluted out of the column at specific times (retention time). Longer retention times (RT) are synonymous with apolar elements while polar elements have shorter retention times. Compounds are determined based on their retention time in the column in a graph called a "chromatogram", versus the method used for detection: mass spectrometry, refractive index, UV detector, etc. HPLC can be distinguished between analytical and preparative type depending on the main purpose. Analytic HPLC aims to separate the components of a sample and is used for qualitative and quantitative analysis. Alternatively, HPLC preparative is employed to isolate and purify a specific substance from a mixture. Analytic HPLC can be employed to determinate the conditions of separation, to be applied for preparative HPLC.[161]

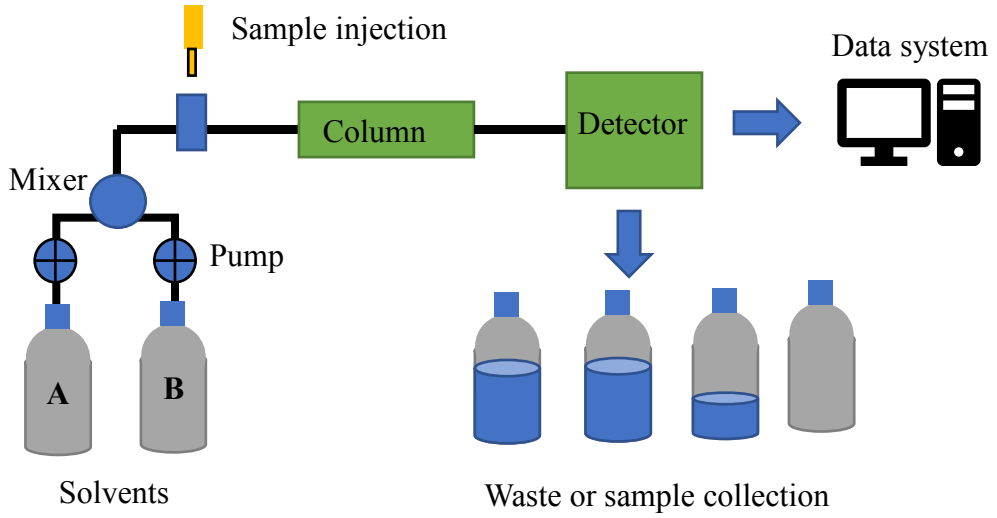


Figure 2.3. *Schematic representation of HPLC.*

2.2.5 Liquid chromatography-mass spectrometry

Liquid chromatography-mass spectrometry (LC-MS) is an analytical technique for the analysis of liquid mixtures. As it can be applied for the analysis of large, polar, ionic, thermally unstable and involatile compounds, it finds application in the analysis of biological samples and is widely employed in organic chemistry as an analysis and purification tool. LC-MS combines the resolving power of HPLC and the detection specificity of mass spectrometry (MS). Following chromatographic separations by HPLC, compounds elute off the column, de-solvated into the gas phase, ionized, and then introduced into the MS instrument for mass analysis. Among the possible ionization methods, ESI is widely employed, being an atmospheric pressure process and thus easy to use and interact with HPLC and LC separation.[20]

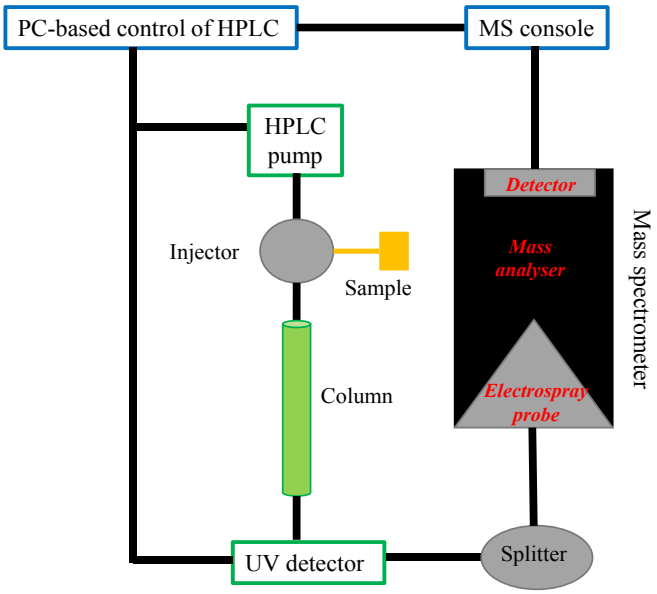


***Figure 2.4**. Schematic representation of LC-MS.*

LC-MS provides the molecular weight and structural information of the compounds after the separation by LC, allowing for the identification and quantification of sample components. More information can be achieved using MS in combination with other LC detectors. Diode array detector acquires data on selected ultraviolet (UV) and visible (Vis) wavelengths and spectra. The use of both a UV detector and mass selective detector allow to employ the two sets of data simultaneously to identify and quantify the compounds. MS detector can be used with non-UV responsive analytes while UV-diode array detection (DAD) helps to identify the presence of non-ionizable compounds. [162]

2.3 Solid substrate analysis and characterization

2.3.1 Contact angle

Contact angle measures the wettability of a surface by a liquid. It is defined by the angle measured at the three-phase interface between air, a liquid drop and a solid (Figure 2.5).

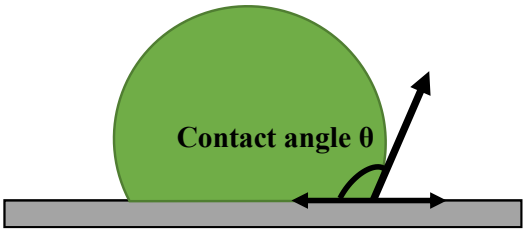


Figure 2.5. *Schematic representation of contact angle.*

Contact angle is used for the determination of hydrophobicity/ hydrophilicity of a surface, through the strength of interaction between a liquid and a solid. Different solvents can be used for this purpose, but water is the most common. As shown in Figure 2.6 (left) the surface of a solid is considered to be hydrophilic, with strong interactions with an aqueous solution, when the contact angle θ is close to zero. On the other hand, a hydrophobic surface results in higher contact angles than 90° for similar droplets (Figure 2.6 right).[163, 164]

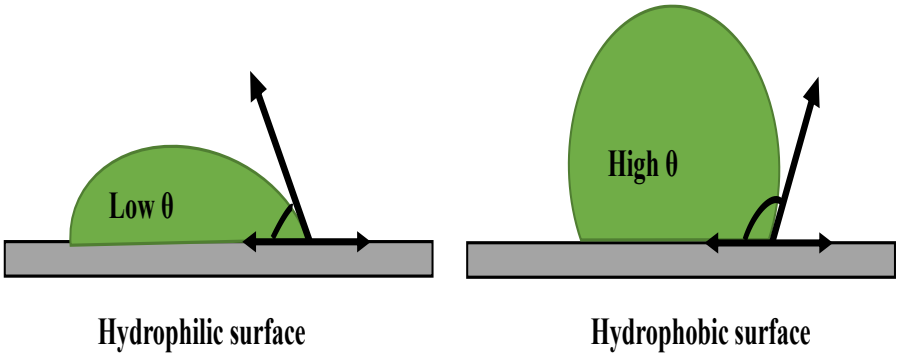


Figure 2.6. *Contact angle schematic representation of hydrophilic(left) and hydrophobic (right).*

The measurements are conducted by a tensiometer that works via dynamic physical force or optical measurements. The first employs the variation in weight when the solid interacts with a liquid, while optical tensiometry measures the shape of the droplet on a surface over time. The contact angle can be recorded statically by placing a liquid droplet on the sample surface and measuring the angle (the static sessile drop method) or dynamically by measuring the angle while increasing

or decreasing the droplet volume (the dynamic sessile drop method). The advancing and receding angles are therefore calculated while increasing and decreasing the droplet volume, respectively (Figure 2.7). The difference between these angles gives the hysteresis which indicates the roughness, smoothness and quality of the self-assembled monolayer formed at the investigated surface.[165]

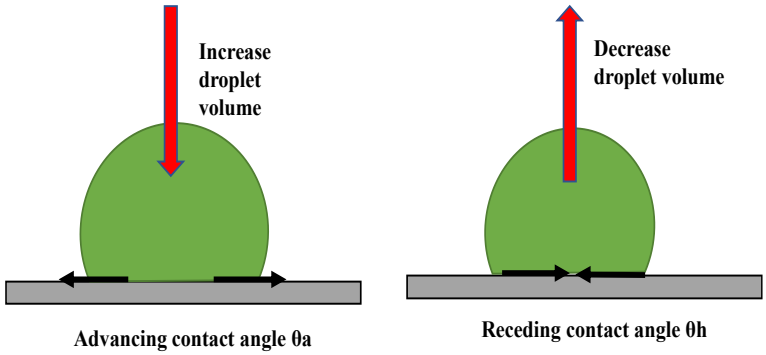


Figure 2.7*. Dynamic contact angle analysis which measures advancing contact angle θa (right) and receding contact angle θh (left).*

2.3.2 Ellipsometry

Ellipsometry is a very sensitive, non-destructive technique used to characterize optical properties of surfaces, as well as film thickness. The characterization of surfaces, interfaces and thin films is possible by analysing the change in a polarized light beam upon reflection at an oblique angle in respect to the sample. Ellipsometry measures the phase shift (Δ) and the amplitude component (Ψ) of the reflected light. A light source produces a light that is polarized by the polarization generator, which allows the passage of light with a specific electric field. The orientation of the generator permits parallel waves to incise perpendicularly to the plane of incidence of the sample. Upon reflection, the linearly polarized light becomes elliptically polarized and can be reflected into the polarization analyser and the detector. The detector then converts the reflected light into an

electronic signal, generating ellipsometry parameters. Models representing the sample are constructed by a computer software. By using regression analysis, the experimental data are fitted to the computed values. The thickness of the self-assembled monolayer is found by the best fit, in which experimental curves overlap with the modelled ones. [166, 167]

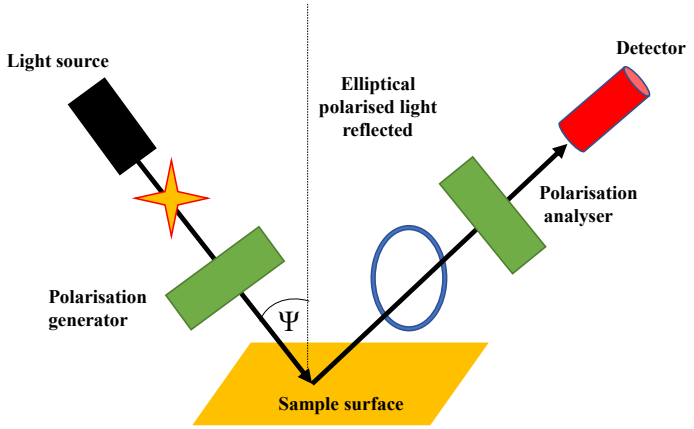


Figure 2.8. *Schematic representation of an ellipsometry experiment.*

2.3.3 Dynamic light scattering (DLS)

DLS is a technique for measuring the size of particles typically in the sub-micron region. It is based on the Brownian motion of dispersed particles, that assumes that they are constantly colliding with solvent molecules. The particles' movement and speed are derived from the collisions and is dependent on their diameter, with smaller particles moving at higher speeds than those that are larger. In this way, it is possible to calculate the hydrodynamic diameter by measuring the speed of particles, knowing the other parameters that influence particle movement. The Stokes-Einstein equation describes mathematically the relationship between the size of a particle to its translational diffusion coefficient, that measures its speed in the solvent:

$$d(H) = \frac{kT}{3\pi\eta D} \qquad \text{Equation 2-1}$$

Where d(H) is the hydrodynamic diameter, D is the translation diffusion coefficient, k is the Boltzmann constant, T and η are respectively temperature and viscosity of the liquid. To obtain the diffusion coefficient, a sample in a cuvette is exposed to a light, originated by a single frequency laser, that is scattered in all directions if particles are present. The scatter light is recorded at a fixed angle over time (Figure 2.9). The variation in intensity of the signal allows the determination of the diffusion coefficient and, by using the previous equation, the particle sizes present in the samples.

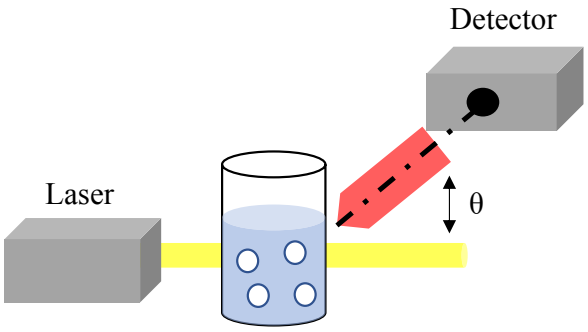


Figure 2.9. *Schematic representation of DLS instrument.*

The movement of the particles is monitored by the collection of scattered light, that is not constant, over a certain time. Due to the higher speed, small particles show faster fluctuation. In contrast, larger particles result in higher amplitude between maximum and minimum scattering intensity (Figure 2.10a). The range of DLS size determination is defined by the nature of the measured fluctuation that needs to be only based on Brownian motion. For example, particles which are too large can sediment causing incorrect estimations, while particles which are too small do not scatter much, leading an insufficient measurement signal. If everything is correct, the measurement should look like an irregular wave that shows the scattered light by unit of time, then it is transformed into a decay function known as the correlation function (G2). From this point the onset of decay can be calculated, meaning the average time that the particles need to change their position. Small

particles move quickly, so the decay is fast. Larger particles move more slowly and therefore the decay of the correlation function is delayed (Figure 2.10b). The delay time is proportional to the diffusion coefficient. From the fitting of the delay time, the polydispersity index (PDI) can also be obtained, and it describes the broadness of the particle size distribution. A particle size distribution chart can also be obtained, relative intensity of light scattered versus various size ranges, which gives more information about different sized populations within the sample (Figure 2.10c). Since the scattering intensity become exponentially proportional to particle size, the intensity function of distribution can be expressed also as a volume or number-dependant. The distribution in function of volume or number is more suitable for smaller particles in which the intensity of scattering is lower.[168]

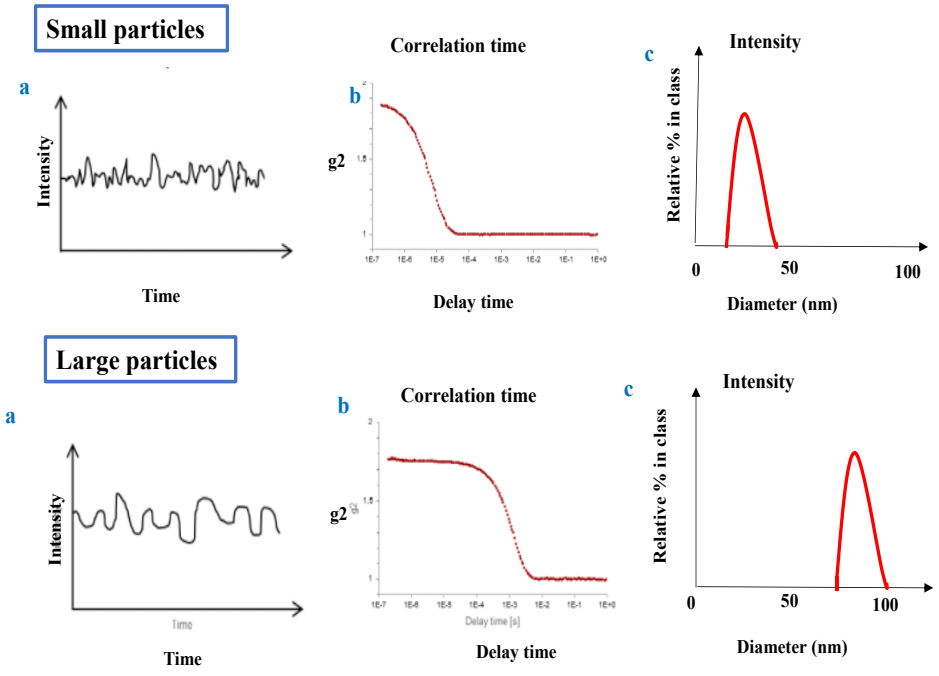


Figure 2.10. *Comparison between small (up) and large particles (down). Intensity vs time (**a**), correlation function versus delay time (**b**). Particle size distribution-based intensity (**c**).*

2.3.4 Zeta potential

Zeta potential is the charge developed at the interface between a particle surface and the liquid medium. This property gives information about functionality and stability of the particle. The functional groups on a particle surface react with the medium where it is dispersed, resulting in a surface charge and the accumulation, through electrostatic attraction, of oppositely charged ions. The attracted ions form two different layers called the Stern and diffuse layer which differ by the strength of the bond; relatively strong for the Stern layer and loosely bound for the diffuse layer. The Zeta potential is defined as the voltage in proximity of the diffuse layer where it meets the surrounding liquid, known as the slipping plane (Figure 2.11).

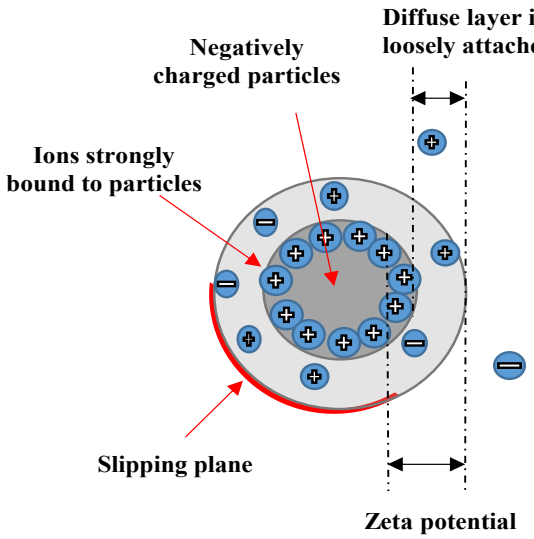


Figure 2.11. *Schematic representation of electrical double layer and zeta potential.*

Nanoparticles with low charge could lead to sedimentation followed by flocculation and conjugation due to the lack of repulsive forces. In contrast, two particles with high zeta potential at opposite signs do not agglomerate due to the repulsive electrostatic forces. Zeta potential is commonly measured by electrophoretic light scattering (ELS), employing the mobility of particles

under the application of an electric field generated by a laser crossing the sample. A special capillary cell with two electrodes is used (Figure 2.12), allowing the application of a voltage to the liquid sample inside the cell. The charged particles move though the medium at different rates which is measured through light scattering and is proportional to the zeta potential. It is higher for particles which moves faster and low for particles with a slow rate of movement.[169]

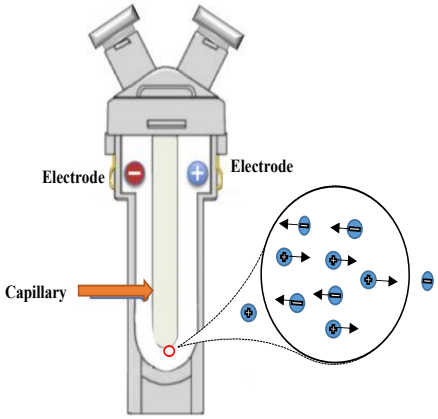


Figure 2.12. *Capillary cuvette (cell) used for the measurement of zeta potential.*

The laser light crosses the sample, generating a frequency shift of scattered light. It is employed to measure the speed of particles and converted into a value of electrophoretic mobility. Knowing solvent dielectric constant (ε), viscosity (η) and other constants, zeta potential ζ is calculated from electrophoretic mobility U_E using the Henry Equation.[170]

$$U_E = \frac{2\varepsilon\zeta}{3\eta} f(Ka) \qquad \text{Equation 2-2}$$

2.3.5 Thermogravimetric analysis (TGA)

Thermogravimetric analysis (TGA) is a technique in which the mass of a sample is monitored over time, as temperature increases slowly. It is commonly used as a characterization method for inorganic material containing organic matter. TGA can be used to determine the

composition/purity of a sample by measuring the mass loss, due to the organic material burning, as a function of temperature. Furthermore, it can also be employed to evaluate thermal stability or chemical decomposition of specific materials. A TGA instrument involves a precision balance contained into a furnace. A sample pan is introduced, following a purge with an inert gas, that controls the environment prior to heating. The data are plotted as residual weight versus temperature, as shown in Figure 2.13.[171]

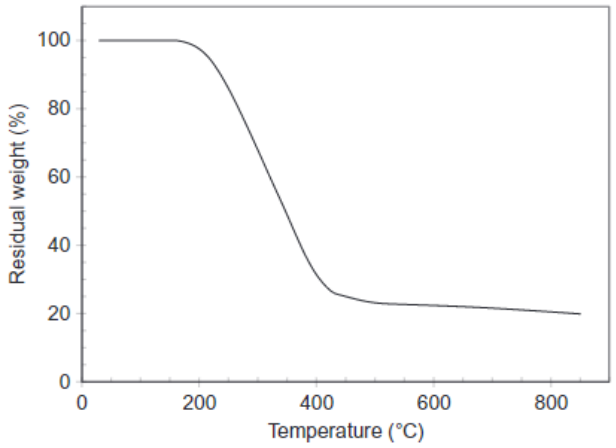


Figure 2.13. *Example of thermal curve by TGA.*

CHAPTER 3: ASSESSMENT OF SEVERAL BORONIC-BASED FLUORESCENCE SYSTEMS

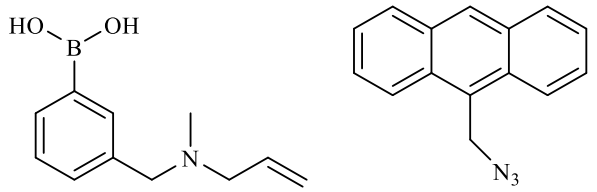
This chapter describes the first sensing systems investigated for saccharides detection. The design, structure and fluorescence experiments are included.

3.1 PET fluorescent sensing system based on phenylboronic acid and anthracene

The first sensing system consisted of two single units: phenylboronic acid as a receptor and an anthracene dye as a fluorophore. The employment of single units allowed them to act independently of each other. The anthracene fluorescence would be modulated by a PET (Photoinduced electron transfer) mechanism upon sugar binding to phenylboronic receptor. Phenyl boronic acid (PBA) with an amino group was demonstrated to promote the interaction with saccharides at a suitable pH (section 1.4.1). Anthracene probe was also selected because it is widely used as a probe in fluorescence applications due its commercial availability, photophysical property and handling ease.[172] Fluorescence-based PET was employed as the transducer mechanism due to its relative ease of implementation (Section 1.5.1). Both units would be immobilised together into solid support, that was supposed to promote the interaction, reducing the distance between each other (2-3 nm). Similarly to the (2-(((anthracen-9-ylmethyl) (methyl)amino) methyl) phenyl) boronic acid sensor reported in the literature,[173] the system aims to provide an efficient fluorescence response following saccharide binding.

The fluorescence sensing system selected is composed of (3-((allyl (methyl) amino) methyl) phenyl) boronic acid **1**, acting as receptor and 9-(azidomethyl) anthracene **2**, as fluorophore unit. Differently compared to the system reported in literature [173] , BA derivative with amino group

in *meta* was selected over *ortho* position. It was expected a similar behaviour of boronic acid unit, despite different position. A comparable fluorescence property of meta substituted BA boronic acid derivatives towards sugar detection has been verified.[174] Moreover, it was predicted that the position could facilitate sugar binding once into solid substrate, via reducing steric effect.



1 **2**

Figure 3.1. *Chemical structures of (3-((allyl(methyl)amino) methyl) phenyl) boronic acid **1**; 9-(azido methyl) anthracene **2**.*

As described in section 1.4.1, the binding of sugar by boronic acid **1** is potentially promoted through the formation of hybridized borate anions using a basic environment. The fluorescence of anthracene was theoretically quenched through a PET mechanism, by the nitrogen electron pair belonging to boronic acid that acts as donor to excited fluorophore. The binding between BA moiety and sugar is predicted to reduce the quenching effect, by strengthening the N-B interaction restoring the fluorescence of the dye and thus displaying the desired fluorescence response (Figure 3.2).[121] The designed system aims to enhance the sensitivity, generating the desirable fluorescence response only upon the binding of a specific sugar.

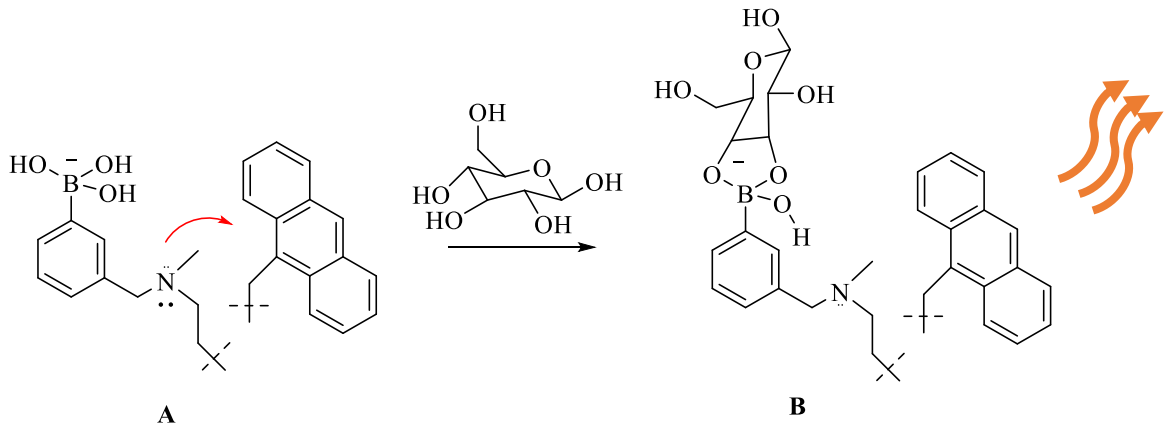


Figure 3.2. *A) Supposed PET mechanism between BA (**1**) towards anthracene dye (**2**) B) Sugar binding followed by suppression of PET and re-establishing of anthracene fluorescence.*

The approach aims to immobilise the fluorescence sensing system components onto SiO_2 surface, selected as a solid support. Thus, both structures of **1** and **2** have been modified to enable further reaction onto the surface by radical addition[100] by an alkene group in **1** and copper (I)-catalysed azide-alkyne cycloaddition (CuAAC) by an azide group in **2** (Figure 3.1).[175]

As shown in Figure 3.3 the strategy provided the deposition onto the surface of the two units **1** and **2**, occurring through reaction with a suitable terminal group of N-acrylamido-4-oxo-4-(prop-2-yn-1-ylamino) butanoic acid. It acted as a spacer between the fluorescence system components and the surface, previously functionalized with amino groups, through SAM formation (section 1.6.1).

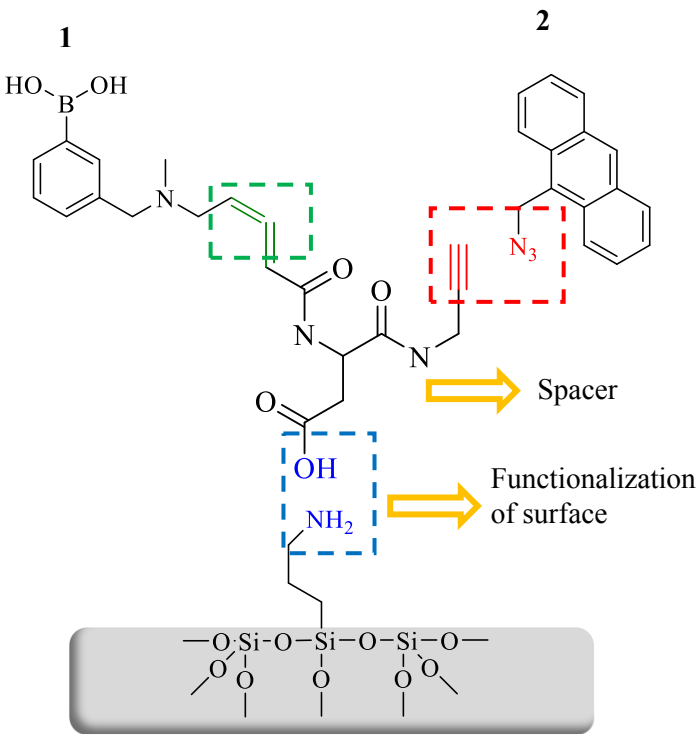


Figure 3.3. *Schematic representation of the two units involved **1** and **2**, spacer with suitable terminal group. Incorporation into the surface functionalized.*

3.2 Fluorescence-based sensing system: design and fluorescence experiments

The proposed fluorescence sensing system was composed of **1** and **2**, as reported in Figure 3.1 which were expected to interact through a PET process between the amino groups of **1** and the fluorophore **2**.

1 was synthesized starting from PBA derivative with bromomethyl group in *meta* position and N-allylmethylamine **4** (Figure 3.4). The reaction was conducted in dimethyl sulfoxide (DMSO) at 60 °C and promoted by triethylamine as base. **2** was previously synthesized by the research group through reaction of 9-(chloromethyl) anthracene with sodium azide (NaN_3).[176]

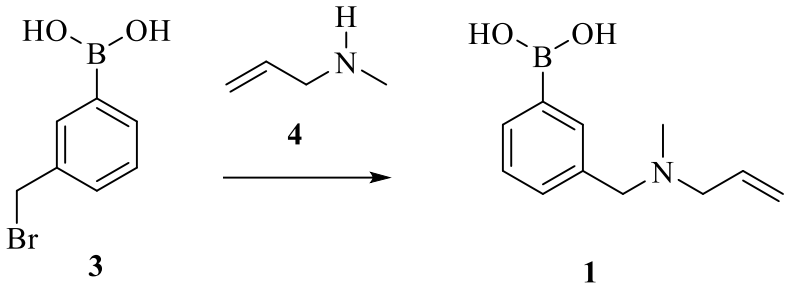


Figure 3.4. *Synthesis scheme of **1**.*

Preliminary studies were performed to assess the quenching of the unlinked compounds. First, solutions of **2** at different concentrations (0.01 to 2 µM) were analysed to evaluate the concentration-dependent fluorescence intensities, the solubility of the fluorophore in aqueous solution and the optimal concentration for further experiments (Figure 3.5).

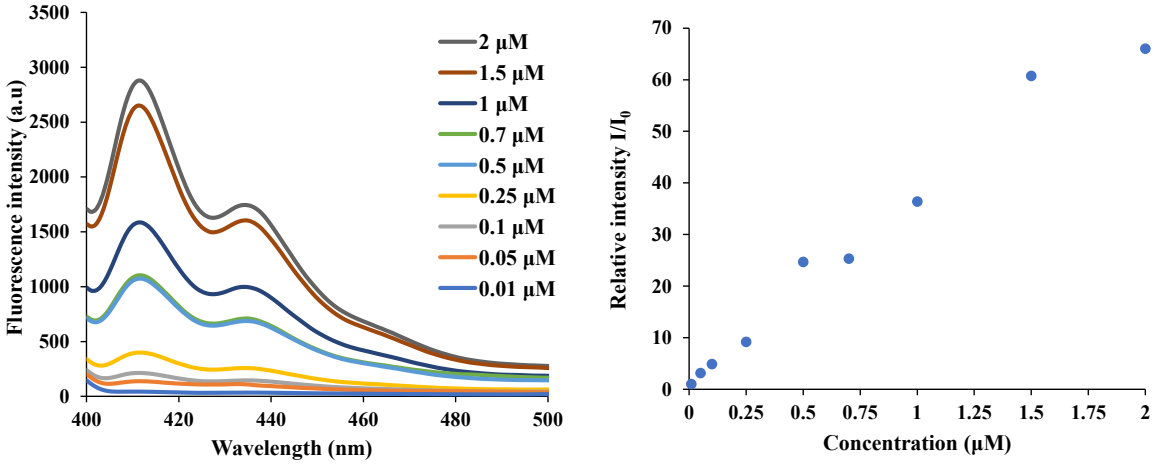


Figure 3.5. *Fluorescence spectra of **2** at different concentrations in water (λ_{ex} 350 nm). Relative intensity vs concentration at λ_{em} 412 nm.*

A concentration of **2** around 0.5 µM was selected as reference concentration to evaluate the behaviour of dye with **3**. Moreover,, since the formation of excimer is determined by excitation and concentration of the fluorophore, being a complex between two same species, higher

concentration could favour the process.[177] Experiments mixing **2** with **1** (0.01; 0.1; 1; 10; 100 µM) in water are shown in Figure 3.6. Preliminary results showed an increase (177 %). in fluorescence intensity upon the addition of **1**.

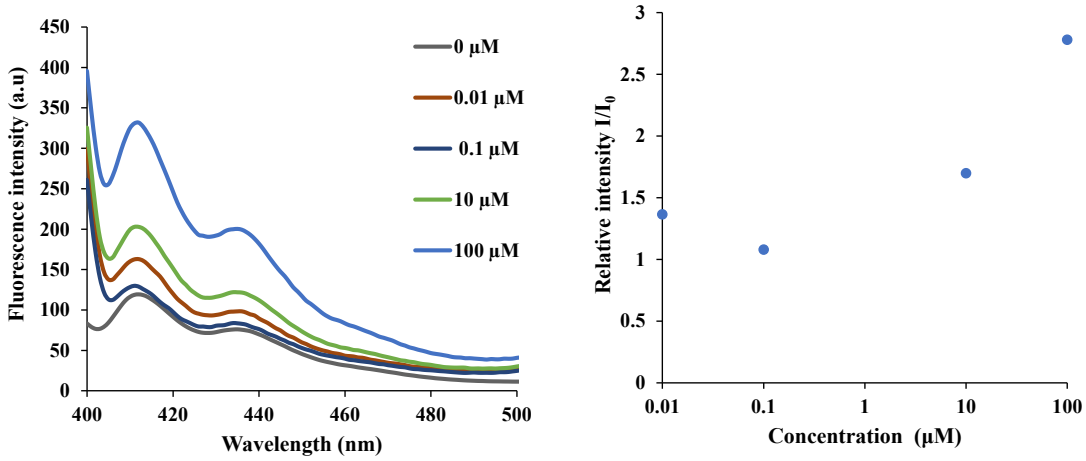


Figure 3.6. *Fluorescence spectra of **2** (0.5 µM) with **1** and different concentrations in water (λ_{ex} 350 nm). Relative intensity vs concentration at λ 412 nm.*

At low concentration of **2**, it was observed a slight decrease of fluorescence. However, by increasing the concentration of **2**, it is possible to notice the increase of fluorescence. These preliminary results suggested the absence of a quenching effect from **1** versus anthracene. Experiments between **2** and a pyridinium chloride **5** were performed to evaluate the quenching effect on the fluorescence of the dye. Despite the structure of **5** differs compared to the units **2**, the aim was evaluated the effect of nitrogen group towards fluorescence of dye. Moreover, **5** is reported in literature as quencher towards fluorescence of anthracene, thus it was considered suitable to observe the establishment of quenching or not. [178] Pyridinium chloride **5** was prepared by mixing pyridine and hydrochloric acid. Measurements of **2** at 10 µM in the presence of pyridinium chloride **5** (2.5; 12.5; 25; 37.5; 50 mM) in ethanol (EtOH) were conducted.

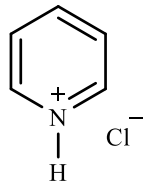


Figure 3.7. *Chemical structure of pyridinium chloride* ***5****.*

Since both fluorophore and quencher move freely in solution, quenching of fluorescence is thought through a collisional mechanism. As shown in Figure 3.8, the fluorescence intensity decreases when **5** concentration increases, showing the pyridinium molecules act as a quencher.

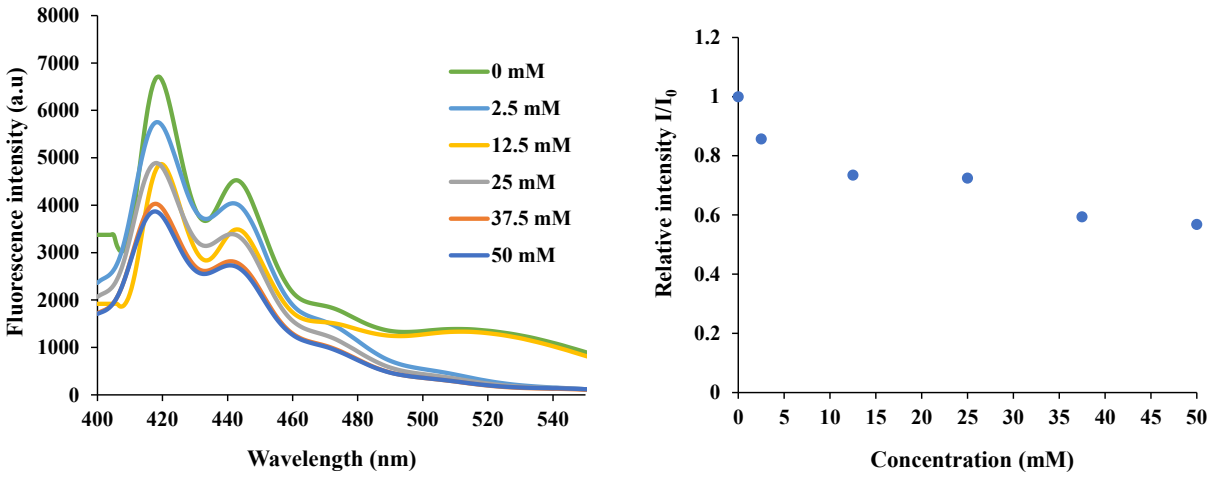


Figure 3.8. *Fluorescence spectra of* ***2*** *(10 μM) with* ***5*** *at different concentrations in EtOH (*λ_{ex} *350 nm). Relative intensity vs concentration at λ 420 nm.*

The formation of an emission band at 520 nm was observed from concentration at 12.5 mM. It was supposed the formation of an excimer. To ensure that the fluorescence response observed were not influenced by the solvent EtOH, experiments with **2** and **5** were repeated in aqueous solution.

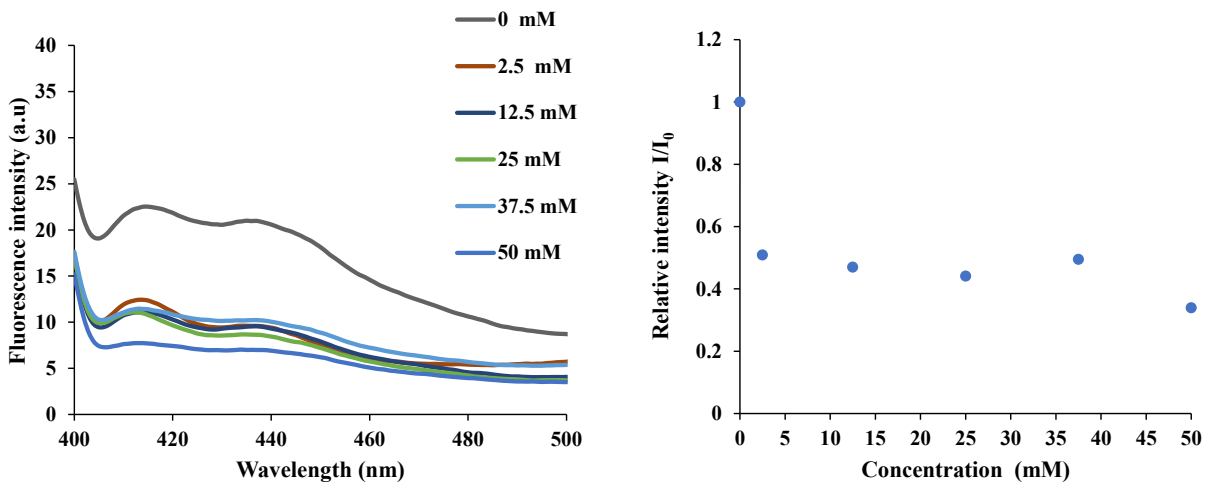


Figure 3.9. *Fluorescence spectra of* ***2*** *(10 μM) with* ***5*** *at different concentrations in water (λ_{ex} 350 nm). Relative intensity vs concentration at λ 412 nm.*

Although at higher concentrations of **5** the decrease in fluorescence intensity was less marked compared to previous results, steep decrease in fluorescence intensity was observed in the presence of **5** suggesting that quenching had occurred (Figure 3.9). One reason of broad peak observed was attributed to some effect by solvent on fluorescence, such as Raman scattering.

It was hypothesized that the combination of a high concentration of quencher and solvent could have a role in the fluorescence quenching process. Thus, new experiments of **2** with **1** at the same concentration and solvent used in the previous experiment were conducted. However, the expected quenching effect was not observed. Instead, a fluorescence intensity increase was seen, as reported in Figure 3.10.

The lower fluorescence intensity of **2** at 10 μM compared to previous experiments could be attributed to the presence of **5** and its lower solubility to compare to **1**. It was believed that the also **2** contributed to the overall fluorescence intensity. To confirm and for control purposes, fluorescence spectra of **1** solution in water (2.5; 12.5; 25; 37.5; 50 mM) and EtOH (5; 25; 75; 100

mM) were recorded. An emission peak at a wavelength that overlaps with one characteristic peak of the anthracene probe (λ_{em} 450 nm) was observed. The fluorescence intensity was higher in EtOH than in water, confirming the hypothesis that the choice of solvent influences the fluorescence response of **1** (Figure 3.11).

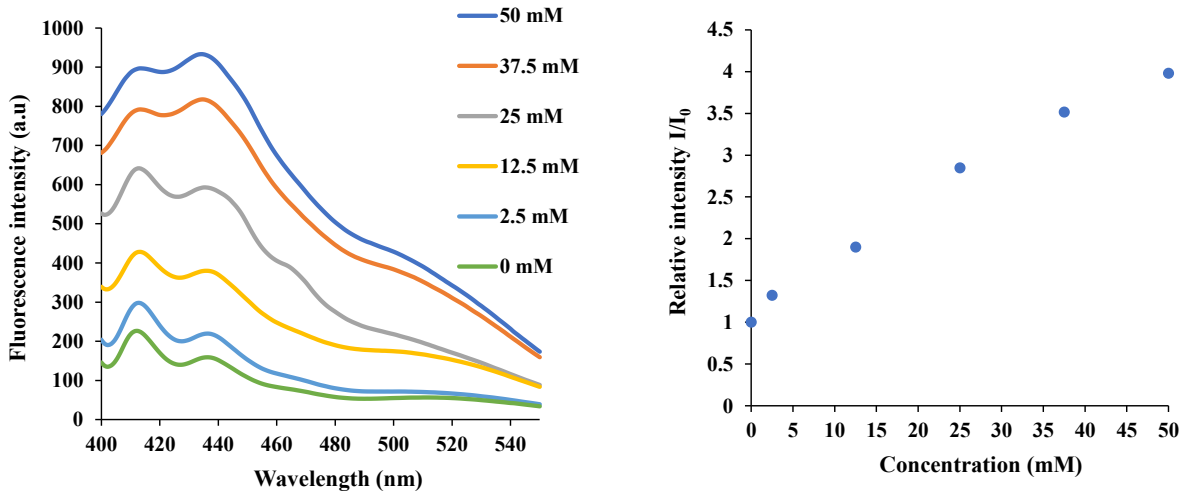


Figure 3.10. *Fluorescence spectra of* ***2*** *(10 μM) with* ***1*** *at different concentrations in water (λ_{ex} 350 nm). Relative intensity vs concentration at λ 412 nm.*

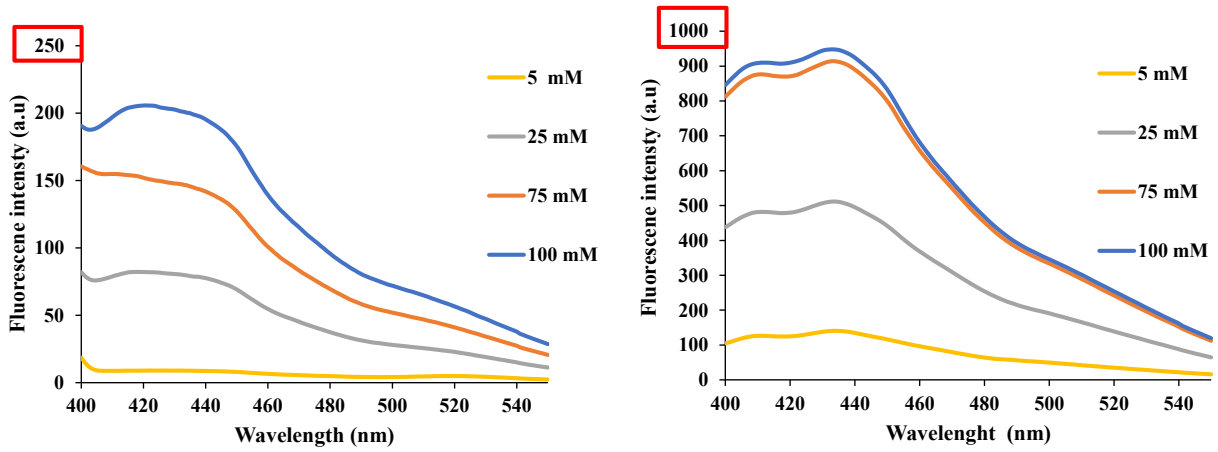


Figure 3.11. *Fluorescence spectra of* ***1*** *at different concentrations in water (left) and EtOH (right) (λ_{ex} 350 nm). The higher values of the fluorescence intensity axis are red labelled.*

The experiments were also performed in aqueous 0.1 M sodium dodecyl sulfate (SDS) solution to evaluate the effect of surfactants on fluorescence intensity. Spectra reported in Figure 3.12, show an opposing trend to that expected. The fluorescence intensity increases with increasing concentrations of **1**.

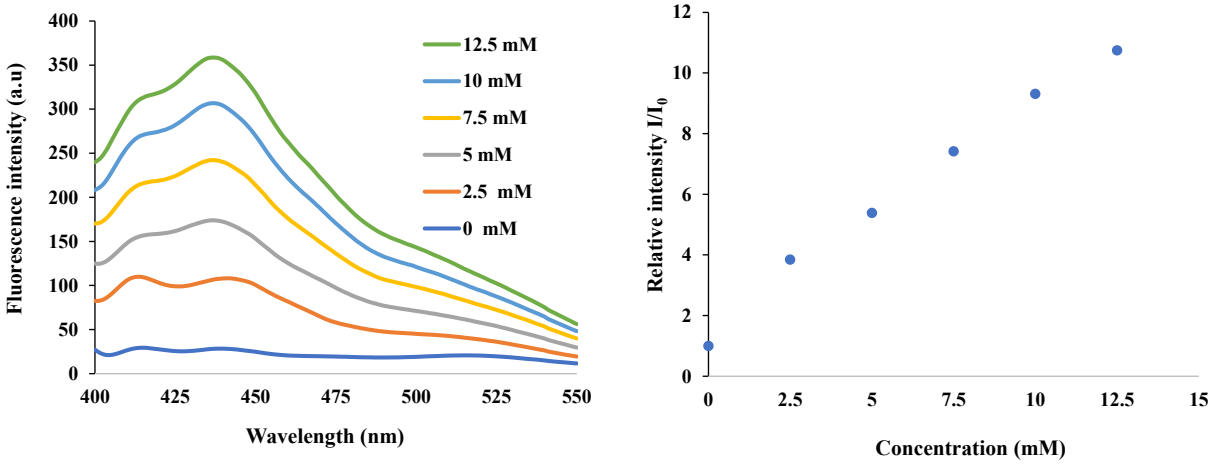


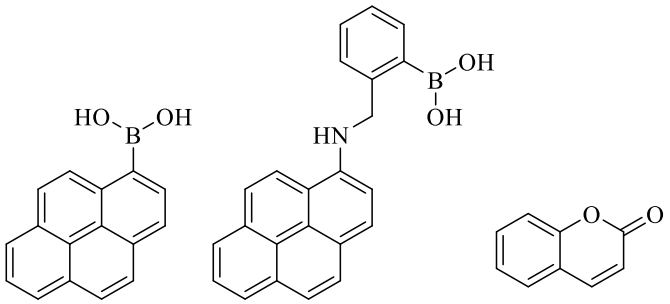
Figure 3.12. *Fluorescence spectra of* ***2*** *(1 μM) with* ***1*** *at different concentrations in an aqueous SDS (0.1 M) solution (λ_{ex} 350 nm). Relative intensity vs concentration at λ 440 nm.*

The fluorescence spectra of **2** displayed a fluorescence intensity enhancement as the concentration of **1** increased, increasing the overall fluorescence signal in the system. The proposed fluorescent system was supposed to work through a quenching PET mechanism, following suppressed by addition of sugars. However, it was verified that **1** did not quench the fluorescence of **2** in the condition tested. Instead, an enhancement of fluorescence response was observed, suggesting that the boronic acid does not quench the fluorophore. Different theories, controversial and still under investigation have been developed to explain the fluorescence mechanism of the sensor. [125] Thus, it was concluded that the fluorescent system's structure required changes to improve the interaction between the two units. However, further step has to involve experiments with sensors units incorporated into the surface, which could improve their interaction. The aim was achieving a

fluorescence response upon saccharides binding, modulated by a mechanism independent of solvent condition employed. The first step of sensor involved is to test fluorescence performance in solution, to ensure that the sensing is not affect by matrix factors.

3.3 FRET fluorescent sensing system: pyrene boronic-acid based sensor and coumarin probe

Since the first system proved unsuccessful, an alternative approach aimed to design a fluorescence sensing system by boronic acid as receptor unit included in the structure of fluorophore. Pyrene was selected as the fluorophore unit, owing to its higher fluorescence quantum yield (0.69) compared to the anthracene (0.31) probe previously used.[179, 180]. The interaction of two units was investigated by direct incorporation of boronic-acid moiety into the structure of the fluorophore through covalent bond formation (sensor **6**) or through an alkyl chain with an amino group as a linker (sensor **7**). To explore also alternative fluorescence mechanism to PET, FRET was proposed due to its wide use in sensing [80] and surface applications. Indeed, it can occur at longer distances (10-100 Å) compared to PET.[178] The final fluorescence signal was aimed to be achieved through interaction between a pyrene boronic acid-based sensor and a coumarin probe, enabling FRET process. The designed sensors acted as a donor while the coumarin as an acceptor, according to the photophysical properties of the pyrene dye. Coumarin (**9**) was selected for the preliminary experiments due to the numerous examples of FRET couples involving coumarin and pyrene found in the literature. [133, 181-183] Figure 3.13 reports the structure of the components of the system, forming the second sensing system.



6 **7** **9**

Figure 3.13. *Structure of pyrene based boronic-acid sensors (sensors **6** and 7) and coumarin probe **9**.*

The designed sensors differed by their connection with boronic acid unit and for the fluorescence mechanism involved that enable the interaction with the acceptor probe. Saccharide binding was expected to cause a change of fluorescence emission of pyrene. It was projected the establishment of FRET mechanism occurs upon the change of fluorescence emission of sensor (donor) such as significative increase or shift to interact with coumarin probe. This fluorescence change will enable interaction with the acceptor probe, allowing a suitable overlap with its adsorption band to provide the sensing signal by FRET mechanism. The establishment of FRET process was projected to improve the fluorescence response. Indeed, it was aimed to heighten the fluorescence performance of the system by optimising the concentration and ratios of the units involved. Further steps involve the incorporation of each unit into selected surface.

Sensor **6** aimed to establish FRET mechanism through fluorescence increase upon saccharides binding, providing the desired signal (Figure 3.14).

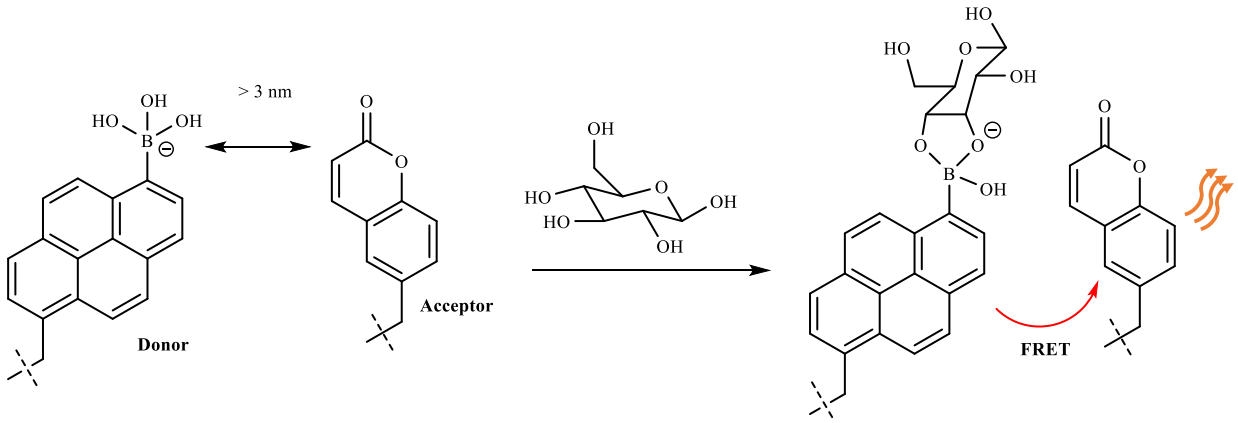


***Figure 3.14**. Scheme of mechanism involving sensor **6**: interaction between donor **6** and acceptor probe **9** provides a fluorescence signal by FRET mechanism following saccharide binding.*

Alternatively, a different mechanism where the BA moiety was incorporated through a linker on the structure of sensor **7** was also investigated. The direct connection of amine of the fluorophore was supposed to bring a spectral change upon saccharide binding. The expected shift of emission band of sensor is to attribute to a change of environment of nitrogen, leading a change of its energy levels. As consequence the fluorescence of dye connected is also affected. This dipole moment change between the units of sensor allows the ICT mechanism to occur. It was expected that the binding of saccharides causes a shift of fluorescence emission of the pyrene through an ICT mechanism (Figure 3.15a). The fluorescence change achieved of sensor **7** (donor) enables the establishment of FRET by interaction with coumarin probe (Figure 3.15b).

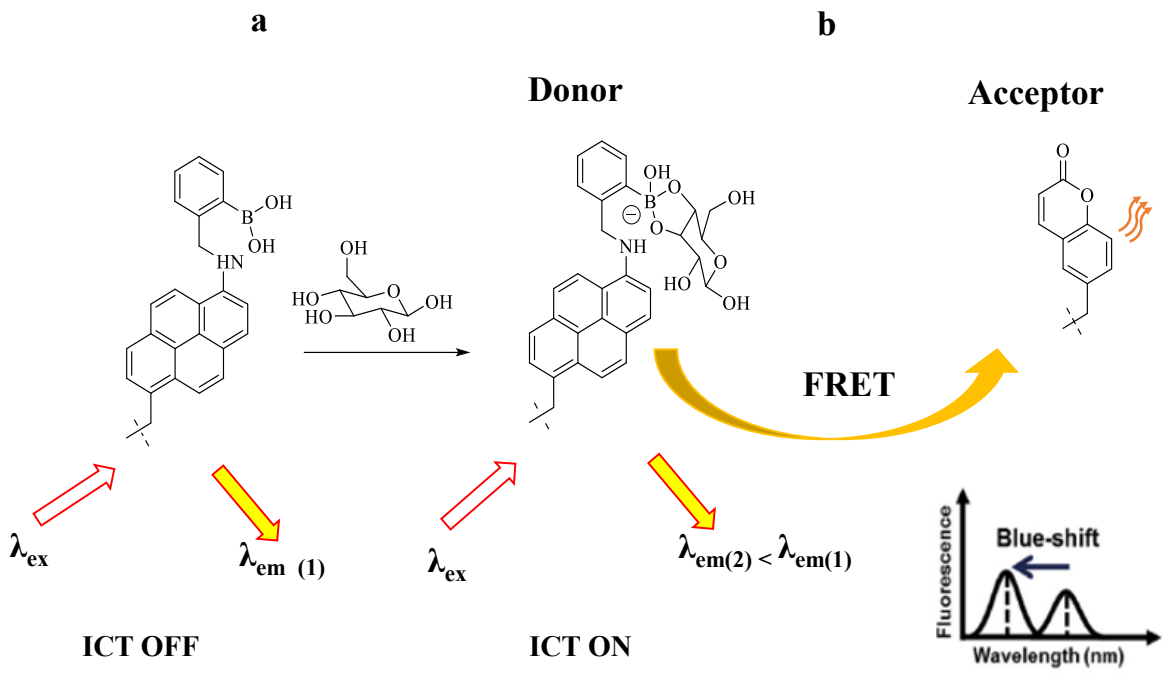


Figure 3.15. *Scheme of mechanism involving sensor **7**: interaction between sensor **7** and saccharides bring the establishments of ICT (a). The process enables the interaction between sensor **7** acting as donor and acceptor probe **9** and provides a fluorescence signal by FRET mechanism (b).*

As FRET can be used on surfaces, the functionalisation of the structure of the acceptor and donor to allow immobilisation onto the surface must also be considered. FRET has been found to be established on the surface of silica nanoparticles.[114] Moreover their stability, recyclability and biocompatibility provide advantages over the silicon wafers employed in the previous chapter, and render them a suitable alternative solid support. [184]

3.3.1 Sensor **6**: fluorescence experiments

Based on a reported system for detection of catecholamines, commercial pyrene-1-boronic acid (PBA) **6** was selected as the first candidate to induce FRET with coumarin **9.** The fluorescent system designed by the group of Chaicham involved a pyrene-boronic acid as donor and coumarin

probe as acceptor in FRET couple (Figure 3.16A). A fluorescence intensity decrease of PBA and the formation of emission band at 450 nm along the addition of catecholamine (B) was noticed. Following the addition of coumarin aldehyde, they observed the fluorescence intensity decrease of PBA (donor) and the fluorescence increase of coumarin (acceptor). This has verified the establishment of the interaction between the probes and thus FRET process (C). [133]

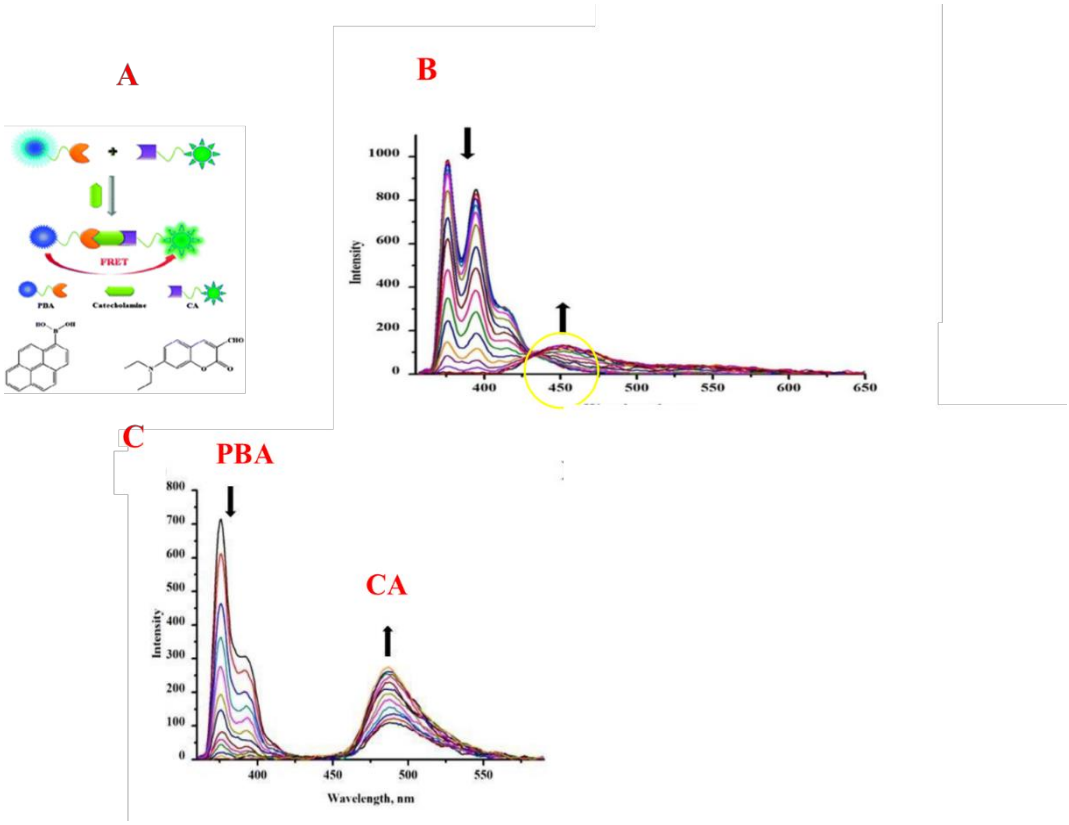
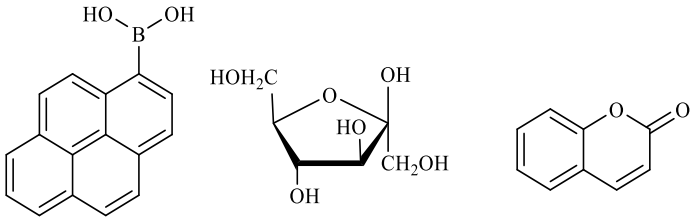


Figure 3.16. *Assembled complex for catecholamine sensing by a FRET process. Emission spectra (right) of pyrene dye as reported in literature: fluorescence intensity decrease with catecholamine addition and increase with coumarin (CA). Image adapted from reference [133].*

D-Fructose **8** was selected as a reference saccharide to evaluate the binding and sensitivity of the system.



6 **8** **9**

Figure 3.17. *Chemical structures of pyrene-1-boronic acid* ***6****; D-fructose* ***8*** *and the probe coumarin* ***9****.*

Preliminary experiments of excitation spectra of 1-Pyreneboronic acid **6** in water, according to the λ_{em} observed in the literature (380 nm),[179] were conducted to select a suitable excitation wavelength. As shown in Figure 3.18, the maximum intensity was observed at 344 nm, which was therefore selected as the optimum excitation wavelength for the next fluorescence experiments.

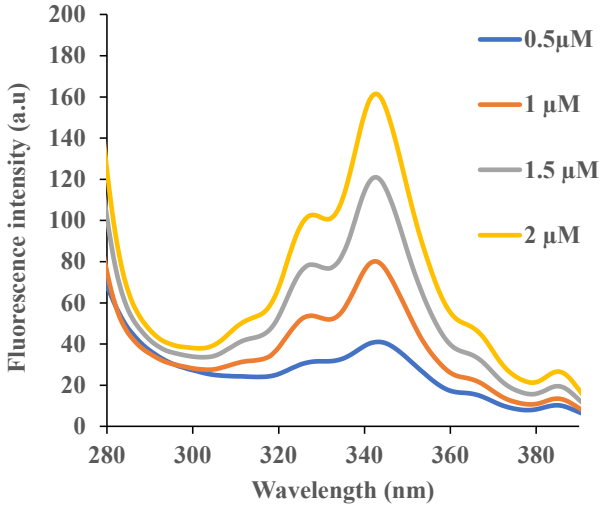


Figure 3.18. *Excitation spectra (λ_{em} 380 nm) of* ***6*** *in water at different concentration (0.5; 1; 1.5; 2 µM).*

Emission spectra of solutions of **6** at different concentrations (0.5 to 2 µM) were performed to evaluate the concentration-dependent fluorescence intensities and to determine the ideal

concentration going forward. Indeed, the excimer could form at higher concentration (1-2 µM), aligning with that seen in the literature.[15]

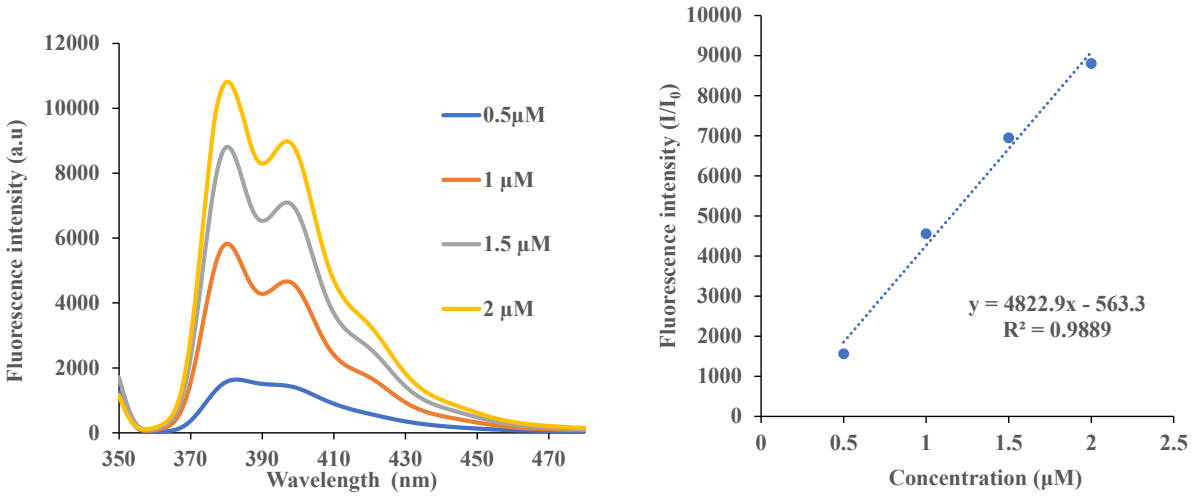


Figure 3.19. *Fluorescence spectra (λ_{ex} 344 nm) of sensor* ***6*** *in water at different concentration (left). Relative intensity versus concentration at λ 380 nm (right).*

As shown in Figure 3.19, a linear response of fluorescence intensity versus concentration was established, confirming the solubility of **6** in water. As the low fluorescence intensity observed with **6** at 0.5 µM was deemed too low, a concentration of 1 µM was considered suitable and comparable in terms of the intensity recorded. It was therefore selected as the optimal concentration. To promote the binding between PBA and D-Fructose **8**, the experiments were conducted in aqueous buffer (HEPES, 100 mM Na_2SO_3, 20 mM NaCl). Using this buffer instead of aqueous solution meant the pH could be modified.

The first experiments were conducted between 1 µM of sensor **6** in aqueous buffers solution at pH 7.4 with D-Fructose **8** (0; 1; 2; 5; 10 mM) to evaluate the effect of boronic acid moiety on **6** and its interaction with sugars. The spectra reported in Figure 3.20 (left) show a fluorescence intensity increase (193 %) of **6** by addition of **8** suggesting the establishment of an interaction between both

molecules. However, the behaviour observed was in contrast with what has been previously reported in the literature, that was a decrease of fluorescence intensity.[133] The system reported was based on PBA and the interaction with different catecholamine species. To investigate the fluorescence response of sensor **6**, further experiments were performed evaluating effect of pH, and solvent.

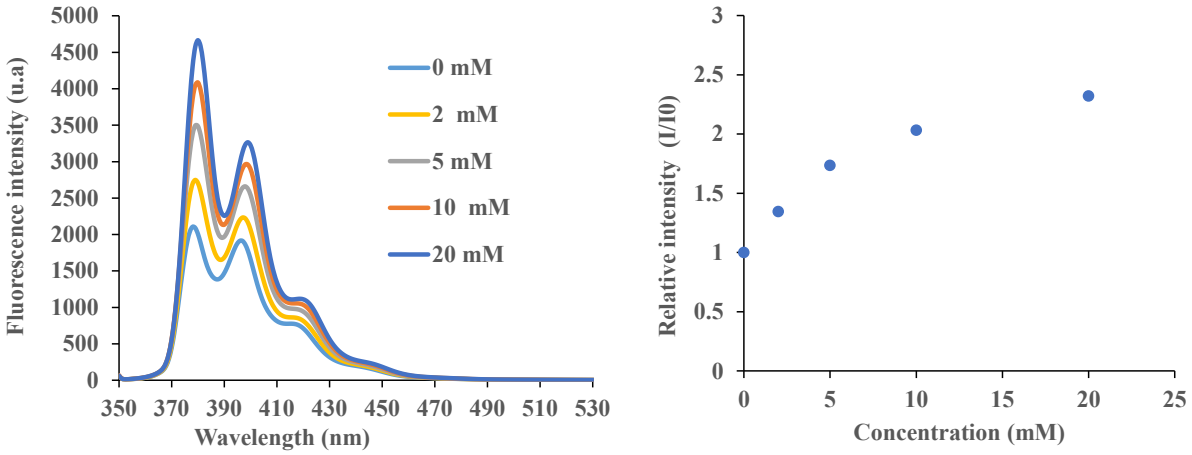


Figure 3.20. *Fluorescence spectra of* ***6*** *(1 μM) at* λ_{ex} *344 nm with* ***8*** *at different concentrations in buffer solution (100 mM* $Na_2S_2O_3$*, 50 mM HEPES, 20 mM NaCl, pH 7.4). Intensity vs concentration at λ 380 nm (right).*

The experiments were repeated in aqueous buffer solution at higher pH (≈ 9), as a stronger binding of sugars has been demonstrated in more basic medium.[185] A smaller increase in fluorescence intensity (18 %) compared to the previous results was noticed (Figure 3.21). The fluorescence response still differed from that expected from the literature. Additionally, the fluorescence response observed was less evidenced at basic pH, where higher sugar binding to the boronic acid was expected.[39]

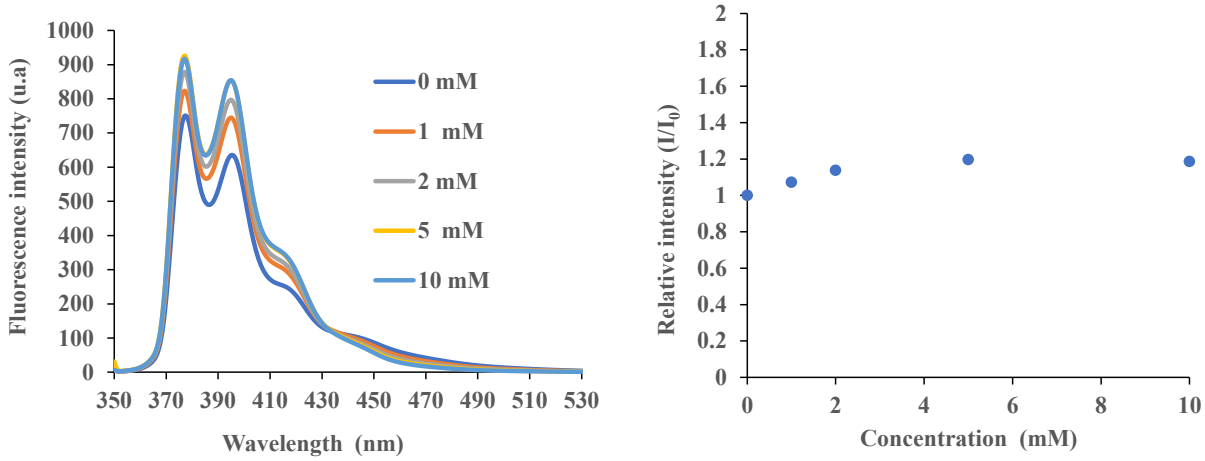


Figure 3.21. *Fluorescence spectra of* ***6*** *(1 μM) at* λ_{ex} *344 nm with* ***8*** *at different concentrations in buffer solution (100 mM* $Na_2S_2O_3$*, 50 mM HEPES, 20 mM NaCl, pH 9). Intensity vs concentration at λ 380 nm (right).*

The experiments were repeated in methanol (MeOH) to assess if the solvent affected the fluorescence response. The experiments were performed with a slight difference in concentration range (0; 2; 5; 10; 20 mM) to evaluate the response of sensor with higher concentration of D-Fructose **8**. An increase of fluorescence intensity (103%) with gradually more concentrated solutions was observed for **8** at 10 mM (Figure 3.22), as in the previous results. It was supposed that the fluorescence response observed here, was not dependent on the solvent.

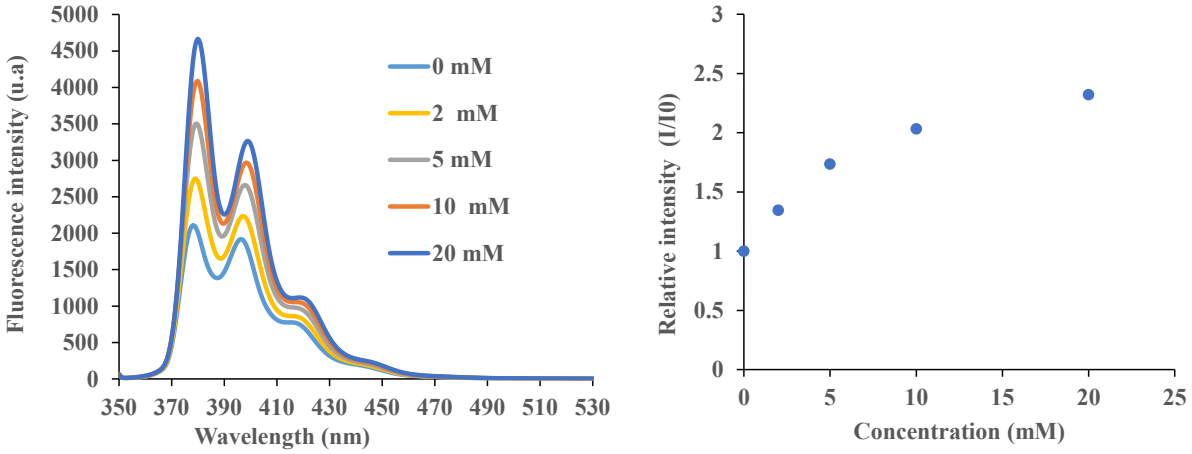
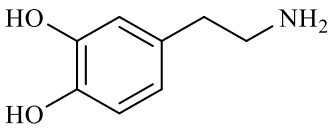


Figure 3.22. *Fluorescence spectra of* ***6*** *(1 μM) at* λ_{ex} *344 nm with* ***8*** *at different concentrations in MeOH. Intensity vs concentration at λ 380 nm (right).*

The results observed with D-Fructose **8** contrasted with the expected trend, wherein a decrease in fluorescence was expected upon sugar binding. Further experiments were performed with a similar compound employed in the system reported in the literature, where it a fluorescence decrease was observed. Experiments between **6** and dopamine **10** were conducted to evaluate the quenching mechanism. Among the catecholamines employed in the reported system, dopamine **10** was selected due to the presence of two-hydroxyl groups, conferring a similarity to the D-Fructose used previously. The structure also involved an amine group with an ethyl chain attached, as shown the Figure 3.23.



10

Figure 3.23. *Chemical structure of dopamine* ***10****.*

The fluorescence spectra reported in Figure 3.24 shows a fluorescence intensity decrease in response to **10**, in contrast to the effect of D-Fructose **8**, confirming that the expected quenching effect was occurring.

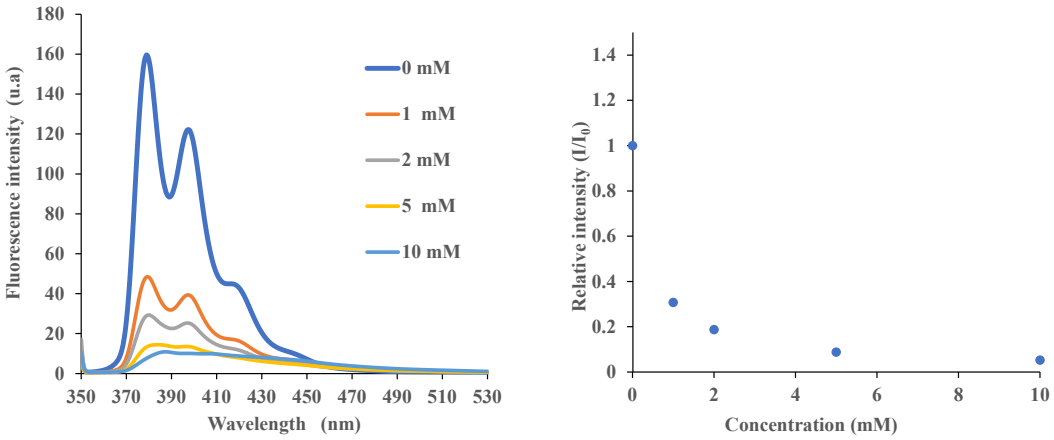


Figure 3.24. *Fluorescence spectra of* ***6*** *(1 μM) at* λ_{ex} *344 nm with* ***10*** *at different concentrations in buffer solution (100 mM* $Na_2S_2O_3$*, 50 mM HEPES, 20 mM NaCl, pH 7.4). Intensity vs concentration at λ 380 nm (right).*

Moreover, in the literature reported PBA system, red shift in the emission spectra of PBA upon the addition of dopamine was observed (using catecholamine as reference), as marked in Figure 3.25. This was attributed to the excimer band of pyrene, hypothetically induced by the reaction of catechol and PBA. However, as shown in Figure 3.24, no shift upon the addition of **10** was seen.

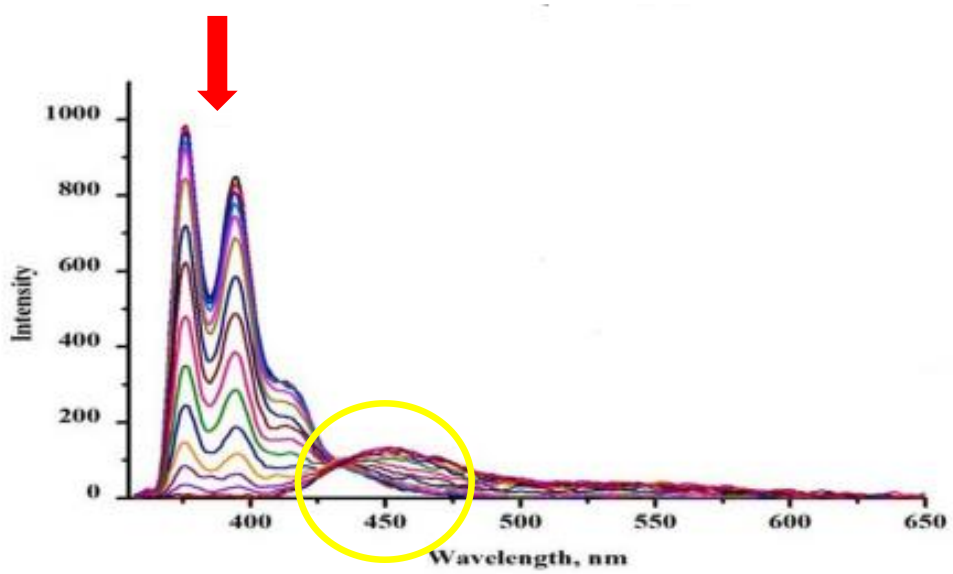


Figure 3.25. *Emission spectra of PBA with different concentration of dopamine. Decrease of fluorescence intensity (red arrows) and red shift at 450 nm (yellow circle). Image adapted from literature [133].*

The experiments were repeated in aqueous buffer solution at higher pH (≈ 9) to examine if this could affect the fluorescence properties of the probe. A stronger fluorescence decrease upon addition of 1 mM of **10** was observed (Figure 3.26). The decrease of fluorescence became less marked at higher concentrations of **10**. Moreover, at concentrations of 2 mM and above, a shift in the emission spectra at 450 nm was seen, as verified in the reported system. However, the intensity of this peak was marginally increased compared to that reported, as noticeable in Figure 3.25.

In the spectra reported in Figure 3.26, it is possible noticed the presence of an emission band at 450 nm. It was attributed to the formation of excimer, as it was observed in the system reported in literature. However, the fluorescence intensity observed was very low compared to the example reported, as shown in Figure 3.16.

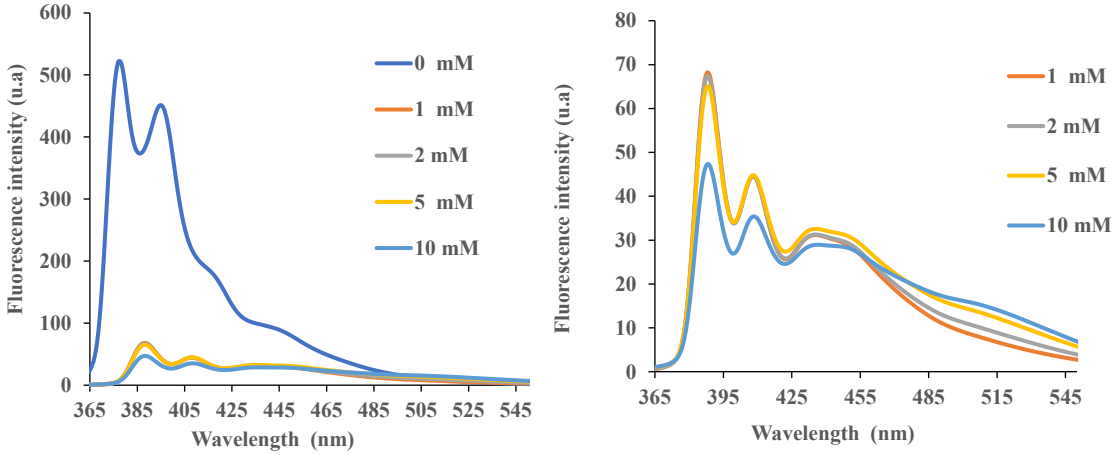


Figure 3.26. *Fluorescence spectra of* ***6*** *(1 μM) at* λ_{ex} *344 with* ***10*** *at different concentrations in buffer solution (100 mM* $Na_2S_2O_3$*, 50 mM HEPES, 20 mM NaCl, pH 9). Focus on smaller fluorescence intensities (right).*

An increase and a decrease in the fluorescence of **6** was seen upon addition of D-Fructose **8** and dopamine **10** respectively, evidencing binding. The opposite fluorescence responses seen for D-Fructose and dopamine can be potentially explained by the presence of the amino group in **10** which might act a fluorescence quencher of **6**. Moreover, the formation of excimer pyrene band at higher intensity was not detected, in contrast with that reported. Whilst experiments were carefully conducted to mimic that reported in the literature, method reproducibility is a known, wide-spread issue. Therefore, a method detail may have been omitted which could influence the results obtained here. The performance of sensor **6** was in contrast with what was expected upon the D-Fructose addition. However, preliminary experiments with coumarin **9** were performed to investigate if the fluorescence response of **6** following addition of **8**, was able to establish a successful interaction and allow FRET mechanism, as shown in the Figure 3.14. The structure of coumarin **9** (Figure 3.17) is different compared to what reported to literature [133]. However, it was considered suitable for preliminary FRET experiments.

FRET experiments

As aforementioned, coumarin is widely used as the acceptor in a FRET couple with pyrene, therefore preliminary experiments with coumarin (**9**) were performed. The emission wavelength of sensor **6** was 380 nm, while the excitation wavelength of coumarin was reported as 350-400 nm. [186] Preliminary experiments with **6** (1 μM) acting as the donor and coumarin **9** (30 μM) as the acceptor were conducted to investigate the FRET process and the fluorescence response upon D-Fructose addition (10 mM).

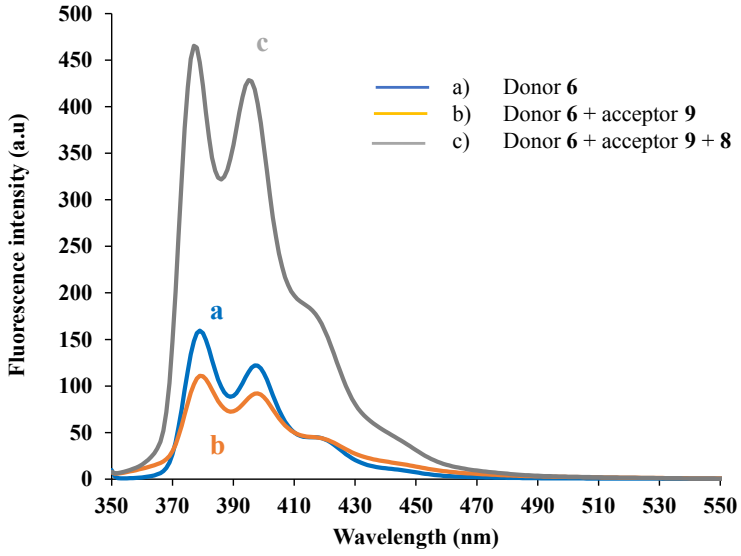


Figure 3.27. *Fluorescence spectra of donor* ***6*** *(a); donor and acceptor* ***9*** *(b); and donor, acceptor plus sugar* ***8*** *(c) in buffer solution (100 mM $Na_2S_2O_3$, 50 mM HEPES, 20 mM NaCl, pH 9) at λ_{ex} 344.*

The fluorescence spectra reported in Figure 3.27 shows a slight fluorescence decrease compared to sensor **6** alone (a) and with **9** added (b). This may indicate an interaction between the two probes through the hypothesized FRET mechanism. There was a marked increase in fluorescence intensity upon addition of **8**, suggesting the successful binding between BA and sugar. A possible reason of the fluorescence increase could be justified with the establishment of additional interaction with

coumarin upon the sugar addition, or some disaggregation mechanism. However, no further experiments were performed to investigate and understand completely the process. Moreover, no change in the fluorescence emission of coumarin **9** was observed, which was supposed to be involved for achieve the detected signal. This was attributed to the reciprocal photophysical properties in terms of absorption and emission of the probes. Emission and excitation wavelength were too close to allow a suitable excitation of coumarin **9**. Different coumarin derivatives with a more suitable excitation wavelength must therefore be investigated. Moreover, the FRET efficiency of the couple could be optimized by varying the concentration of sensors.

Although a fluorescence response of **6** was observed upon saccharide addition, a more marked change in fluorescence intensity was required to establish the interaction with another probe to achieve FRET. Additionally, it was theorized that the fluorescence increase was affected by pH and solvent since a slight increase at basic pH (18 %) and a less marked response in MeOH (103 %) compared to aqueous solution at pH 7.4 (193 %) was seen. The reason for this behaviour was not clarified and could cause an issue for achieving the FRET mechanism. Furthermore, PBA has been previously employed as sensor for saccharides detection.[32, 187-189] This work aimed to the development of new sensing system, to be improved for highly sensitive saccharides detection.

Sensor **7** was designed with the aim of achieving a more marked fluorescence change upon sugar binding and enable a FRET process. Improvement of structure and alternative sensing mechanism were investigated.

3.3.2 Sensor 7: design and fluorescence experiments

Sensor **7** was designed to promote the incorporation of BA into the structure through an alkyl chain with an amino group. They reported an internal charge transfer (ICT) fluorescent saccharide

sensor, composed of 2-formyl benzeneboronic acid and aniline as the dye. They observed a shift of emission maxima from 404 nm to 362 nm upon saccharide binding. Sensor **7** involved a pyrene probe, an amino group directly linked to it, which acted as a quencher, and a phenylboronic acid as saccharide receptor (Figure 3.28). The sensor was planned to provide a blue shift (decrease in wavelength) in the emission spectra. It was anticipated that the shift could be enhanced using PBA as the receptor and pyrene as the dye. Moreover, as reported in the literature, the presence of an amino group in an *ortho* position, thus closer to BA moiety compared to in *para* position, can improve the affinity binding with diols. [190] The change in fluorescence emission achieved with saccharides binding aimed to allow the interaction with coumarin and provide the final FRET process (Figure 3.15).

The synthesis of sensor **7** involved a nucleophilic substitution of 1-aminopyrene **11** with 2-(bromomethyl) phenylboronic acid **3b**, following the scheme below.

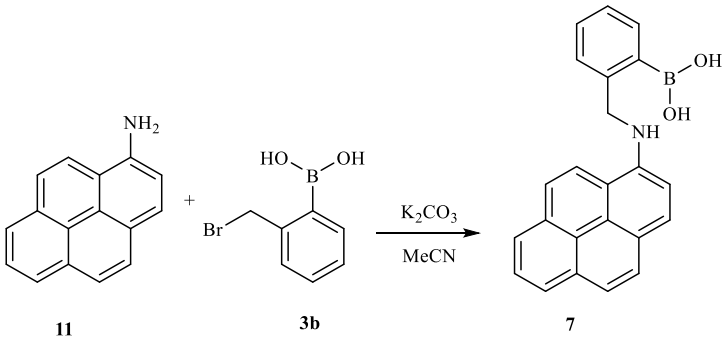


Figure 3.28. *Synthesis scheme of sensor **7** from starting materials **11** and **3b**. Reaction condition adapted from a reported procedure [191].*

The reaction product was isolated by chromatographic column [Hexane / Ethyl acetate 1:1 (Hex) /(EtOAc) and analysed by NMR. Preliminary analysis of the NMR spectra suggested the

successful synthesis of the desired product. By comparing the NMR spectra of the starting material **11** and **3b** (Figure 3.29a & b, respectively) and that of the reaction product (**c**), both the characteristic aromatic peaks (8-7 ppm) belonging to pyrene and the benzene ring can be seen in spectra c. The amino group peak (≈ 7.0 ppm) did however disappear in spectra a. Moreover, the peak (≈ 5.0 ppm) attributed to the proton closest to bromide in **3b** (**b**) is slightly shifted (≈ 4.7 ppm) in the product's spectra (**c**).

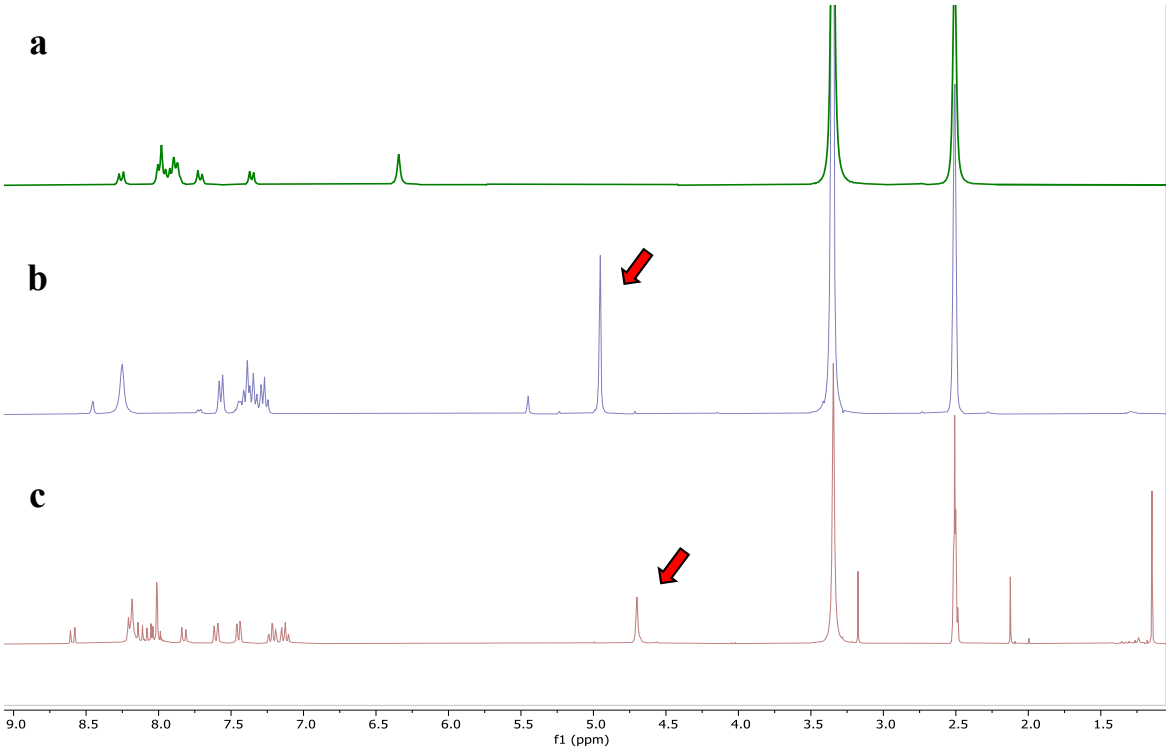


Figure 3.29. *Comparison of NMR spectra in DMSO-d6: a) 1-aminopyrene **11** b) 2-bromomethyl) phenylboronic acid **3b**, and **c**) reaction product. Arrow indicates the shift of peak (5 ppm) from **b** to **c**.*

To further confirm the desired product was formed, mass spectra of the reaction product was conducted. In contrast with what was hypothesized with the NMR spectra, the main peak shown in Figure 3.30 did not correspond to the desired product **7** (calculated 350.14). Instead, the found m/z 486.21 (yellow label) was attributed to $[M+H]^+$ of the di-substituted derivate **12** (Figure 3.31).

The other minor peaks were attributed to the desired product **7** (m/z 351.14) and to the starting material **3b** (m/z 216.09).

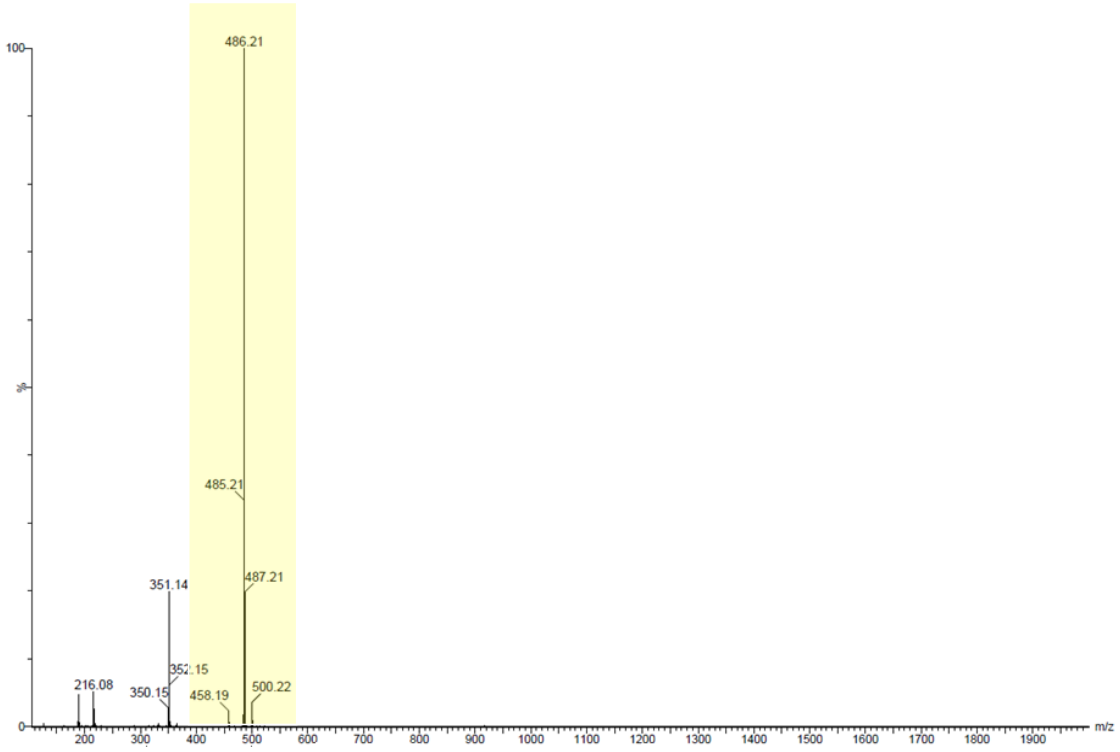
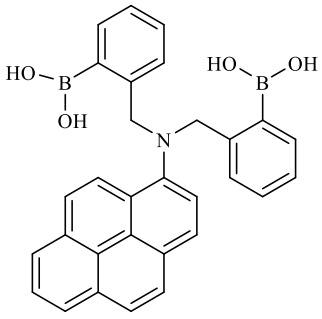


Figure 3.30. *Mass spectrum of recovered product with peak m/z 486.21 in evidence.*



12

Figure 3.31. *Chemical structure of the substituted derivate **12**.*

Following these unexpected results, alternative conditions involving different ratios of starting material **11** and **3b**, temperature, time and purification were evaluated to achieve sensor **7** without the di-substituted product. The same reaction solvent (MeCN) was used across the experiments summarised in Table 3.1.

Table 3.1 *Reaction conditions for the synthesis of 7.*

Test	Ratio **11/ 3b**	Time (h)	Temperature (°C)	Atmosphere
a	1:1.5	24	25	Air
b	1:1	24	25	Air
c	1:1	24	90	Air
d	1:1	8	25	Argon
e	1:1	5	90	Argon

Since an excess of **3b** on **11** could increase the likelihood of forming di-substituted product, the reaction was conducted with the reagents at equal concentration (test **b**). Preliminary analyses were performed by TLC with dichloromethane (DCM)/MeOH 1 % as eluent. Comparing starting material and product, a large excess of unreacted **11** was observed. The reaction (test **c**) was therefore repeated with an increased temperature (~ 90 °C) slightly higher to the reflux temperature of MeCN (82 °C). It was expected that a high temperature could promote the conversion of starting material **11** and achieve the final product. The mass spectra reported in Figure 3.32 of the product related again to the di-substituted derivate, corresponding to the main peak at m/z 486.21 (yellow label). The peak at peak 218.16 (blue label) was attributed to starting reagent **11**.

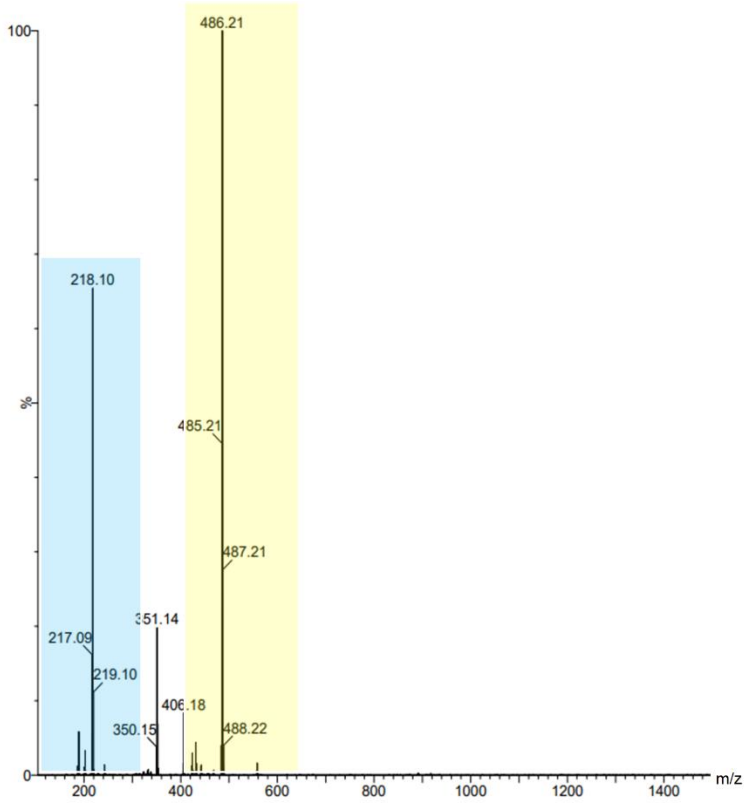


Figure 3.32. *Mass spectrum of product of test* ***c*** *shown in the Table 3.1 with peak at m/z 218.10 9 (blue) and at m/z 486.21 (yellow) evidenced.*

Since the results, it was supposed that a higher temperature increases the reactivity, leading to the formation of di-substitute product. A new strategy was therefore employed, following an alternative procedure reported in the literature [190] in which a shorter reaction time (8h), room temperature and inert atmosphere were used. The inert atmosphere was supposed to enhance the reactivity, avoiding the formation of side product. The mass spectra of the reaction product achieved with test **d** (Figure 3.33) show the peak of the desired product (m/z 351.14-orange peak) suggesting an improved conversion with this method. Although the desired product **7** was achieved following this method (d), the m/z attributable to starting reagent **11** was still seen (peak 218.16-blue label).

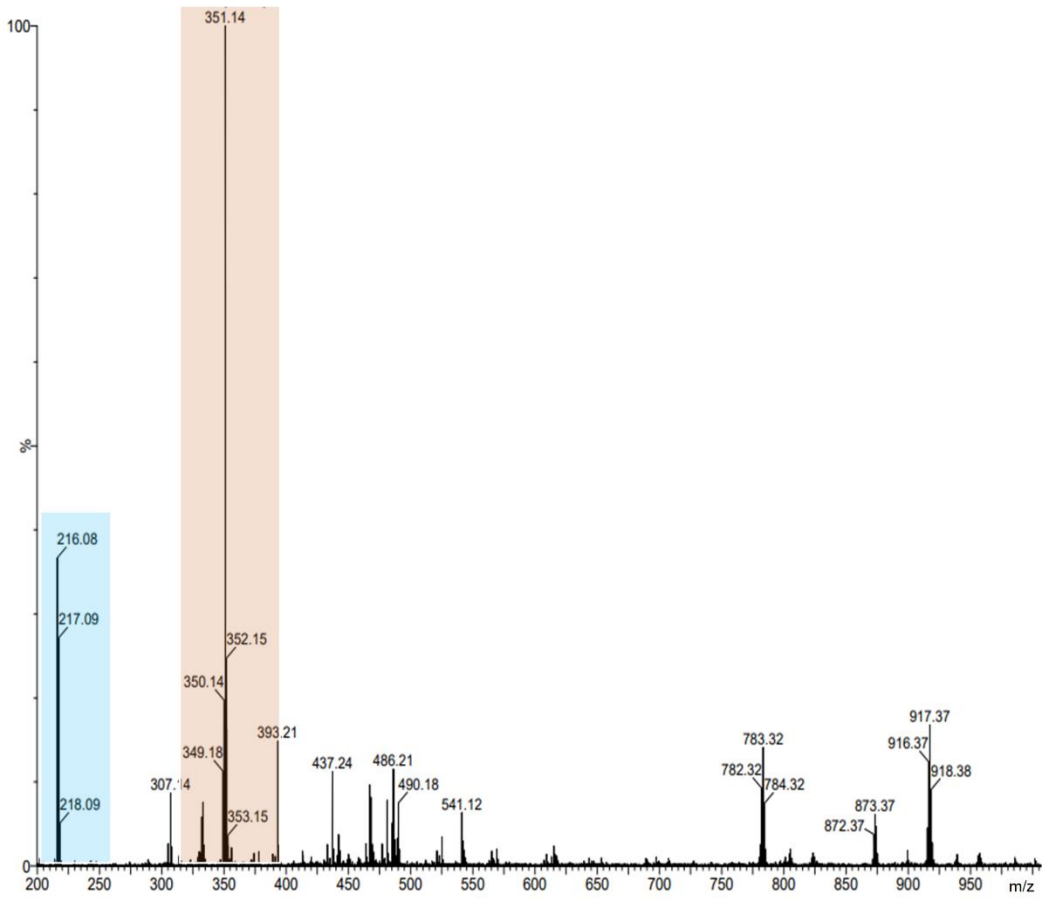


Figure 3.33. *Mass spectrum of product following condition* ***d*** *shown in the Table 3.1.Peak at m/z 351.14 (orange) and 218.16 (blue) evidenced.*

New test **e** was conducted following the condition of previous test **d** but monitoring the progress of reaction by TLC analysis until **11** was totally consumed. The reaction was monitored by TLC every two hours, using DCM/Hexane/MeOH 1 % as eluent system. Specific TLC stains were employed; ninhydrin to identify amino groups[192] and curcumin for boronic acid.[158] The selected stains allowed the amino group of **11** and boronic acid of **3b** starting materials to be identified, to examine whether the final product was achieved The starting material **11** was very visible by ninhydrin test, being a primary amine, whilst the desired product involving a secondary amine showed a less marked signal.

Alternatively, a tertiary amine, such as in the di-substituted derivate **12**, does not stain. In Figure 3.34, TLC plates (on silica gel substrate) at three different time points (after 2, 4 and 5 hour) are reported. Each plate was subjected to analysis by curcumin (***a***, ***c*** and ***e***) and ninhydrin (***b***, ***d*** and ***f***). The spot of starting materials and reaction product were compared through their retention factor (Rf) and marked by colour with TLC stain. After 2 hours, in TLC ***a*** (curcumin stain) the presence of a spot assigned to **3b** can be observed (purple label in Figure 3.34). In TLC ***b,*** (ninhydrin stained) a marked signal attributed to the primary amine of starting material **11** at low RT was also observed (red label in Figure 3.34). Being low polar, **11** travelled slowly and only moved a short distance on the TLC plate. After 4 hours the same results were observed, as shown in TLC plates **c** and **d**. After 5 hours, in TLC plates **e** and **f**, the spot at different RT to that of the starting material was seen; the spot had a stronger signal upon curcumin stain (TLC ***e***) and a weaker coloured stain with ninhydrin test (TLC ***f***) compared with the previous one (yellow circles). The weaker spot was supposed to arise from secondary amino presence, and thus attributable to the desired product **7**. It was therefore concluded that five hours was the optimum reaction time, allowing for completion of the reaction without the formation of side product.

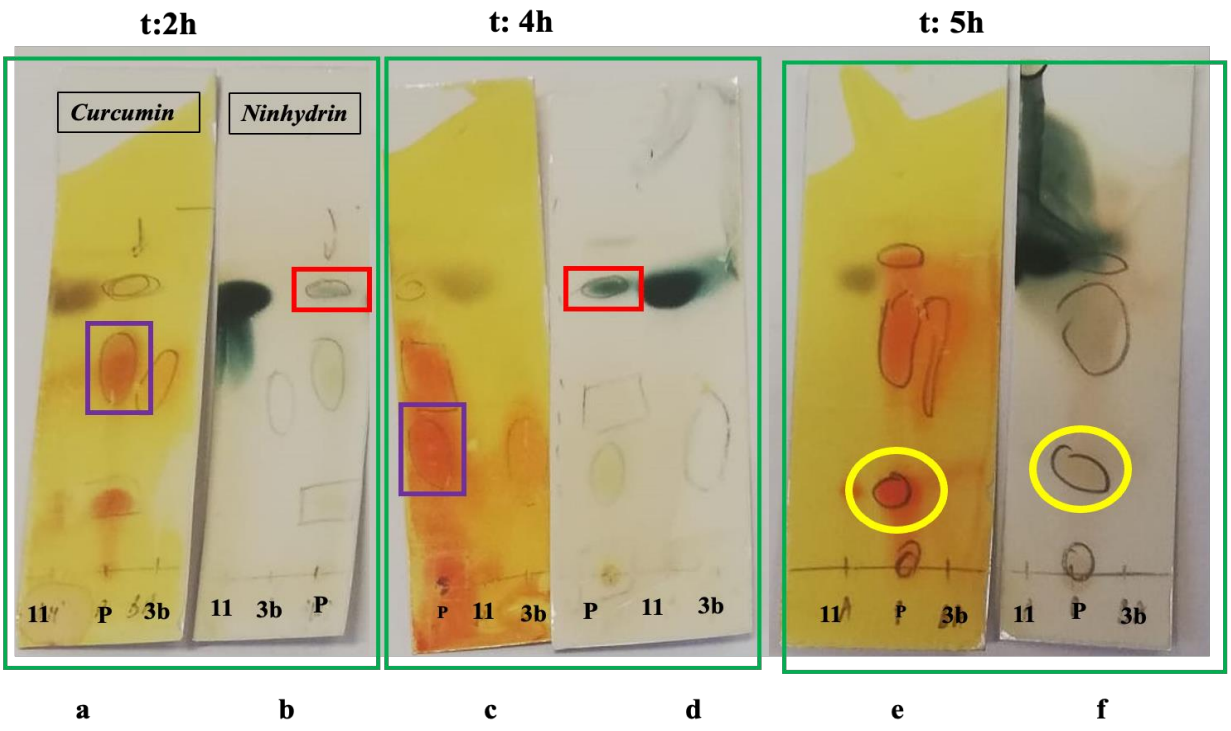


Figure 3.34. *TLC plates, subjected to curcumin test (left)) and ninhydrin (right) at different reaction time (2, 4 and 5 hours). Red label shows primary amine by (**11**), purple label refers to boronic acid reagent (**3b**), yellow circles the supposed final product (**7**).*

Due to these results, the reaction according to test **e**, as reported in Table 3.1, was repeated. DCM/hexane was employed as the eluent system with increasing percentage of MeOH to promote the separation of the desired final product. The TLC plate, subjected to ninhydrin test reported in Figure 3.35, shows different spots at a suitable Rf, validating the chosen conditions for the separation. The spot at the top was attributed to the starting material **11** (a). **11** being the less polar compound moved higher up the plate. As the boronic acid moiety was involved, both starting material **3b** and the desired product were more polar and thus, move slowly and were dependent on the addition of MeOH to the eluent system. The spot on the bottom and the middle spot were attributed to **3b** and the desired product **7**, respectively (Figure 3.35c).

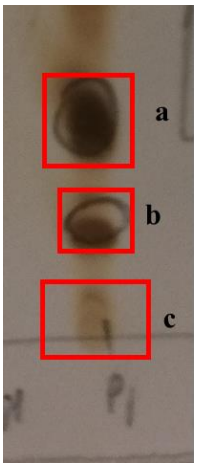


Figure 3.35. *TLC plate, subjected to ninhydrin strain, of product following conditions* ***e****, reported in Table 3.1, showing three spots, attributed to* ***11****(a)* ***3b*** *(c) and (b) desired product* ***7****.*

In contrast to the results observed by preliminary TLC studies, the mass spectra of the fractions collected by chromatographic column did not support these results (Figure 3.36). The first fraction corresponded to the starting material **11** (m/z 218.10-blue label) as shown in Figure 3.36a. The mass spectra of the second and third fractions, reported in Figure 3.36 b & c, showed a mixture of products. They include the di-substituted product **12** (m/z 486.19-yellow label) and the desired product (m/z 352.15-orange label), as well as starting material **11** (m/z 218.10-blue label). Only in the third fraction could the presence of reagent **3b** (m/z 216.10-pink label) be seen by a small peak. It was therefore concluded that despite the preliminary promising studies, the chromatography column was not suitable for the separation of **7**. Alternative separation techniques were therefore investigated, such as LC-MS.

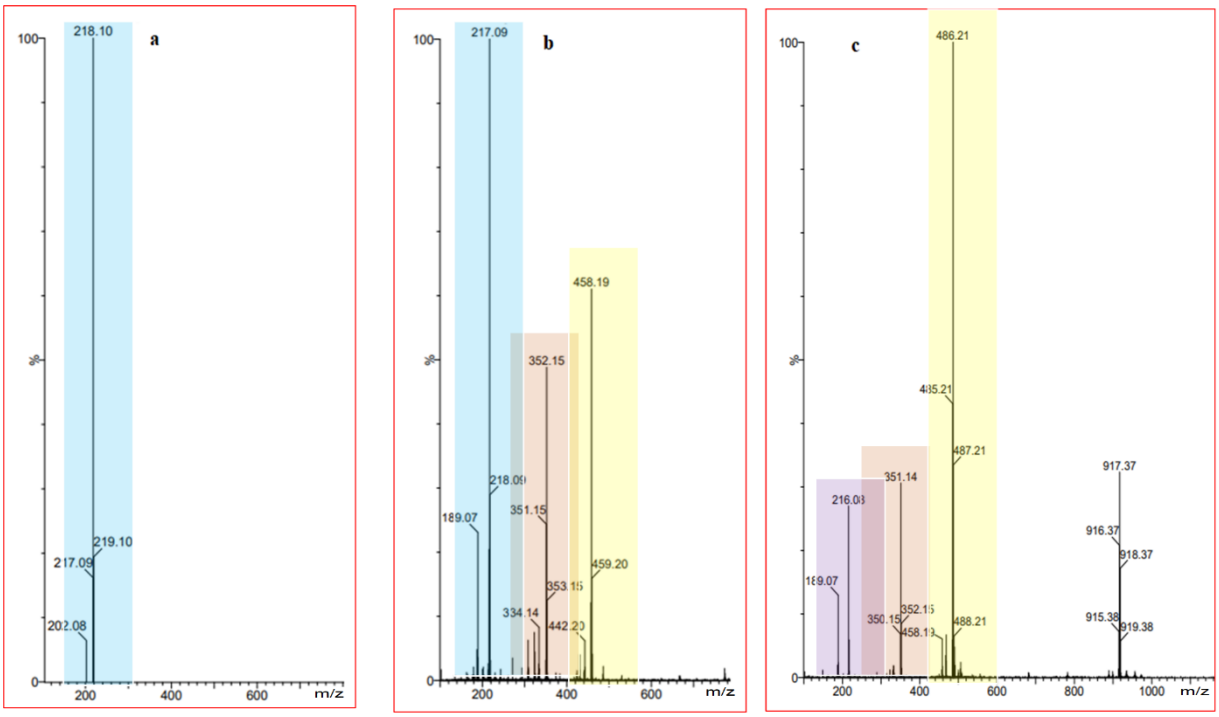


Figure 3.36. *Mass spectra of first, second and third fraction (a, b and c) collected by chromatography column of reaction product following conditions* ***e****, reported in Table 3.1.Peak at m/z 218.10 (blue), 216.10 (pink) and 486.19 (yellow) evidenced.*

The reaction was repeated, and the reaction product was analysed by LC-MS to allow the separation and identification of single compounds through mass spectra. The first chromatograms shown in Figure 3.37a and b, involved a system with water (solvent 1) and MeOH or MeCN as solvent 2, following preliminary gradient conditions reported in Table 4.2. Due to the low separation observed in both methods, a solution of 0.1 % trifluoroacetic acid (TFA) was added to promote the separation and the definition of single peaks (Figure 3.37a2 and b2). Using MeOH (Figure 3.37a2) over MeCN (b2), achieved a higher level of separation.

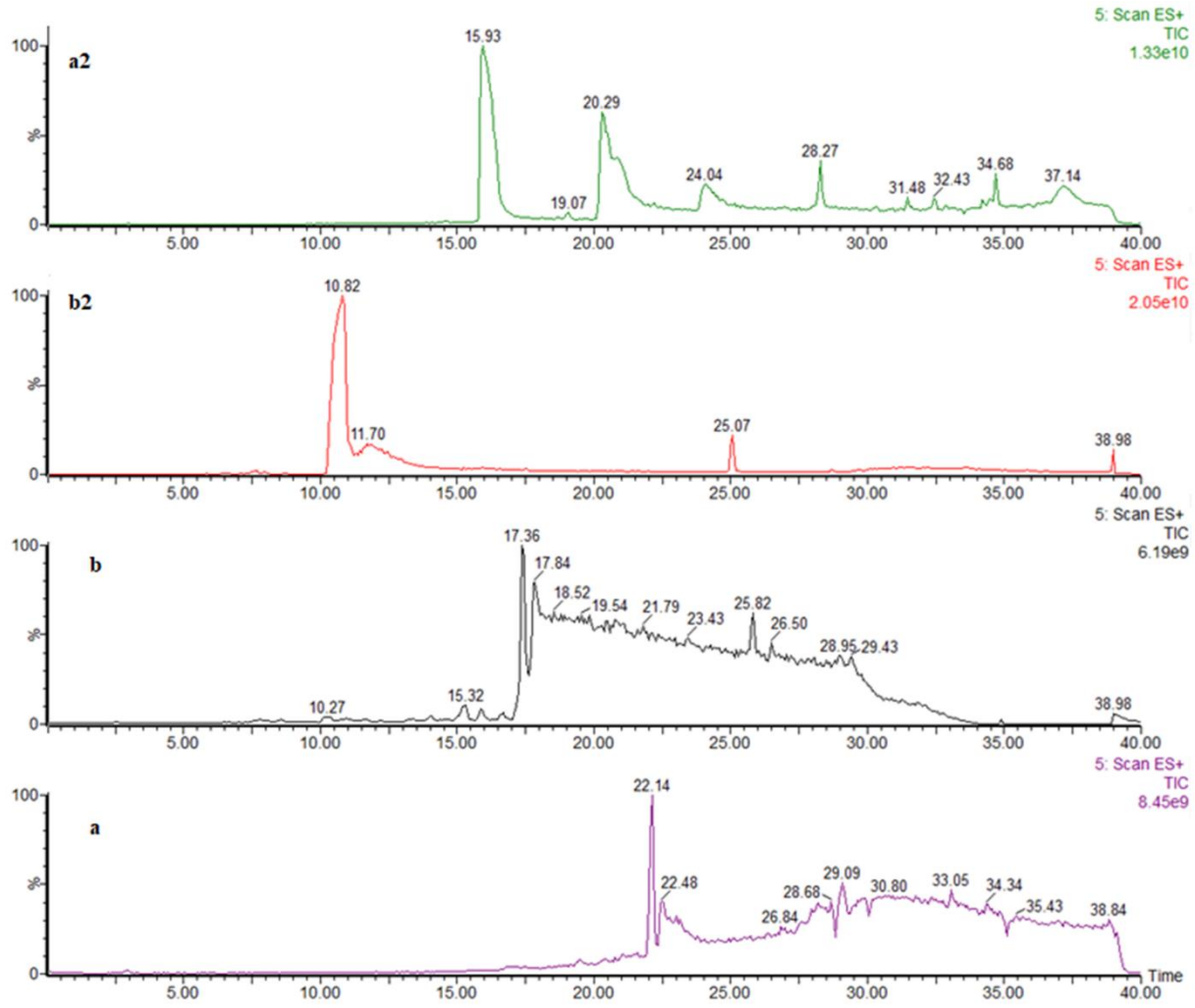


Figure 3.37. *Chromatograms achieved following the gradient condition reported in Table 3.2 a) water/ MeOH b) water/MeCN, a2-b2) with the addition of TFA 0.1 %.*

Table 3.2. *Gradient condition, applied to achieve chromatogram (a/a2, b/b2) reported in Figure 3.37.*

Method	Time	Water %	MeOH (a) % // MeOH + TFA (a2)
a/a2	0 30 35 35.10 40	70 0 0 70 70	30 100 100 30 30
		Water %	**MeCN (b) % // MeCN+ TFA (b2)**
b/b2	0 30 35 35.10 40	70 0 0 70 70	30 100 100 30 30

However, the analysis of the mass spectra of the single compounds (Figure 3.38B) identified with different RT in the chromatogram, (Figure 3.38A) did not confirm the successful purification of the desired product. **11** (m/z ~217-yellow label) was identified in all mass spectra while **3b** was identified in all except the peak at RT 15.33 (1). The peak with m/z 189 may be attributed to fragmentation product of **3b** (orange). The conditions employed may have resulted in the unsuccessful separation of the desired product. Consequently, new parameters were investigated such as gradient change, time and type of solvents.

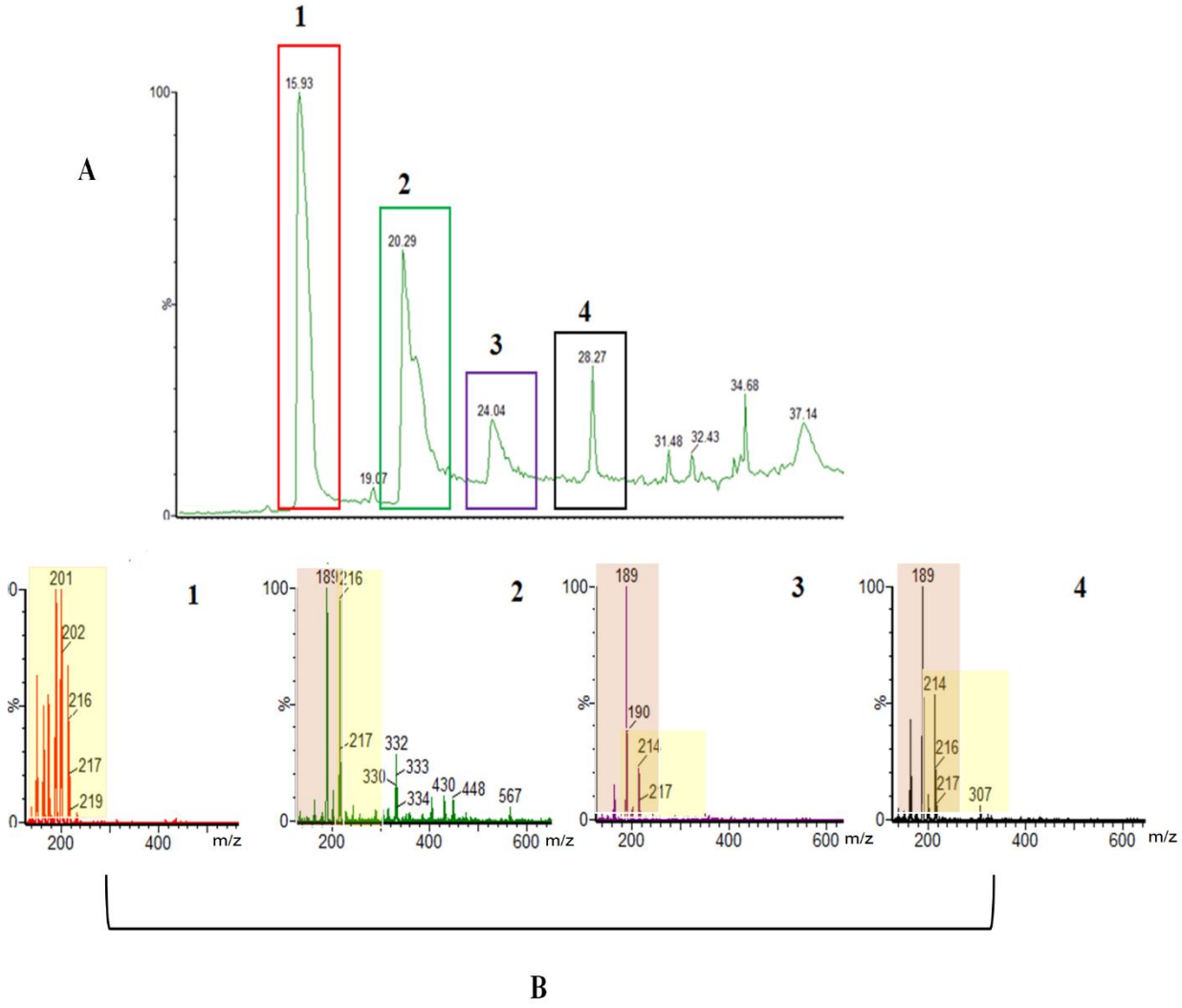


Figure 3.38. *Chromatograms achieved employing system water/ MeOH plus TFA 0.1 %, following the gradient condition reported in Table 3.2 (A). Mass spectra of the main peak identified 1-4 (B). Peak at m/z 189 (red) and 217 (yellow) evidenced.*

It was expected that the desired separation could be obtained by increasing the amount of MeOH. Indeed, as observed by TLC analysis the presence of MeOH enabled the movement of boronic acid-based compounds along the column. Thus, new gradient conditions employing different starting amounts of MeOH were investigated (Table 3.3). As used previously, 0.1 % TFA was employed to improve the separation in each experiment.

Table 3.3 *Gradient condition, applied to achieve chromatogram reported in Figure 3.39.*

Method	Time	Water %	MeOH (a) % // MeOH + TFA (a2)
c	0 30 35 35.10 40	30 0 0 30 30	70 100 100 70 70
		Water %	**MeCN (b) % // MeCN+ TFA (b2)**
d	0 30 35 3510 40	20 0 0 20 20	80 100 100 80 50
		Water %	**MeCN (b) % // MeCN+ TFA (b2)**
e	0 30 35 35.10 40	50 0 0 50 50	50 100 100 50 50
		Water %	**MeCN (b) % // MeCN+ TFA (b2)**
f	0 30 35 35.10 40	95 0 0 95 95	5 100 100 5 5
		Water %	**MeCN (b) % // MeCN+ TFA (b2)**
g	0 30 35 35.10 40	95 25 25 95 95	5 75 75 5 5

Analysis of the chromatograms reported in Figure 3.39 showed that the use of a low percentage of MeOH to start the gradient and then an increase to 100 % (**f**) or 75 % (**g**) did not improve the separation (Figure 3.39**f** and **g**). A better separation of the peaks following method **c-d-e** with a higher amount of MeOH, respectively 70, 80 and 50 %, was seen compared to the preliminary conditions applied and reported in Table 3.2. (Figure 3.39 **c-d-e**). Moreover, the chromatogram **e** showed the most acceptable separation, in which more distinct peaks were seen.

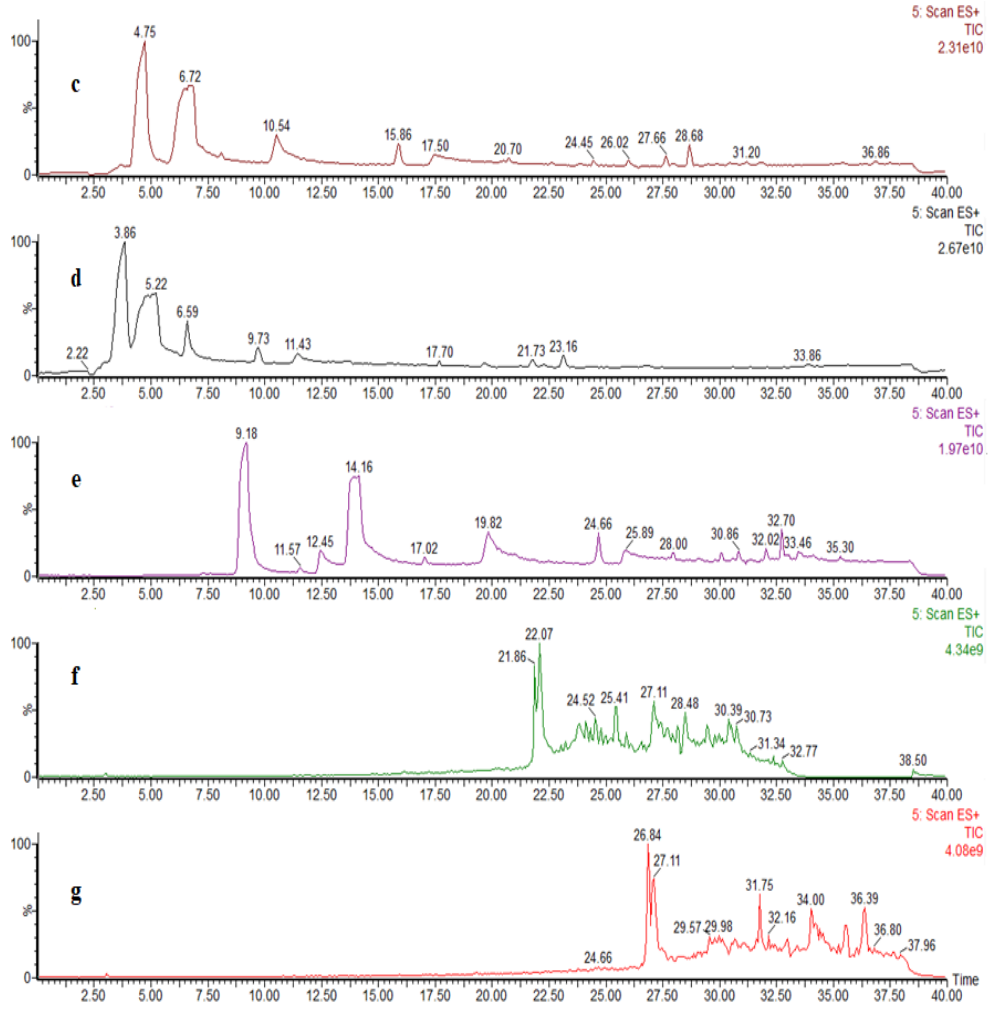


Figure 3.39. *Chromatograms achieved following the gradient condition reported in Table 3.3 (**c-g**) with an eluent system a) water and MeOH with the addition of TFA 0.1 %.*

Mass spectra of the main peaks of chromatogram **e** (Figure 3.40A) were investigated to find the peak (retention time) of the desired product. From the mass spectra 1-5 as showed in Figure 3.40 B no peaks corresponding to the m/z of the desired product (351) were observed. As in previous results, it is possible to notice the peak attributed to the starting material **11** and **3b**, as highlighted in yellow (aminopyrene **11**) and orange (1-Bromo PBA **3b**) in Figure 3.40B. Based on these results, it was assumed that the chosen conditions resulted in retention of the final product in the column.

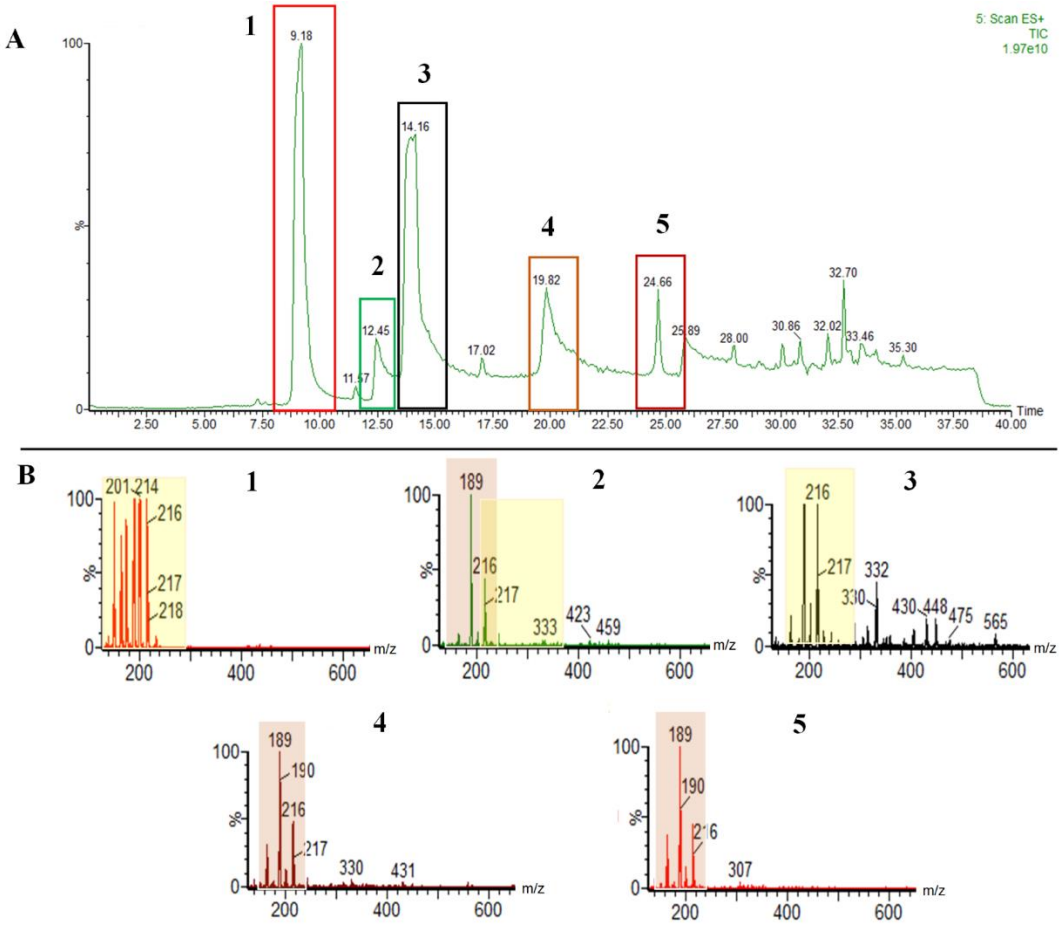


Figure 3.40. *Chromatograms achieved employing method* ***e*** *shown in Table 3.3 (**A**). Mass spectra of the main peak identified 1-5 (**B**). Peak at m/z 189 (red) and 217 (yellow) evidenced.*

Despite exploring different conditions, sensor **7** could not be completely isolated from the products mixture. However, it was decided to perform fluorescence experiments with the di-substituted product **12** achieved with the first conditions (Test a) reported in Table 3.1. The synthesis of product **12** was verified through mass spectra, as shown observe in Figure 3.30. Although it was not the desired sensor designed, it was projected that the structure of **12** would allow the behaviour of sensor-based ICT mechanism to be investigated. The aim was to evaluate if a shift in the emission spectra occurred, as expected, upon saccharide binding.

Preliminary excitation spectra experiment of pyrene were conducted to select the maximum excitation wavelength. Excitation spectra of **12** were recorded at the emission wavelength of the pyrene probe reported in the literature (380 nm).[133]

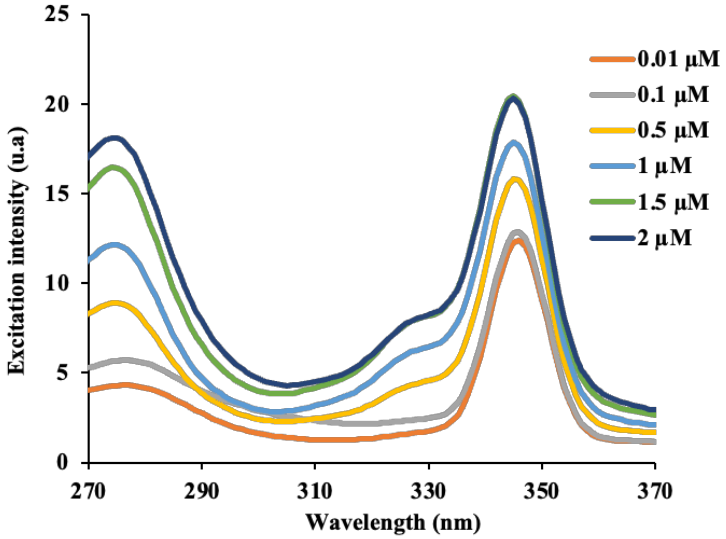


Figure 3.41. *Excitation spectra a λ_{em} 380 nm of **12** in water at different concentration (0.01; 0.1;0.5; 1; 1.5; 2 µM).*

Following emission spectra of **12** were recorded at λ_{ex} 344 nm, the maximum excitation wavelength observed. Next aim was to evaluate the solubility of the sensor in water and to select

the optimum concentration for further experiments. As shown in Figure 3.42a, a linear response of fluorescence intensity versus concentration was established, confirming the solubility of **12** in water. Since an acceptable fluorescence intensity was seen at the lowest concentration 0.01 µM of synthesized sensor **12** (Figure 3.31), this concentration was selected and used in further experiments.

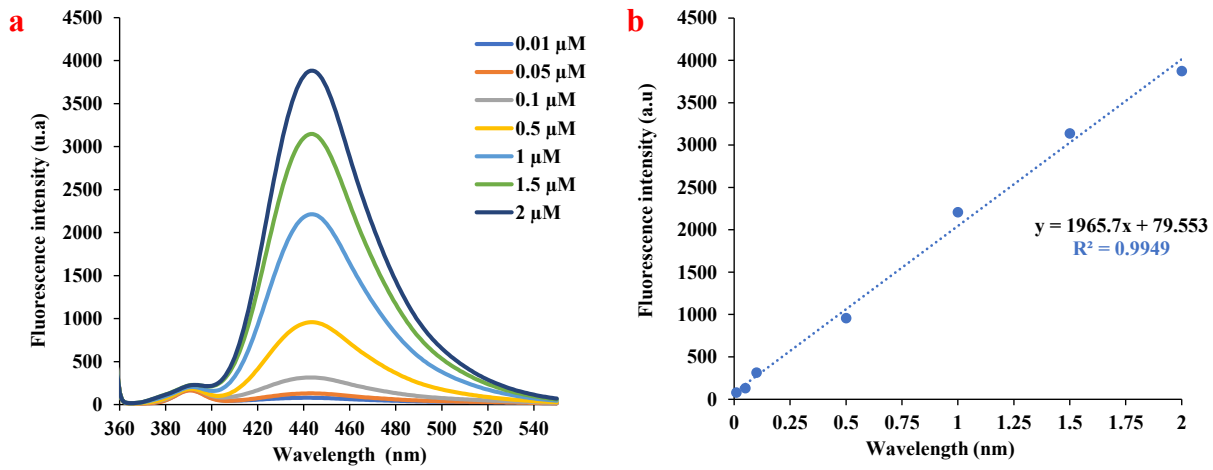


Figure 3.42. *Fluorescence spectra at λ_{ex} 344 nm of sensor **12** in water at different concentration (a). Fluorescence intensity versus concentration at λ 445 nm (b).*

Fluorescence experiments between **12** and D-Fructose **8** at different concentrations (0.01; 0.01; 0.1; 1;10; 100; 1000 µM) were conducted in aqueous buffer solution at pH 7.4 (Figure 3.43) and pH 9 (Figure 3.44). Since the purpose was to evaluate the appearance of a shift in the emission spectra upon saccharide binding, a smaller concentration of D-Fructose was employed. However, the emission spectra shift predicted was not detected in either of the fluorescence spectra shown in Figure 3.43 and Figure 3.44. It was therefore determined that the ICT mechanism was not involved. In both of spectra, it is possible to notice a peak at 385 nm, mainly at basic pH. It was attributed to Raman band of water. Moreover, it was observed a difference starting fluorescence

intensity value of sensor in absence of **8**. These results suggest an effect, not examined, of pH towards the fluorescence properties of sensor.

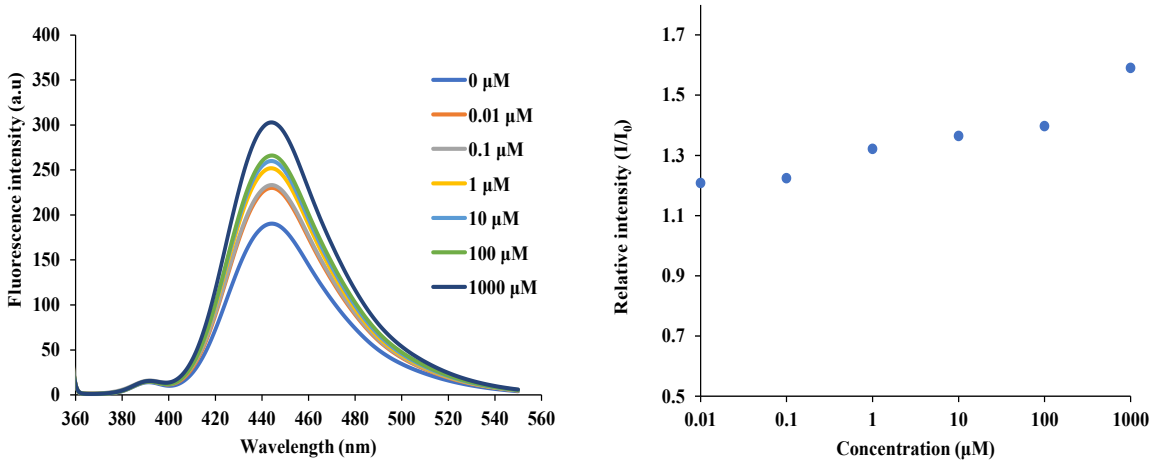


Figure 3.43. *Fluorescence spectra of* ***12*** *(0.01 µM) at* λ_{ex} *344 nm with* ***8*** *at different concentration in in buffer solution (100 mM* $Na_2S_2O_3$*, 50 mM HEPES, 20 mM NaCl, pH 7.4). Intensity vs concentration at λ 445 nm (right).*

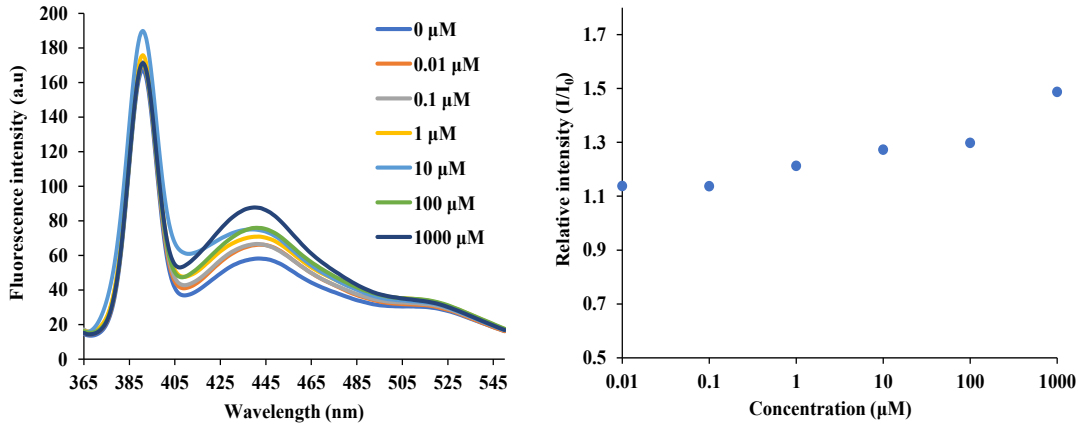


Figure 3.44. *Fluorescence spectra of* ***12*** *(0.01 µM) with* ***8*** *at different concentration in in buffer solution (100 mM* $Na_2S_2O_3$*, 50 mM HEPES, 20 mM NaCl, pH 9). Intensity vs concentration at λ 445 nm (right).*

Since a visible shift was not seen, it cannot be verified whether an ICT mechanism was involved. Although it has not been assessed, the reason could be attributed to the presence of two boronic acid moiety in product **12**. Since it has not been possible to synthesize sensor **7**, it was not possible perform fluorescent experiments to evaluate a potential establishment of ICT mechanism in the sensor as designed. However, a higher fluorescence intensity increase upon saccharides binding was observed, compared to that seen with sensor **6** at the same concentration of D-Fructose **8** (1 mM). Indeed, in a solution at pH 7.4 an increase of 57 % with sensor **6** (Figure 3.20), and an increase of almost 59 % with sensor **12** (Figure 3.43). Moreover, sensor **12** showed an increase of 48 % at pH 9 compared to the 7 % increase of sensor **6** in the same conditions (Figure 3.21) These results suggested that the presence of amino group could promote the binding towards saccharides. It was anticipated that the fluorescence response could be amplified by the presence of a single boronic acid moiety, instead of two, as in **12**. Nevertheless, the fluorescence response observed was not considered to evaluate the FRET mechanism. No experiments with **9** were conducted.

3.4 Summary and outlook

The first sensing system provided a PET mechanism between boronic acid derivative as receptor **1** and anthracene **2**, as fluorophore units. The interaction between the units was predicted to be strengthened with the future immobilisation onto a solid support. However, fluorescence experiments recorded between the components **1** and **2** did not show fluorescence quenching upon addition of **1** to **2**. Indeed, its addition to **2** showed a slight fluorescence increase, in contrast to the expected result. It was proved that no PET mechanism occurred and so the fluorescent system did not act as planned. Consequently, it was concluded that the structure of the fluorescent system required improvement to promote the interaction between the two units. Moreover, an alternative fluorescent mechanism was investigated to improve the response upon saccharide binding.

The second sensing system involved a boronic acid-based pyrene and coumarin **9**, and their interaction to allow a FRET process for saccharide detection. The boronic acid was incorporated into the structure of the fluorophore by a direct connection (sensor **6**) or through an alkyl chain with an amino group as a linker with a phenylboronic acid (sensor **7**). Sensors **6** and **7** were planned to bring a suitable change in fluorescence properties upon sugar binding to enable the interaction with coumarin **9**. Sensor **6** was expected to display a fluorescence intensity decrease upon the saccharide binding, as observed with the catecholamine sensing systems reported in the literature. However, a fluorescence increase following the addition of D-Fructose was observed here. Fluorescence experiments between sensor **6** and dopamine **10**, employed in the reference system, displayed a fluorescence intensity decrease. The reason was attributed to the presence of amino group in **10**, expected to incite a quenching mechanism towards pyrene. However, the fluorescence response exhibited was not considered suitable for the sensing application. Moreover, there was not an efficient interaction with coumarin **9** to establish a FRET mechanism. Sensor **7** was designed, expecting a noticeable shift in the emission spectra upon sugar binding caused by ICT mechanism. Despite different attempts, the desired compound, isolated from the products mixture, was not obtained. To investigate the behaviour of the sensor-based ICT mechanism, fluorescence experiments between the di-substituted product **12** and D-Fructose were performed. No noticeable shift in the emission spectra upon sugar binding was observed. However, the system displayed a higher fluorescence increase compared to sensor **6**. These results suggested that the presence of amino group could improve the interaction with saccharides. Moreover, it was expected that a suitable linker between the amino group and the fluorophore could further strengthen the fluorescent mechanism that modulates the signal response. Whilst the fluorescence response of sensor **7** was not verified, focus was shifted away from the purification of sensor **7** towards a new

sensing system. The structure of the sensing system needed to be improved to ensure a suitable fluorescence response upon saccharide binding, enabling the interaction with an additional probe and thus the FRET process. Moreover, since ICT mechanism is also influenced by the matrix, a more predictable and frequently used mechanism such as PET was favoured for the next sensing system.

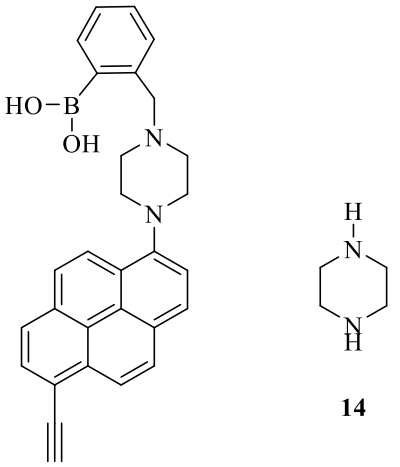
CHAPTER 4: FLUORESCENT SENSING SYSTEM BASED ON PET-PYRENE BORONIC ACID SENSOR

4.1 Introduction

The previous sensing system involved a boronic acid-based pyrene (sensor **6** and **7**) and coumarin **9** and their interaction to allow a FRET process. Sensor **6** based on boronic acid directly connected to the structure of pyrene, displayed a fluorescence increase following the addition of D-Fructose. The response observed was not considered significative (157 %) to be employed for sensing applications. Moreover, an efficient interaction with coumarin **9** to establish a FRET mechanism was not observed. Sensor **7** involved the incorporation of boronic acid moiety to the pyrene dye through an alkyl chain with an amino group as a linker with a phenylboronic acid. Due to insufficient yield of the compound desired, isolated from the product mixture, fluorescence experiments were performed between the di-substituted product **12** and D-Fructose. The higher fluorescence response compared to sensor **6** evidenced the effect of amino group in improving the interaction with saccharides. However, this response was not considered sufficient to enable the interaction with coumarin **9** to allow FRET process. The FRET mechanism is promoted by a suitable overlap between the emission of the donor and the absorption spectra of acceptor. Thus, the fluorescence response of the sensors followed the sugar binding must bring a markable change in the emission spectra. A wide range of high sensitivity boronic acid-based sensors have been developed in the recent years. The novelty of this work consists of developing a sensing system based on the interaction of surface-confined independent units to provide the final fluorescence response.

From the previous sensor investigation, it was concluded that the structure of the sensing system needed to be improved, with a suitable linker between the amino group and the fluorophore. It was projected to strengthen the fluorescent mechanism that modulate the signal response. Since ICT mechanism depends also on the solution and environment condition to occur, a more predictable and employed mechanism such as PET was favoured for the next sensing system. Therefore, this chapter is focused on the design and synthesis of a PET-based sensor with an enhanced structure that involves a defined amino based linker between the boronic acid moiety and the fluorophore. The aim was to enhance the fluorescence response upon sugar binding and allow the interaction with an additional probe through the FRET process.

According to the literature, PET mechanism can be promoted by increasing the electron-deficiency of the fluorophore moieties and including a longer and more rigid alkyl spacer. Based on a 4-amino-1,8-naphthalimide fluorophore reported by Liu et al,[127] a fluorescence pyrene analogue (sensor **13**) was designed, integrated with the phenylboronic acid receptor through piperazine **14** as the linker characterized by a semi-rigid structure (Figure 4.1). It was expected to strengthen the interaction between the amino group and the boronic acid and modulate the fluorescence response by PET mechanism. Furthermore, the structure was decorated with ethynyl groups to allow immobilisation onto silica surfaces.



13 **14**

Figure 4.1. *Chemical structure of sensor **13** and piperazine **14**.*

Fluorescence experiments of the designed sensor were conducted to evaluate the signal response upon the binding with sugars. Since the structure of sensor **13** was novel, a thorough investigation of its photophysical properties by absorption spectra, solubility test and pH titration were required. Indeed, the presence of acetylene group and piperazine can affect the fluorescence of pyrene. As planned in the previous chapter, the fluorescence response achieved upon sugar binding by PET was employed to establish an interaction with the coupled probe through FRET process. The role of the sensor **13** was investigated both as donor then acceptor in the FRET couple. In contrast with the previous system designed. With the aim of incorporating the sensors onto solid substrates in mind, easily functionalizable dyes and with reported photophysical properties were chosen. Common functionalized groups such as acetylene group could bring a bathochromic shift (higher wavelength) [193] and amplify the quantum yield of a probe used as acceptor.[194-197] It was expected that the shift of emission spectra of acceptor reduced the requested overlap. Moreover, it was theorised that the high difference between quantum yield of donor and acceptor would make the FRET signal response following the sugar binding less noticeable. Furthermore, the role of pyrene

probe as acceptor in FRET couple is less investigated. The photophysical properties, their concentration relating to the optimum ratio, and structure of the probes have been investigated to improve the FRET efficiency. [114, 198, 199] The use of an additional process such as FRET antenna or surplus effect were also considered to promote FRET selectivity and efficiency.[79] The final stage of this work looked to immobilise sensor **13** onto the surface of silica nanoparticles through functionalisation of the sensor's structure, as previously exhibited by the group of Qian (Section 1.8).[146] The probes involved in the FRET process have been selected for the inclusion of a suitable functionalization group. Discussion and preliminary experiments with silica nanoparticles are described in chapter 5.

This chapter reports the design of the main components of sensor **13,** along with an explanation of their function. A detailed discussion about synthesis strategies of sensor **13**, including analysis and purification procedures, are provided. Fluorescence experiments were conducted to evaluate the photophysical properties of the sensor, its ability to bind sugars and the resulting final fluorescence response. Preliminary FRET experiments between the sensor and different probes are also described herein.

4.2 Sensor 13: design

Pyrene was selected as the probe due to its higher fluorescence quantum yield (0.69) compared to other fluorophores,[200] and the associated versatility of structure modification. To enable its immobilisation onto surfaces, an acetylene group was selected and added due to its widely reported functionalization procedure.[201] Moreover, according to the literature it should not compromise the fluorescence properties of the probe. [200, 202] Fluorescence quenching could occur instead with different group such as halogen or amino groups.[203] The structure of sensor **13** involved a semi-

rigid piperazine (**14**) that was believed to act both as a fluorescence quencher and a spacer for the receptor moiety. Due to its semi rigid, planar structure, it was thought that piperazine promoted fluorescence quenching by twisted intramolecular charge transfer (TICT) promoted PET. TICT caused the maximum charge separation (positive-negative), stimulating the PET process. [128] Following the excitation, TICT states were performed, and a strong positive electron filed on 4-position nitrogen, that accelerates the PET process. The semi-rigid structure of piperazine guaranteed a short distance between the two nitrogen atoms, promoting the interaction with boronic acid with sugar and the quenching effect towards fluorophore. [128, 204] The interaction with sugars by boronic acid (BA) moiety located in *ortho* position, should promote the interaction B-N, interrupting the PET process and restoring the fluorescence of the sensor (Figure 4.2).

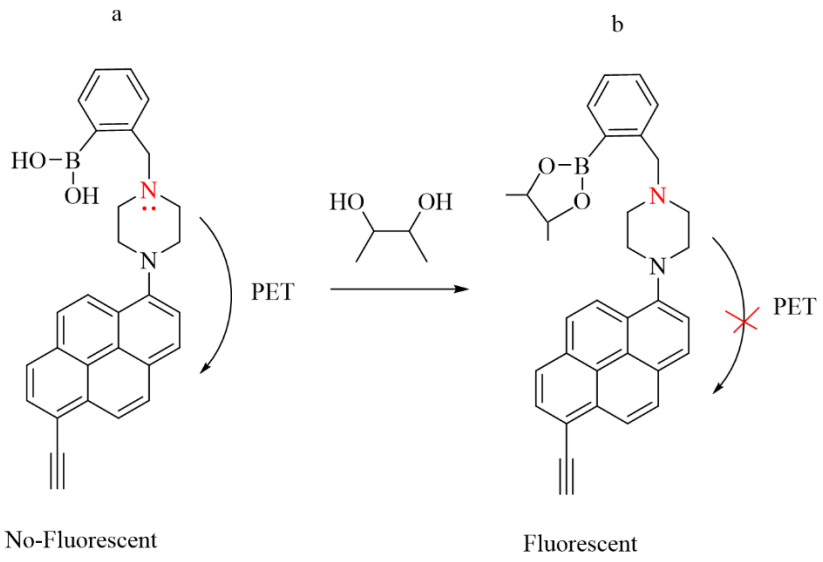


Figure 4.2. *Scheme of fluorescence mechanism involved in sensor* ***13*** *modulated by sugar binding by BA.*

Since the sensor (**13**) was composed of two single units, contrary to the sensor described in chapter 3, the Rehm-Weller equation can be used to calculate the energy change which can be used to evaluate whether the PET process is established. [70]

$$\Delta G = E(D^+/D) - E(A^+/A^-) - \Delta G_{00} - \frac{e^2}{\varepsilon d} \qquad \text{Equation 4-1}$$

The redox potential of pyrene (acceptor) and of piperazine (donor) were noted from the literature. The oxidation potential of pyrene ($E(D^+/D)$), is 1.16 V,[205, 206] while the reduction potential of piperazine ($E(A^+/A^-)$), is 1.96 V.[207] The excited state energy of pyrene fluorophore (ΔG_{00}), is 3.34 eV. The last term represents the coulombic energy of ion pair (e) following the electron transfer process, where ε is the dielectric constant and d the distance between the charges. Taking acetonitrile as reference solvent, the ratio (e^2 / εd) is 0.06 eV. [70] The estimated ΔG is -0.28 eV. The negative value of ΔG proved that PET was energetically possible. The quencher behaviour of piperazine towards the pyrene probe was tested through preliminary fluorescence studies. Fluorescence spectra of pyrene **15** (0.1 μM) were recorded with piperazine **14** at different concentrations (0-100 mM) in water to highlight the quenching response. The results reported in Figure 4.3 show a decrease in fluorescence intensity upon the addition of **14**, confirming its quencher role and suitability for its incorporation into the design of sensor **13** sensor.

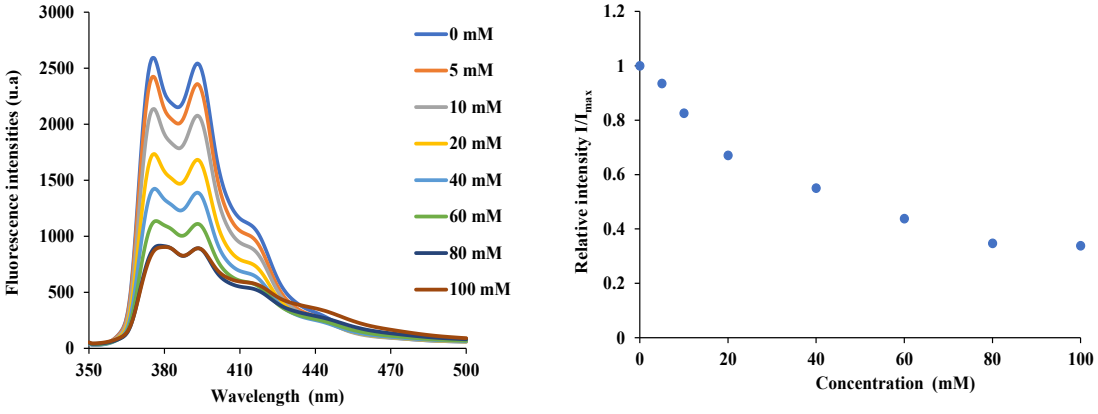


Figure 4.3. *Fluorescence spectra of* ***15*** *(0.1 μM) at* λ_{ex} *344 with* ***14*** *at different concentrations in water. Relative intensity vs concentration at* λ_{em} *376 nm (right).*

4.3 Synthesis and purification

The retrosynthetic route reported in Figure 4.4 shows the starting approach proposed for sensor **13** synthesis, that included five main steps. The methodology involved the reaction between 1,6-dibromopyrene (**15b)** and 1-boc-piperazine (**14b**) for **step 1** of synthesis. **15b** was employed due to the higher reactivity compared to the monobromide pyrene. Furthermore, the second atom of bromine allowed the next functionalization (**step 2**). **18** can be obtained through a Sonogashira coupling reaction, between **16** and trimethylsilyl acetylene **17** (TMS acetylene) followed by TMS deprotection (**step 3**).[200, 208] After the deprotection of the Boc group (**step 4**) to achieve **20**, **13** can be synthesised by reaction with 2-(bromomethyl) phenylboronic acid **3b** (**step 5**).

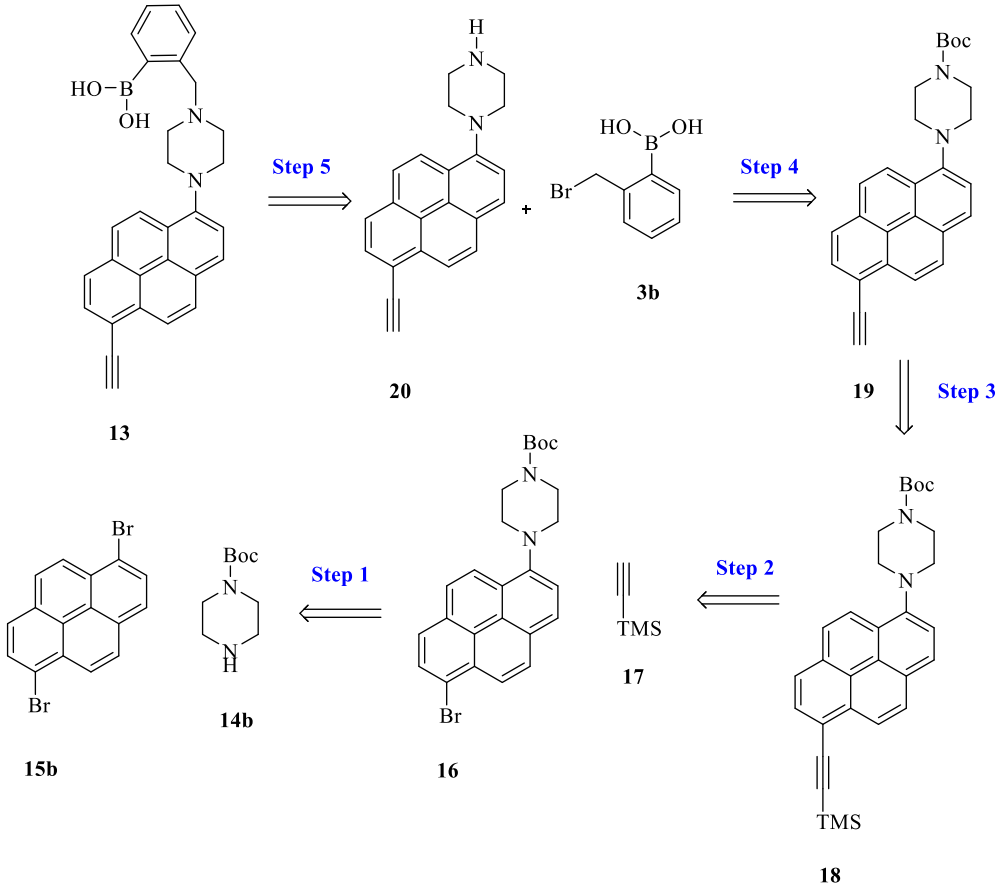


Figure 4.4. *Retrosynthetic route of sensor **13** (step 1-5).*

Conferring to the retrosynthesis route, each step was performed to evaluate the best reaction conditions to yield the desired product. Although each step reactions are reported in the literature, the reactivity of the product changed due to the protective groups, Boc (**step 1**) and TMS-acetylene (**step 2**) and their next deprotection reactions (**step 3** and **4**). Different condition reactions and changes in the reaction sequence were evaluated.

The first step consisted of incorporation of piperazine group to pyrene structure. Di-bromo substituted pyrene **15b** was employed to have a secondary amine group for the next functionalization (**step 2**). Tert-Butyloxycarbonyl (Boc) is a common protecting group for amines Piperazine involving Boc group (**14b**) was employed to increase the reaction selectivity towards **15b**, avoiding the functionalisation of both the amino groups of piperazine (Figure 4.5).

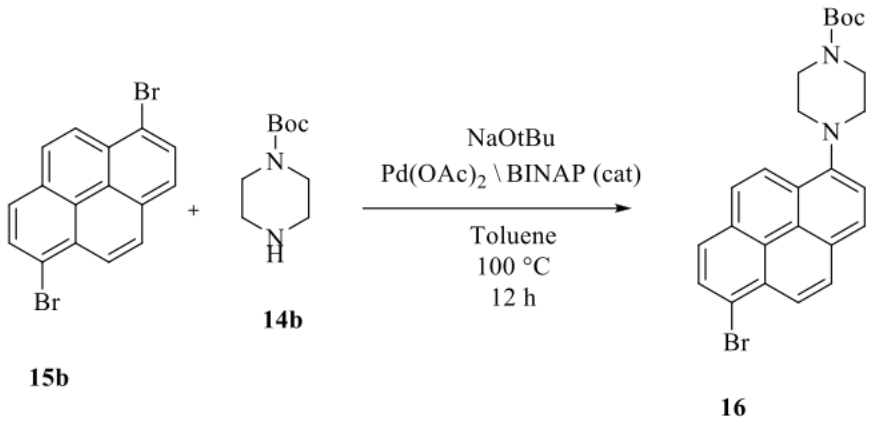


Figure 4.5. *Reaction scheme of step 1 for the synthesis of* ***16****.*

Synthesis of **16** was verified by NMR spectra, where the Boc group peak (~1.5 ppm) [209] is noticeable (Figure 4.6). The main peak observed in mass spectra (m/z 467) corresponds to the mass expected of **16** $[M+H]^+$, confirming successful synthesis. Furthermore, peaks relative to m/z

411 and 365, respectively peaks **a** and **b**, were attributed to the fragmentation of t-Boc group (a= m/z 411) and total loss of the Boc group (b = m/z 365), as reported in Figure 4.7.

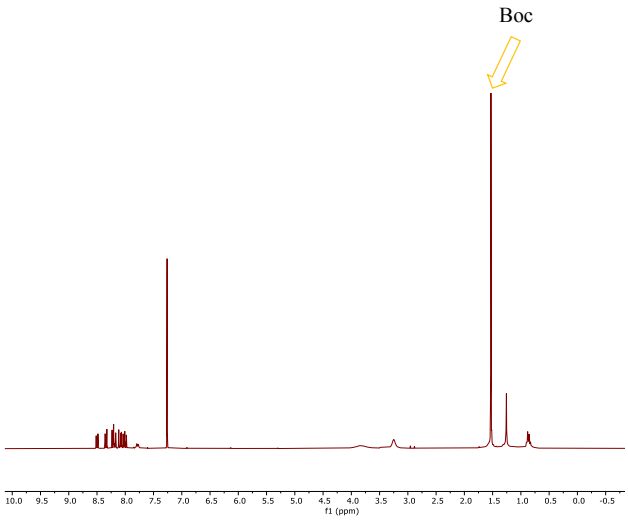


Figure 4.6. *NMR spectra of* ***16****, with Boc peak shown with an arrow.*

.

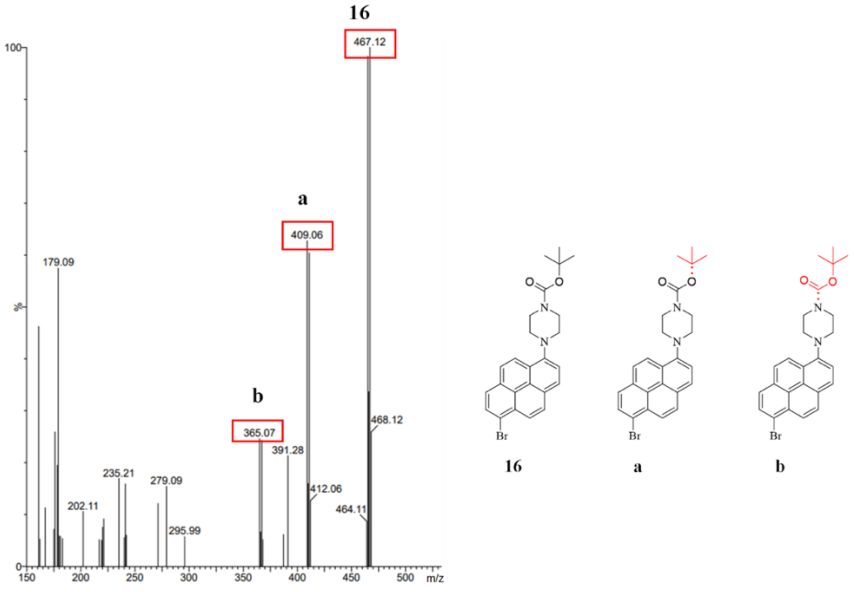


Figure 4.7. *Mass spectra of* ***16*** *(left). Relative structure of compounds for peaks* ***a*** *and* ***b*** *with the relative fragments lost in red (right).*

The next steps involved the introduction of TMS acetylene (**17**) by reaction of **16** in dry Et_3N and ethynyl-trimethylsilane **17** with $Pd(PPh_3)_2Cl_2$ /CuI as catalyst. The following deprotection TMS employed tetra-n-butylammonium fluoride (TBAF) in tetrahydrofuran (THF) to achieve the product **19**. The reaction was verified by comparing the NMR spectra, as reported in Figure 4.9. The products **18** and **19** were confirmed by NMR spectra. The appearance of the peak of the TMS group (~0.5 ppm) proved the synthesis of **18** while the peak attributable to ethynyl group peak (~ 3.5 ppm) verified the successful synthesis of **19**. In the same spectra, it is possible to notice that the previous peak of the TMS group is absent, confirming its successful deprotection.

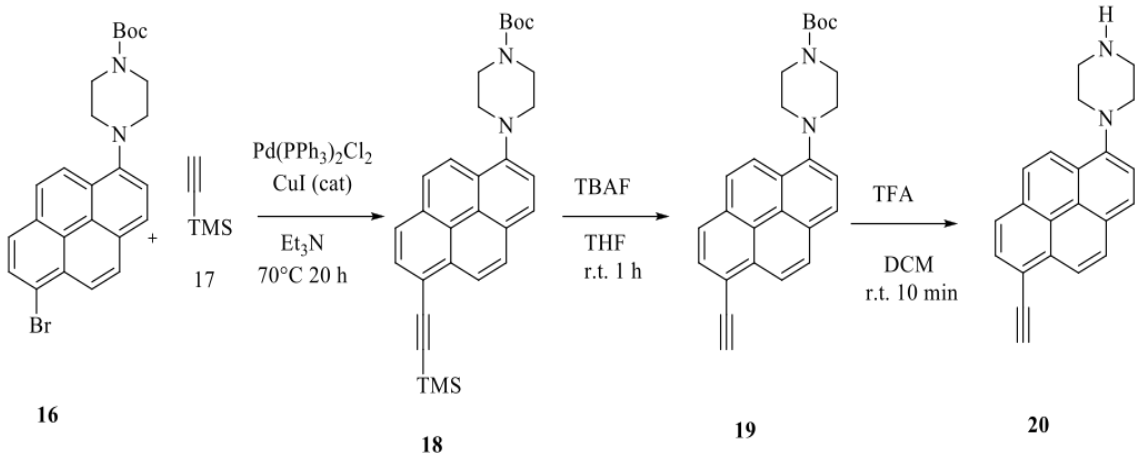


Figure 4.8. *Scheme of step 2-4 with reaction conditions.*

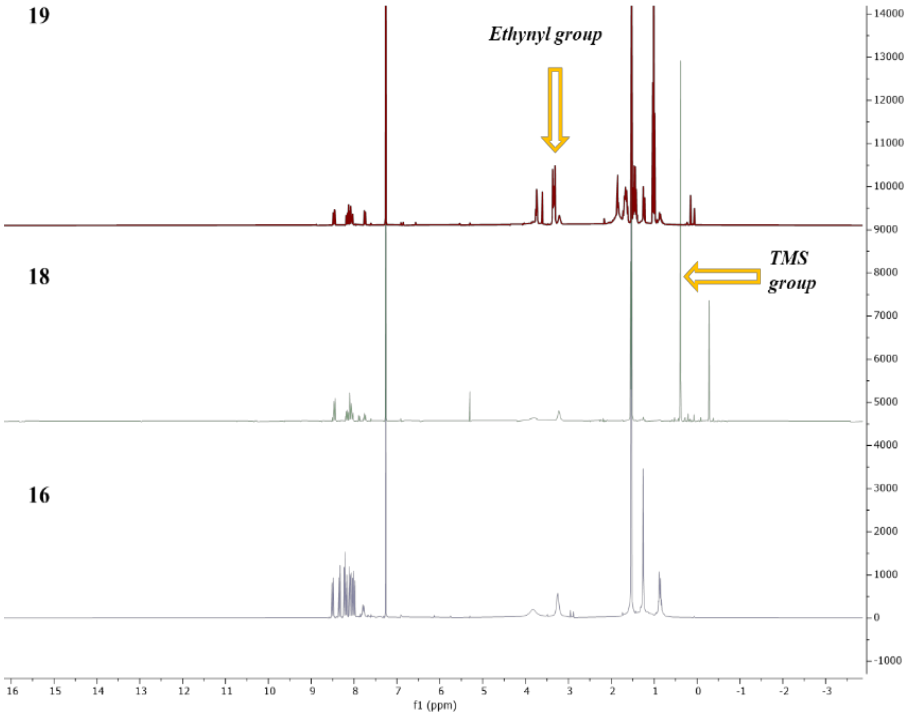


Figure 4.9. *Comparison NMR spectra of* ***16****,* ***18*** *and* ***19*** *with TMS and ethynyl group peaks shown with an arrow.*

The final step, before the reaction with **3b**, provided the deprotection of Boc (step 4 in Figure 4.4). This procedure was widely reported and occurs through carbamate hydrolysis in acidic conditions.[210] The starting material **19** was dissolved in dichloromethane (DCM) with a solution of trifluoroacetic acid (TFA) at room temperature for 10 min.[211]

Examining the NMR spectra reported in Figure 4.12, the characteristic peak of Boc is absent (~1.5 ppm-orange label) suggesting the successful Boc deprotection. However, analysis of the mass spectra reported in Figure 4.10 has not verified the formation of the desired product **20**. The mass was attributed to the formation of alternative methyl ketone **21** [m/z 329.17], as shown in Figure 4.11. This reaction was supposedly caused by the acetylene group's instability in acidic conditions. Although rare, an example of this reaction has been reported in the literature.[212] The other small

peak (m/z 429.22) was attributed to methyl ketone derivative with Boc group, not subjected to deprotection.

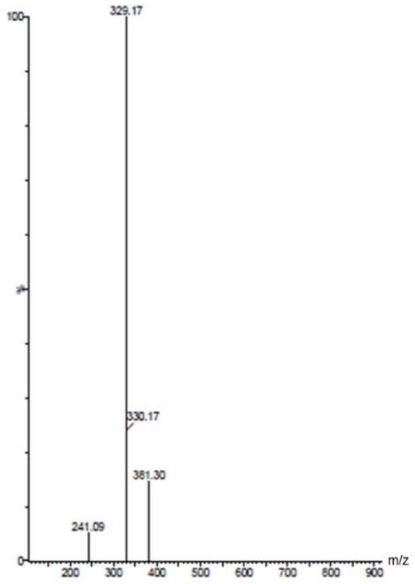


Figure 4.10. *Mass spectra of reaction product following Boc deprotection (left) with main peak 329.17.*

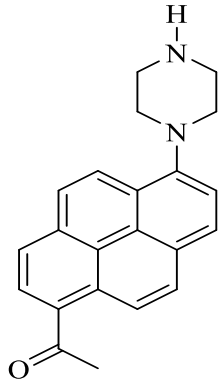


Figure 4.11. *Chemical structure of side product of* ***21****.*

A further investigation of the NMR spectra (Figure 4.12) has evidenced the presence of a small peak around 3.2 ppm that could be attributed to methyl group (green label), identified by mass spectra. Since the low concentration of product obtained, it has not been possible record 13C NMR spectra for a deeper investigation. To avoid doubt regarding side product formation, following

separation by column chromatography each product was analysed by mass spectra. It was considered a superior analysis technique to verify the formation of undesired product of the reaction compared to NMR spectra. Indeed, despite NMR spectra clearly showing the appearance or disappearance of the peak of interest, it was difficult to notice the small change due to side products, as verified for side product **21**.

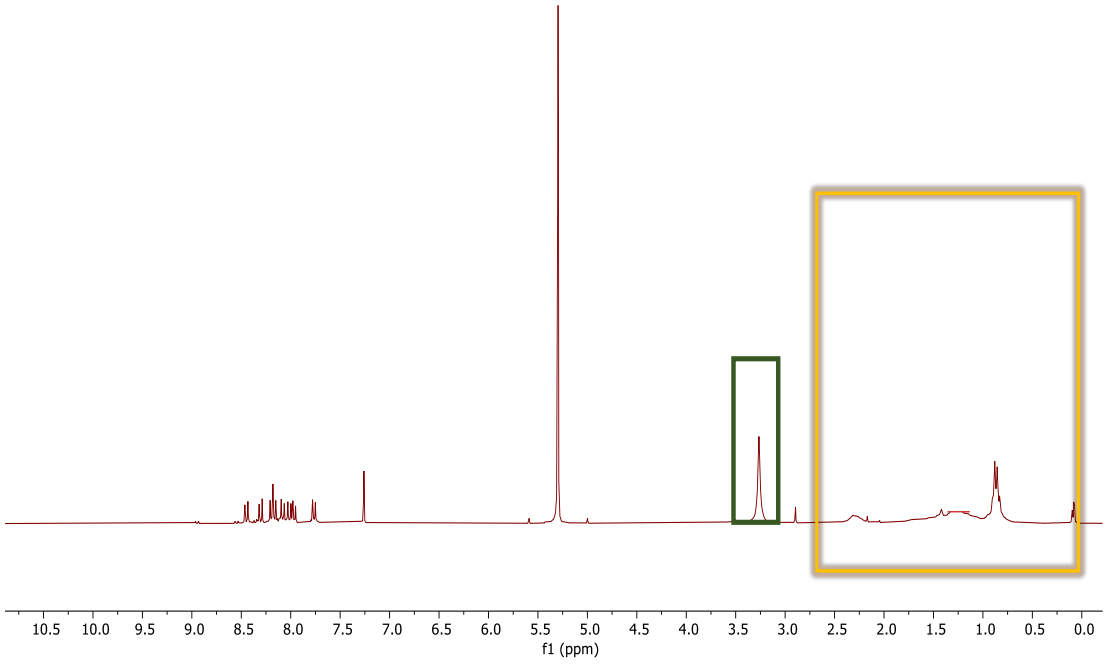


Figure 4.12. *NMR spectra of product following Boc deprotection. Absence of peaks around 1.5 ppm (orange label). Marked peak 3.2 ppm (green label).*

It was proposed that ethynyl group was sensitive to acidic conditions due to its high reactivity. Therefore, to avoid the formation of side product **21**, the reaction of Boc deprotection was conducted with the compound **18**, before the deprotection of TMS, assuming its higher stability compared to **19** (Figure 4.13). Nevertheless, formation of the undesired product **21** was still verified by mass spectra, suggesting that the instability of the TMS group was easily removed in acidic conditions and subjected to reaction.

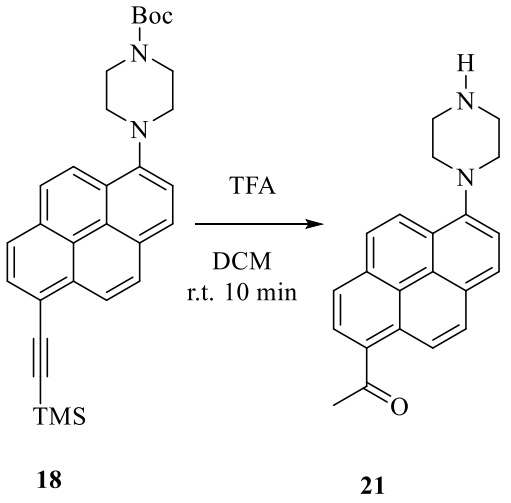


Figure 4.13. *Scheme of reaction of* ***21*** *with reaction conditions.*

Another strategy involved the Boc deprotection of **16**, followed by the introduction of TMS group (**17**). The purpose to achieve the final product **18b**, avoiding side product formation due to TMS or ethynyl group instability.

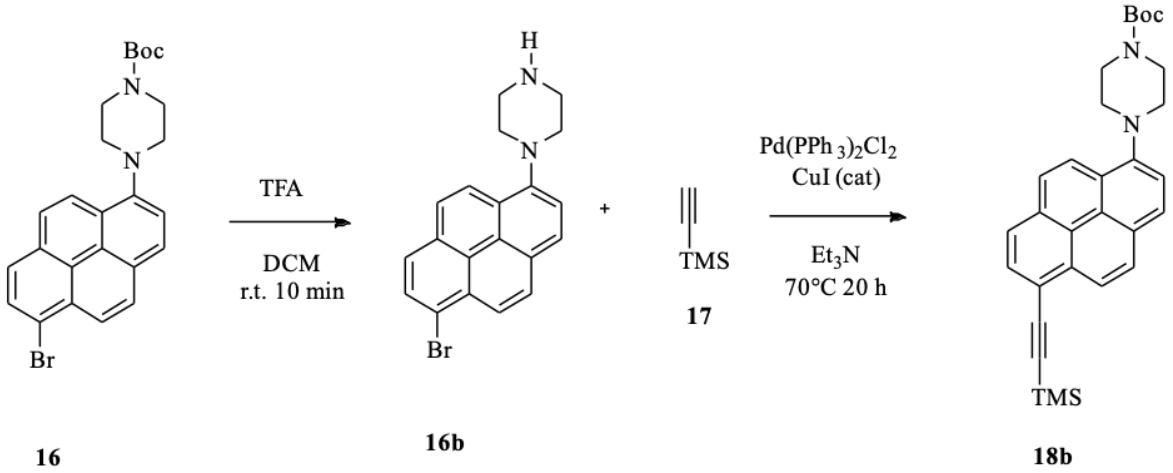


Figure 4.14. *Reaction scheme of* ***18b*** *with reaction conditions.*

However, the absence of Boc group in **16b** changed the reactivity and solubility of the reagent. The reaction employed previously to achieve **18** through Sonogashira reaction (Figure 4.14) failed to yield the product. The mass spectra reported in Figure 4.15a shows the peak attributable to the

desired **18b** (m/z 383.19-yellow circle) but also the presence of other compounds. All the products corresponding to other peaks had not been identified. However, it was expected that some may arise due to the presence of the starting material **16** not fully being deprotected, which brings the formation of side products. A preliminary TLC analysis did not reveal a suitable separation between the compounds. Moreover, the purification through column chromatography became more complex, due to the presence of the free amino group of **16b**. Another reaction was made using dimethylformamide to increase the solubility, aiming to improve the yield of **16b** and facilitating the next purification. The mass spectra reported in Figure 4.15b did not reveal the presence of the desired compound. Moreover, the boiling point of dimethylformamide (DMF) (153 °C) is higher than DCM (39.6 °C) making the removal of solvent more difficult. Since product **18** was obtained with acceptable yield (54%), focus was shifted to implementing new strategies of Boc deprotection instead.

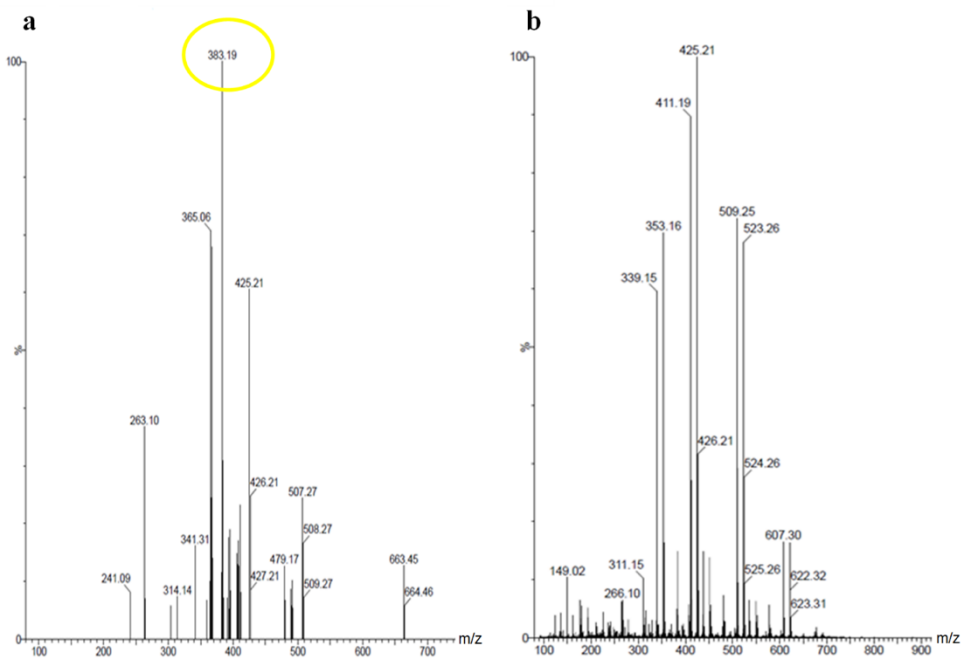


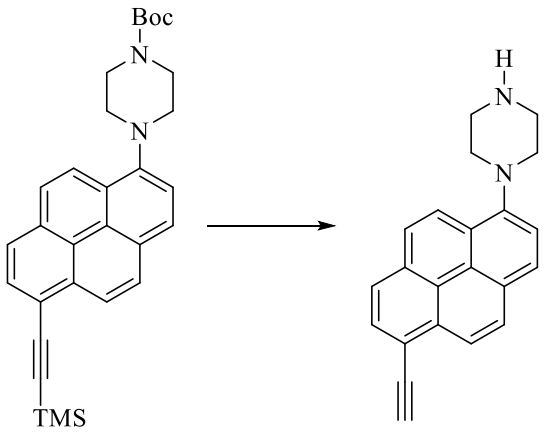
Figure 4.15. *Mass spectra following test a* ***(a)*** *and b* ***(b)*** *to achieve* ***16b****. Peak at m/z 383.19 (yellow circle) evidenced.*

As a result, new reagents for Boc deprotection were investigated. The aim was to determine the suitable pH condition of reaction,[213] required for Boc deprotection of **14,** avoiding side reaction of the TMS group. The main challenge consisted of finding a reaction under suitable acidic conditions to allow the Boc deprotection of amine group of piperazine **14** (pK_b 4-5). Different Boc deprotection procedure have been reported, depending on nature of amino group involved. Table 4.1 describes some of the methods investigated to evaluate their efficacy towards **14**.

Table 4.1 *Boc deprotection methods used* ***(a-d)****.*

Method	Conditions
a	Tetra-n-butylammonium fluoride TBAF/THF [214]
b	Fluorinated Alcohols: 1,1,1,3,3,3-Hexafluoro-2-propanol (HFIP) [215]
c	6M HCl / H_2O [216]
d	HCl (4M) / Dioxane [217]

The method **a** aimed to bring the deprotection of the TMS group and Boc at one single step to achieve the final compound **20** (Figure 4.16).



18 **20**

Figure 4.16. *Reaction scheme of* ***20*** *according to method* ***a****.*

The first attempt was made at room temperature, but deprotected product was not observed, so the reaction was attempted at a higher temperature (70°C). The comparison between NMR spectra reported in Figure 4.17 before (1) and after (2) the reaction shows the presence of the Boc peak in both spectra (~1.5 ppm-green arrow). Whereas the TMS group peak (purple arrow) is absent in spectrum 2 (Figure 4.17), meaning the conditions employed were suitable for TMS deprotection

but not for the deprotection of the Boc group. Further experiments with a longer reaction time (overnight) did not show the desired product either.

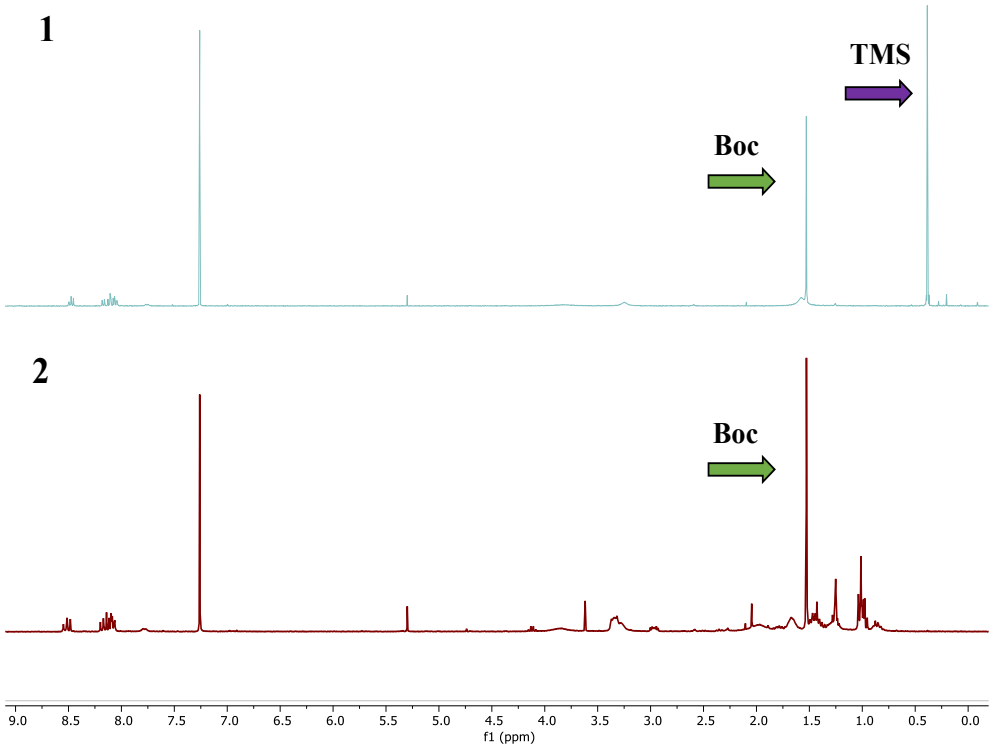
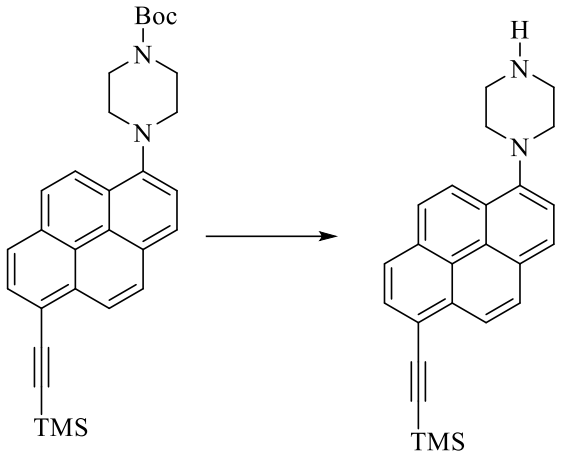


Figure 4.17. *Comparison between NMR spectra before (1) and after the reaction (2) reported in Figure 4.14, following condition of method* ***a*** *as reported in Table 4.1. Boc (green) and TMS (purple) peak evidenced with arrows.*

The literature procedure,[214] adapted for method **a**, was employed for aromatic and heterocyclic aromatic amine with pKa 9-10 and pKb 7-8 respectively. The reason for the unsuccessful reaction was attributed to the difference in basicity of the amines employed in the literature compared to piperazine **14** (pKb 4-5). As aromatic amines are less basic (pKa 9-10 and pKb 7-8), they were more easily subjected to Boc deprotection under mild conditions. Since the deprotection of Boc required selective conditions, the next methods (**b-d**) were focused only on Boc deprotection, as shown in the figure below.



18 **18b**

Figure 4.18. *Reaction scheme of* ***18b****.*

As reported in the literature, fluorinated alcohols,[215] can be exploited as solvents for Boc deprotection. Thus, method **b** employed HFIP as the solvent at reflux temperature, aiming to achieve the cleavage of Boc, without affect the reactivity of TMS group. Although the literature [215] reported its successful application to piperazine compounds, the mass spectra of the reaction product revealed the predominant presence of the starting material **18** (m/z 483), suggesting low conversion to the final product **18b** (m/z 383.19). This can be attributed to a different reactivity of the piperazine once bound to pyrene.

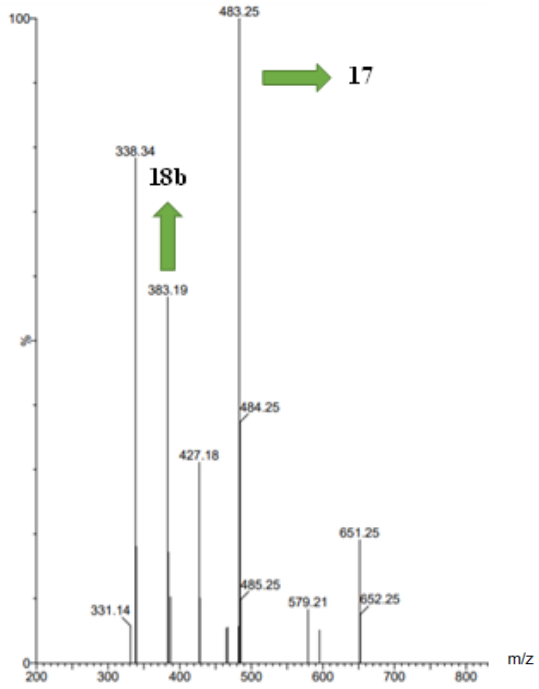


Figure 4.19. *Mass spectra following the scheme reported in Figure 4.18 according to condition of method* ***b****, reported in Table 4.1.Peat at m/z 383 (****18b****) and 483 (****17****) evidenced with green arrows.*

Assuming that Boc deprotection needed stronger conditions, method **c,** an aqueous solution of HCl was used. However, as with the previous method, Boc deprotection was not achieved, possibly due to the low solubility of starting material **18** in aqueous solution. Consequently, alternative solvents such as dioxane, was investigated, adapting the reported procedure.[217] A longer reaction time (5h) compared to the original procedure (30 min) was employed. Decisively, with these conditions, deprotection was successful as seen in the NMR spectrum reported in Figure 4.20 (left). Whilst the Boc group peak was absent, the peak representing the TMS group was present. Although the mass spectra (Figure 4.20 right) showed the presence of the desired compound **18b** (m/z 383), the fully deprotected compound **20** was also revealed, signifying the presence of mixed

products. However, it was believed that having mixed product would not cause a problem in the following reaction, because undesired product, methyl ketone **21**, is absent.

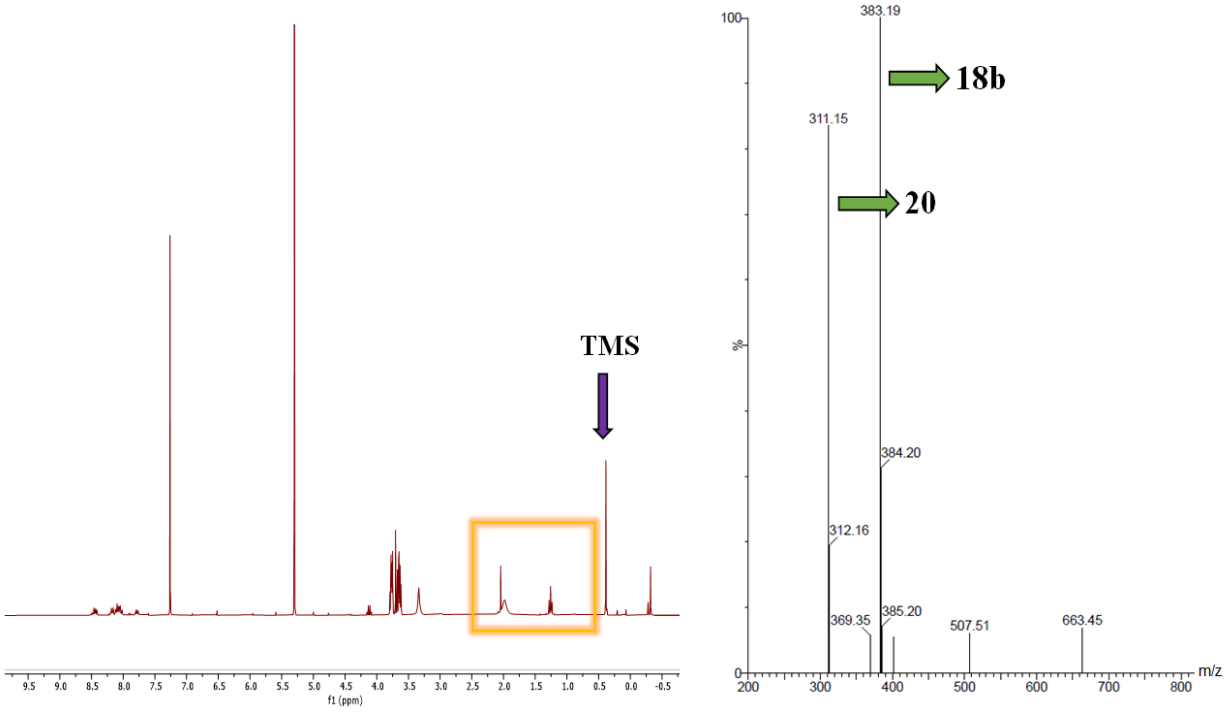
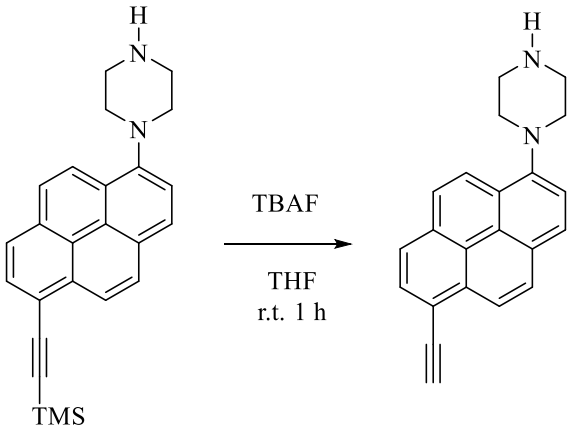


Figure 4.20. *NMR (left) and mass spectra (right) of reaction product following the scheme reported in Figure 4.18, according to condition of method* ***d*** *as reported in Table 4.1. In NMR spectra TMS peak (purple arrow) and absence of Boc peak (orange label). In MS spectra, peak at m/z 311 (**20**) and 383 (**18b**) are evidenced with green arrows.*

Following the successful deprotection of the Boc group, the next reactions involved the total deprotection of TMS group, allowing the subsequent reaction with boronic acid derivative **3b**.



18b **20**

Figure 4.21. *Reaction scheme to achieve **13**, from starting **18b**, previously subjected to TMS deprotection (**20**).*

The reaction of TMS deprotection was performed with a solution of 1M of TBAF in dry THF. The reaction was verified by comparison of NMR spectra of **18b** and **20 (**Figure 4.22), the absence of TMS peak (purple arrow) in the NMR corresponding to **20**, suggested that successful deprotection had occurred.

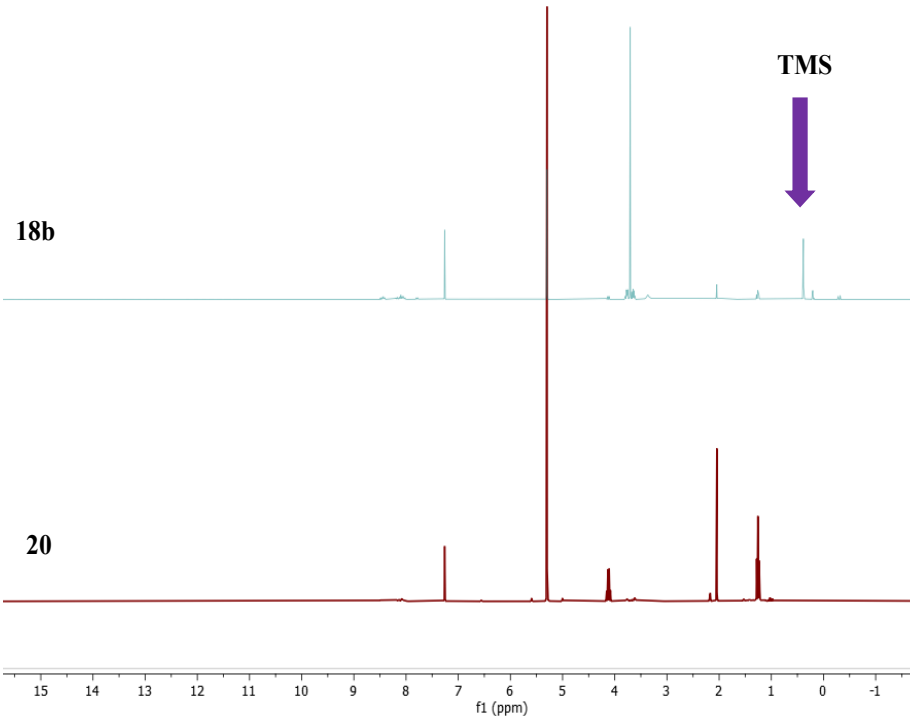


***Figure 4.22**. Comparison NMR spectra of **18b** and **20** with TMS peak evidenced with purple arrow.*

The mass spectra in Figure 4.23 shows the presence of some undesired product. The peak **1** (m/z 242.99) was attributed to tetrabutylammonium as a residue from the reaction with TBAF. The peak **2** (m/z 311.16) corresponded to the desired product **20** [$M+H^+$]. The peak **3** (m/z 399.21) was thought to be a complex between the final product **20** (without TMS) and a residue of solvent (dioxane) from the previous Boc deprotection according to the conditions of method **d** (Table 4.1).

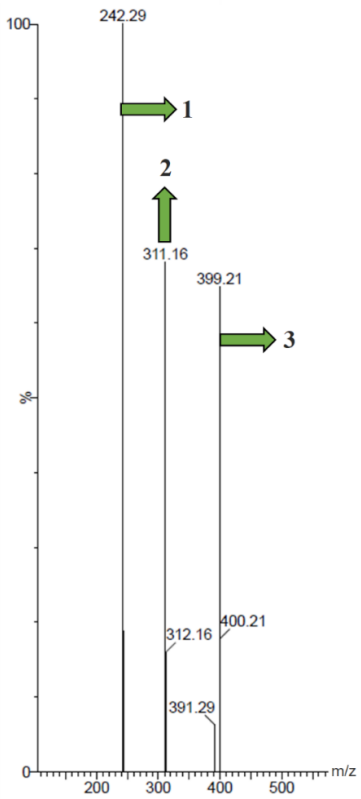


Figure 4.23. *Mass spectra of reaction product followed the scheme reported in Figure 4.21.Peak at m/z 242.29 (**1**), 311.16 (**2**) and 399.21 (**3**) evidenced with green arrows.*

As the presence of residual solvent (dioxane) was observed following the method **d** (Table 4.1) for Boc deprotection, so new reactions conditions were investigated. The aim was also to prevent the deprotection of TMS group (**18b**), and the formation of mixed products as seen in the mass spectra reported in Figure 4.20. Two alternative methods, **e** and **f**, reported in Table 4.2 were investigated to selectively deprotect the Boc group, leaving the TMS group intact.

Table 4.2. *Boc deprotection method approached (**e-f**).*

Method	Conditions
e	HCl (2M) / Et_2O [218]
f	HCl (4M) / MeOH [219]

Reaction conditions following method **e** did not produced a complete Boc deprotection. Assuming the concentration of HCl used was too low (2M), method **f** used a more concentrated HCl solution (4M) in MeOH, to enhance the solubility of starting material **18**. Moreover, it was assumed the use of MeOH as solvent allowed the easier purification of the desired product through a silica chromatographic column. The separation of the pure desired product was achieved by employing a short chromatographic column and the slow addition of MeOH. The Figure 4.24 reports the NMR spectra of **18** (**a**) in which the Boc group (~1.5 ppm) was still present and of the product **18b** (**b**) where the Boc peak is absent. Additionally, the TMS peak was present in both spectra.

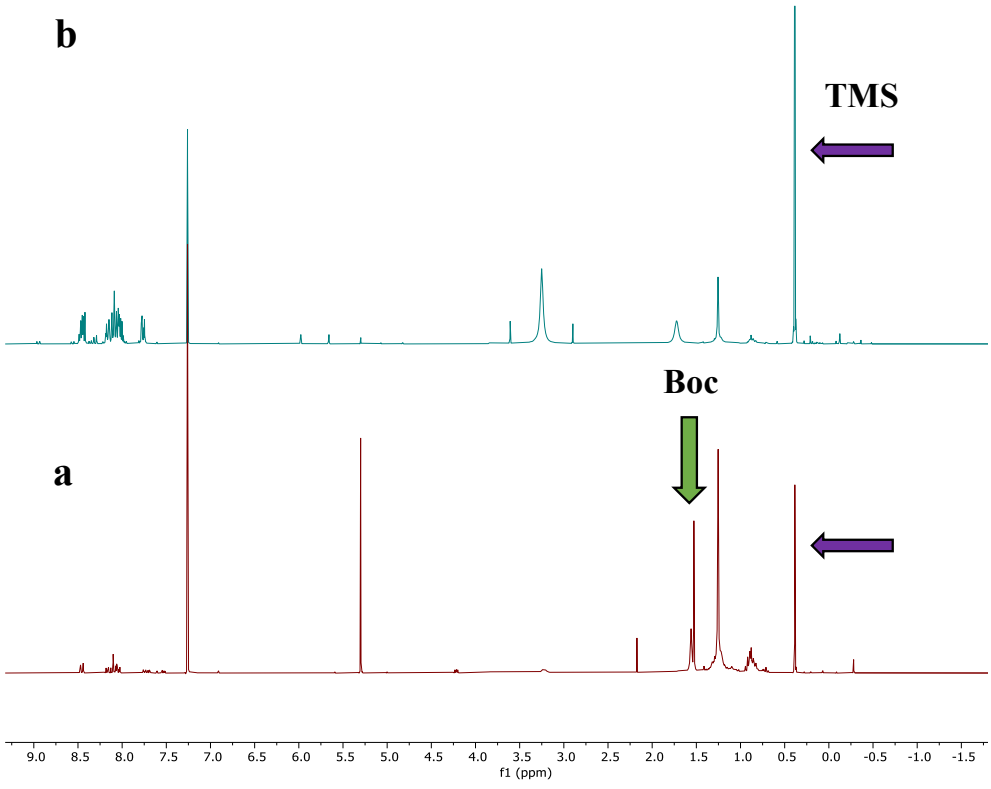
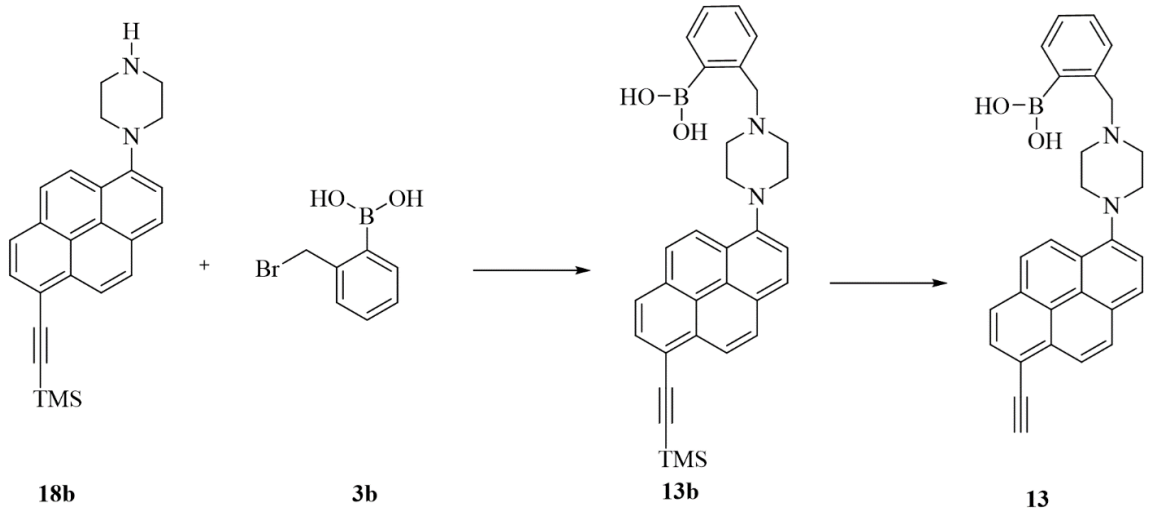


Figure 4.24 *Comparison NMR spectra of the two fraction,* ***a*** *and* ***b****, isolated by chromatographic column of reaction product following conditions of method f as reported in Table 4.1. TMS (purple) and Boc peak (green) evidenced with arrows.*

In contrast with the reaction scheme reported in Figure 4.21, a new approach provided the TMS deprotection as the final step following the reaction between **18b** and **3b**. It was expected that the presence of the ethynyl group could affect the reaction, due to reaction competition of **3b** with thus group. Figure 4.25 reports the reaction scheme adopted.



18b **3b** **13b** **13**

Figure 4.25. *Reaction scheme to achieve **13** though formation of **13b**.*

To preserve the TMS group, the reaction with boronic **3b** was performed in mild conditions: weak base as Et_3N, dry solvent (DMF) and at room temperature. The completion of the reaction was verified by TLC analysis and confirmed by NMR and mass spectra. By comparing the NMR spectra, the distinctive groups of the starting material **3b** and **18b** in the spectra of product **13b** can be observed (Figure 4.26). The peak relative to **3b** is at 7.2 ppm (yellow label) and the TMS peak of **18b** at 0.5 ppm (purple label). The mass spectra also confirmed the presence of desired product (Figure 4.27). The main peak (m/z 517) was attributed to the desired product **13b**, while the small peaks were ascribed to **13**, the fully deprotected product (m/z 445).

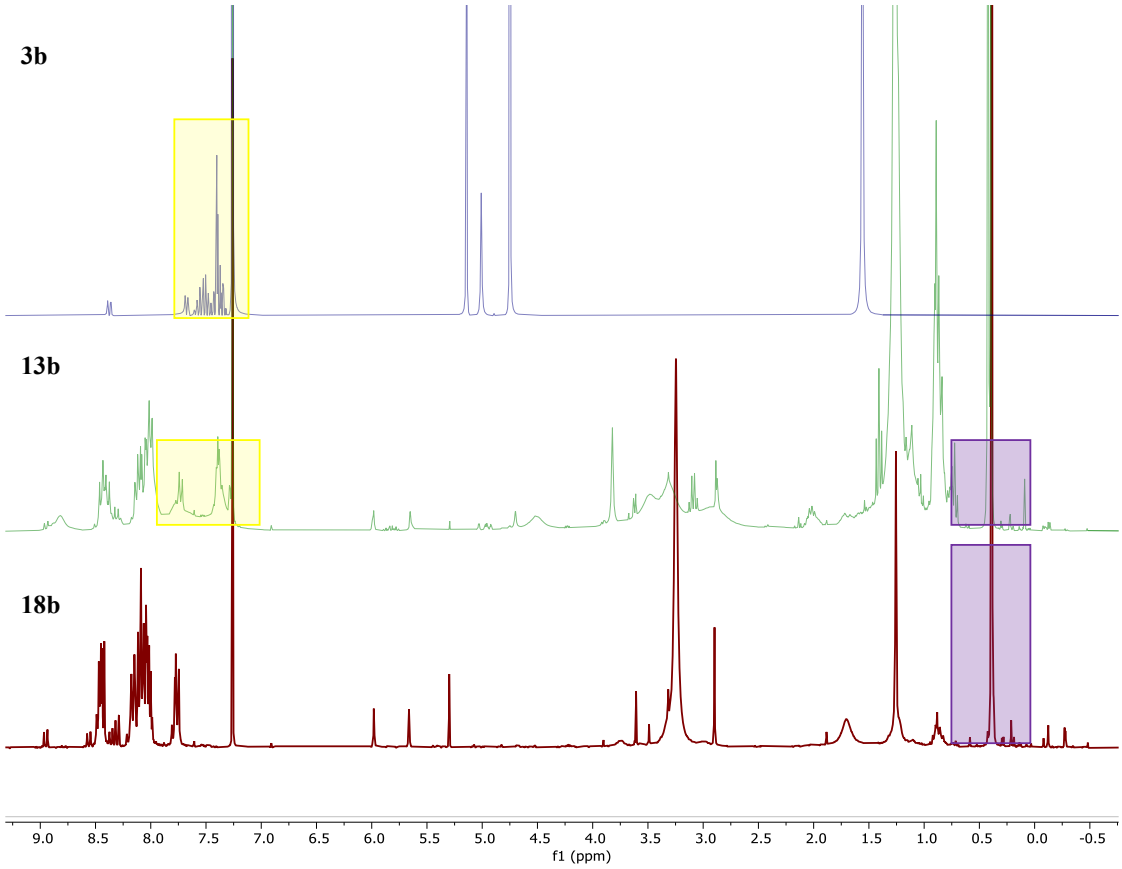


***Figure 4.26**. Comparison NMR spectra of **3b**, **18b** and **13b**. Peaks at 7.2 ppm (yellow) and 0.5 (purple) evidenced.*

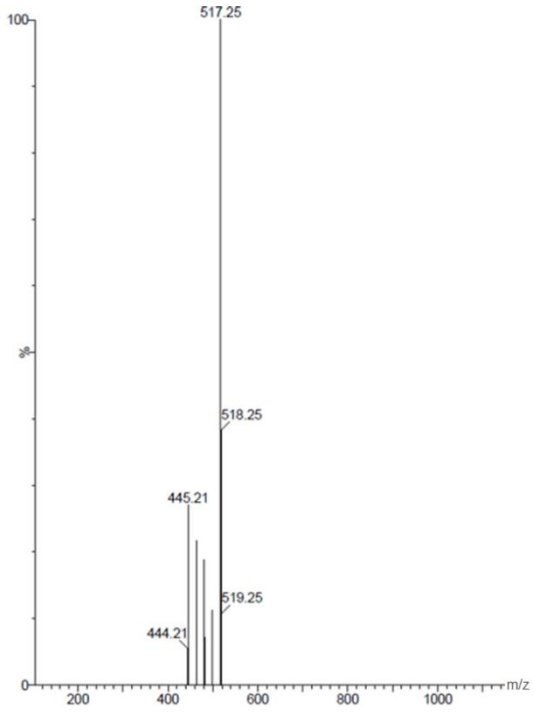


Figure 4.27. *Mass spectra of expected product* ***13b*** *following the scheme reported in Figure 4.25.*

Because of the previous issues with the purification of amine and boronic acid compounds, **13b** was analysed by LC-MS to evaluate the conditions for a further separation through preparative HPLC. The method, already employed in the previous chapter for sensor **7**, involved an eluent system of water and MeCN + TFA 0.1 %, following the gradient condition reported in Table 4.3.

Table 4.3. *Gradient condition followed to achieve chromatograms reported in Figure 4.28.*

Method	Time	Water %	MeCN + TFA 0.1 TFA %
a/a2		30	70
	30	0	100
	35	0	100
	35.10	30	70
	40	30	70

In the chromatogram reported in Figure 4.28, the main peak is seen at RT 20.02. Analysis of mass spectra (right) demonstrated that the peak corresponded to the desired product **13b** (m/z 517). The compound was successfully isolated through preparative HPLC and verified by NMR spectra.

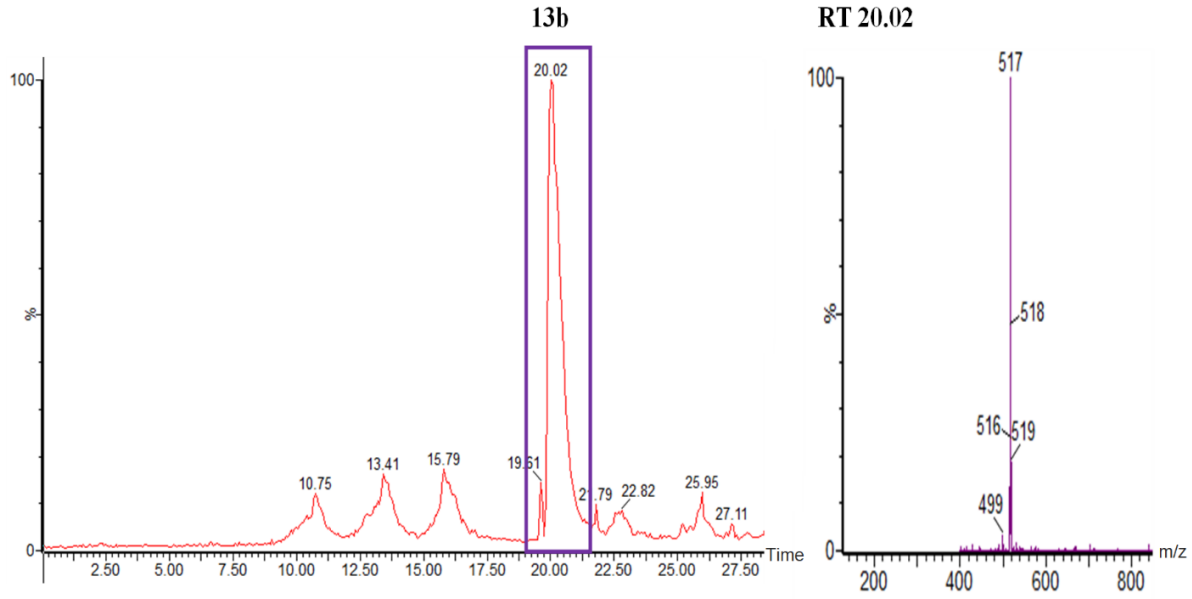


Figure 4.28. *LC-MS chromatogram of* ***13b*** *following method reported in Table 5.2. Peak at RT 20.02 (purple label) evidenced. Mass spectra of peak at RT 20.02 (right)*

Moreover, the successfully separated compound **13b** was noticeable in LC-UV chromatograms, reported in Figure 4.29. The purity level of the compound was estimated at *86* % by integration of the main peak at RT 20.25.

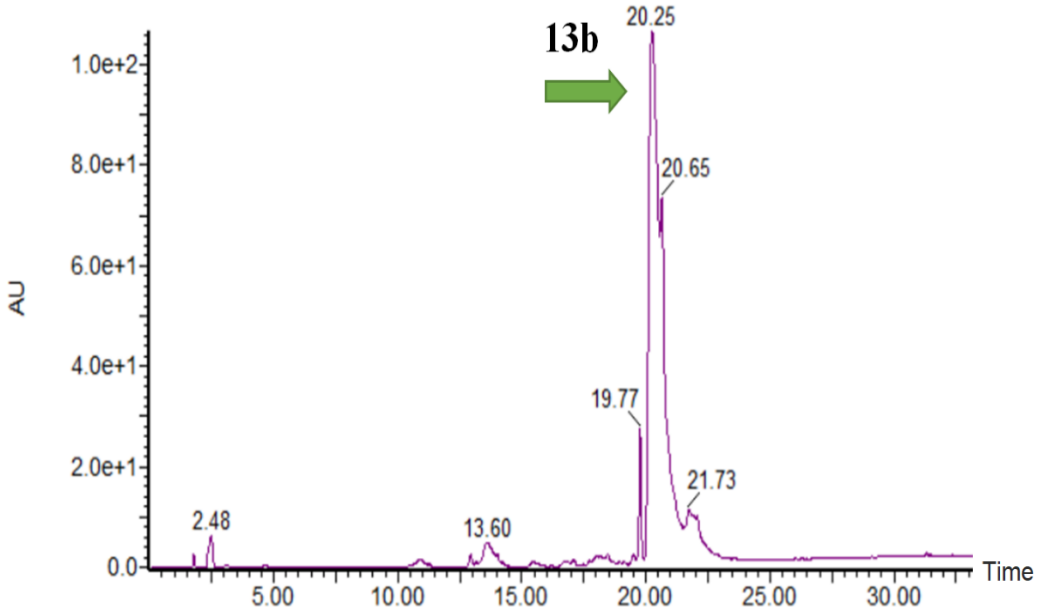
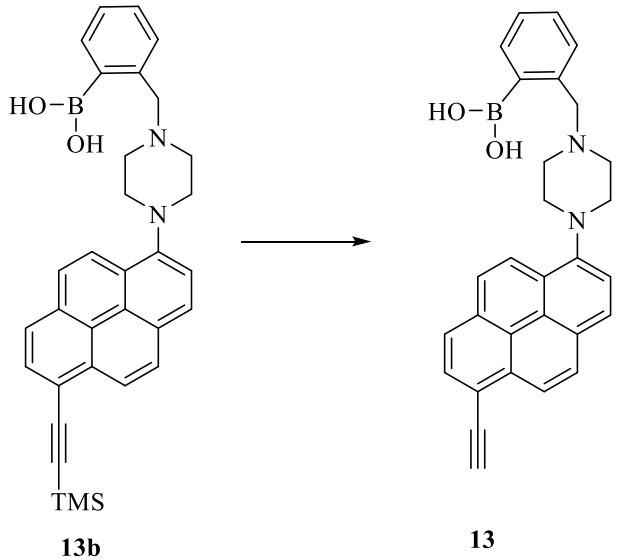


Figure 4.29. *LC-UV chromatograms of* ***13b****. Peak at RT 20.25 (green arrow) evidenced.*

The next step concerned the TMS deprotection to yield the final sensor **13**, employing the same conditions used previously (TBAF/ THF).



13b **13**

Figure 4.30. *Reaction scheme for synthesis of* ***13****.*

Since the absence of characteristic TMS peak in the NMR spectra of **13**, it was assumed that successful deprotection had occurred. However, the comparison between NMR spectra of the compound before (**13b**) and after the reaction (**13**) suggested the formation of a side product. Some unexpected peaks were also seen, as highlighted in orange in Figure 4.31.

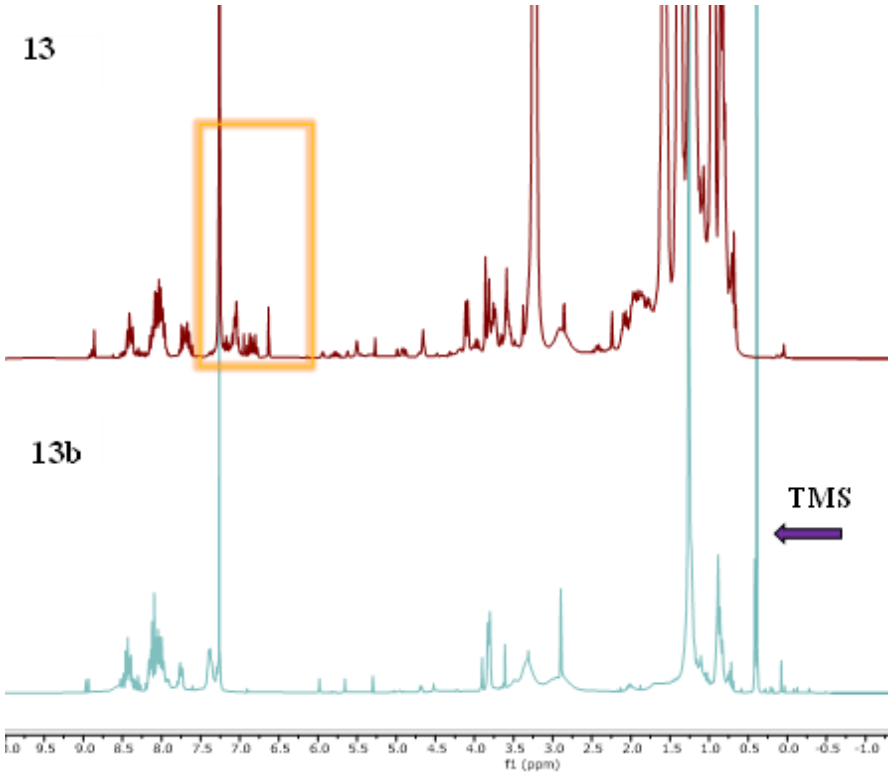


Figure 4.31. *Comparison NMR spectra of* ***13*** *and* ***13b****, following the reaction scheme reported in Figure 4.29. Interested peak (orange) and TMS (purple arrow) evidenced.*

In support of this, the mass spectra reported in Figure 4.32 confirmed the presence of an undesired product. The peak **1** (m/z 242.29) was attributed to tetrabutylammonium as second product following the reaction with TBAF, as previously observed (Figure 4.23). The peak **3** (m/z 446.22) referred to the desired product **13**, while peak **2** (m/z 418.20) was attributed to the oxidized product on BA moiety (**22**) as reported in Figure 4.32.

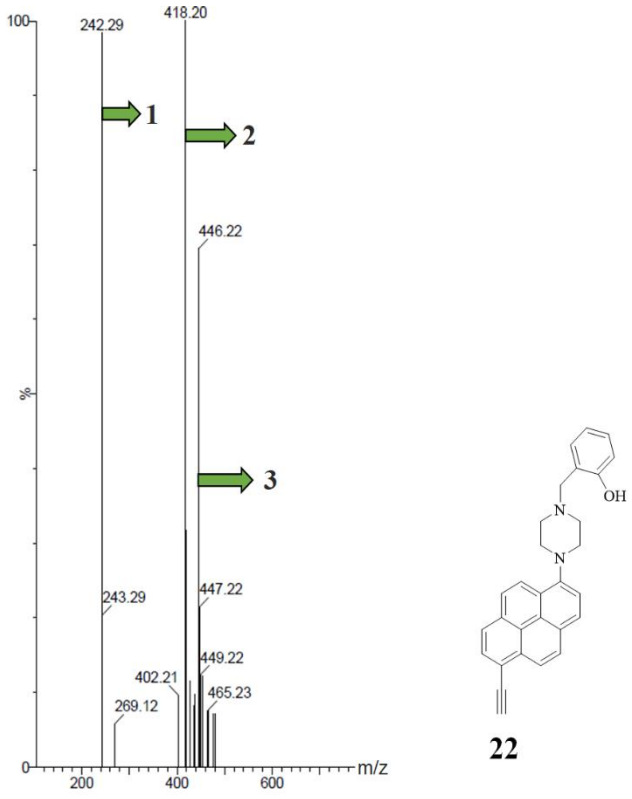


Figure 4.32. *Mass spectra of reaction product, following scheme reported in Figure 4.25, with peak* ***1*** *(m/z 242.29)* ***2*** *(418.20) and* ***3*** *(446.22) evidenced (left). Chemical structure of* ***22*** *(right), attributable to peak* ***2****.*

As reported in the literature, some boronic acid derivatives can be subjected to oxidation or even protodeboronation at select conditions.[218] Additionally, the presence of amino atoms such as piperazine in closer proximity can strengthen this propensity.[220] The process was described to be promoted by high temperatures, basic conditions and radical-generating solvents, as for example THF, employed for the deprotection reaction of TMS. In face of these results, TMS deprotection was performed following an alternative procedure. Sodium carbonate in MeOH was selected over TBAF to avoid the tetrabutylammonium impurities observed before. The reaction was conducted at room temperature and the reaction time was increased to support the complete conversion of

starting material. The expected product was achieved following the new conditions and was analysed by LC-MS. The gradient conditions were maintained as reported in Table 4.3 while different combinations of solvents were investigated, as shown in Table 4.4.

Table 4.4. *Gradient condition, applied to achieve chromatogram reported in Figure 4.33.*

Method	Solvent 1 (%)	Solvent 2 (%)
a	Water	MeCN + TFA 0.1%
b	Water	MeCN + FA 0.1 %
c	Water	MeOH + TFA 0.1 %
d	Water	MeOH + FA 0.1 %

The Figure 4.33 shows the chromatograms corresponding to the different methods (**a**-**d**) used. As shown in Figure 4.33 the greatest separation between the desired product **13** (orange label) and the oxidised product **22** (green label) was achieved though method **d**. Latter gradient conditions were applied for the purification of the reaction product through preparative HPLC.

.

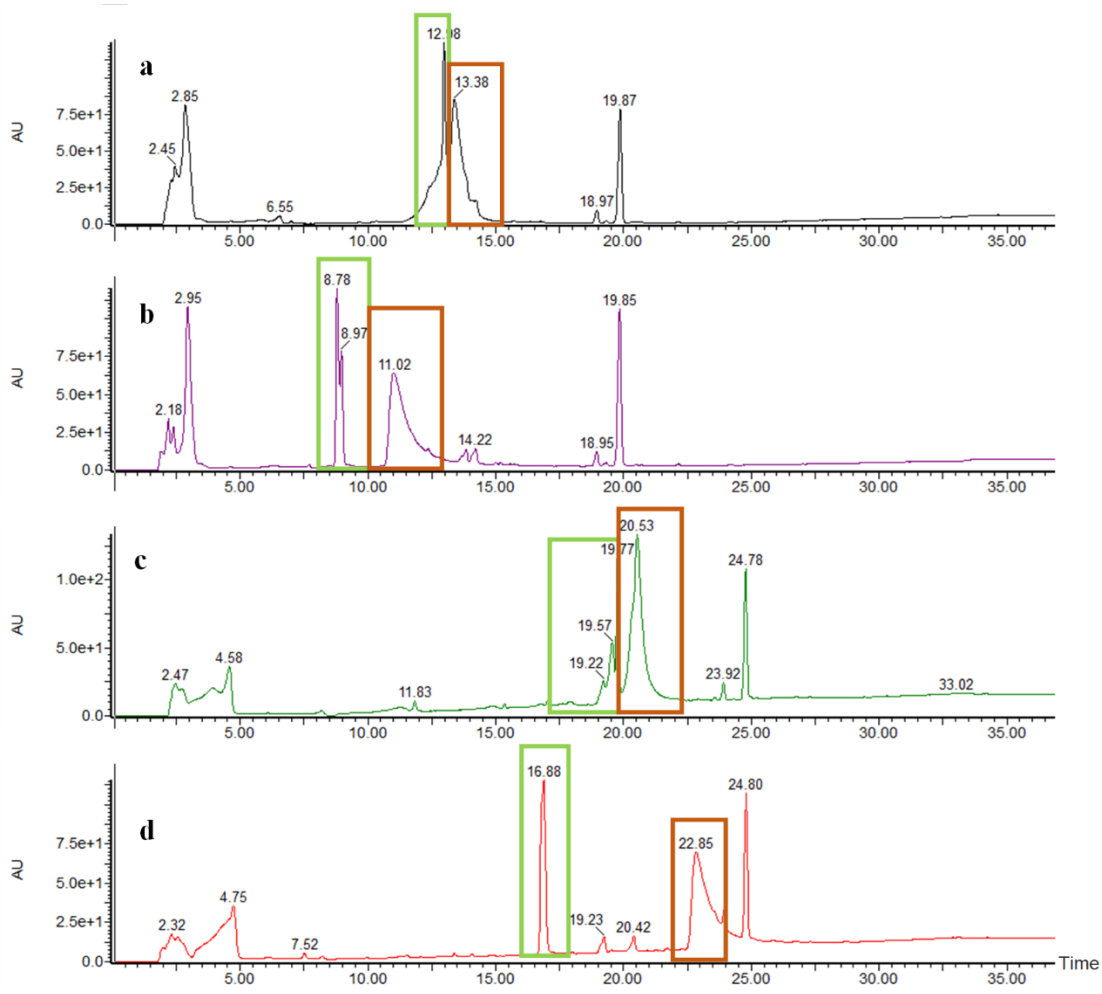


Figure 4.33. *Chromatograms of reaction product **13** (Figure 4.29) following method **a-d**, according to gradient conditions reported in Table 4.4. Peak of **13** (orange label) and **22** (green label) evidenced.*

The purified compound was analysed by LC-MS, as reported in Figure 4.34. Analysis of the peaks 1 (RT 17.02) and 2 (RT 22.60) by mass spectra suggested the separation was not successful in contrast to what has been observed in the chromatograms **d** reported in Figure 4.33. Peaks 1 and 2 were attributed to the phenol **22** (1) and to the desired **13** product (2) respectively.

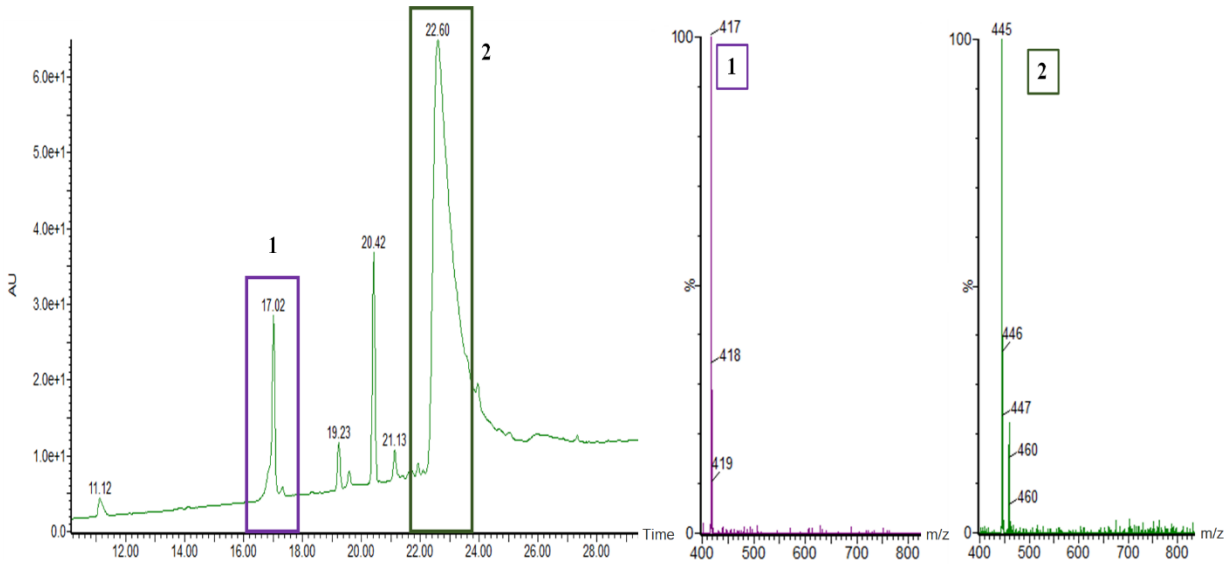


Figure 4.34. *UV chromatogram by LC -UV of **13** following HPLC preparative (left). Peak at 17.02 (1-purple) and 22.60 (2-green) evidenced. Mass spectra of peak **1** (RT 17.02) and **2** (RT 22.60) (right).*

It was concluded that the boronic acid moiety was very sensitive to the temperature and to the basic conditions that were required for TMS deprotection. To avoid side reaction of the BA moiety under these required conditions, 2-Bromomethylphenylboronic acid pinacol ester **3c** was selected as an alternative method to achieve the final product. It had not been selected previously because it implied an addition step of deprotection. The reaction scheme reported in Figure 4.35 shows the strategy adopted.

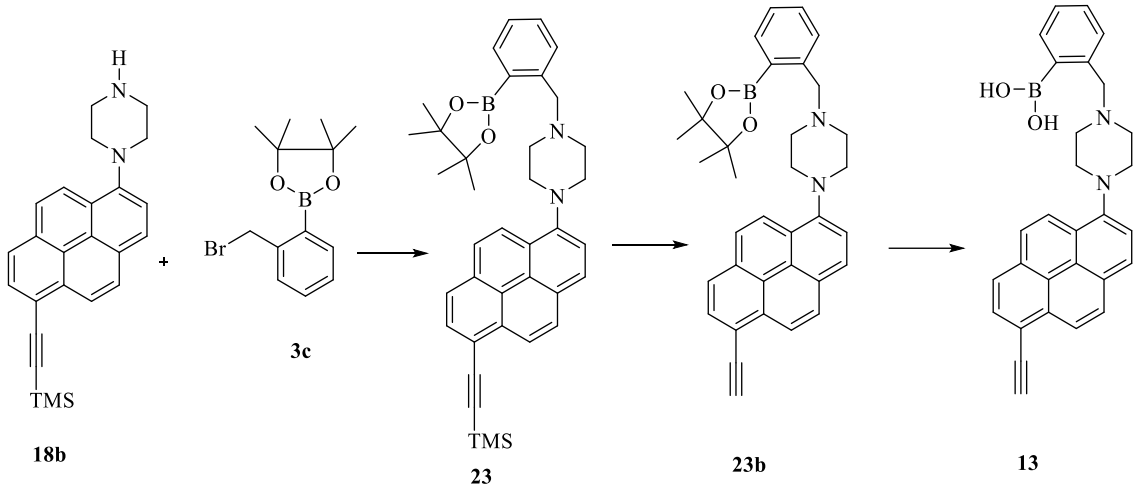


Figure 4.35. *Reaction scheme to achieve **13**, involving **3c**.*

The compound **18b**, containing the TMS group, was subjected to further purification by preparative HPLC, following the gradient reported in Table 4.3 (Water/ MeCN plus TFA 0.1 %). Neutralization of TFA before the complete removal of solvent was required to avoid the formation of side product such as ketone **21**. To avoid the deprotection of TMS group which occurs in basic conditions, a mild base such as Et_3N or a solution of solid sodium carbonate was employed. However, even in the mild basic condition used, the formation of side product **21** and the deprotection of TMS group was still seen. Instead, the solution was successfully treated with a basic resin which allowed the complete neutralization of TFA without adding any reagents that may affect future reactions.

Figure 4.36 shows the comparison of LC-UV chromatograms of the **18b** before (1) and after (2) being subjected to preparative HPLC. In chromatogram 2, a single peak was observed, confirming the purity of the compound.

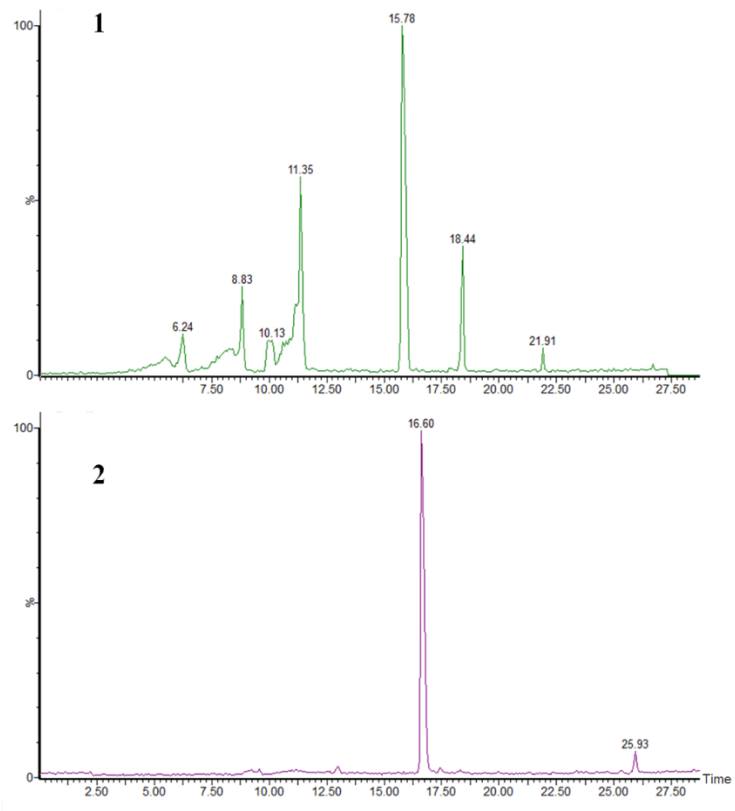


Figure 4.36. *LC-UV chromatograms of* ***18b*** *before (1) and after (2) HPLC preparative.*

Next, the reaction of **18b** with **3c** was conducted (Figure 4.35) in the same conditions employed for **3b,** with triethylamine (Et_3N) as base, in DMF and at room temperature (24h). Figure 4.37 reports the mass spectra of the reaction. It is possible to observe a main peak (m/z 318.26), that was attributed to an undesired compound due to the reaction between **3c** and Et_3N.

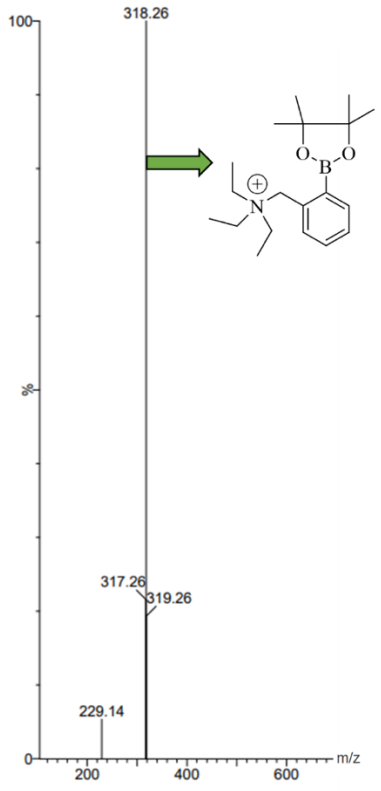


Figure 4.37. *Mass spectra of product of reaction between* ***18b*** *and* ***3c****, using* Et_3N*.Peak at 316.26 evidenced. Chemical structure of relative compound is reported.*

The reaction was repeated employing K_2CO_3 as base (two equivalent), increasing the reaction time (48h) to enhance the conversion of starting material **18b**. The reaction successfully yield product **23**, that was analysed though LC-MS for the next purification. Table 4.5 reports the eluent systems evaluated for this LC-MS analysis. The gradient conditions were maintained the same as reported in Table 4.3, but solvents (Table 4.5) were modified to look for a good separation.

Table 4.5. *Methods applied to achieve chromatogram reported in Figure 4.37.*

Method	Solvent 1 (%)	Solvent 2 (%)
e	Water	MeCN + TFA 0.1 %
f	Water	MeCN + FA 0.1 %
g	Water	MeOH + TFA 0.1 %
h	Water	MeOH +FA 0.1 %
i	Water	MeCN + TFA 0.05 %
j	Water	Buffer pH 5

Analysis of the mass spectra of each chromatogram peak determined that desired product **23** possessed the highest RT, as indicated with red labels in Figure 4.38. With method **h**, **23** was less noticeable compared to all the other chromatograms. In the chromatograms **e**, **f** and **g,** a second peak was also seen, attributable to **13b**, that arises from the deprotection of alkyl pinacolyl boronate esters (yellow label). The reason was attributed to the acidic conditions employed for the separation.

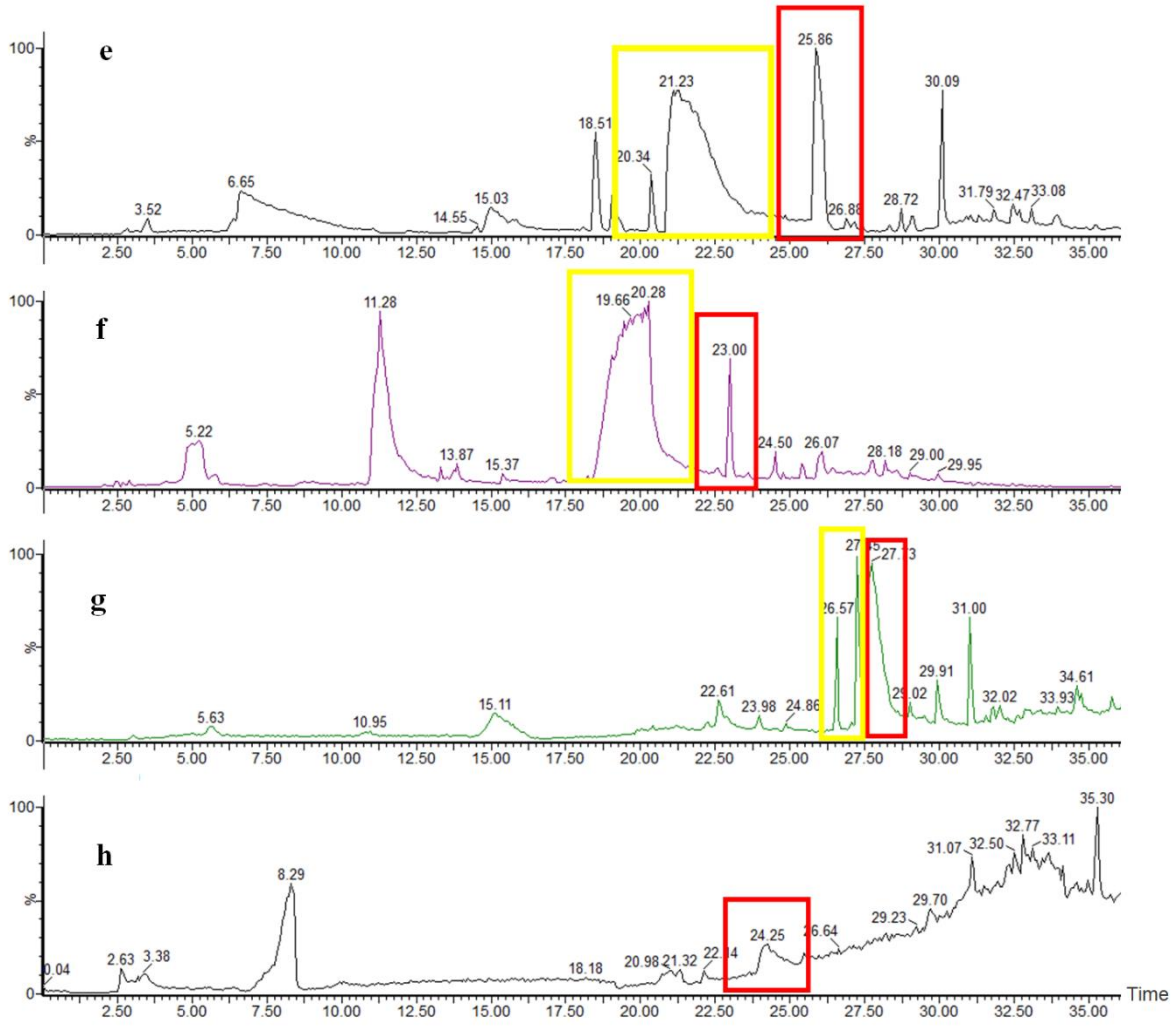


Figure 4.38. *Chromatograms of reaction product* ***23*** *(Figure* 4.35*) following method* ***e-h****, described in Table 4.5. Peak of* ***13b*** *(yellow label) and* ***23*** *(red label) evidenced.*

Thus, two alternative methods involving milder conditions were investigated; a solution of MeOH with a lower percentage of TFA 0.05 % (**i**) compared to previous methods (0.1 %), and a buffer solution at pH 5 (**j**). However, the peak attributable to **13b** was still noticed in both chromatograms, as indicated in yellow in Figure 4.39.

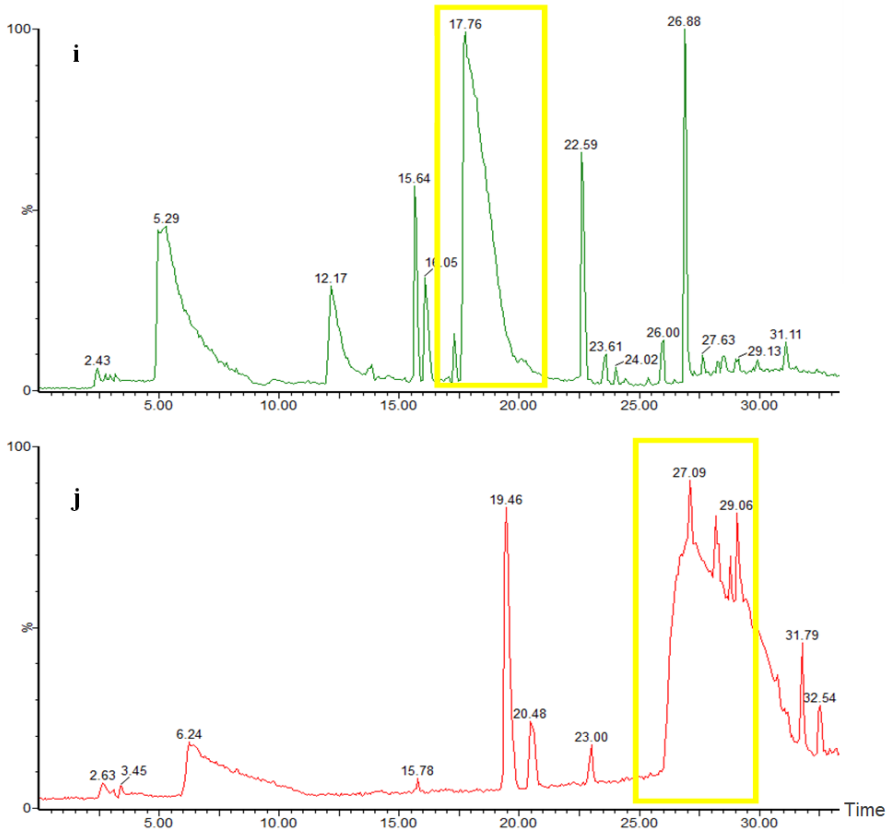


Figure 4.39. *Chromatograms of reaction product* ***23*** *(Figure* 4.35*) following method* ***i-j****, described in Table 4.5. Peak of* ***13b*** *(yellow label) evidenced.*

After comparison of the results, method **e** led to the most effective separation. Thus, these conditions were applied to yield the final product by preparative HPLC. HPLC chromatograms revealed two different peaks (Figure 4.40left). The mass spectra of the isolated fractions 1 and 2 (right) identified a mixture of product that involves both **23** and **13b**, suggesting separation had not been successful.

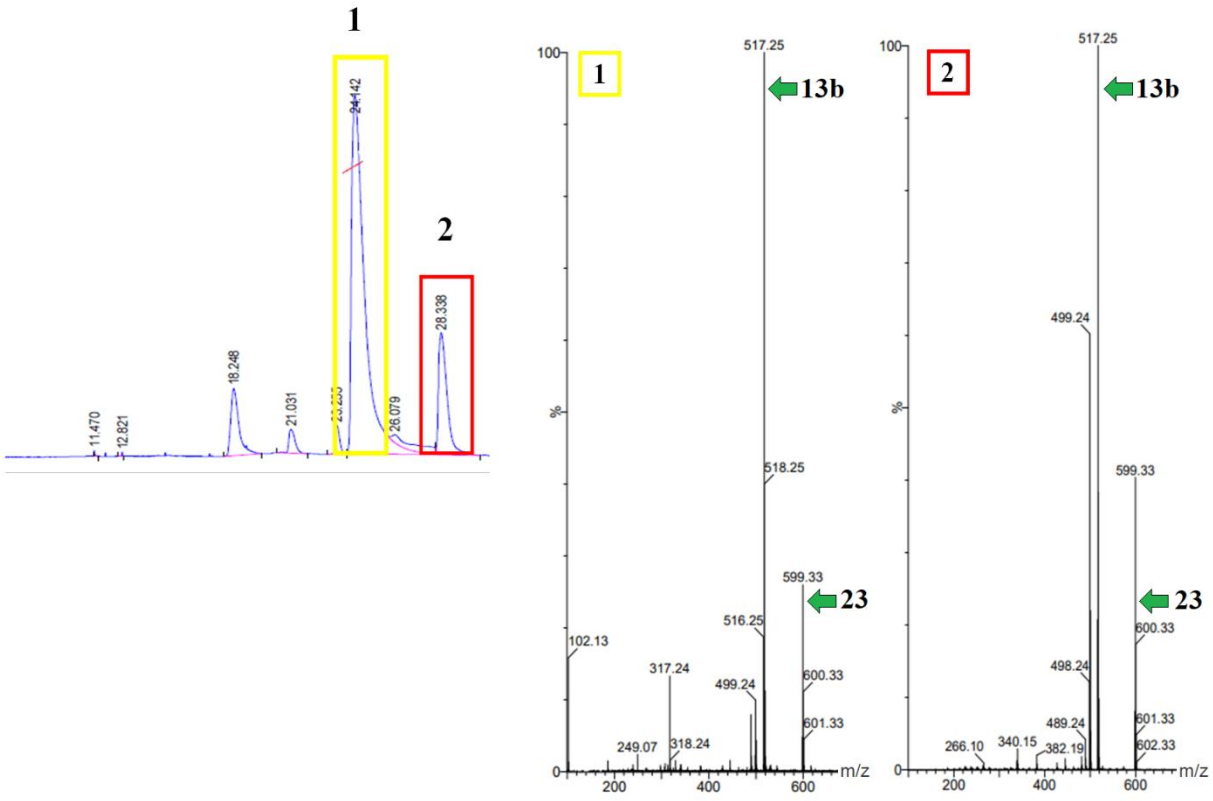


Figure 4.40. *HPLC chromatograms of product **23** according to method **e** reported in Table 4.5. Mass spectra relative to fraction collected at peak **1**(yellow label) and **2** (red label) (right).*

Due to these results, it has been agreed to perform the next step of the synthesis (Figure 4.43) without steps of purification of the intermediate products. The aim was to avoid side or undesired product due to the possible conditions employed during the purification. The deprotection of the TMS group to achieve **23b** was performed with sodium carbonate (Na_2CO_3) to avoid the formation of side product **21**. The reaction was confirmed by mass spectra as reported in Figure 4.41, where the main peak (m/z 527.29) was attributed to **23b**.

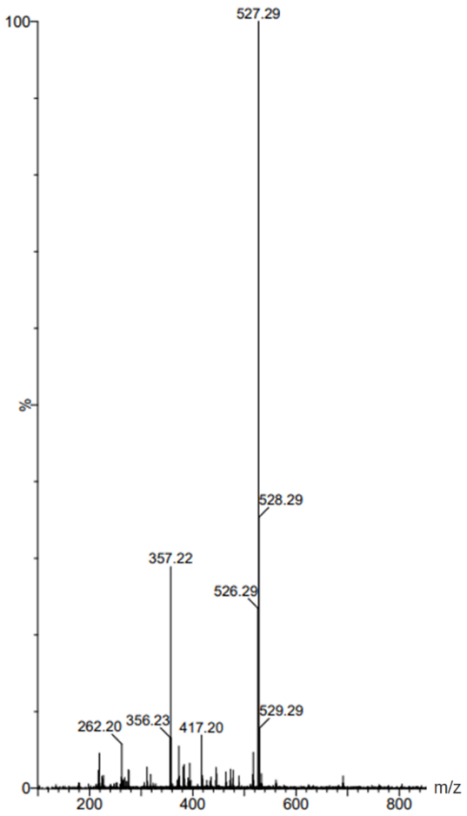


Figure 4.41. *Mass spectra of reaction product following TMS-deprotection of* ***23*** *(Figure 4.35).*

The last step involved the deprotection of alkyl pinacolyl boronate esters in **23b** (Figure 4.35). Two methods have been investigated to achieve the successful deprotection. The first one employed the use of diethanolamine (DEA) according to a literature procedure.[221] The deprotection reaction was expected to occur through transesterification with diethanolamine (DEA) followed by acid hydrolysis. The mass spectra of reaction product revealed the formation of the DEA-boronate compound, as reported in Figure 4.42 (m/z 586.31). However, the followed reaction of hydrolysis was insufficiently efficacious to achieve the final product.

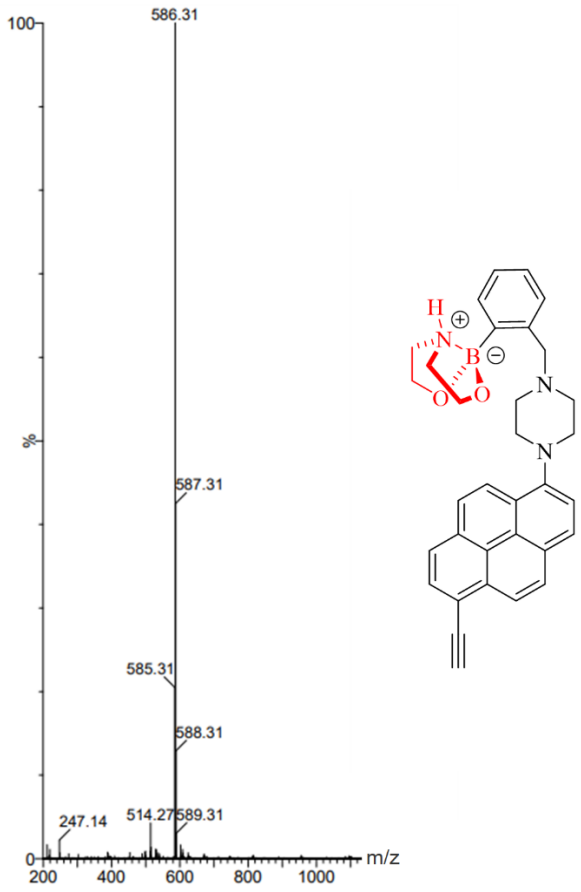


Figure 4.42. *Mass spectra of reaction product following the first method for the deprotection of alkyl pinacolyl boronate esters. Chemical structure of relative compound is reported.*

The second method to achieve the deprotection of alkyl pinacolyl boronate esters employed methylboronic acid as reagent, as reported in the literature.[222] The reaction was performed under mild acidic conditions to preserve the ethynyl groups. Due to the risk of formation of the oxidized product, the reaction was handled avoiding any source of heat. The final product was verified by mass spectra as reported in Figure 4.43. Regardless of the presence of the mass attributable to **13** (m/z 445.21)**,** the presence of a mixture of products was apparent.

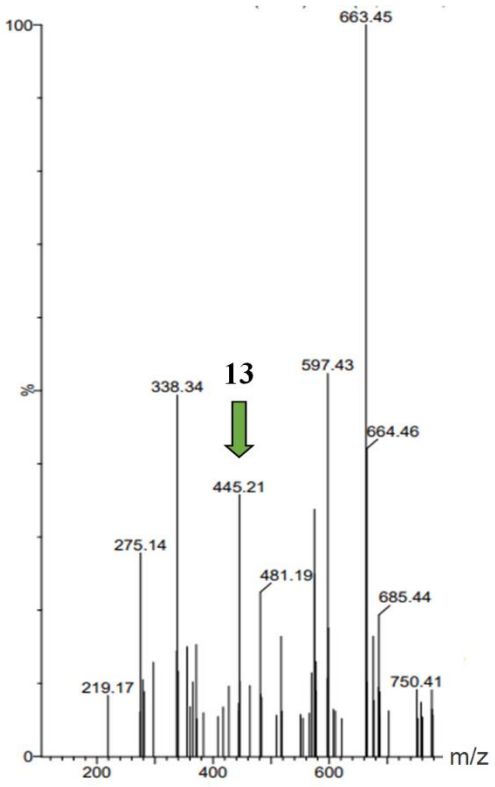


Figure 4.43. *Mass spectra of reaction product* ***13****, following the scheme reported in Figure 4.34.Peak at m/z 445.21 (****13****) evidenced with green arrow.*

The reaction mixture was analysed by LC-MS, following the conditions of method **e** (Table 4.5). Product purity was calculated at 35% by integration of the relative peak, detected by LC-UV chromatogram (Figure 4.44).

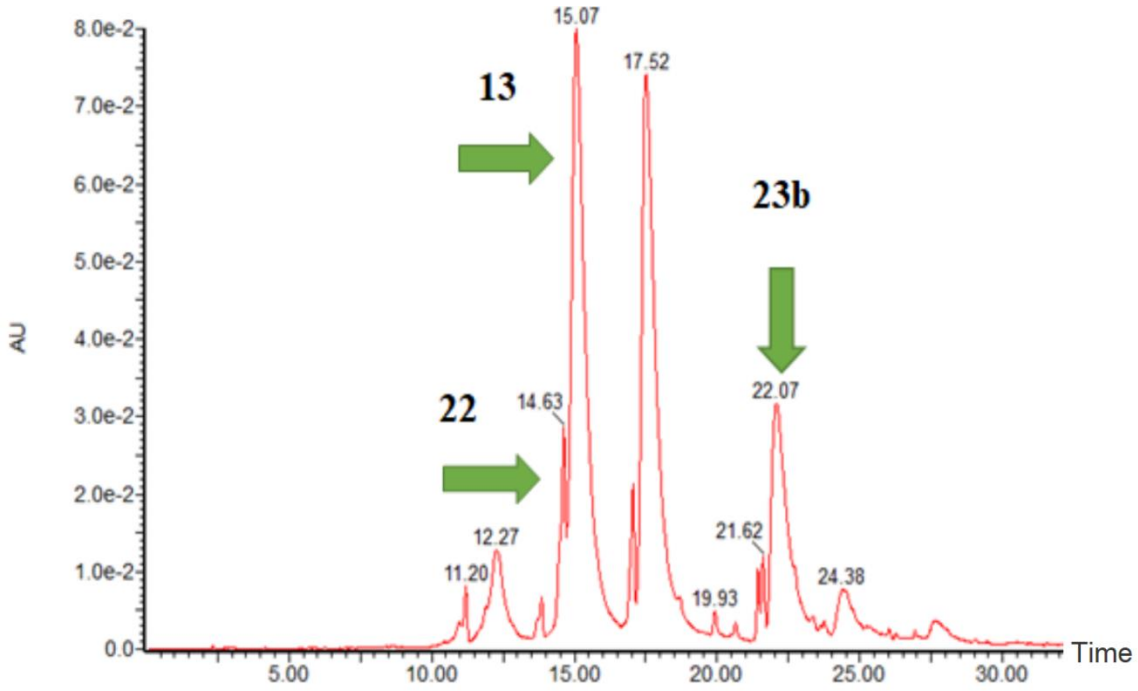
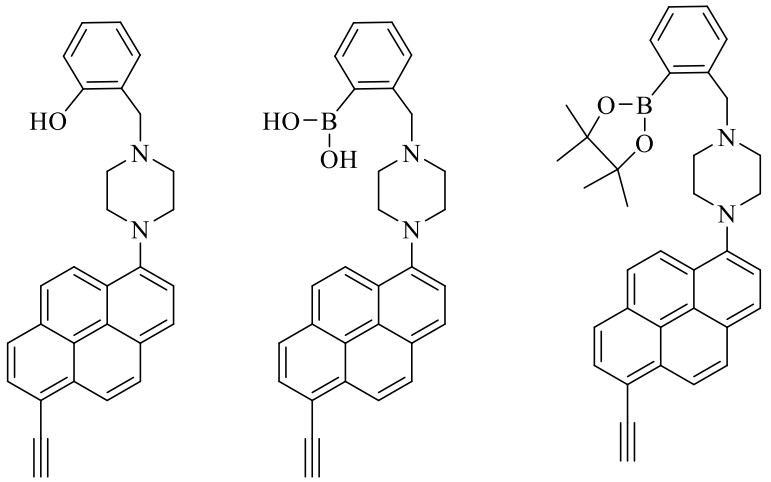


Figure 4.44. *LC-UV chromatograms achieved according to method e conditions as reported in Table 4.5.Peak at RT 14.63 (**22**), 15.07 (**13**) and 22.07 (**23b**) evidenced with arrows.*

As expected, a mixture of products was observed, explaining the low product purity determined. Due to the low stability of the final product, the formation of fragment ions did not allow the identification of all the compounds present. The mass spectra of peaks evidenced were analysed and were attributed to the oxidized product **22** (RT 14.63), the desired product **13** (RT 15.07) and the starting material **23b** (RT 22.07).



22 **13** **23b**

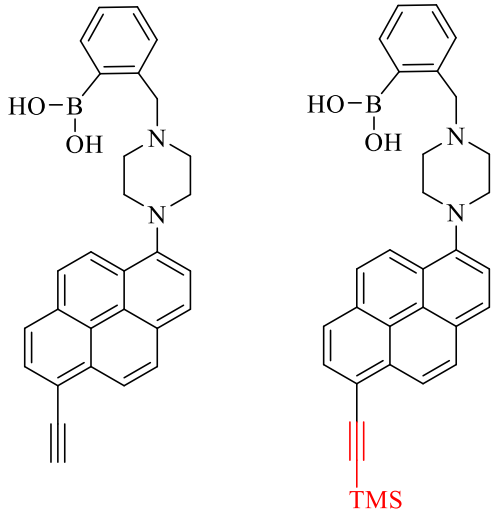
Figure 4.45. *Chemical structure of compound **22**, **13** and **23b**.*

The presence of **23b** suggested that the deprotection conditions were not completely suitable and needed improvement. A different amount of methylboronic acid or increasing reaction time could promote yield desired product. LC-MS technique allowed the identification of the products of reaction, giving more information regarding secondary products. However, since the low stability of **13** towards temperature and acid, the condition employed during the separation with LC-MS or HPLC could cause side reactions such as oxidation, or degradation of the desired product. Consequently, the success of the reactions could not be verified. Alternative techniques to achieve a complete separation of desired product must be investigated. Complete characterization of sample with 1H and 13C NMR has not conducted, due to the presence of product as mixture and low purity.

4.4 Fluorescence experiments

The intermediate compound **13b** that involved TMS-group as shown in Figure 4.25, was synthesized. It was isolated and purified, estimating at 86% purity level from LC-UV chromatograms reported in Figure 4.29. The main cause affecting the purity of the sample was attributed to the formation of the oxidized product, equivalent to the compound **22** (Figure 4.45)

but including the TMS-group. Since it was difficult to achieve the final desired compound **13** by separation from the mixing of product, preliminary fluorescence experiments were conducted with **13b**. It was expected that the response towards saccharides of **13b** were similar to that of the desired product. The main difference between the two structures was the presence of the TMS group linked to the pyrene probe which should not interfere with the interaction between diols and the PBA receptor (Figure 4.46).



13 **13b**

Figure 4.46. *Chemical structure of **13** and **13b**.*

Fructose was employed as a standard monosaccharide to evaluate the binding with BA receptor. The selectivity of the sensor was tested by performing experiments with different monosaccharides (Figure 4.47). Sorbitol and Glucose were selected as they are commonly used to evaluate boronic acid binding, due to their abundance in the blood and thus important for sensing application. Moreover, they are both affordable and widely available. [33, 115, 223]

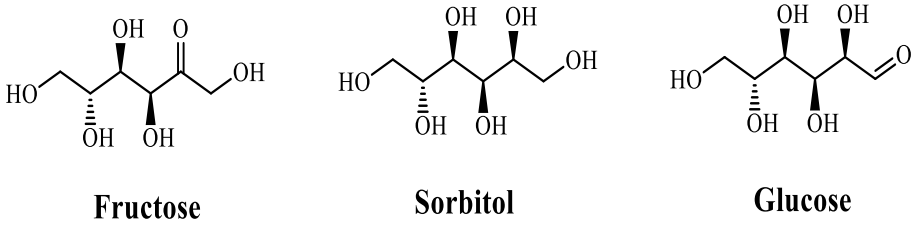


Figure 4.47. *Chemical structure of monosaccharides: Fructose, Sorbitol, Glucose.*

Preliminary experiments were performed in solutions to evaluate the behaviour of sensors towards saccharides. The role of solvent used to dissolve the compounds and the solvent used to record the spectra was investigated. The final aim consisted of the incorporation of the sensor onto the surface of silica nanoparticles. However, the sensitivity and overall performance of sensors need to be investigated in solution first.

Due to the low solubility of the organic probe, a highly concentrated solution of **13b** was prepared in DMF, and then diluted in water. Absorption spectra of **13b** at different concentrations were recorded (Figure 4.48a). Since a signal response with the lowest concentration (10 μM) was observed, 10 μM was selected for the further fluorescence experiments. The solubility of the sensor in aqueous solution was evidenced by the linear response of absorbance versus concentration of **13b** at 390 nm (Figure 4.48b).

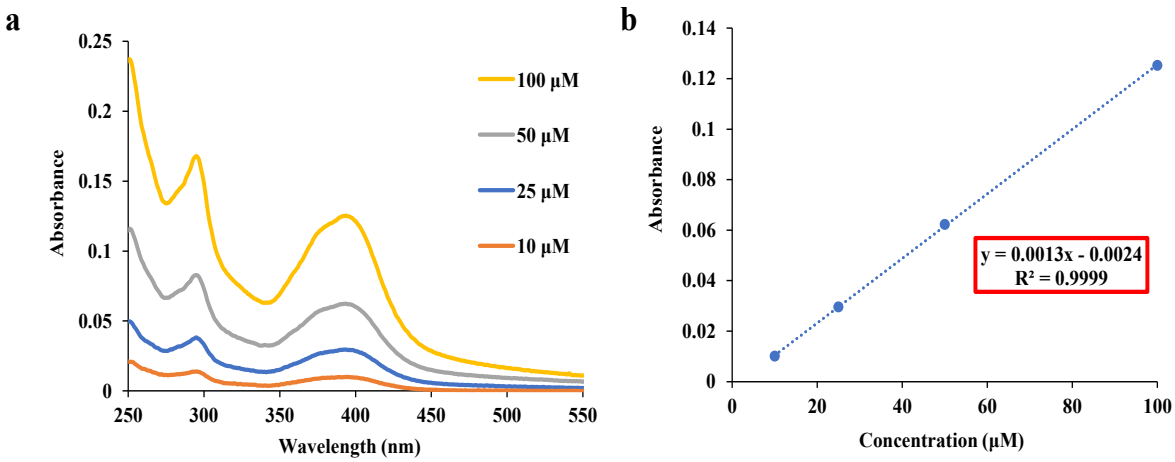


Figure 4.48. *Absorption spectra of sensor* ***13b*** *in water. Absorbance versus concentration at* λ_{abs} *390 nm.*

A highly concentrated solution of **13b** was also prepared in DCM, however due to its immiscibility in water, the solution was prepared by completely drying the solvent under vacuum (overnight). It was then dissolved in large amounts of water to afford a low concentrated solution. A set of diluted solutions (0; 0.1; 0.2; 0.5; 1; 2; 5; 10 µM) were prepared from a high concentrated stock solution and subjected to fluorescence measurements. The aim was to investigate the effect of the starting solvent (DCM and DMF) on the fluorescence properties of sensor and evaluate the maximum fluorescence signal.

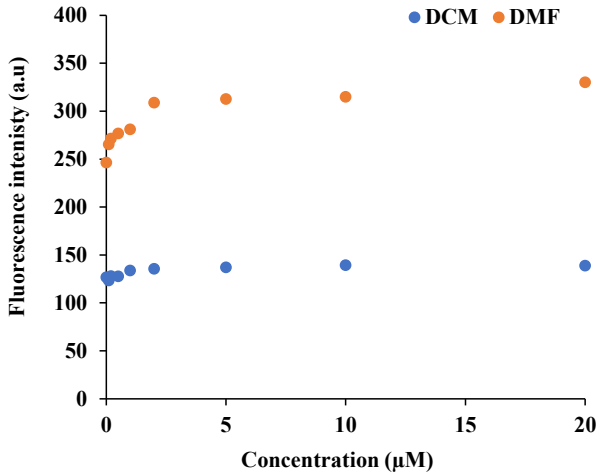


Figure 4.49. *Relative intensity (a.u) versus concentration. Comparison between solution prepared by dilution of stock solution of* ***13b*** *dissolved in DCM or DMF.*

As shown in Figure 4.49, the solution in DMF had a higher fluorescence signal compared to the solution with DCM. Therefore, DMF method was selected in the further experiments. Once the absorption and emission spectra were recorded, the Stokes shift was determined by the difference between the maximum absorption and emission wavelengths. A Stokes shift of 66 nm was calculated (Figure 4.50). A large Stokes shift (>100 nm) aids to reduce self-quenching processes that could cause a decrease in fluorescence intensity. Although the Stokes shift value was lower than required to prevent self-quenching, it was expected that the further immobilization of the sensor onto the surface of silica nanoparticles would prevent this effect.

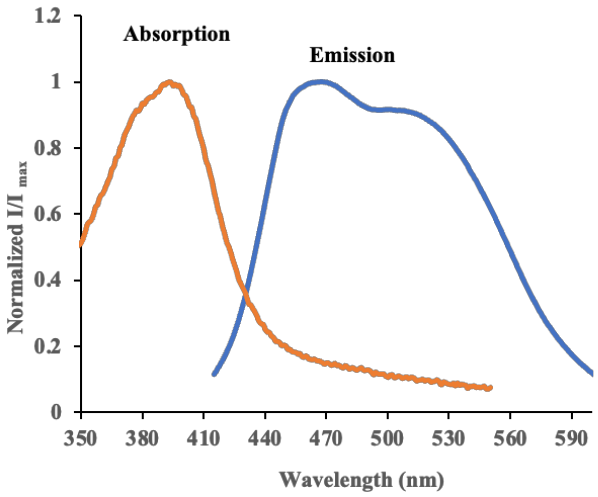


Figure 4.50. *Normalized absorption and emission spectra of* ***13b*** *in aqueous solution.*

To ensure that the fluorescence properties of the sensor were not affected by the polarity of solvent, absorption and fluorescence experiments were conducted in water with different percentages of MeOH and MeCN, and in pure organic solvent (Figure 4.51).

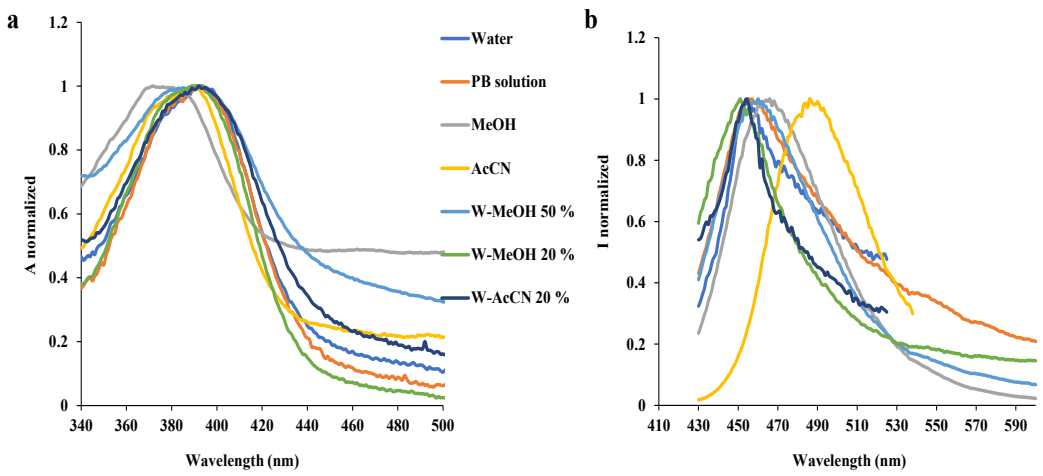


Figure 4.51. *Normalized absorption (a) and emission (b) spectra of* ***13b.***

In Table 4.6 absorption maxima and the respective emission maxima in different solvents are reported. As shown, the calculated extinction coefficient ε and the Stokes shift did not increase when the MeOH and MeCN solutions were used, compared to water (66 nm). The sensor displayed a marked bathochromic shift of emission spectra (λ_{em} 473 nm) when dissolved in the less polar solvent (MeCN). The highest extinction coefficient molar ε were detected in pure MeOH and MeCN. This may be due to the higher solubility of the probe in organic solvents compared to water. Although, since in the polar solvents the orbital energy of HOMO decreases, it was expected that the PET process would be supported.[224]

Table 4.6. *λ_{abs} and λ_{em} of absorption and emission spectra of* ***13b*** *in different solvent. Extinction coefficient molar ε and Stokes shift calculated.*

Solvent	*λ_{abs} (nm)*	*λ_{em} (nm)*	*ε (M^{-1} cm^{-1})*	*Stokes shift (nm)*
Water	390	456	1182	66
PB solution (pH 7.4)	391	445	999	61
MeCN	390	473	2122	83
MeOH	372	462	3801	90
Water-MeOH 1:1	380	462	1683	82
Water-MeOH 20 %	392	453	1272	61
Water-MeCN 20 %	392	458	1326	66

As consequence of these results, it was concluded that experiments can be conducted in aqueous solution, strengthening the PET mechanism involved and consequently increase the probability of fluorescence emissions following the sugars binding. To investigate the effect of the selected solvent, fluorescence experiments of water at different excitation wavelengths were conducted. Typical Raman scattering bands can be recognized by a shift of emission wavelength changing the excitation wavelength. Experiments with the probe **13b** (10 μM) were performed to investigate the wavelength at which these bands occur. The aim was to identify the excitation wavelength to allow a suitable fluorescence intensity response of the probe, avoiding overlapping with Raman bands of water.

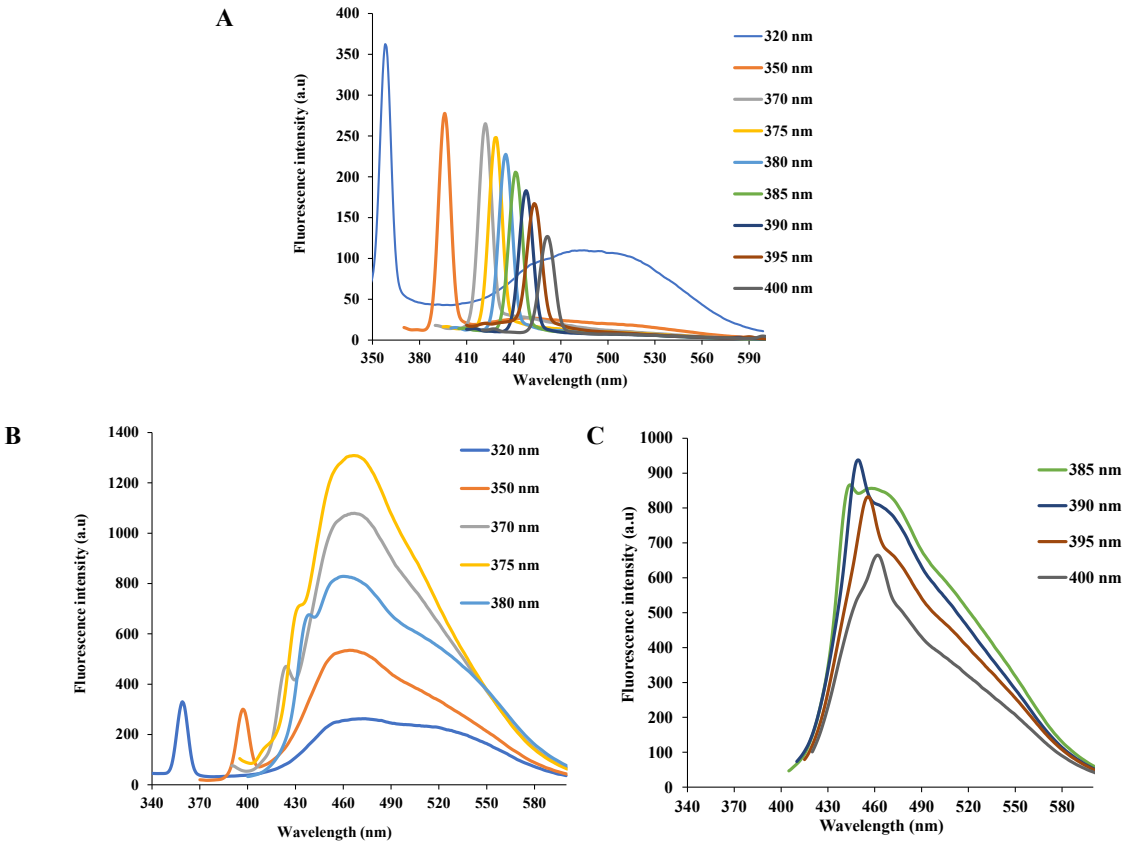


Figure 4.52. *Emission spectra of water (A) and* ***13b*** *in water (B-C) at different excitation wavelengths (320-400 nm).*

Figure 4.52A show a shift of emission spectra of water, verifying the typical Raman bands. In Figure 4.52B and C, it is shown how the fluorescence spectrum of **13b** was affected by the Raman bands of water. In proximity of the wavelength corresponding to the emission maxima of probe (λ_{em} 456 nm), the Raman band of water overlaps the emission band of the probe. Consequently, a decrease of fluorescence intensity was detected alongside a band distortion.

Figure 4.53 reports the fluorescence intensity at maximum emission (λ_{em} 456 nm) versus different excitation wavelengths. The intensity increased until λ_{em} 375 nm, and then decreased markedly. Due to the low fluorescence intensity of the sensor, involving the PET process, the effect of water and the overlapping of Raman bands predominates. To avoid this effect, the next fluorescent

spectra have been recorded at a specific excitation wavelength (λ < 390 nm), because distinct bands can be identified at λ 320, 350, 370,375, 380 nm, (Figure 4.52B). It was expected that this method would avoid an overlap with the Raman bands of water and the emission band of the probe, and thus prevent the decrease of fluorescence intensity.

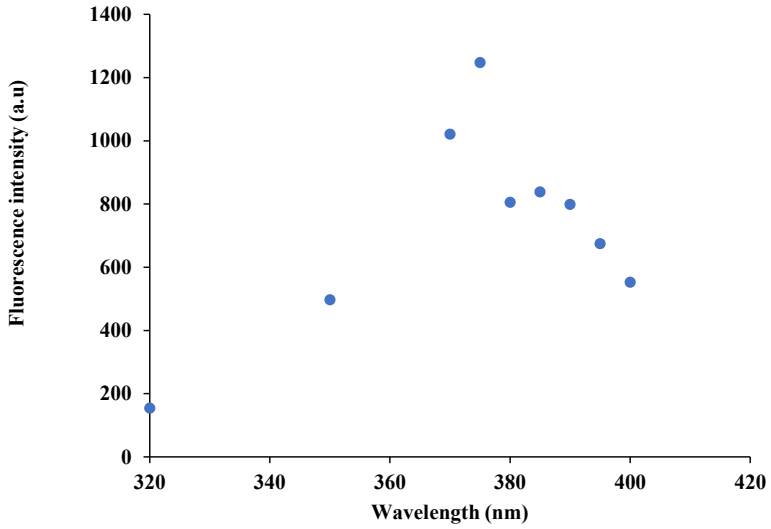


Figure 4.53. *Fluorescence intensity of* ***13b*** *(10 μM) in water at λ 456 nm versus different excitation wavelength (320-400 nm).*

After determining the most suitable excitation wavelength, the next experiments focused on investigating the behaviour of the sensor towards D-Fructose. Experiments were conducted in buffer solution.

Phosphate buffer solution (PBS) was selected due to its simple preparation and the absence of compounds that influence the properties of the sensor. A 50 mM phosphate buffer was selected to avoid interferences of high concentration buffer, while keeping the buffering ability.[225]

The effect of PBS on the emission spectra was investigated, as similarly done for water. As reported in Figure 4.54 (right), the fluorescence intensity at fixed emission wavelength (450 nm) decreased as the excitation wavelength increased. Unlike with water, an early fluorescence intensity decrease (λ_{ex} 375 nm), with the maximum value at 350-360 nm, was observed. 360 and 390 nm were investigated as excitation wavelengths for the further experiments.

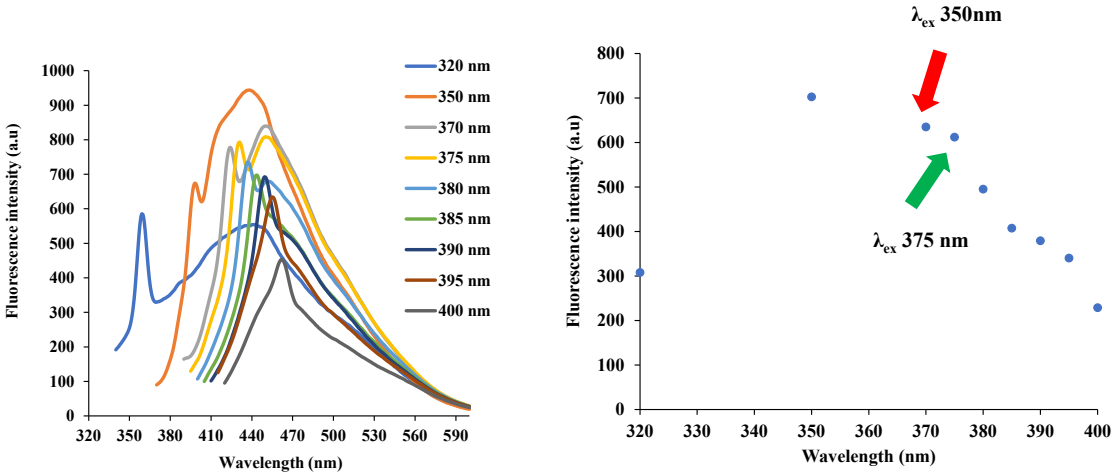


Figure 4.54. *Emission spectra of* ***13b*** *(10 µM) in PBS (left) at different excitation wavelengths (320-400 nm). Fluorescence intensity at λ 450 nm versus excitation wavelengths. λ_{ex} 350 nm (red) and 375 nm (green) evidenced.*

Due to the low fluorescence intensity of the probe due to the involved PET mechanism, the effect of solvent and the Raman bands was strongly visible. It was expected that the fluorescence intensity would increase after binding with sugars, due to the suppression of PET mechanism involved. However, a change of intensity signal, by changing the excitation wavelength, was observed. Thus, different excitation wavelengths were considered as although the aim was to avoid the effect of the Raman bands, the optimum excitation wavelength resulting in the highest emission intensity also need to be elucidated.

The next experiments focused on fluorescence properties of the sensor in the presence of saccharides. The pH profile of the sensor **13b** was investigated to understand the sensing mechanism toward the sugars. A proposed pH-dependent behaviour of the probe **13b** is described by the scheme shown in the Figure 4.55. At neutral pH, **13b** should not exhibit fluorescence due to electron transfer process from the amino group of piperazine (**a**). The establishment of an interaction between boron and amino group would cause a reduction of the basicity of the amino, making its electron pair less available. This interaction will strengthen upon saccharides binding. At low pH the protonation of the amine was believed to restrain the electron transfer from the amino to the fluorophore, resulting in high fluorescence (**b**). While in a more basic environment, the piperazine will be deprotonated, restoring the quenching effect by electron transfer leading to a fluorescence intensity decrease (**c**).

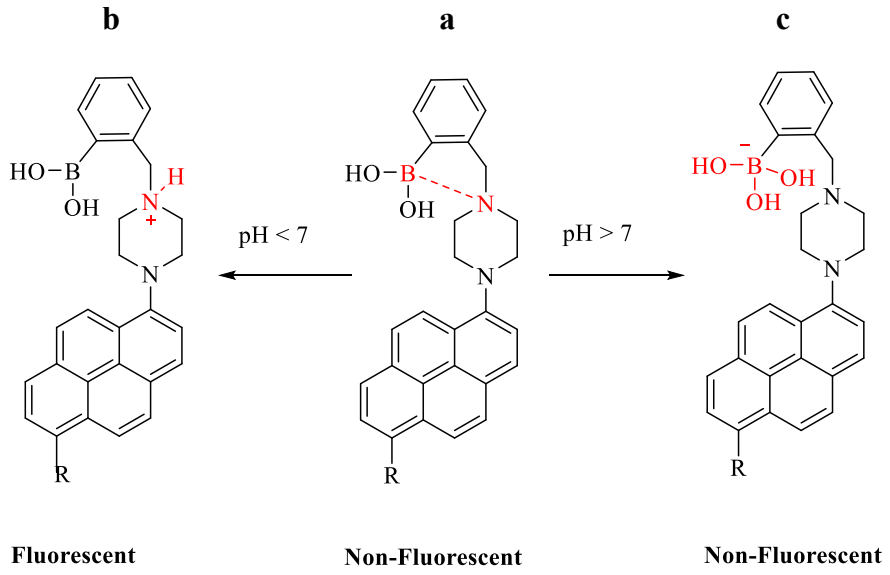


***Figure 4.55**. Proposed scheme of **13b** behaviour from acid (b) neutral (a) and basic (c) pH.*

The pH-dependent fluorescence emission behaviour of **13b** (10 µM) was investigated through fluorescence titration, where the pH was gradually increased. The fluorescence emission spectra

at λ_{ex} 390 nm were recorded upon addition of basic solution to evaluate the whole pH range. Following the same procedure, fluorescence spectra of the basic solution with gradually increasing pH were also performed as a control, allowing the emission spectra of the probe to be normalised to a blank solution, as reported in Figure 28 (Appendix).

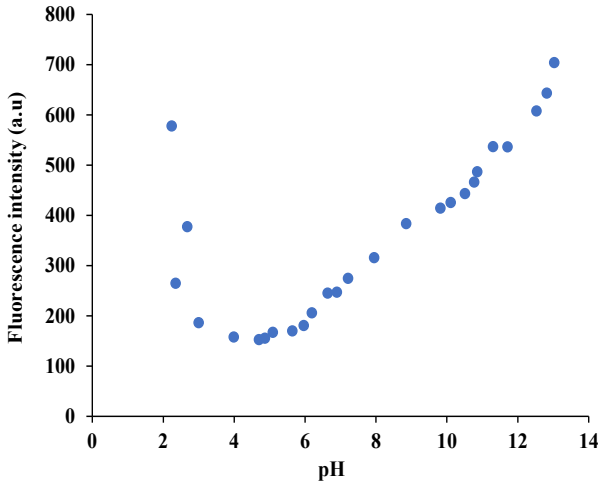


Figure 4.56. *Fluorescence intensity pH profiles of* ***13b*** *(10 μM) in 50 mM PB solution at λ 450 nm. Emission spectra recorded at* λ_{ex} *390 nm. Complete emission spectra reported in Figure 28 (Appendix).*

The Figure 4.56 reports fluorescence intensity profile at λ 450 nm. It is possible seen that the intensity was high at acidic pH (<3) as expected due to the protonation of amine, blocking the electron transfer to the fluorophore, and restoring the fluorescence. However, in contrast to what was predicted (Figure 4.55), the fluorescence continued to increase even at more basic pH. Indeed, it was expected a restoring of quenching effect by piperazine, once be deprotonated. The reason for this behaviour was attributed to the presence of the TMS group. It was thought that strong basic conditions led to the deprotection of the TMS groups, leaving the free acetylene group which enhanced the fluorescence intensity.[193, 203]

The binding with diols is known to increase the acidity of BA, due to an increased electron deficiency of the boron centre which acts as Lewis acid. [118] The expected behaviour of the sensor in the presence of diols is reported in Figure 4.57. It was expected that the interaction between boron and amine (**a**) became stronger upon the diol binding, restoring the fluorescence by suppression of PET mechanism (**a2**). The presence of D-Fructose brings a fluorescence change of sensor over a large pH range. It was expected two different pKa values 1 and 2 ascribed respectively to the tertiary amine (1) and to PBA (2), following the binding with saccharides. In acidic conditions (pH < pKa1), the fluorescence was supposed to be restored due to the protonation of amine (**b2**). In strong basic conditions (pH > pKa2), the interaction between boron and amino was too weak to suppress the electron transfer, resulting in the lack of fluorescence observed (**c2**). For sensing application, the sensor aims to perform at physiological pH (7.4).

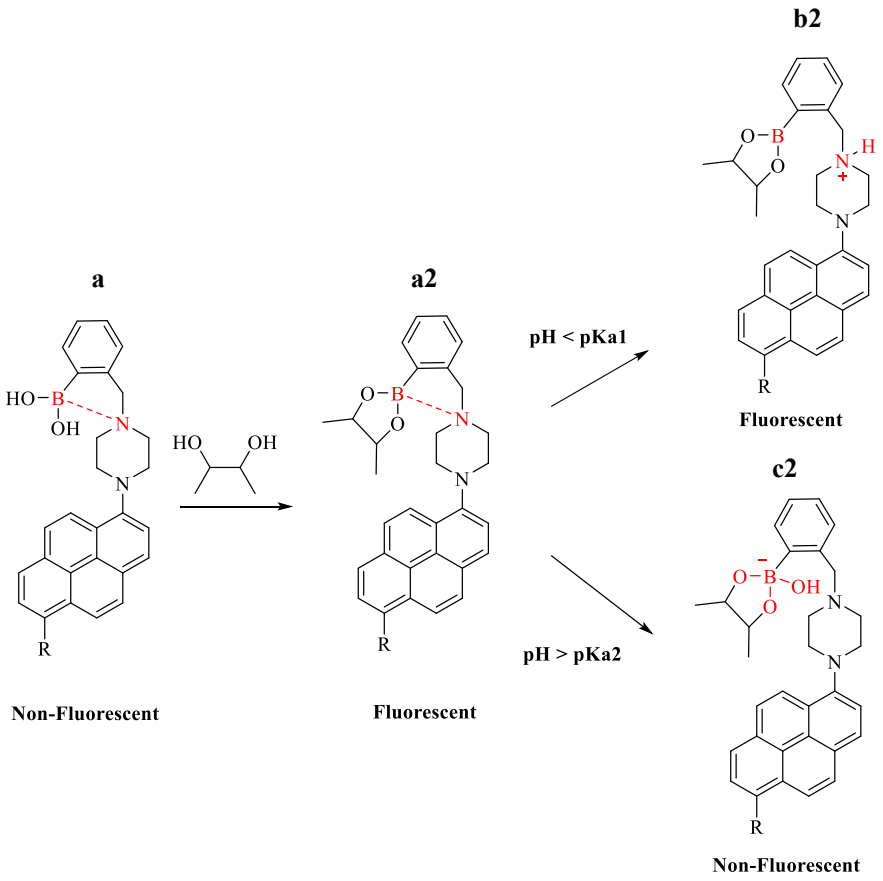


Figure 4.57. *Proposed scheme of* ***13b*** *behaviour over a change of pH, with diol-interaction.*

As reported in the literature,[43] the binding between phenyl boronic acid and saccharides occurs primarily at basic pH (around pH 8). Since the basicity of amino group was projected to be reduced due to the formation of the N-B bond[226], the binding between sensor **13b** and saccharides was expected to occur at the lower pH of physiological pH. This supports the suitability of the sensor for biological application.

The pH fluorescence titration was repeated with the addition of D-Fructose at high concentration (100 mM) to investigate the establishment of the binding, and to determine the pH that this occurs. The complete emission spectra are reported in Figure 29 (Appendix). The results reported in Figure 4.58 reports the fluorescence intensity pH profile at λ 450 nm versus pH of **13b**. It is

noticeable an enhancement of fluorescence intensity with D-Fructose (orange) compared to sensor alone in solution (blue), confirming the formation of the interaction. However, an increase of fluorescence intensity at high pH (> 10) was also observed. In contrast, the fluorescence of the sensor with D-Fructose was expected to decrease at high pH. The electron transfer from amino group of piperazine to the fluorophore is restored, due to the deprotonation of piperazine at basic environments. The fluorescence intensity profile detected was not able to provide information regarding the pH range in which the binding with saccharides occurs at. Moreover, it has not been possible to calculate the values of pKa1 and pKa2.

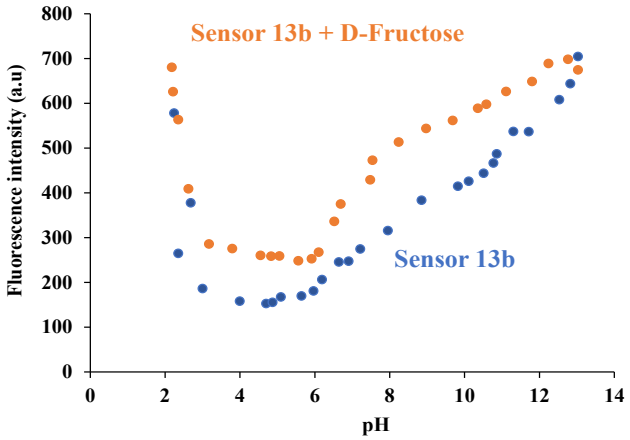
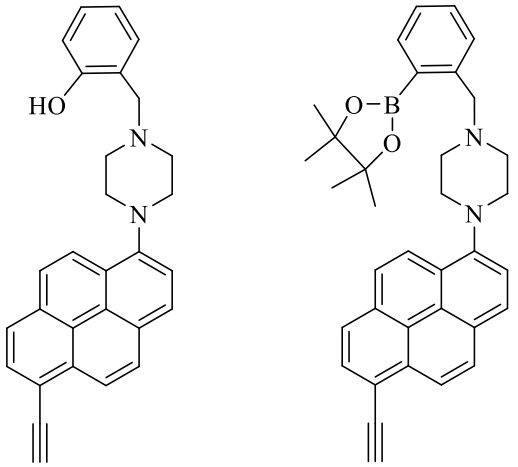


Figure 4.58 *Comparison of fluorescence intensity pH profiles of* ***13b*** *(10 μM) with (orange) and without D-Fructose 100 mM (blue) in 50 mM PB solution at λ 450 nm. Emission spectra recorded at* λ_{ex} *390 nm.*

Since the fluorescence response observed did not follow the expected trend, the probe **13b** was not considered suitable to evaluate the sensing ability of the sensor toward saccharides. Further experiments were performed with designed sensor **13** which had the low purity level of 35 %. The reason for the low purity was due to the main presence of the oxidized product **22** and of the product **23b**, that involved the BA pinacol ester. The low stability of product towards temperature

and acid conditions made techniques, such as LC-MS or HPLC, unsuitable for the purification and isolation of final product. Indeed, the establishment of side reactions such as oxidation, or degradation represented an issue to achieving the desired sensor with higher purity percentage. As the sensor was present in a mixture, it was expected that the presence of other compounds would interfere with its fluorescence. They could be excited at the same wavelength of the sensors or reduce the fluorescence intensity due to side processes such as collisional quenching, energy transfer, charge transfer, or the heavy-atom effect.[227] However, it was expected that the presence of **22** and **23b** would not affect the interaction with sugars, due to the lack of BA free unit receptor. It was thought that the effective binding and the sensitivity towards saccharides could be successfully evaluated by performing experiments with sensor **13** as mixed solutions.



22 **23b**

Figure 4.59. *Chemical structure of **22** and **23b**.*

Spectroscopic properties of the final designed sensor **13** were investigated. Absorption and relative emission spectra were recorded. The absorbance spectrum of probe **13** could only be recorded at a high concentration (100 μM). Conversely to the absorbance signal of **13b**, involving TMS, that was detected at a lower concentration (10 μM), as shown in Figure 4.48. This was due to a lower

solubility of **13** in aqueous solution and due to the presence of impurities. Moreover in Figure 4.60a, a higher absorbance of **13b** was seen compared to **13**. The absorbances of two sensors are not comparable since different concentration and purity. However, the aim was investigated the maximum excitation and emission wavelength, to evaluate the role of TMS group. To gain more information regarding the excitation wavelength of the probe, excitation spectra of **13** at 10 µM was conducted, assuming the same emission wavelength of **13b** (450 nm).

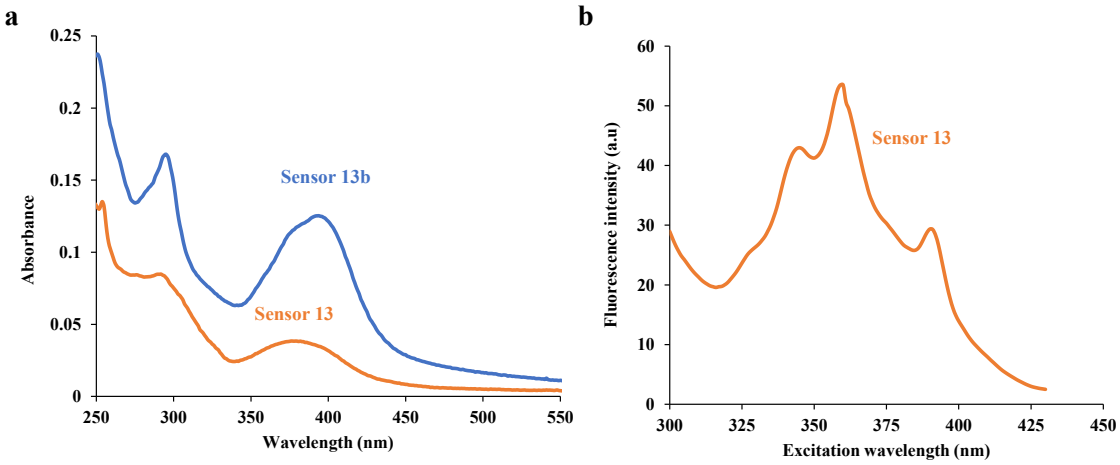


Figure 4.60. *Comparison of absorption spectra of sensor **13b** and **13** in aqueous solution (a). Excitation spectra of **13** at λ_{em} 450 in water (b).*

The excitation spectra reported in Figure 4.60b show a different excitation wavelength compared to **13b**. The 360 and 390 nm were selected as excitation wavelengths to perform next fluorescence experiments. 360 nm was the excitation wavelength with highest intensity in the excitation spectrum, while 390 nm was the one used for the previous sensor **13b**. In Figure 4.61, a higher fluorescence intensity for the shorter excitation wavelength (360 nm) was observed. Furthermore, at this excitation wavelength the impact of Raman bands of water was lower as observed in Figure 4.52.

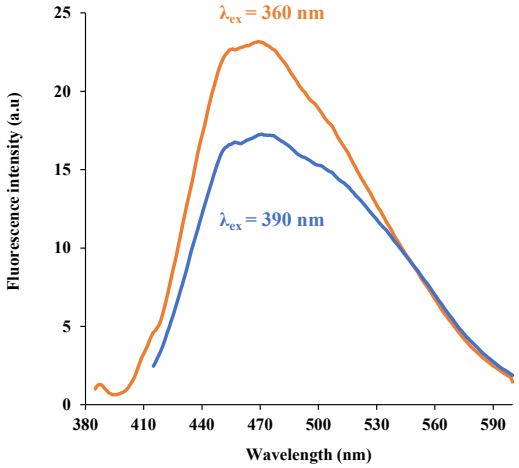


Figure 4.61. *Emission spectra of* ***13*** *(10μM) at different excitation wavelength, λ 360 nm (orange) and 390 nm (blue).*

As with **13b**, the pH profile of **13** was investigated to understand the sensing mechanism towards sugars. The fluorescence emission pH profile of **13**, was recorded at both excitation wavelengths (360 and 390 nm) as reported in Figure 30 (360 nm) and 31 (390 nm) in the Appendix. Figure 4.62a reports fluorescence intensity pH profile at λ 450 nm, for both excitation wavelengths. Alongside, Figure 4.62b shows the fluorescence response of **13b** at different pH. Comparing the spectra of **13** and **13b**, there is a difference in the fluorescence intensity trends of both sensors, with an intensity decrease at high basic environment (pH > 10) for **13** (a) and the opposite for **13b** (b). This trend confirmed that the fluorescence intensity increase observed in **13b** was due to the deprotection of the TMS group in basic conditions.

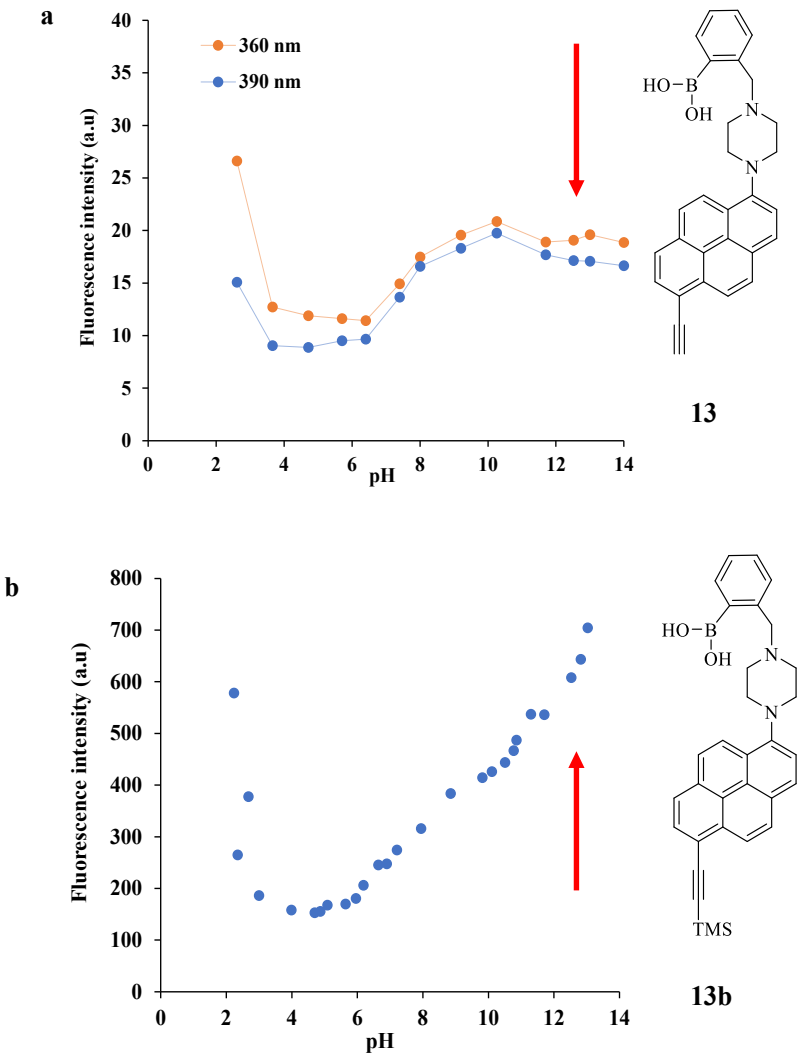


Figure 4.62. *Fluorescence intensity pH profiles of* ***13*** *10 µM at* λ_{ex} *360 and 390 nm (a) and* ***13b*** *(b)at* λ_{ex} *390 nm in 50 mM PB solution with λ 450 nm.*

Through the titration curve, the two pKa values of **13** can be approximated. First in the region where the fluorescence intensity starts to decrease, around 4 (pKa1), and the second before the intensity starts to decrease again, around 10 (pKa2). The pH fluorescence titration experiments

were repeated in presence of D-Fructose at high concentration (100 mM), selecting λ_{ex} = 360 nm due to the better response seen at this wavelength.

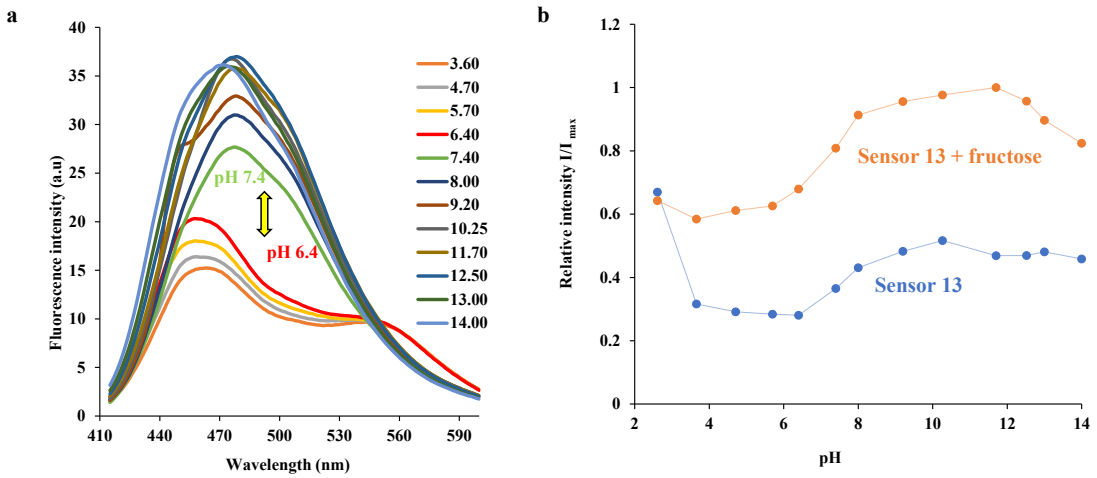


Figure 4.63 *Fluorescence intensity pH profiles of* ***13*** *(10 µM) with of D-Fructose at λ_{ex} 360 nm (a). Comparison of fluorescence intensity pH profiles of* ***13*** *(10 µM) with and without D-Fructose (100 mM) at. λ 476 nm in 50 mM PB solution. (b).*

Figure 4.63a shows an enhancement of fluorescence intensity and a shift of maximum emission around pH 7.4. This increase of fluorescence intensity verified the successful binding between the probe and D-Fructose. The observed red-shift in emission wavelength was assumed to be due to the deprotonation of piperazine, which strengths the electron push-pull effect on the probe. In Figure 4.63b, the relative intensities of sensor **13** with and without D-Fructose (100 mM), at λ_{em} 476 nm, versus pH are reported. Although binding at pH 7.4 was confirmed, further experiments were conducted at a slightly basic pH (~8) to ensure a stronger interaction between sensor and saccharides.

The sensing ability of **13** towards saccharides was evaluated through fluorescence titration of the sensor (10 µM) with gradual addition of D-Fructose to reach concentrations in the mM range (0-

200 mM). Results reported in Figure 4.64A show a concentration-dependent increase in florescence intensity response with D-Fructose until a plateau was reached (B). Furthermore, a linear trend was seen up until 18 mM, as shown in graph C (Figure 4.64).

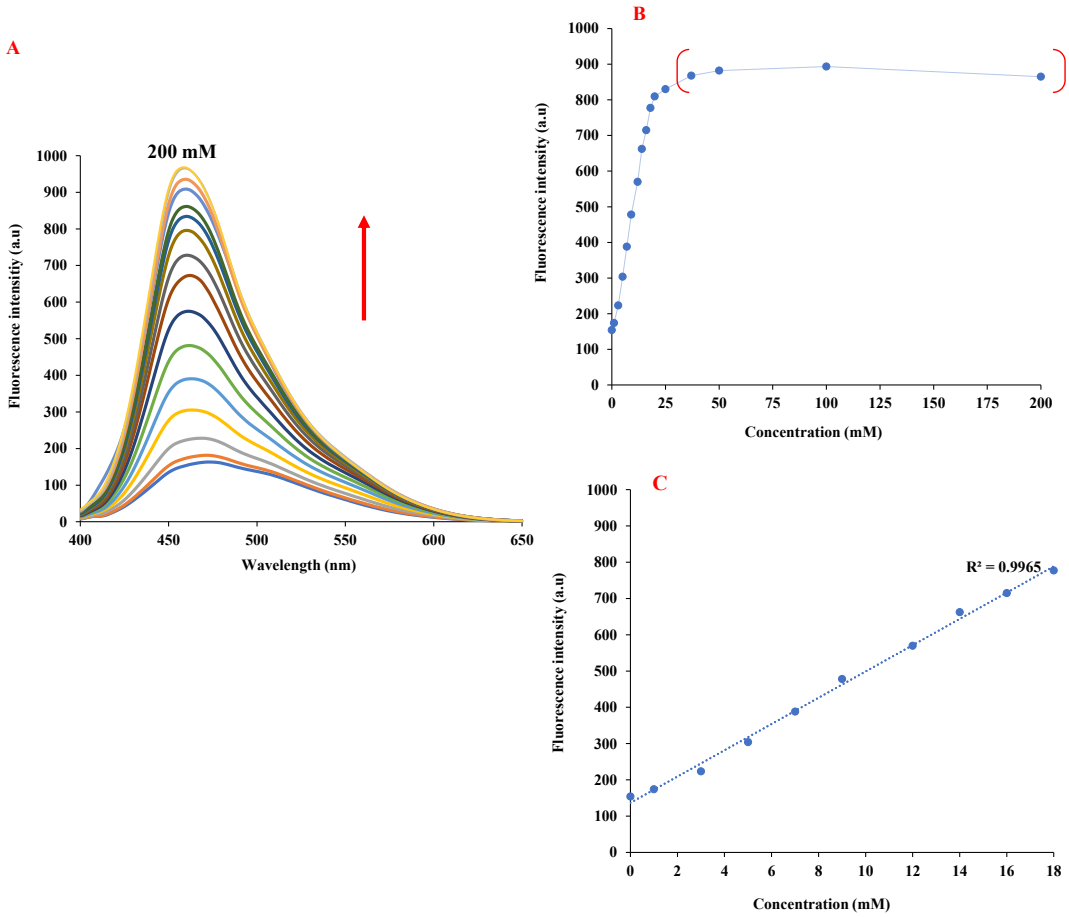


Figure 4.64. *Fluorescence emission of **13** (10 µM) with different concentration of D-Fructose (0-200 mM) in 50 mM of PB solution at λ_{ex} 360 nm (A), Fluorescence intensity versus concentration 0-200 mM (B) and 0-18 mM (C) at λ 460 nm.*

The experiments were repeated with different saccharides, as reported in Figure 4.47, to evaluate the selectivity of sensor **13**. D-Sorbitol (**a**) and D-Glucose (**b**) induced similar spectral changes, as shown in Figure 4.65. Higher fluorescence intensity was observed for D-Sorbitol suggesting the

stronger binding with **13**, followed by D-Fructose and D-glucose, in accordance with the reported literature. [3, 228, 229]

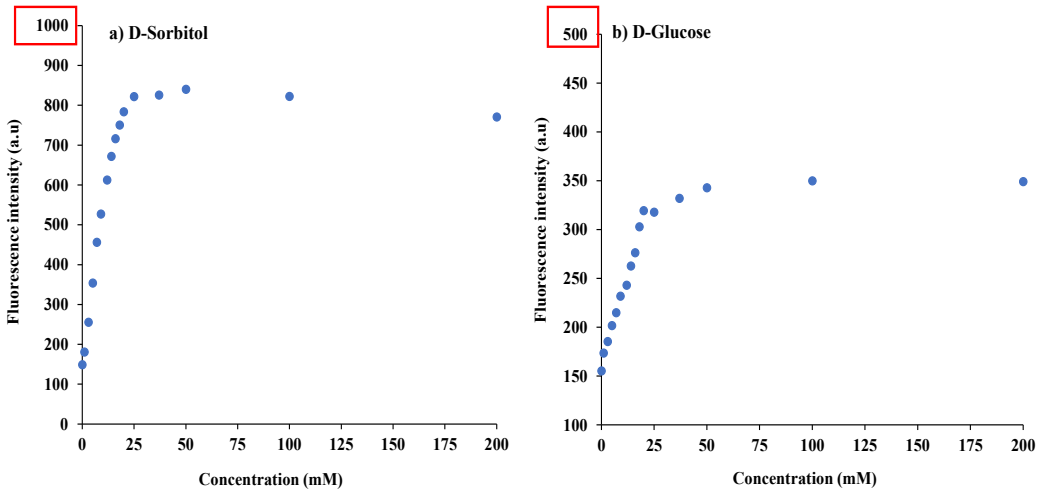


Figure 4.65. *Fluorescence intensity of* ***13*** *(10 µM) at* λ_{ex} *360 nm versus concentration (0-200 mM) of D-Sorbitol (a) and D-Glucose (b) at λ 460 nm.*

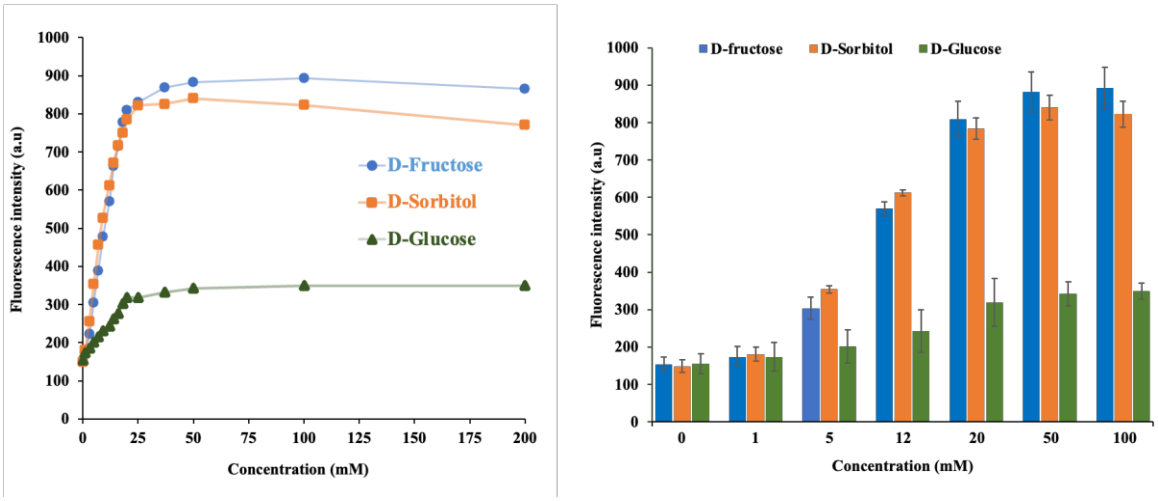


Figure 4.66. *Comparison between fluorescence intensity of* ***13*** *versus D-Fructose,D- Sorbitol and D-Glucose concentration.*

Figure 4.66 shows the fluorescence response of **13** towards the sugars selected. **13** was proved to have a higher sensitivity for D-Fructose and D-Sorbitol than D-Glucose, again in agreement with the literature.

Binding constants were calculated employing the Hill equation assuming 1:1 stoichiometry. [230]

$$I = I_0 + \frac{A \times C}{K_D + C} \qquad \text{Equation 4-2}$$

Where I is the fluorescence intensity, while C is the concentration of the sugar selected. The equation provides: K_D is the dissociation constant, I_0 is base fluorescence and A is maximum fluorescence.[231]

The detection limit (LOD) and limit of quantification (LOQ) were calculated by Sb/k, where Sb is the standard deviation of the blank measurements multiplied by 3 for LOD and by 5 for LOQ. k is the slope of the line achieved by plotting fluorescence intensity versus concentration (Figure 4.67).

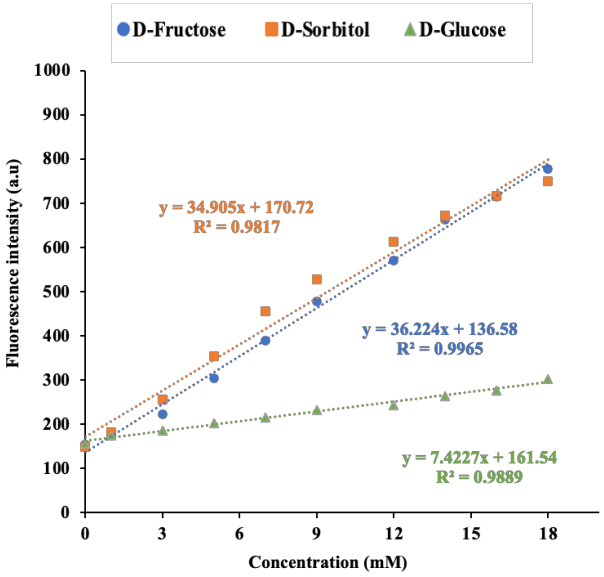


***Figure 4.67**. Fluorescence intensity of **13** at λ 460 nm versus concentration (mM) of D-Fructose, D-Sorbitol, or D-Glucose. Determination of LOD by slope of relative line plotted.*

The table below summarises association constants LOD and LOQ for the sugars tested. The binding constants between sensor **13** and sugars decreased in the order D-Sorbitol> D-Fructose > D-Glucose, as found also in literature.[127, 229, 232] However, the value were lower compared to literature sensor. The reason was attributed to the low purity of compound, used to perform the experiments.

Table 4.7. *The association constants (Kas) between sensor **13**, their detection limit (LOD) and quantification limit (LOQ).*

	D-Fructose	*D-Sorbitol*	*D-Glucose*
K_D/mM	9.5	6.9	12.7
K_A/M^{-1}	104.9	144.3	78.6
LOD/mM	0.27	0.28	1.33
LOQ/mM	0.91	0.94	4.44

Determination quantum yield

Quantum yield Φ of sensor was calculated to verify the application in saccharides detection. Despite not being able to isolate **13** from the products, its quantum yield was calculated. A low value was expected due to the PET mechanism involved. **13** has been calculated through a relative method,[63] by using a standard with known quantum yield. 7-Diethylamino-4-methylcoumarin was selected as the standard since absorption (λ_{max} 380 nm) and emission (λ_{em} 460 nm) maxima wavelengths are comparable with the designed sensor.

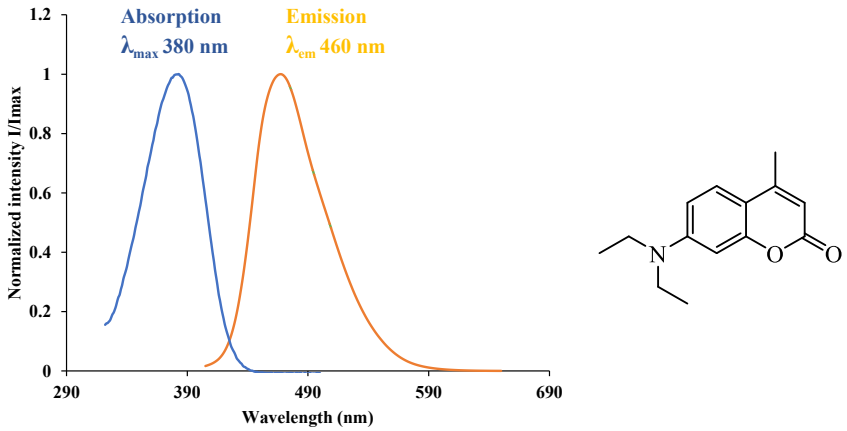


Figure 4.68. *Normalized adsorption and emission spectra of 7-Diethylamino-4-methylcoumarin (left) and chemical structure (right).*

Φ_x (sample unknown) was determined employing the following equation.[233]

$$\phi_x = \phi_{st} \left[\frac{A_{st}}{A_x}\right]\left[\frac{F_{st}}{F_x}\right]\left[\frac{D_{st}}{D_x}\right] \qquad \text{Equation 4-3}$$

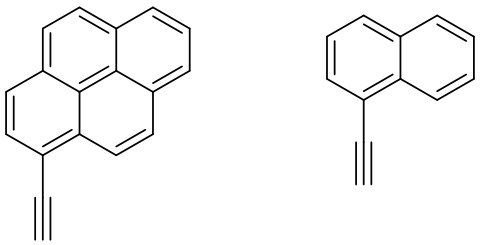
Φ_{st} (standard) of 7-Diethylamino-4-methylcoumarin is 0.055 in water according to the literature.[234] Absorbance of sensor **13** (A_x) and standard (A_{st}) were determined, by recording absorbance spectra at the excitation wavelength of the standard (λ_{max} 380 nm). F_{st} and F_x represent the areas of fluorescence spectra of the standard and sample (x) respectively, subjected to spectral correction. Both absorbance and fluorescence spectra were conducted in the same solvent and in the same conditions for each probe. The values were adjusted via dilution ratio D. The quantum yield Φ of the sensor **13** was negligible (0.00019) due to the involved quenching mechanism of PET, as demonstrated with the fluorescent experiments reported in Figure 4.64. However, the value determined belonged to sensor **13**, which was involved in a mixed product. The presence of these impurities could affect the quantum yield of the probe, displaying a lower value. As the value of probe **13** isolated from the mixture product could not be determined, it was decided not to calculate

the quantum yield of the sensor in the presence of D-Fructose. Following the successful synthesis of isolated **13**, the Φ of sensor **13** alone and in presence of D-Fructose will be calculated and compared to evaluate the strength of PET mechanism involved and the effective binding. Although Φ determined did not correspond to pure probe **13**, the value determined further supports the idea that PET mechanism is involved. Furthermore, it suggested the potential application and promising efficacy for saccharides detection.

Preliminary FRET experiments

Due to the fluorescence results gained upon sugar binding, preliminary experiments were conducted to evaluate FRET mechanism as an additional process for the sensing system. The system based on the designed sensor and an additional probe aimed to enhance the fluorescence response previously observed.

The performance of the system was planned to be further improved by antenna or surplus effect, manipulating the concentration of the probes involved to achieve this. Sensor **13** was investigated to act both as an acceptor and a donor. When **13** acts as the acceptor, a donor probe with a suitable emission wavelength overlapping the absorption spectra of the acceptor is required. When **13** acts as a donor, its emission needs to match with the absorption spectra of the acceptor probe. The structure of the probes should involve a group that enables their immobilisation onto a solid substrate, as designed in sensor **13**. However, the presence of an additional group could change the fluorescence properties of the dye. For example, it was verified how acetylene groups could bring a shift of emission or increase the quantum yield of a probe.[194, 196] This was taken into account to select dyes with fluorescence properties to ensure the overlap for FRET process. 1-ethynylpyrene (**24**) and 1-ethynylnaphathalene (**25**) were the best candidates, as they widely reported in the literature, and commercially available. [235-239] They were therefore selected as the donor in the FRET couple, while sensor **13** employed as the acceptor (Figure 4.69). [240-243]



24 **25**

Figure 4.69. *Chemical structure of 1-ethynylpyrene (**24**) and 1-ethynylnaphathalene (**25**).*

By mixing donor and acceptor (sensor **13)**, a decrease in the donor's fluorescence emission was expected due to FRET, while acceptor emission should not increase much due to PET quenching. Following sugar binding with **13**, the fluorescence emission of the acceptor was expected to increase (as shown in scheme of Figure 4.70) and emission of the donor to further decrease.

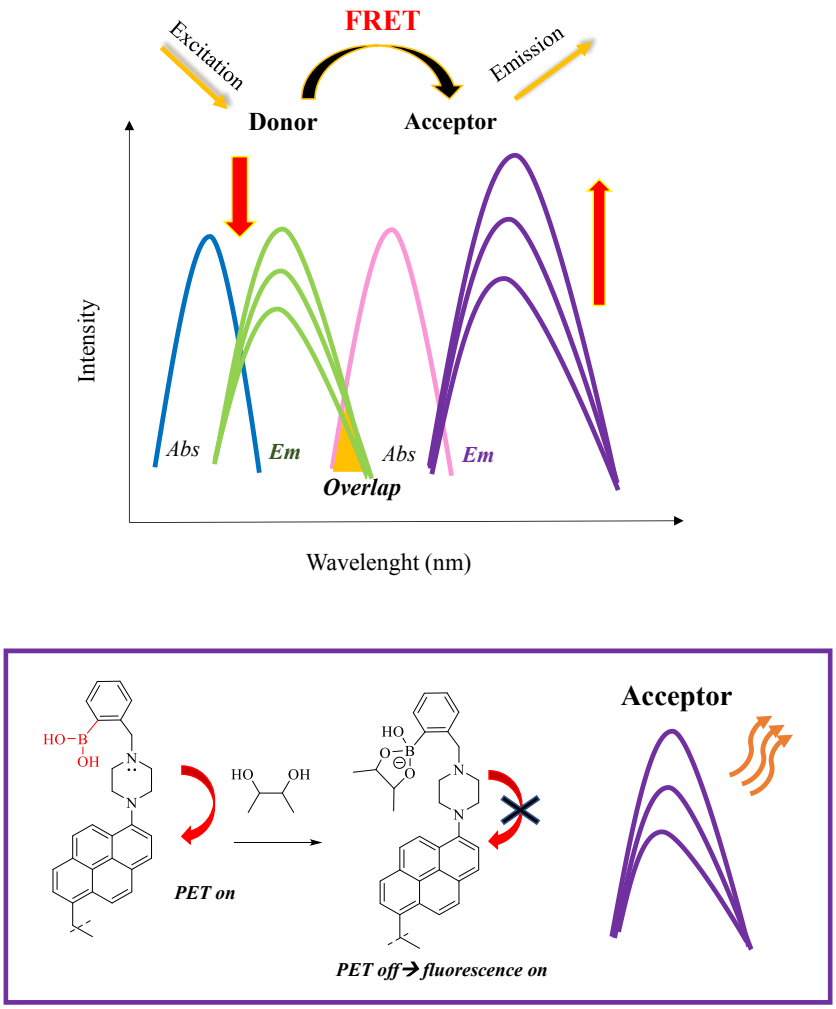


Figure 4.70. *Scheme to show the interaction between the sensor **13** acting as acceptor in FRET process.*

The absorption spectra (a) of **24** was examined at different concentrations (10; 25; 50 and 100 μM). The lowest concentration was designated to evaluate the fluorescence properties of **24**, comparing two excitation wavelengths, 343 nm and 326 nm, as reported in Figure 4.71b. To solely excite donor **24** and not sensor **13** (λ_{ex} 360 nm), an optimum wavelength of 326 nm was selected.

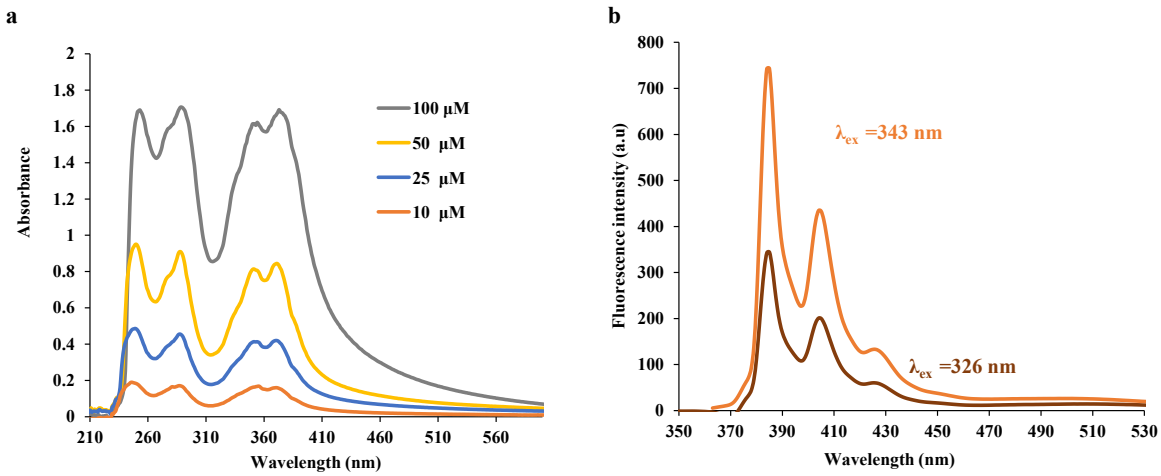


Figure 4.71. *Absorption spectra of* ***24*** *(a) at different concentration and fluorescence spectra (b) of* ***24*** *(10 µM) at different excitation wavelengths (343 and 326 nm) in water.*

Figure 4.72 shows the overlapping (yellow evidenced) of the donor **24** emission and the acceptor **13** excitation spectra (at λ_{ex} 390 nm), confirming the suitability of the probe selected.

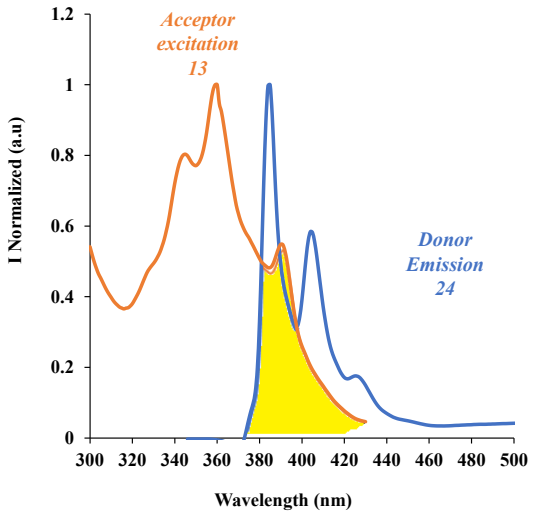


Figure 4.72. *Normalized acceptor* ***13*** *excitation and donor* ***24*** *emission spectra. Overlapping evidenced (yellow).*

Since using a small concentration help to avoid self-quenching processes that could cause to a fluorescence signal decrease,[244] **24** was used at low concentrations.

Results reported in Figure 4.73 show the fluorescence spectra of **24** (0.2 µM) acting as the donor, its fluorescence response with the acceptor **13** (10 µM), and the response following addition of D-Fructose (2; 10; 25 µM). The experiments were conducted in PBS, at pH 8 to promote the binding with D-Fructose. A decrease of fluorescence emissions of donor **24** and an increase of fluorescence emission of acceptor **13** were expected. In Figure 4.73, a decrease of fluorescence intensity at emission wavelength of donor (λ = 384 nm) and an increase at one of acceptor 13 (λ = 460 nm) was shown. The results verified the establishment of an interaction between the two probes.

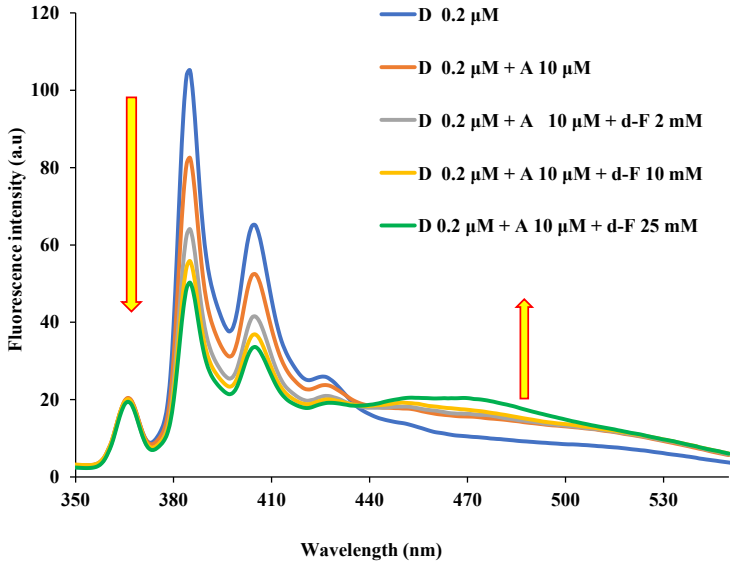


***Figure 4.73**. Fluorescence spectra of donor **24** 0.2 µM, donor **24** plus acceptor **13** (10 µM) and donor plus acceptor plus D-Fructose (2;10;25 µM) in PBS (pH 8). Fluorescence decreases at λ 384 nm and increase at λ 460 nm evidenced with yellow arrows.*

Fluorescence experiments were repeated with **24** at high concentration (0.5 and 1 µM), maintaining a fixed concentration of **13**. The Figure 4.74 and 4.75 report the relative fluorescence

intensity respectively at emission wavelength of donor D (Fig. 4.74) and acceptor A (Fig. 4.75). Each measurement was repeated three times, and the results represent the average of fluorescence intensity recorded with relative standard deviation calculated. The graphs allow comparison of the intensity of the donor at different concentrations and the fluorescence response of acceptor **13** above different concentrations of D-Fructose. The aim was to investigate which concentrations of donor **24** caused the strongest fluorescence intensity decrease following the interaction with acceptor **13**. Similarly focusing on maximum emission wavelength of donor **24**, the aim was to evaluate the concentration at which the most marked decrease occurred.

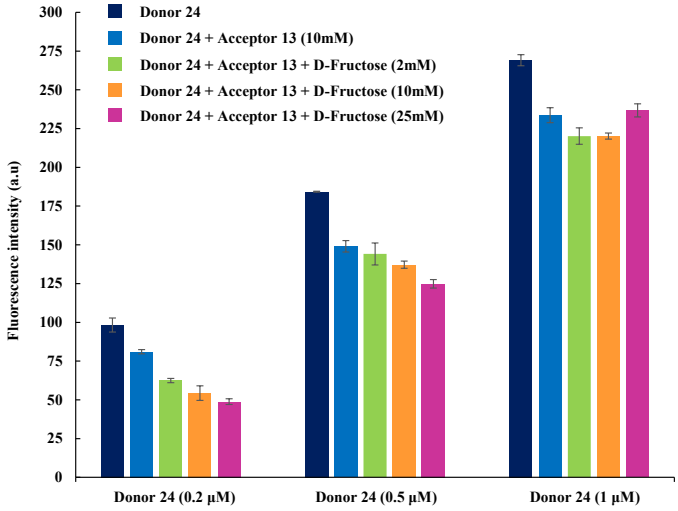


Figure 4.74. *Comparison of the fluorescence intensities between donor **24** at 0.2; 0.5; 1 µM, donor **24** 0.2; 0.5; 1 µM plus acceptor **13** (10 µM) and donor 0.2; 0.5; 1 µM plus acceptor plus D-Fructose (2;10;25 µM) at **λ 384 nm.***

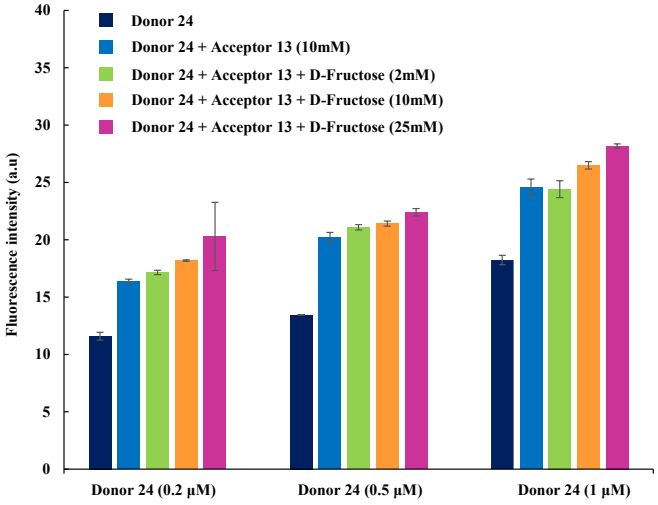


Figure 4.75. *Comparison of the fluorescence intensities by donor **24** 0.2; 0.5; 1 µM, donor **24** 0.2; 0.5; and 1 µM plus acceptor **13** (10 µM) and donor 0.2; 0.5; 1 µM plus acceptor plus D-Fructose (2;10;25 µM) at **λ 460 nm.***

Focusing on the emission wavelength of the donor (Figure 4.74), all tested concentrations of **24** showed a marked fluorescence intensity decrease compared to each other. Similarly, a marked increase in fluorescence intensity in the acceptor's emission spectra upon D-Fructose addition was seen in Figure 4.75. The interaction between donor **24** and acceptor **13** through FRET was confirmed due to this observed fluorescence decrease in emission of the donor and the increase of the acceptor. However, the response following the D-Fructose addition in the FRET couple was not as striking as expected (16.45 ± 6.76) compared to the performance of sensor 13 (400 %), as observed in (Figure 4.64).

The probe **25** (Figure 4.69) was selected as an alternative non-pyrene-based donor probe, to evaluate the interaction between two different probes. The aim was to achieve an improved interaction with sensor **13**. The experiments were repeated with the same conditions as used

previously. Emission spectra was recorded only to 10 µM as selected concentrations. Absorption measurements may require higher concentration compared to fluorescence. Absorption (a) and emission spectra (b) of **25** were recorded to determine the suitable emission wavelength, identified as 334 nm (Figure 4.76).

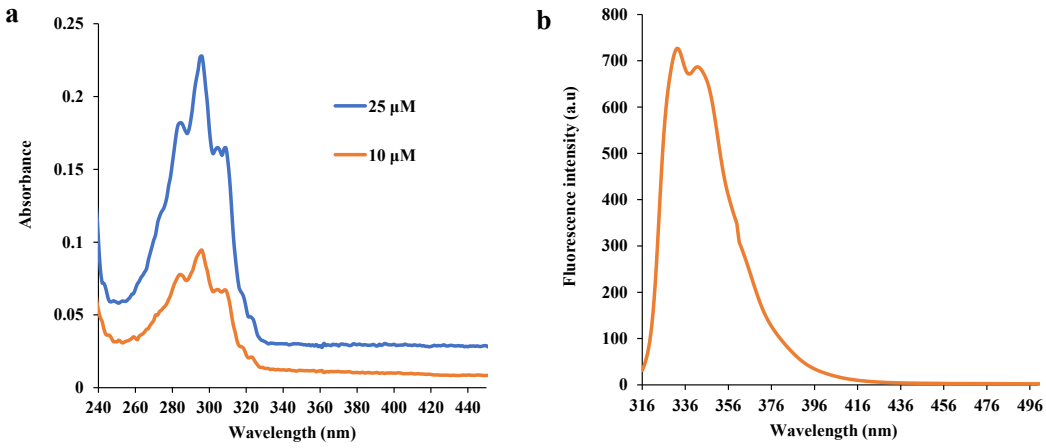


Figure 4.76. *Absorption spectra of **25** (a) and fluorescence spectra (b) at 10 µM at different wavelengths in water.*

The overlap between the two spectra (yellow evidenced) respectively emission of **25** and excitation of **13**, demonstrated the suitability of probe **25** to act as a donor in a FRET application (Figure 4.77).

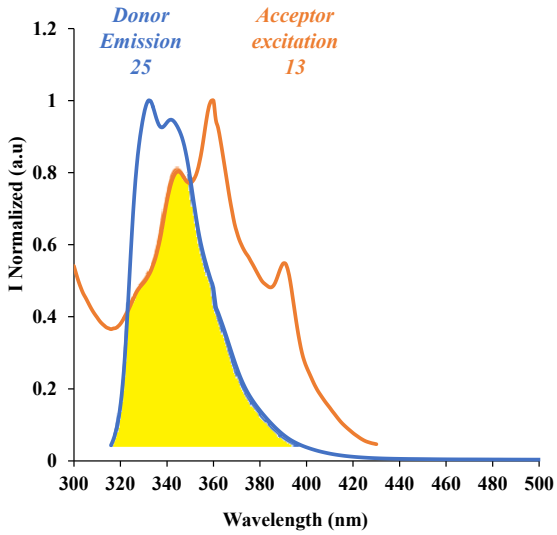


Figure 4.77. *Normalized acceptor **13** excitation and donor **25** emission spectra. Overlapping (yellow) evidenced.*

Comparing with the results reported in Figure 4.72, the overlap occurs at 350 nm, which differed from that seen with donor **24** (390 nm). Fluorescence spectra of **25** (λ_{ex} 296 nm) as the donor at 0.2 µM, together with the acceptor **13** (10 µM) and upon addition of D-Fructose (2; 10; 25 µM) were recorded. As shown in Figure 4.78, the peak fluorescence intensity in the emission of **25** (λ 334 nm) decreased suggesting that the interaction with acceptor **13** was successful. Furthermore, an increase of signal at the emission wavelength of the donor (λ 460 nm) was observed following the addition of D-Fructose.

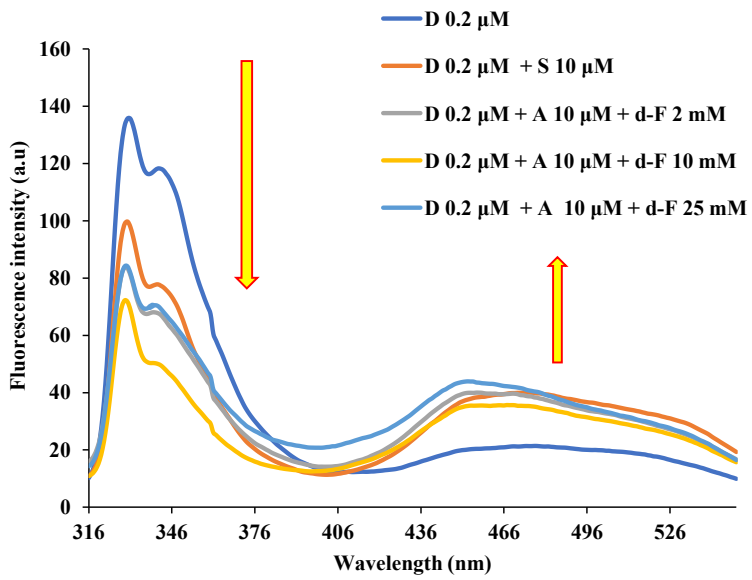


Figure 4.78. *Fluorescence spectra of donor **25** 0.2 µM, donor **25** plus acceptor **13**, (10 µM) and donor plus acceptor plus D-Fructose (2;10;25 µM) in PBS (pH 8). Fluorescence decrease at λ 334 nm and increase at λ 460 nm evidenced with yellow arrows.*

Since a marked change in the fluorescence response was not seen when a high concentration of the previous donor **24** was used (Figure 4.75), fluorescence experiments were repeated with donor **25** only at 0.5 µM. Figure 4.79 and 4.80 show the results observed at the two-emission wavelengths, 334 nm and 460 nm. As below, the results represent the average of three measurements with standard deviation calculated.

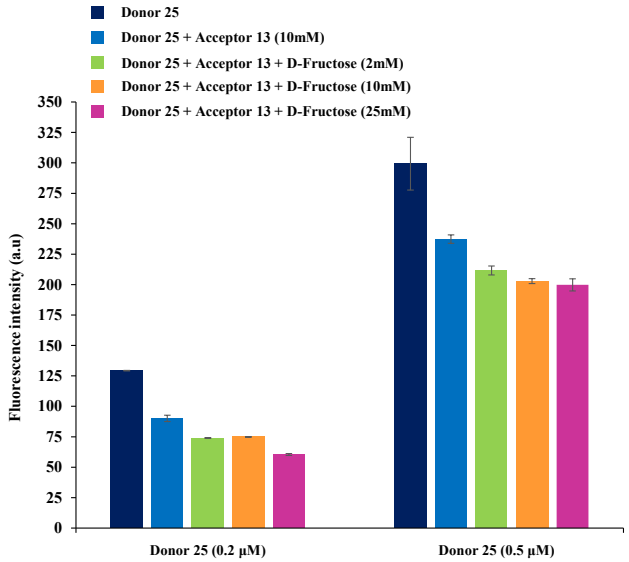


Figure 4.79. *Comparison fluorescence intensities by donor* ***25*** *0.2; 0.5 µM, donor* ***25*** *0.2; 0.5; 1 µM plus acceptor* ***13*** *(10 µM), and donor 0.2; 0.5 µM plus acceptor plus D-Fructose (2;10;25 µM) at* ***λ 334 nm****.*

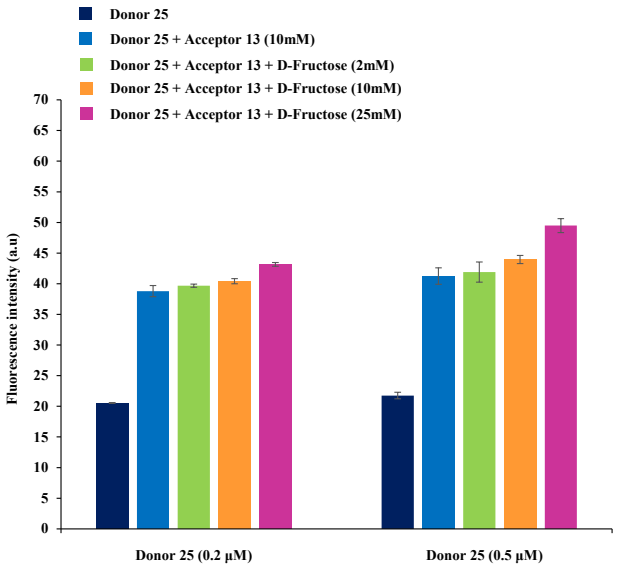


Figure 4.80. *Comparison fluorescence intensities by donor* ***25*** *0.2; 0.5 µM, donor* ***25*** *0.2; 0.5 µM plus acceptor* ***13****, and donor 0.2; 0.5 µM plus acceptor* ***13*** *plus D-Fructose (2;10;25 µM) at* ***λ 460 nm****.*

As shown with **24**, the concentration did not affect the fluorescence response. However, a fluorescence emission decrease of the donor and an increase of fluorescence emission of the acceptor was observed, suggesting an interaction between donor **25** and acceptor **13** through FRET. As observed with **24**, the fluorescence response was not comparable with sensor **13** (15.61 ± 6.15).

The fluorescence signal response of the two probes 1-ethynylpyrene **24** and 1-ethynylnaphathalene **25** at 0.2 µM with acceptor **13** and with D-Fructose addition were compared. Figure 4.81 shows the relative fluorescence intensity of **24** and **25** at 384 nm (left) and 334 nm (right). These wavelengths correspond to the maximum emission wavelength recorded for **24** (384 nm) and **25** (334 nm).

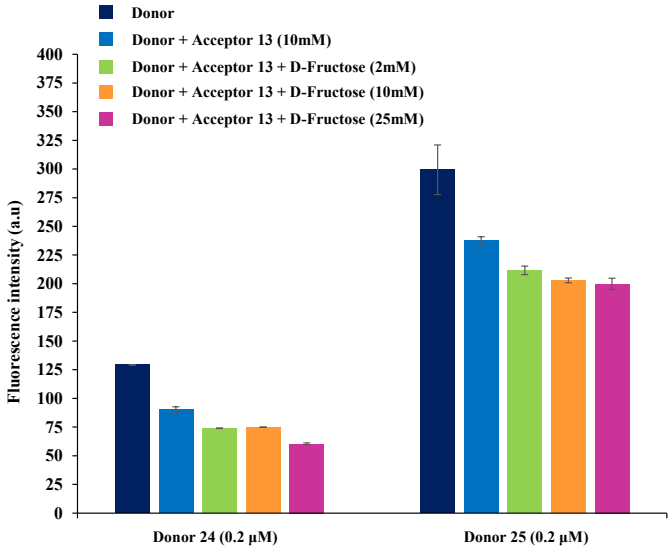


Figure 4.81. *Comparison between fluorescence intensities of donor **24** and **25** (0.2 µM), donor plus acceptor **13** (10 µM), and donor plus acceptor plus D-Fructose at λ_{em} **384 nm** (24) and **334 nm** (25).*

Both probes employed as donors displayed a fluorescence intensity decrease when acceptor **13** was added. These results suggested an interaction between the two probes. Figure 4.82 reports the

fluorescence intensity of **24** and **25** at 460 nm, identified as the maximum emission wavelength of acceptor **13**.

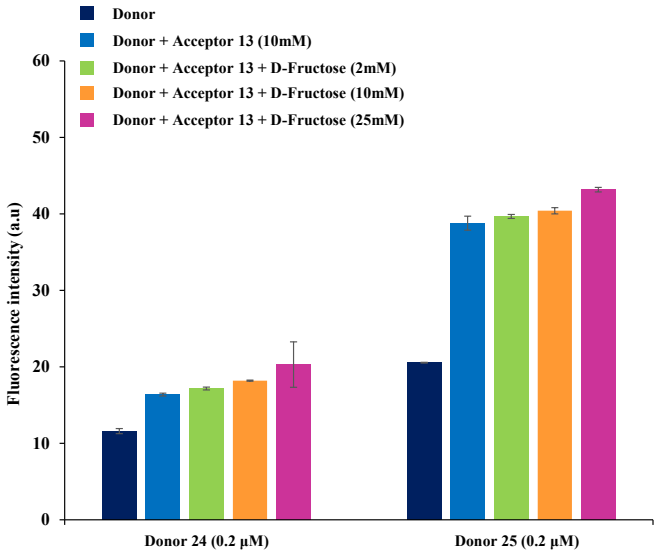


Figure 4.82. *Comparison fluorescence intensities by donor **24** and **25** 0.2 µM, donor plus acceptor **13** (10µM) and donor plus acceptor plus D-Fructose at* λ_{em} ***460 nm**.*

As expected, a fluorescence intensity increase following the addition of **13** was seen. No marked change in fluorescence response following the D-Fructose addition was observed, independent of the probe used. This was attributed to the large difference in quantum yield between the donors and the acceptor, involved in the PET process. It was thought that the fluorescence, re-established upon the sugar binding by PET suppression, was not sufficient to achieve a comparable quantum yield as the donor. Consequently, despite evidence of an interaction between the probes, the system did not provide a significant improvement compared to just sensor **13**. Detected fluorescence response was higher for **25** compared to **24**. This may be due to the lower quantum yield of naphthalene dye **24** (0.16) compared to pyrene dye **25** (0.69).[180] The lower difference between the quantum yields of **13** and **25** was expected to bring a more visible change in the fluorescence

response upon sugar binding. Moreover, both **24** and **13** are pyrene dye-based which could interact with each other by collision and affect the fluorescence response due to self-quenching. Considering the difference of quantum yield between the probes analysed (**24** and **25**) and the sensor **13**, it was hypothesised that a lower concentration of donors (< 0.2 μM) could promote the interaction, enhancing the signal. Increasing the concentration of **13** was not considered as this could increase the possibility of self-quenching occurring. It was expected that a higher fluorescent intensity of acceptor **13** could be achieved by employing probes with an emission wavelength, closer to 360 nm, the excitation wavelength of **13**.

The role of sensor **13** as donor was also investigated. Sulfonated coumarin dye AF430 (**26**) was selected as acceptor, due to its functionalized structure involving an acetylene group, and to its reported excitation wavelength (at 450 nm) could be suitable for FRET application with **13.**

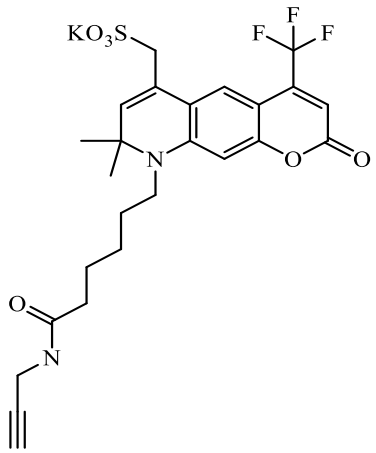


Figure 4.83. *Chemical structure of sulfonated coumarin dye AF430 (**26**).*

The fluorescence intensity increases of sensor **13** following the binding with saccharides was anticipated to enable the interaction with the acceptor probe. A consequent increase in fluorescence emission of acceptor through the FRET process, as reported in Figure 4.84.

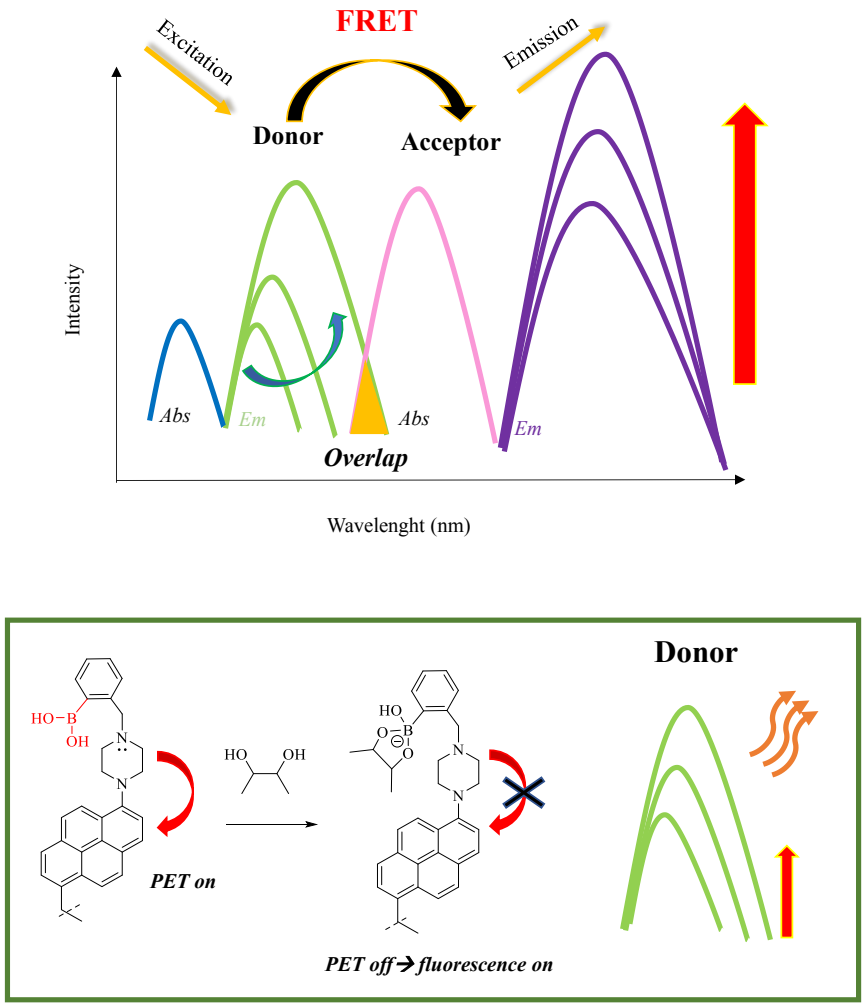


Figure 4.84. *Scheme to show the interaction between the sensor **13** acting as donor in FRET process.*

Photophysical properties of **26** were investigated recording absorption (a) and fluorescence spectra (b) at two concentrations of 10 μM and 25 μM (Figure 4.85).

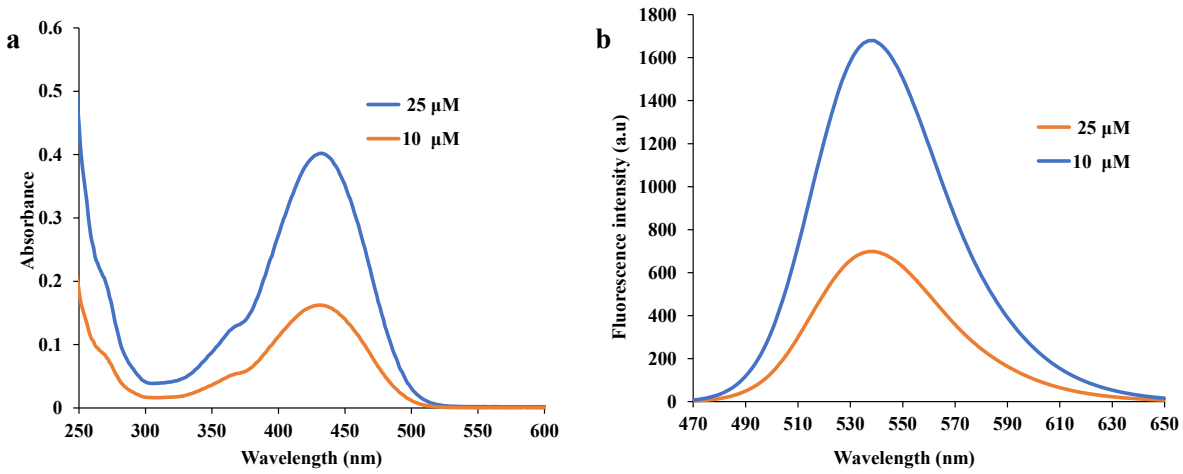


Figure 4.85. *Absorption spectra (a) and fluorescence spectra (b) of* ***26*** *in water.*

To enable **26** to act as the acceptor, an overlap between absorption spectra with the emission spectra of the donor was required. Figure 4.86 reports the suitable overlapping of respective spectra.

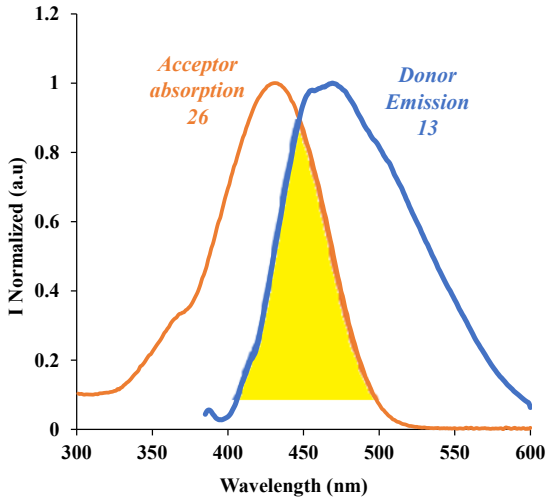


Figure 4.86*. Normalized absorption spectra of acceptor* ***26*** *and emission spectra of donor* ***13****. Overlapping (yellow) evidenced.*

In this case, mixing donor (sensor **13)** and acceptor should not make a big change due to PET quenching of the donor's fluorescence emission, so not much FRET interaction was anticipated. It was expected that donor **13** would interact more with acceptor **26** upon the sugar binding. Indeed, the interaction with D-Fructose caused the suppression of PET process and the restoration of fluorescence According to the FRET process, the fluorescence emission of acceptor was projected to increase following the establishment of this interaction. Fluorescence spectra of **26** (1 µM) together with donor **13** (10 µM), at excitation wavelength of latter (360 nm), and following addition of D-Fructose (2;10;25 µM) were recorded in PB solution, pH 8 and reported in Figure 4.87. A fluorescence intensity increase was observed at the emission wavelength of **13** (λ_{em} 460 nm) upon the addition of D-Fructose. However, a marked fluorescence change in emission by acceptor **26** (λ_{em} 540 nm) was not observed.

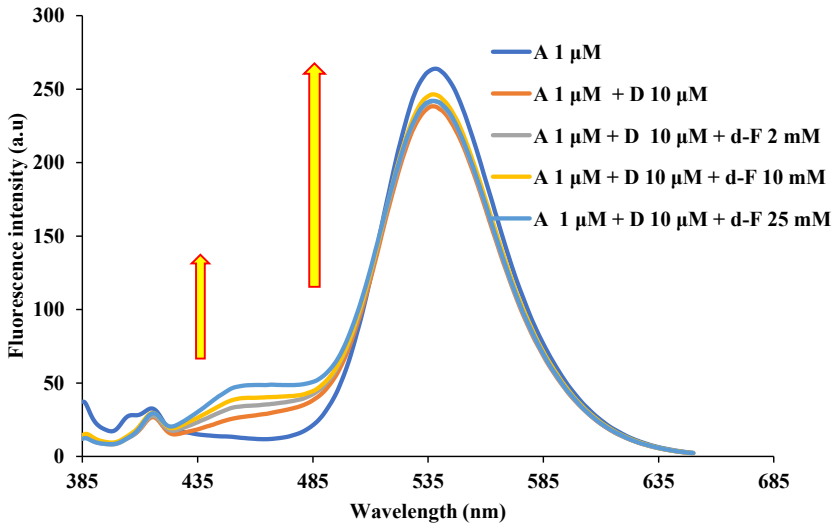


Figure 4.87. *Fluorescence spectra of acceptor* ***26*** *1 µM, acceptor* ***26*** *plus donor* ***13*** *(10 µM) and acceptor plus donor plus D-Fructose (2;10;25 µM) in PBS (pH 8). Fluorescence increase at* λ_{em} *460 nm and 540 nm evidenced with yellow arrows.*

The fluorescence response recorded at 540 nm, identified as maximum emission wavelength of the acceptor, displayed only a slight increase (3.5%). Due to these results, fluorescence experiments were repeated with acceptor **26** at high concentration (5 and 2 μM), without changing the concentration of **13**. Figure 4.88 and 4.89 summarize the relative fluorescence intensity at λ_{em} 460 nm and 540 mm, respectively maximum emission wavelength of donor (460 nm) and acceptor **26** (540 nm). Analogue to the previous experiments. the data shown represent the average of three measurements with standard deviation calculated.

The fluorescence intensity increase observed at 460 nm alongside the addition of acceptor and D-Fructose, λ_{em} of donor **13**, established the successful interaction with sugars and the suppression of PET involved. These results did not suggest the establishment of FRET mechanism (Figure 4.88). Investigation of the fluorescence intensity recorded at 540 nm (Figure 4.89), showed no enhancement of fluorescence intensity of acceptor **26** following the addition of donor and D-Fructose. It was therefore concluded that an interaction by FRET did not occur as predicted. The fluorescence response of **13** was thought to be independent of addition of **26**. It was proposed that the fluorescence emission of **26** was not subjected to a marked change by interaction with **13**, probably due to its lower quantum yield of sensor **13** attributed to the PET involved. The binding with D-Fructose restored the fluorescence of **13,** as verified by enhancement of fluorescence intensity at 460 nm. However, it was thought that the fluorescence re-established upon the sugar binding by PET suppression did not permit the successful interaction with acceptor **26**. Consequently, an interaction between the probes was not verified.

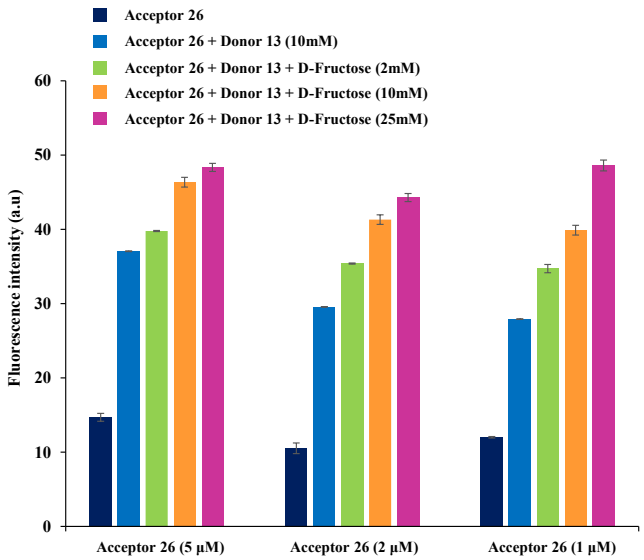


Figure 4.88.**. Comparison fluorescence intensities by acceptor **26** (5, 2 and 1 µM), acceptor **26** plus donor **13** (10 µM) and acceptor plus donor plus D-Fructose (2;10;25 µM) at λ_{em} **460 nm.

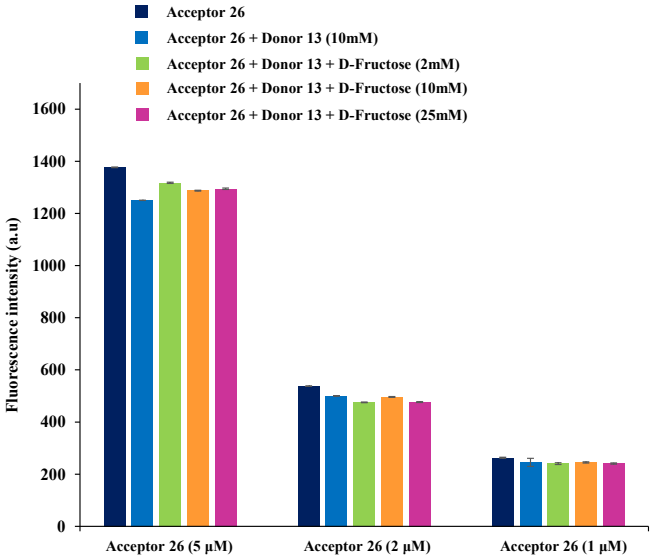


***Figure 4.89.** Comparison fluorescence intensities by acceptor **26** (5, 2 and 1 µM), acceptor **26** plus donor **13** (10 µM) and acceptor plus donor plus D-Fructose (2;10;25 µM) at λ_{em} **540 nm**.*

The results validate the interaction between **13** as acceptor and **24** or **25** donors through FRET. It has not observed the establishment of an interaction between **13** acting and the acceptor **26.** For both systems investigated, with sensor **13** acting as the acceptor or donor, the fluorescence response recorded upon the addition of **13** did not overcome the sole performance of the sensor. One reason proposed was the small quantum yield of sensor **13**. It was assumed that the fluorescence restoration following PET suppression did not allow a significant interaction with the probes investigated. The FRET efficiency depends on different factors such as spectral overlap integral, distance by FRET pairs and dipole-dipole interactions. A suitable overlap between the emission spectrum of donors **24** and **25** and the excitation spectra of **13** was verified (Figure 4.77). Similarly, a spectral overlap between the emission spectrum of sensor **13**, as donor, and the absorption spectra of acceptor **26** was also observed (Figure 4.86). A deeper study to evaluate the distance between probes investigated or the interaction between dipole-dipole has not been performed. Consequently, it was predicted that these factors could also have affected the fluorescence mechanism involved. However, it was expected that the incorporation of the probes onto the surface would help to reduce the distance between the probes, since both would be confined on the surface. Moreover, it was expected that the orientation of dipole and consequently their interaction would be more controlled upon reduced matrix interference.

4.5 Summary and outlook

The third sensing system involved a pyrene-based sensor with the boronic acid connected through the piperazine ring. It acts both as a linker and a fluorescence quencher, ensuring a PET process is involved. The sensor was also functionalized with an acetylene group to allow the future immobilization on the surface of silica nanoparticles. Although the synthesis of sensor **13** was achieved employing a few steps, gaining the desired product was challenging due to side product formation such as **21** (Methyl ketone) or product oxidation (**22**). One issue was the presence of two different protective groups, TMS for acetylene group and Boc for amino group. The deprotection reaction of Boc required acidic conditions, which at same time brought an undesired reaction from TMS groups. Thus, appropriate combination and sequence of reactions was required. Moreover, the separation and purification of the target compound **13** needed to be performed in suitable conditions, to avoid degradation of the product. The presence of the amino and boronic acid groups made the separation by reverse phase chromatographic column difficult. Furthermore, the high sensitivity of the compound to temperature did not allow the use of LC-MS technique because temperature was involved to promote the separation. Heatless alternative purification techniques, such as normal phase chromatographic column or HPLC technique, could be employed to achieve the final sensor at high purity. Since the optimum purification condition was not established the sensor was yielded with low purity (36 %). Alternative separation techniques as well as the optimization of synthesis conditions will enable the product to be obtained with a higher level of purity.

Experiments conducted both with sensor **13** and **13b** showed how the presence of TMS group in **13b** affected the fluorescence properties of the compound. Despite its low purity, the application of sensor **13** in saccharide detection was demonstrated. An enhancement of fluorescence intensity

upon the binding with saccharides at pH 8 was observed. It was evidenced that a PET process first occurred and then was suppressed to restore fluorescence abilities of pyrene. Results obtained by pH titration emission profile suggested that the sensor was able to work at physiological pH (~ 7.4) as well. The higher selectivity of sensor **13** toward D-Fructose and D-Sorbitol compared to D-Glucose was demonstrated. It was believed that the sensing potential of **13** was affected by its low purity. The actual sensitivity and the efficiency of the sensor were therefore expected to be improved when a higher purity compound could be achieved.

Fluorescence experiments performed with sensor **13** and the probes **24** and **25** demonstrated the interaction between **13** as acceptor and **24** and **25** as donor probes. Any enhancements of fluorescence emission by acceptor **26** was observed employing sensor **13** as donor. Consequently, the interaction between **13** acting as the donor and the acceptor **26** was not verified**.** For both systems investigated, with sensor **13** acting as acceptor or donor, the fluorescence response recorded upon the addition of **13** did not overcome the performance of the sole sensor. The low quantum yield of sensor **13** was identified as a possible explanation. It was assumed that the fluorescence restoration following PET suppression did not allow a significant interaction with the probes investigated.

However, it was expected that the FRET efficiency would be improved through the incorporation of the probes onto a solid surface. Indeed, it was expected that the reduced distance between the probes and the favourable orientation between their dipole would improve the performance of the system. Furthermore, the investigation of alternative dyes to those tested has not been excluded. Moreover, a selected ratio between probes employed in FRET process will allow regulation of their interaction and so improve the performance of the sensing system.

Performed studies with the third sensing system (sensor **13**) showed a quenching behaviour of the fluorophore, verifying the role of the length and rigidity of the linker to ensure the fluorescence mechanism PET involved. The synthesized compound displayed fluorescence enhancement after sugar addition in the millimolar range, confirming its application for saccharide detection. The next immobilization of the sensor **13** into silica nanoparticles is expected to improve its performance and sensitivity toward saccharides. Moreover, it has been proved that the fluorescence intensity change produced by the saccharides binding by PET could be employed to establish the interaction with an additional probe, attesting to a FRET process. The final aim will be achieving the incorporation of the sensing system based on sensor 13 and dye as FRET probes coupled onto the surface. This is expected to improve the interaction between the units involved and reduce the matrix interferences. The effect will be promoting the fluorescence response upon saccharides detection through the establishment of FRET process.

The sensor **13** has been functionalized with an acetylene group in the structure of the fluorophore. The presence of azide group on the surface will allow the incorporation of the sensor through a click chemistry reaction as shown in Figure 5.12. (Chapter 5). Moreover, the probes investigated for FRET applications as 1-ethynylpyrene (**24**), 1-ethynylnaphathalene (**25**) and sulfonated coumarin dye AF430 (**26**) involved an acetylene group. Therefore, there can be incorporated onto the selected surface through the same strategy with click chemistry reaction. The final aim will be achieving the incorporation of the sensing system into the surface. This is expected to improve the interaction between the units involved and promote the fluorescence response by the establishment of FRET process.

CHAPTER 5: SURFACE SOLID SUPPORTS

Each system described in the previous chapter is planned to be immobilized onto a silica surface. Indeed, it was predicted that incorporation of the system onto the surface would strengthen the interaction between the units involved. Moreover, it was expected that the system would be less affected by matrix environments. The final aim is to achieve an enhancement of the final fluorescence response, improving the performance of the system. Silicon-based surfaces were selected as solid support due to their transparent and photophysical inert properties, making them suitable for fluorescent sensing application. Moreover, they can be functionalized with terminal groups, allowing the incorporation of the system units onto silicon wafers and silica nanoparticles, which were investigated as potential solid supports. SAM formation on silicon wafers was first investigated, evaluating different deposition techniques through ellipsometry and contact angle measurements. Silica nanoparticles were investigated regarding their size and functionalized groups on the surface to achieve the desired dye-doped nanoparticles. Both silica-based surfaces have been investigated as potential solid substrates for same application as sensing system incorporation.

5.1 SAM formation on silicon wafer surfaces

Silicon oxide wafers (SiO_2) were selected since they allow for easy monolayer characterization by ellipsometry and contact angle. Before performing the functionalisation reaction, an appropriate cleaning procedure was needed to obtain high-quality films and high reproducibility because the presence of contaminants on the substrate can affect the uniformity and homogeneity of the SAM.[245] Among different procedures,[245] piranha solution cleaning is the most suitable to remove both organic and inorganic impurities. It also guarantees the activation of the surface, producing a

thin hydrophilic oxide layer. The chips were carefully cleaned by immersion in piranha solution,[246] a mixture of sulfuric acid (H_2SO_4) and hydrogen peroxide (H_2O_2).

Following the cleaning procedure, the next step involved the functionalization of the silicon wafers by SAM formation. For example, Amino functionalization is a known, versatile procedure and has been verified by XPS studies.[247] The dry deposition technique for SAM formation was selected over liquid deposition, because it helps to prevent the formation of multilayers onto the surface due to the polymerization tendency of amine silane compounds.[112] The method occurred in a sublimation chamber to allow the vaporization of the selected silane held in one or more vials positioned at the bottom of the chamber (Figure 5.1). Chips with an approximate area of 1 cm^2 were placed in different locations (2) on higher support, facing upwards or upside down (1), as shown in the Figure 5.1. After exposing the chamber to vacuum, the silane was evaporated and began to deposit on the chips once the vacuum was stopped and maintained. Finally, the chip was put inside an oven to enhance the crosslinking of the deposited silane to the silica surface (curing). Vacuum, deposition and curing time, as well as chip number and position, were variables studied during the experiments.

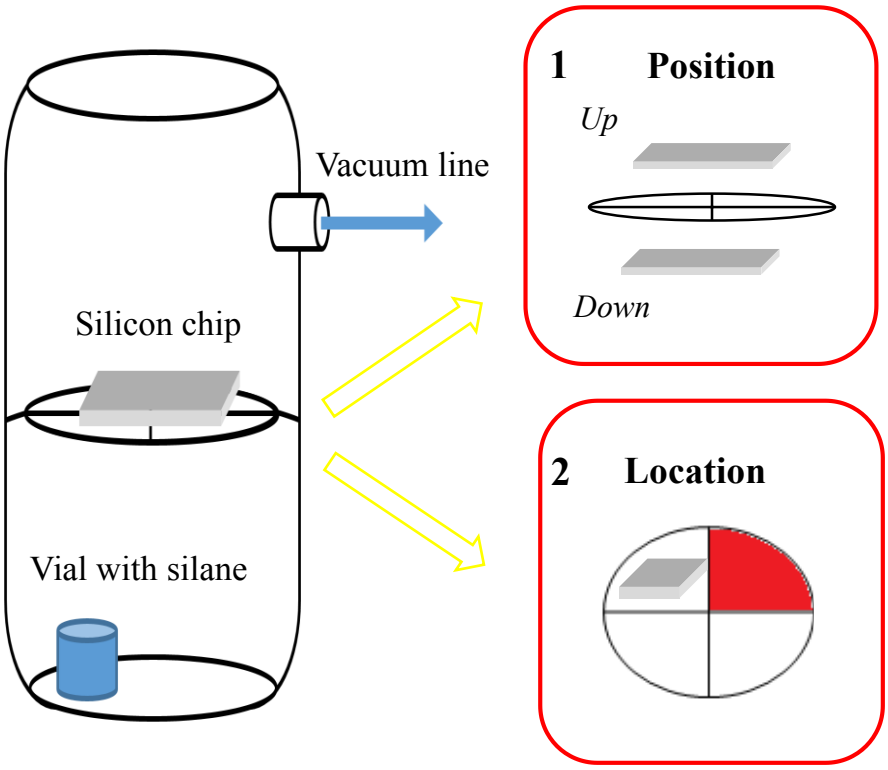


Figure 5.1. *Representation of sublimation chamber: vial with silane silicon chip on support, and vacuum line. Different position up and down (1) and location (2) are shown.*

Ellipsometry and contact angle were used to evaluate the thickness and wettability respectively, to confirm surface functionalization.

Preliminary studies were performed with more hydrophobic thiol groups of (3-mercaptopropyl) trimethoxysilane (MPTMS), which should provide higher contact angle values compared to amino functionalization, due to the hydrophilicity of silicon chips.

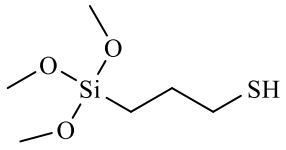


Figure 5.2. *Structure of (3-mercaptopropyl) trimethoxysilane (MPTMS).*

Table 5.1 shows the first condition evaluated. For the first experiments, a different blank chip was used as a reference. Si thermal oxide fitting model was selected as a fitting model for ellipsometry measurements. The theoretical thickness for MPTMS molecule on the surface was calculated as 0.61 nm using ChemDraw 3D.

Table 5.1. *Conditions A-B-C-D for SAM formation with MPTMS.*

Dry deposition						
Conditions	Orientation	N chips	Vacuum time (*min*)	Deposition time (*min*)	Curing time (*min*)	Silane
A	Up	2	5	120	30	MPTMS
B	Down	2	5	120	30	MPTMS
C	Up	4	5	120	30	MPTMS
D	Up	4	30	120	30	MPTMS

The first experiments **A** and **B** were conducted with 2 chips placed in the sublimation chamber. Conversely, experiments **C** and **D** involved four chips distributed symmetrically in the sublimation chamber. Experiment **A** did not show good homogeneity values by ellipsometry measurements, where the relative errors are quite high (Figure 5.4).

An increase in both advancing contact angle (ADV) and receding contact angles (REC) compared to the blank were observed. This change from a hydrophilic to a hydrophobic surface confirmed the successful deposition of MPTMS (Figure 5.3). In experiment **B,** the chips were placed in the downside orientation whilst maintaining the same other conditions as in experiment **A**. The number of chips from two to four (**C**) was increased to achieve an improvement in homogeneity between chips. To allow more exposure of the chips to MPTMS, in exp **D** the vacuum time was

increased to 30 min and three vials containing the silane were used, rather than one as used in exp **A-C**. By contact angle measurements, both the ADV and REC contact angles were enhanced, comparing condition **D** with **C**.

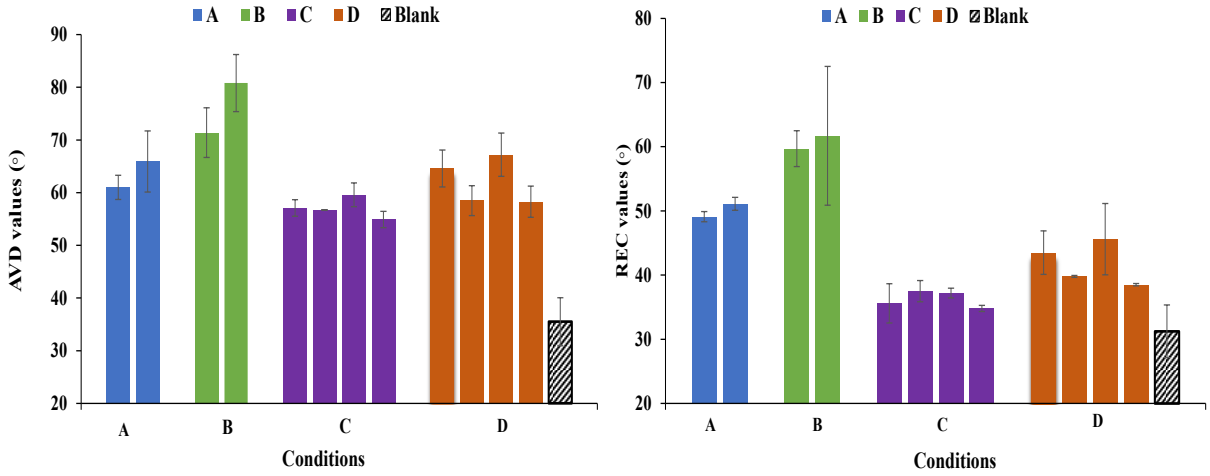


Figure 5.3. *Advancing (left) and receding contact angle of MPTMS SAMs on SiO_2 surface following conditions A-D shown in Table 5.1. Reference values for bare surface (black bar).*

However, the observed thickness values do not correlate with the theoretically calculated values in any of the chips examined. Furthermore, there is a high degree of inter-chip variation within each tested method, as shown in Figure 5.4. Condition **A** and **C** gave measured thicknesses markedly lower than the theoretical thickness, whereas condition **B** and **D** gave sometimes higher measured thicknesses than the theoretical thickness. The higher values found for **B** and **D** may be attributed to the formation of multi-layers. Regardless, there was clearly issues with reproducibility and heterogeneity across chips, mainly in method **D**. Despite producing lower than expected thicknesses, method **C** had the best reproducibility therefore experiments were performed by alternating vacuum and deposition time through cycles.

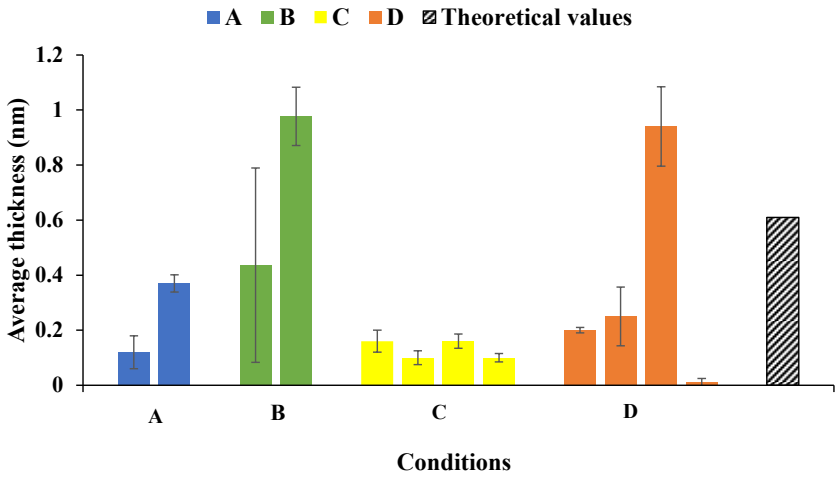


Figure 5.4. *Ellipsometry data for MPTMS SAMs on SiO_2 surface compared to the theoretical calculated values, following conditions A-B-C-D shown in Table 5.1.*

In next experiments, vacuum time and deposition time remained the same but 4 cycles of vacuum/deposition were performed, aiming to increase the deposition rate and achieve homogeneous thicknesses. Different time combinations of both cycles were investigated, as reported in Table 5.2. The position of the chips was also evaluated in method **G**. In addition, the same chips were used as blank reference and subjected to reaction, to achieve a truer representation of the surface.

***Table 5.2**. Conditions E-F-G-H for SAMs formation.*

Dry deposition					
Conditions	Orientation	Vacuum time (min)	Deposition time (min)	Curing time (min)	Compounds
E	Up	5 x 4	25 x 4	30	MPTMS
F	Up	5 x 2	55 x 2	30	MPTMS
G	Down	5 x 2	55 x 2	30	MPTMS
H	Up	5 x 2	55 x 2	30	MPTMS in Et_2O

The measured thicknesses values achieved with first method (**E**) were more than double (1.593 ± 0.075 nm) of the theoretical values (0.61 nm) as it possible to observe in Figure 5.5. Assuming the possible formation of multilayers, the number of cycles of vacuum were reduced and the deposition time (55 min) was increased for two cycles (exp **F**). These experimental conditions gave the most comparable measured thickness to that of the theoretical value (0.65± 0.15 nm). Furthermore, the highest contact angles values were also reached, as it is visible in Figure 5.6, showing the formation of a more hydrophobic surface. The experiments were repeated in the same conditions to evaluate the reproducibility of the model (**F***). Although two chips achieved the thickness value expected (0.64 ± 0.42 nm), the other two chips analysed showed different values which were both too small (0.26 nm) and too high (1.24 nm). The issue of reproducibility therefore persisted, which was also seen in the contact angle results (Figure 5.6). An inverted position of a chip on the support was evaluated to improve this issue (exp **G**). To place the chips in a suitable position upside down, only three chips were analysed. The majority of ellipsometry results, showed higher values (2.17-2.78 nm) than expected, again suggesting that multilayers were being formed at the surface. Moreover, the inverted position did not ensure the stability of the chip on the support, increasing

the possibility of contamination. Returning to the original position, experiments (**H**) were carried out using a solution of MPTMS and diethyl ether (Et_2O) to promote the evaporation rate. Although the measured thicknesses achieved were lower compared to the theoretical thickness (0.28 ± 0.06 nm), there was more consistency across the chips which was also seen in the contact angle data (Figure 5.6).

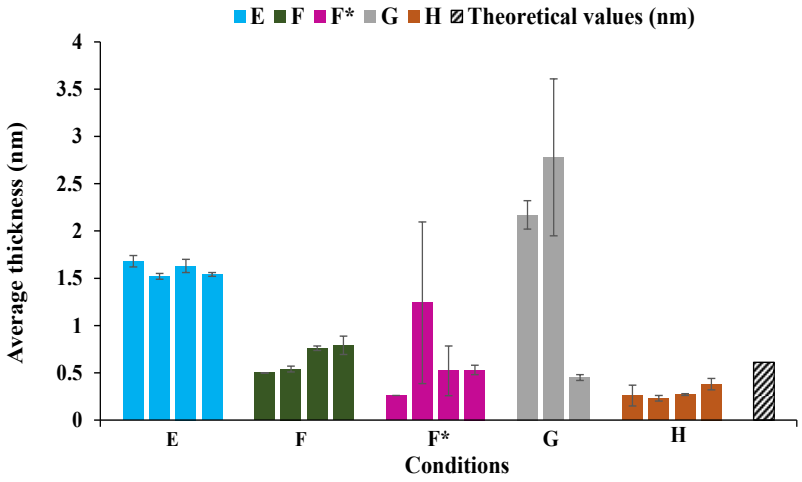


Figure 5.5. *Ellipsometry data for MPTMS SAMs on SiO_2 surface compared to the theoretical calculated values, following conditions E-F-G-H. shown in Table 5.2.*

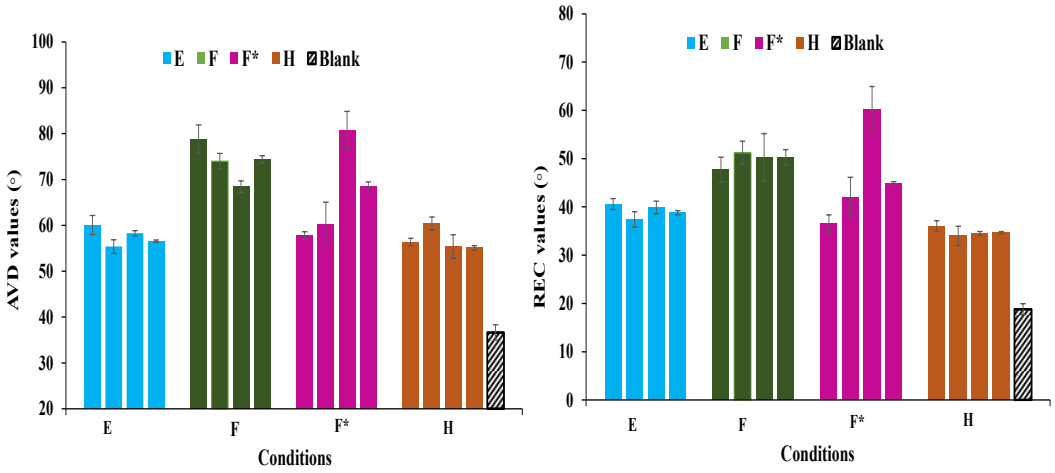


Figure 5.6. *Advancing (left) and receding contact angle of MPTMS SAMs on SiO2 surfaces following conditions E-F-G-H shown in Table 5.2. Reference values for bare surface (black bar).*

Method **H** achieved the best results however different silane were evaluated to achieve improved accuracy. Method **I** was conducted using (3-aminopropyl) trimethoxysilane (APTMS) instead, using the same conditions of **F** (Table 5.3).

Table 5.3. *Conditions I-J for SAMs formation.*

Dry deposition					
Conditions	Orientation	Vacuum time (min)	Deposition time (min)	Curing time (min)	Compounds
I	Up	5 ×2	55 ×2	30	APTMS
J	Down	0.5	55 ×2	No	APTMS

Measured thickness values were compared with the theoretical thickness of APTMS (0.58 nm). it possible observe in Figure 5.7, the value measured following exp **I** was closer to the theoretical value (0.63 ± 0.18 nm). Whereas for method **J**, the chips were placed in downside position and

vacuum and deposition were reduced respectively to 0.5 min and 30 min with no curing time, resulting in measured thicknesses larger than the theoretical (2.08 ± 0.68 nm). Contact angle results were indicative of the presence of APTMS on the surface if they are compared with bare surface (ADV~45° and REC~29°), as shown in Figure 5.8. Furthermore, the very high thicknesses achieved with method J indicate the formation of multilayers.

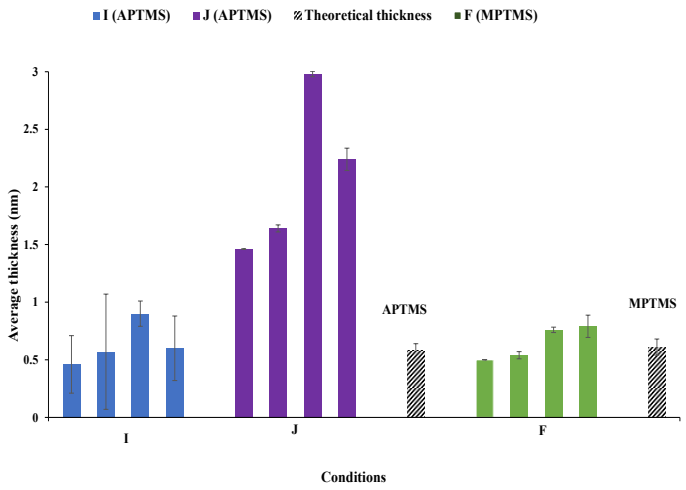


Figure 5.7. *Comparison between ellipsometry data of APTMS and MPTMS SAMs on SiO_2 surface following conditions I-J show in Table 5.3. Theoretical thickness for each silane is taken as reference.*

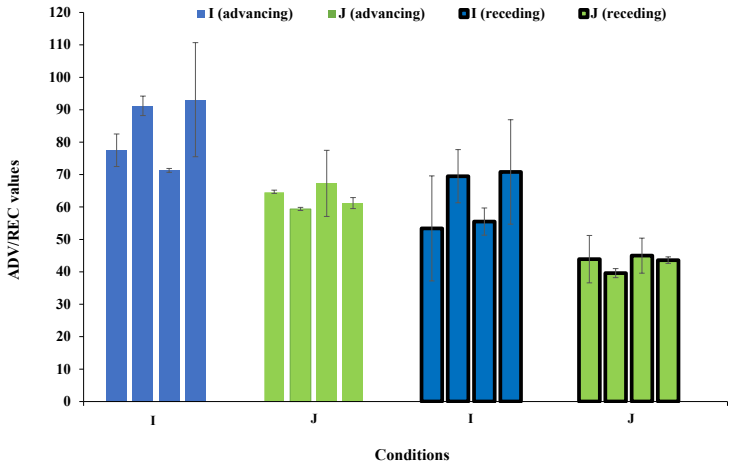


Figure 5.8. *Advancing and receding contact angle of APTMS SAMs on SiO_2 surface following conditions I-J shown in Table 5.3.*

No significant difference in the quality of SAM formation was seen when APTMS was employed instead of MPTMS, therefore a different method of SAM formation involving liquid deposition was investigated.

For this method, MPTMS solution was prepared in toluene (1 mM). Markedly high thicknesses (30.75 ± 18.22 nm) were measured compared to the theoretical value of 0.58 nm, suggesting that polymerization of silane onto the surface had occurred. Moreover, an unacceptable degree of inter-chip variation was seen. The average advancing (79.4± 10.01°) and receding contact angles (56.47± 5.83°) were higher than those for bare SiO_2, confirming the presence of silane (Figure 5.9). Taken together, the contact angle and ellipsometry results support the theory that this method promoted the polymerisation of silane onto the surface.

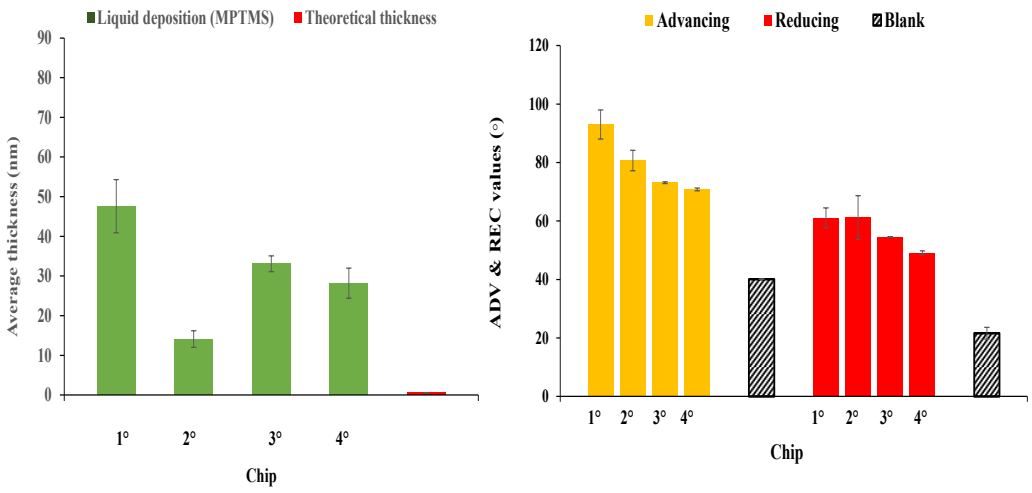


Figure 5.9. *Ellipsometry data (left) and advancing and receding contact angle values (right) for MPTMS on SiO_2 surface by a liquid deposition method. The values are compared with theoretical thickness in ellipsometry measurements. ADV- REC values of bare SiO_2 are used as blank reference.*

To investigate the deposition of silane onto the surface, a different approach using vapor deposition was attempted. Instead of a single measurement for each chip, a larger chip (3×3 cm) was examined at 9 different points, improving deposition rate evaluation (Figure 5.10). Experiments with said chip with MPTMS silane at the same condition as **F** and **G**, were conducted and characterized by ellipsometry.

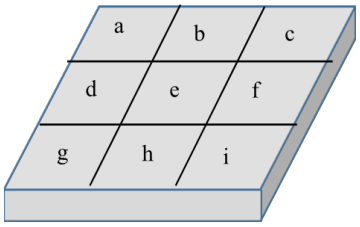


Figure 5.10. *Scheme of chip used during experiments: a physically larger dimension to allow differentiating each position.*

Thickness values observed were smaller (0.24± 0.06 nm) than the theoretical calculated thickness of 0.61 nm in all the points examined (**F2**). An upside-down position of the chip may promote multilayer formation, as seen in Figure 5.11 (**G2**), as all the measured thicknesses exceed the theoretical. In both experiments, different thickness values across the points were observed, suggesting that deposition rates in particularly with exp **G2** did not occur homogeneously on the surface (Figure 5.11). It is thought that the inverted position of chips aggravated the issue.

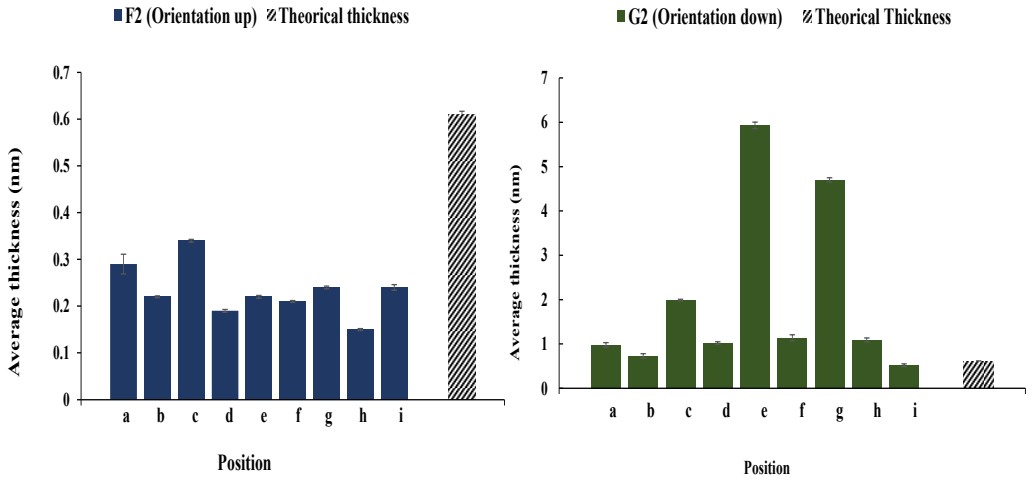


Figure 5.11. *Ellipsometry data of different points (a-i) of one larger chip with orientation up (left) and down (right) following the condition shown in Table 5.3. The values are compared with theoretical calculated thickness TT (red bars).*

The contact angle data verified the successful deposition of silane onto the surface, with method **F** achieving the most satisfactory results. However, ellipsometry data indicated either the formation of multilayers, due polymerisation of silane, or incomplete deposition. Across the experiments, poor homogeneity and reproducibility was consistently seen. Further optimisation was therefore needed to reduce the heterogeneity which could affect the fluorescence properties.

5.2 SiO_2 NPs characterization

SiO_2 NPs was selected next as a potential solid support for the fluorescence sensing system due to their excellent stability, recyclability, biocompatibility, and low toxicity. Dye doped silica nanoparticles can provide an enhancement of fluorescence signal due to the possibility of incorporating several fluorophores onto the surface. Followed by the attachment onto the surface, fluorescence properties of the designed sensor are less influenced by the solvent environment. [54] Therefore, the sensor was predicted to have increased sensitivity, prolonged detection time and better reproducibility if immobilised onto a solid support.[89, 184] The surface of SiO_2 NPs can be readily functionalized with organic molecules through alkoxysilane chemistry, as observed on the surface of silicon wafers (3.2). In contrast with silicon wafers, SiO_2NPs were characterized by techniques such as DLS, zeta potential, IR or transmission electron microscopy (TEM) to evaluate successful functionalization.[248] A suitable spacer between the surface and the probes will guarantee that the functionality of the probe is retained and will impede surface-induced effects such as quenching. The strategy used here provided the functionalization of SiO_2 NPs with azide groups, enabling immobilisation of the designed boronic-based sensor with ethylene group, through CuAAC chemistry with formation of triazole (Figure 5.12). [249]

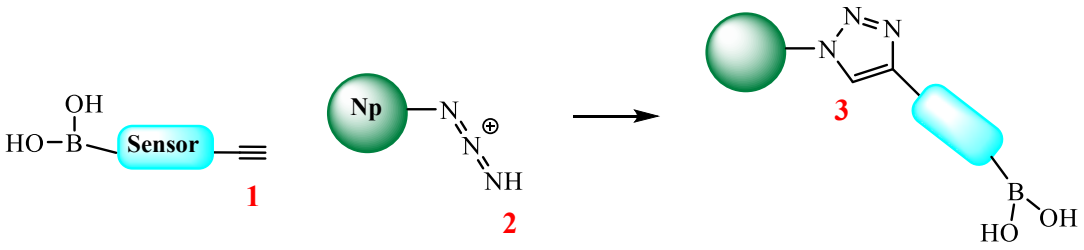


Figure 5.12. *Incorporation of sensor into the SiNPs functionalized surface. CuAAC chemistry reaction between ethylene (**1**) and azide group (**2**) with the formation of triazole (**3**).*

Two strategies (**1** and **2**) for azide functionalization of the surface were evaluated. Strategy **1** involved the direct reaction between SiO_2 NPs and (3-azidopropyl) trimethoxysilane **27**. Strategy **2** provided the starting functionalization of the surface with amino groups following the introduction of an azide group via coupling reaction with 4-azidobutanoic acid **28** (Figure 5.13).

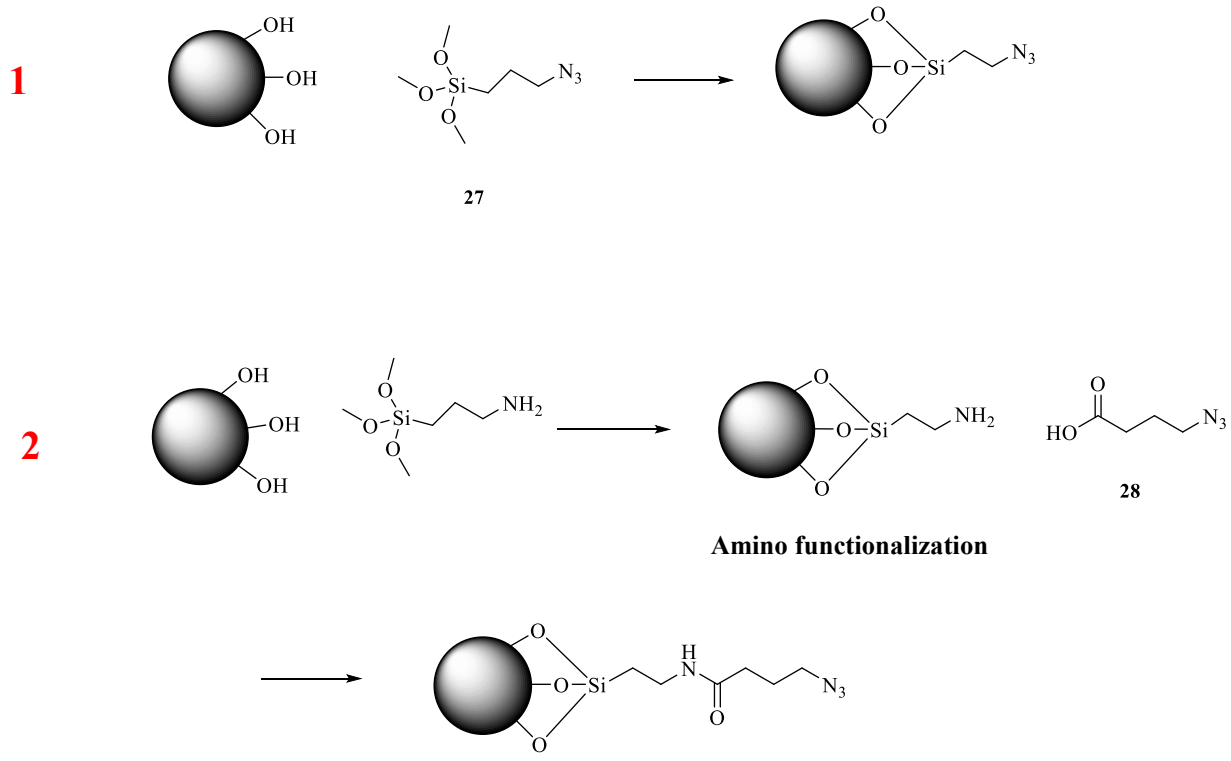


Figure 5.13. *Schematic representation of strategies investigated for the functionalization of SiO_2 NPs, through direct reaction with **27** (1) or 4-azidobutanoic acid **28**, via coupling reaction (2).*

For the preliminary test, SiO_2 NPs were purchased and further subjected to functionalization. In both strategy **1** and **2**, dried silica nanoparticles were selected rather than the solution-dispersed formulation due to their longer-term stability and the possibility of resuspension in a wide variety of solvents.

5.3 Functionalization and characterization

Purchased SiO_2 NPs (100 nm, 250 mg) were characterised by DLS and IR to verify properties such as size, charge and spectra. Among the different sizes available, 100 nm was selected due to its suitability for the dye's incorporation, leading to a higher fluorescence response compared to smaller particles.[42] Furthermore, NP with a higher diameter can be affected by agglomeration and aggregation. [250, 251]

The size of the nanoparticles and zeta potential were determined by DLS, as described in 2.3.3 and 2.3.4).

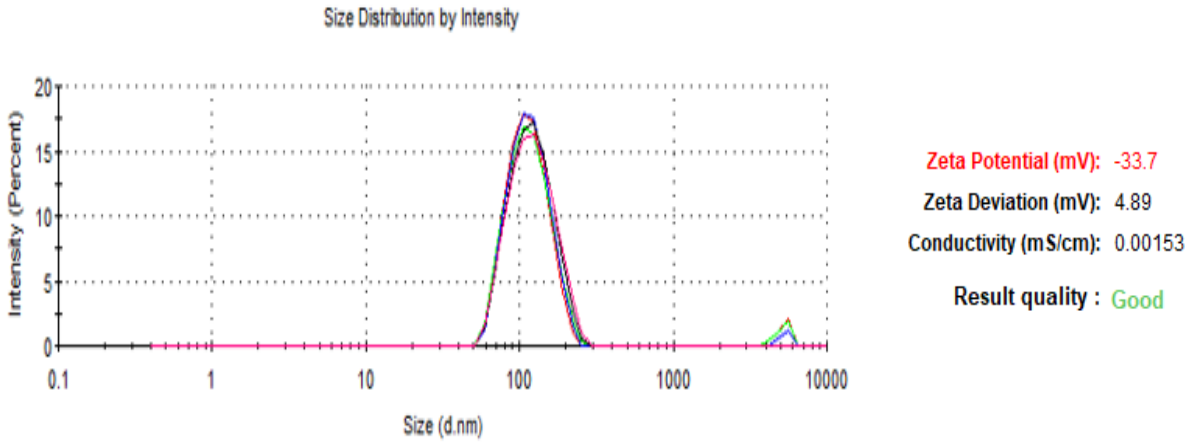


Figure 5.14. *DLS results: size distribution graphs and zeta potential of purchased SiO_2 NPs.*

The results reported in Figure 5.14 confirmed the size of NPs as 80-100 nm. The zeta potential (-33.7 mV) was in accordance with the zeta potential of SiO_2NP reported in literature.[252] Figure 5.15 reports the infrared (IR) spectra of SiO_2 NPs, employed as reference for the next functionalization. In the spectra graph the characteristic band of silica nanoparticles [253] as silanol (Si-OH) symmetric stretching at 3300 cm^{-1} (**a**) and bending vibrations at 1100 cm^{-1} (**b**) can be seen. The peak at 900 cm^{-1} was attributed to stretching vibration of Si-O (**c**).

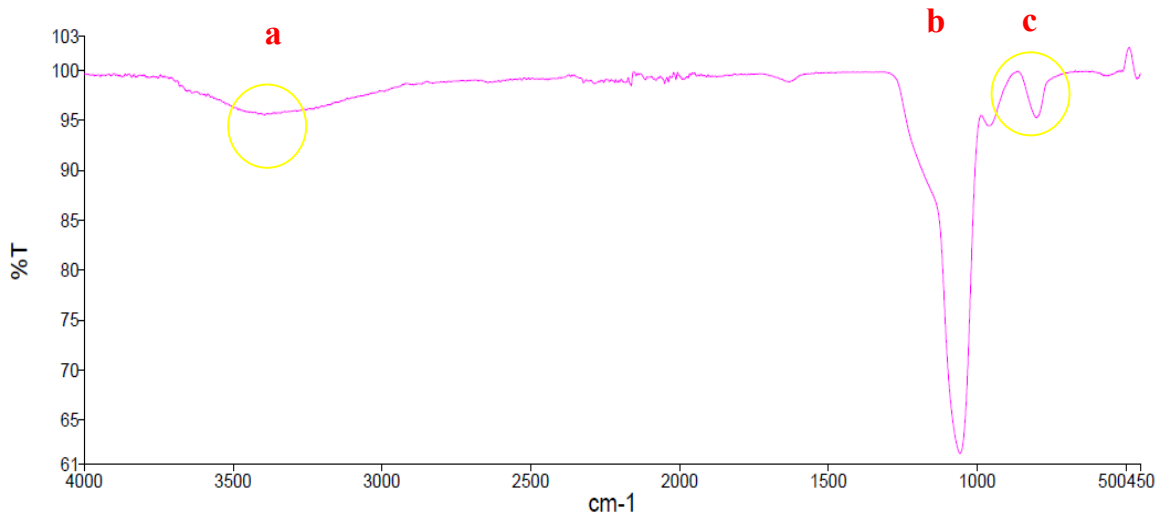


Figure 5.15. *IR spectra of SiO_2 NPs. Si-O-H stretching peak (a), Si-O-Si bending (b) and stretching vibrations of Si-O (c) evidenced.*

Strategy 1

Dried SiO_2 NPs were resuspended in EtOH (1 mL to each 10 mg) and subjected to bath sonification until complete redissolution, according to the redispersing procedure provided by the manufacturer. (3-azido propyl) trimethoxysilane **27** was added directly to the solution of SiNPs in EtOH and left to stir overnight at room temperature (method **a** in Table 5.4). After the reaction, the solution was subjected to centrifugation. The supernatant was removed, and the nanoparticles were collected, washed with EtOH, and dried overnight at 50˚C under vacuum (Figure 5.16).

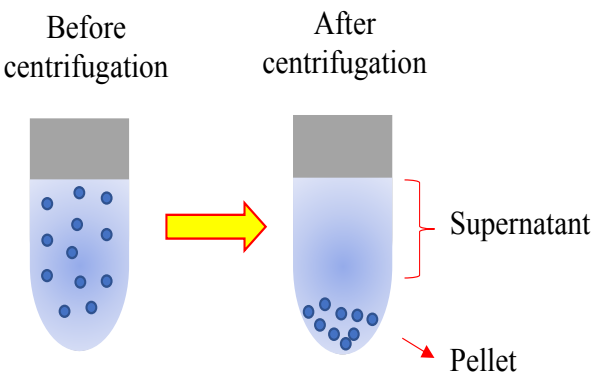


Figure 5.16. *Schematic scheme before and after centrifugation*

An IR spectrum was recorded to evaluate the reaction. There was no difference in the spectra of the bare Si NPs and the NPs that underwent reaction. Furthermore the characteristic peak of the azide group (2110 cm^{-1}),[254] was absent from the spectra, and the zeta potential remained unchanged at -33.5 mV. This data therefore indicate that the reaction had not been successful (Figure 5.17).

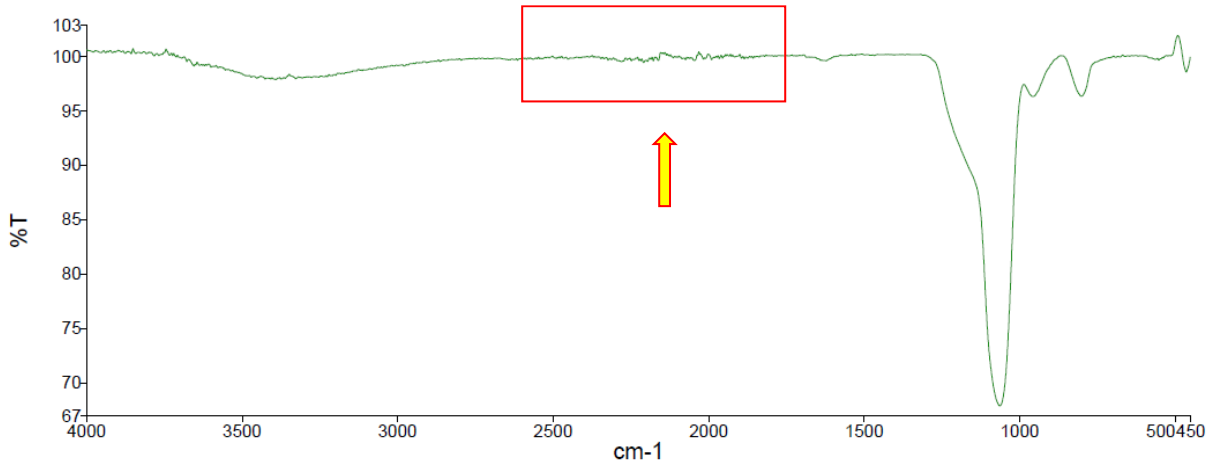


Figure 5.17. *IR spectra of reaction product following method* ***a****. Spectra region of azide group peak (2110 cm^{-1}) evidenced (red label).*

Due to these results, alternative methods were investigated, as summarized in Table 5.4. All the methods provided an excess of silane **27**. Unreacted reagent was removed through the removal of supernatant as to not affect the next reaction.

Table 5.4. *Method employed (**a-i**) for reaction between SiO_2 NPs and (3-azidopropyl) trimethoxysilane **27** according to strategy **1**.*

Method	Solvent	Co-reagent	Temperature (°C)
a	Ethanol	/	25
b	Ethanol /water	/	25
c	Ethanol	Et_3N	25
d	Water	Solution 0.1 M NaOH	25
e	Pyridine	/	25
f	Ethanol	Solution 0.1 M HCl	25
g	Dry MeCN	/	25
h	Dry toluene	/	25
i	Dry toluene	/	90

The reaction was conducted in a mixture of water/EtOH (method **b**), aiming to increase the reactivity of SiO_2 NPs. Analysis by IR did not reveal the desired product. The methods **c**, **d** and **e** employed a basic reagent to enhance the reactivity. No change observed in the IR spectra suggested that a successful reaction had occurred. Neither the use of different dry solvents, such as MeCN (**g**) and toluene (**h**), or heating produced a successful functionalization. To ascertain the absence of azide groups, thermogravimetric analysis (TGA) of bare SiO_2 NPs and reacted ones, following the conditions of method **g** as reported in Table 5.4, was conducted.

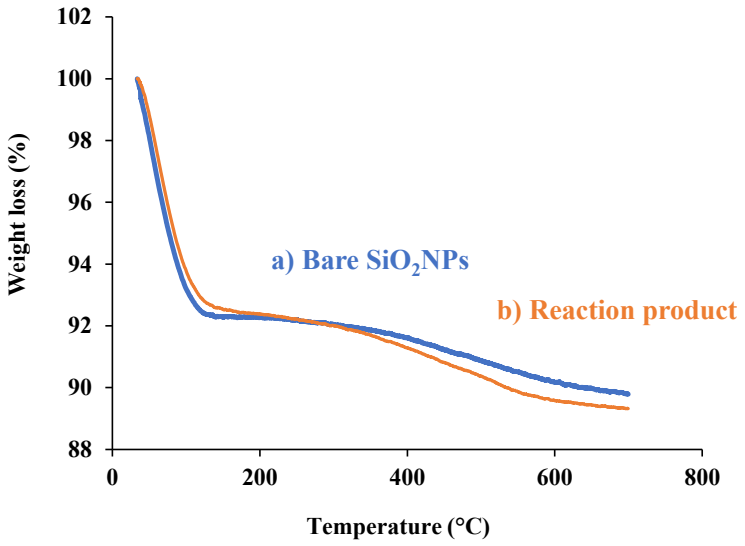


Figure 5.18. *TGA of a) bare SiO_2 NPs b) Silica nanoparticles reaction product following condition of method* ***g****, reported in Table 5.4.*

As shown in the results in Figure 5.18, a very small difference between SiO_2 NPs before (**a**) and after the reaction (**b**) was observed for method **i**. The weight loss difference calculated by TGA was 0.46 %, smaller than that needed to indicate a successful reaction.[255] Furthermore, TGA experiments conducted for reaction products, following methods **h** and **i**, had similar results, validating the absence of the desired group.

The functionalization of SiO_2 NPs with **27** is widely reported in the literature.[101, 256] However, the reason for the unsuccessful reaction occurring here was attributed to the source of **27**. In contrast with the literature, it was not synthesized *in situ* but purchased. It has been concluded that the issues seen with the strategy **1** were attributable to the low reactivity of azide silane towards SiO_2NPs. Moreover, the azide group could be subjected to degradation or collateral reaction with the surface. It was hypothesized that the group could interact with silicon atoms intramolecularly by coordination or by the formation of a five-membered cyclical intermediate. The product would

therefore be more susceptible to cleavage by hydrolysis, similar to the primary amine functionalization mechanism proposed in literature [107] (Section 1.6.1).

Strategy 2

Strategy **2** provided the first step of the functionalization of SiO_2 NPs with 3-(trimethoxy silyl) propan-1-amine APTMS (Figure 5.19).

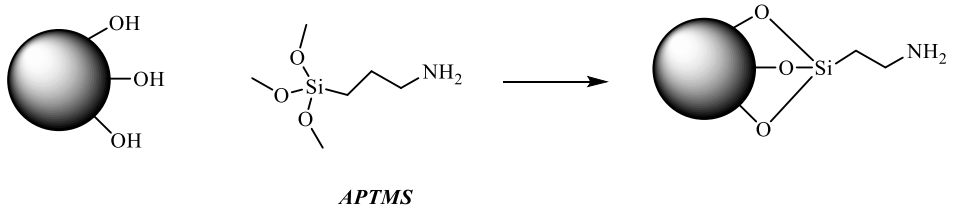


Figure 5.19. *Schematic representation of SiO_2 NPs functionalization by 3-(trimethoxy silyl) propan-1-amine APTMS.*

In strategy **2**, silica aminated nanoparticles were also tested. However, a robust way to quantify the surface bound amines, required for the further coupling reaction, was not found.[257] The functionalization of purchased Si NPs with amine silane was considered as an alternative strategy. As shown in Figure 5.20, an absorption peak at about 3420 cm^{-1}, attributed to N-H stretching vibration, was observed.

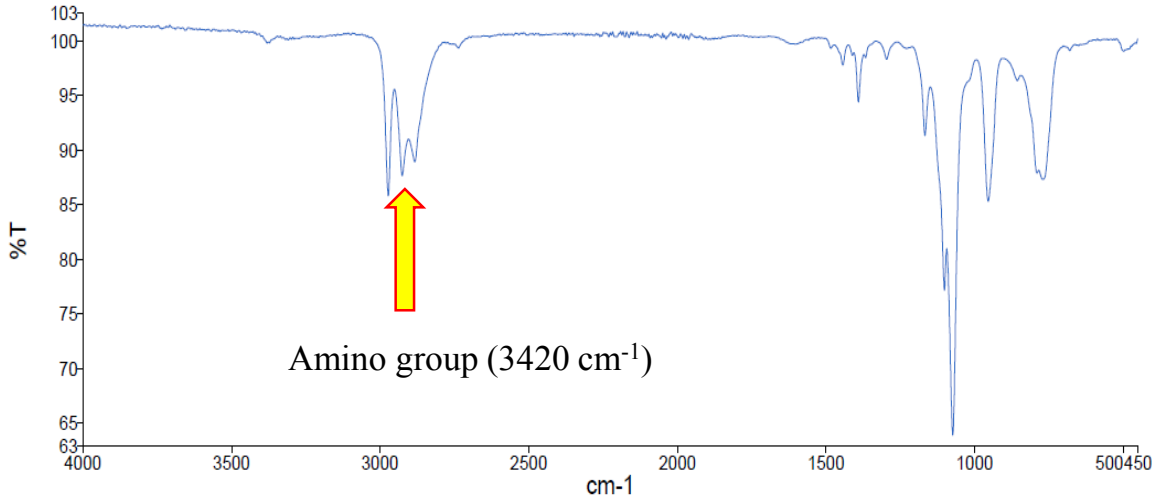


Figure 5.20. *IR spectra of 3-(trimethoxy silyl) propan-1-amine APTMS. Peak at 3420 cm^{-1} evidenced with yellow arrow.*

The reaction between SiO_2NPs and **29** was conducted following method **g** reported in Table 5.4. The functionalization of SiO_2 NPs was verified by IR spectra, as reported in Figure 5.21 (**a**). The characteristic absorption peak of amino group, at about 3420 cm^{-1} was seen (**1**). Moreover, a marked change at 1600 cm^{-1} (**2a**) compared to the IR spectra of bare SiO_2 NPs (Figure 5.21 (**2b**) was observed. The presence of these peaks (**2a**), in contrast with the previous experiments, suggested the successful functionalization of the SiO_2 NP surface.

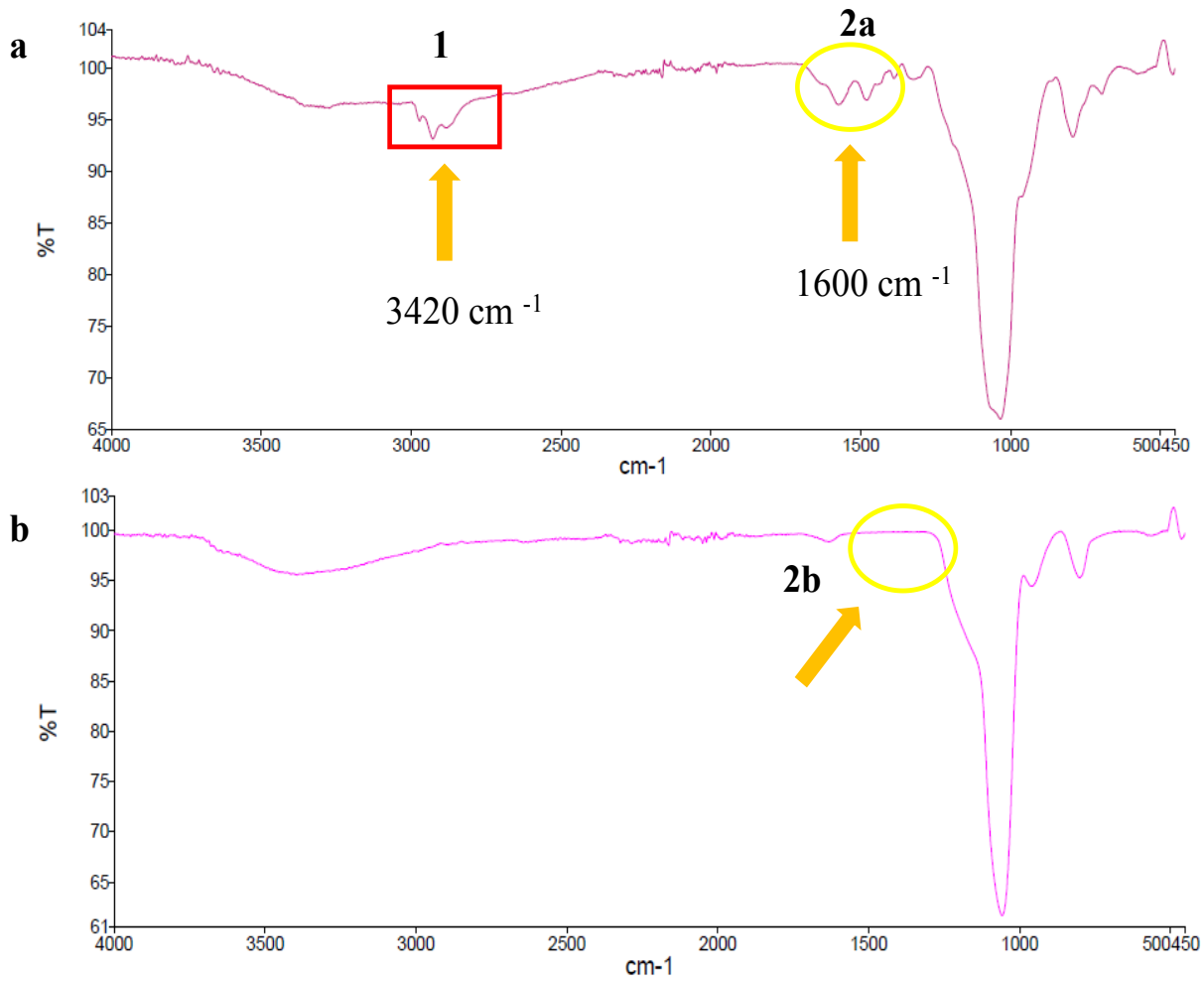
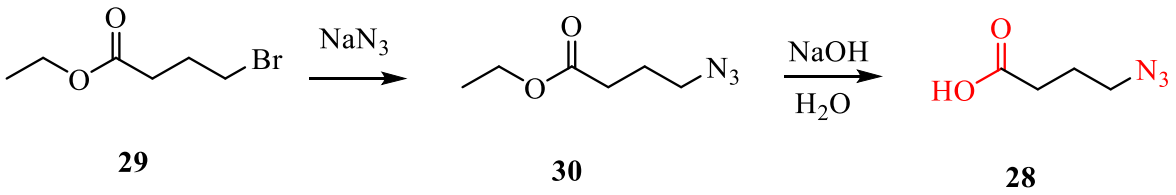


Figure 5.21. *IR spectra of NH_2 SiO_2 NPs (a) and SiO_2 NPs (b). Peak at 3420 cm^{-1} (red), 1600 cm^{-1} (yellow) evidenced.*

The second step involved the reaction with 4-azidobutanoic acid **28** itself synthesized following the scheme reported in

Figure **5.24**. The synthesis of **28** involved the reaction of ethyl 4-bromobutanoate **29** with sodium azide (NaN_3) in DMSO to introduce the azide group (**30**), and the further hydrolysis of the ester in a basic environment to gain the final product **28** (Figure 5.22).



29 **30** **28**

Figure 5.22. *Synthesis scheme of 4-azidobutanoic acid* ***28.***

The presence of carboxylic group in **28** was confirmed by TLC plate with Bromocresol Green Stain. The appearance of the yellow spot on the background verified its presence. Since the distinctive and known peak of azide group in IR spectra, this technique was selected to confirm the formation of final product. The spectrum reported in Figure 5.23 shows the characteristic azide group (2210 cm^{1}), confirming the presence of the group.

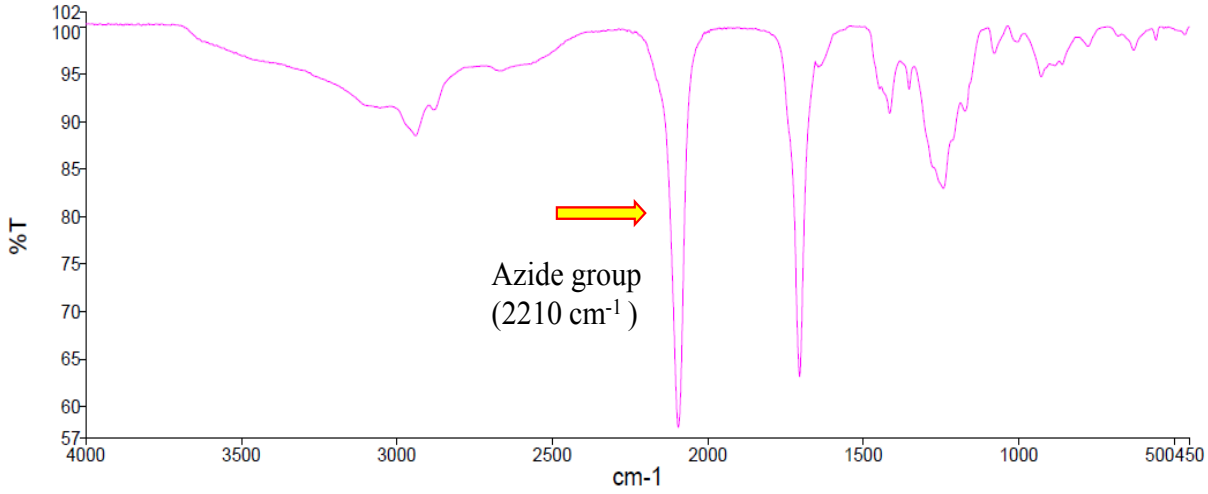


Figure 5.23. *IR spectra of* ***28****. Peak at 2210* cm^{-1} *evidenced with yellow arrow.*

The final step provided a coupling reaction between amino SiO_2NPs and the synthesised product **28**. The crosslinking of carboxylic acid **28** was promoted by carboxyl-reactive crosslinker groups.[258] Ethyl-3-(3-dimethylaminopropyl) carbodiimide (EDC) was a standard reagent, employed due to its water solubility. It activates carboxyl groups for direct reaction with primary

amines via amide bond formation. N-hydroxy succinimide (NHS) was employed in EDC coupling to improve the efficiency of the reaction. EDC couples NHS to carboxyl's forming an NHS ester, a stable intermediate, that allows efficient conjugation to primary amines on the surface of SiO_2 NPs (

Figure **5.24**).

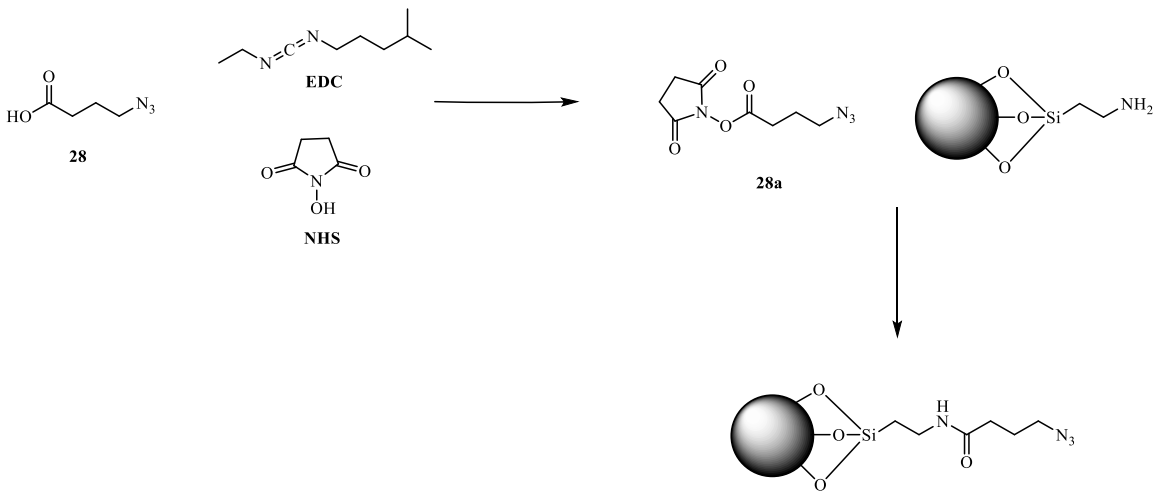


Figure 5.24. *Schematic scheme of strategy **2** complete.*

IR-Spectra of SiO_2 NPs achieved after the reaction (**C**), of bare SiO_2NPs (**A**) and NH_2-SiO_2NPs (**B**) were compared to evaluate the reaction, as reported in Figure 5.25. In the final product's spectra **C**, a new peak (**x**) at 2110 cm^{-1} was seen, attributable to the azide group, suggesting successful functionalization.

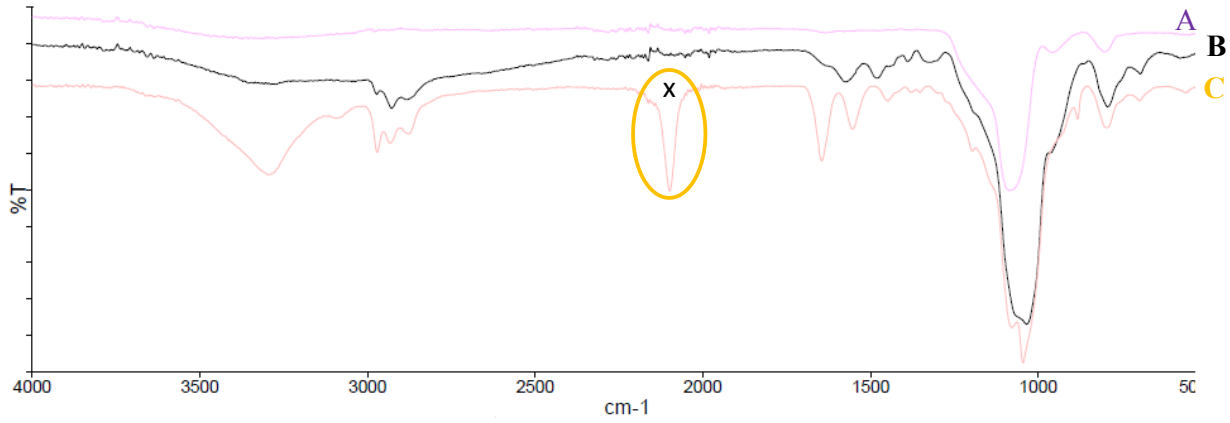


Figure 5.25. *IR spectra of bare SiO_2NPs (**A**) NH_2-SiO_2 NPs (**B**) and SiO_2 NPs product (**C**). Peak at* 2110 cm ^{1}(x) evidenced.

5.4 Summary and outlook

Functionalization with MPTMS of silicon wafers was achieved successfully by SAM (self-assembled monolayers) formation Following test of different method and conditions, the successful formation of monolayer was achieved by dry deposition and confirmed through ellipsometry and contact angle measurements. However, there was a poor homogeneity of deposition across different chips tested and low reproducibility of results. Despite the formation of SAM, it was concluded that is required a further evaluation to improve the homogeneity the quality of monolayers.

Since the wide availability of techniques for SiO_2 NPs characterization as DLS, zeta potential, IR or TEM, SiO_2 NPs have been selected as an alternative solid support for the sensing system. The functionalization with azide group enables the immobilisation of the system onto SiO_2 NPs through click chemistry. Bare dried SiO_2 NPs were selected for the preliminary experiments rather than in solution due to the higher control of functionalization afforded. Despite adopting different

methods, the introduction of azide group on SiO_2 NP surface through direct reaction with **27** according to strategy **1** was unsuccessful. Instead, the azide group was incorporated through reaction between amino-functionalised SiO_2 NPs, previously functionalized with APTES, and **28** (Strategy 2). The reaction vas verified by IR spectra.

Azide functionalization of the surface will enable the next incorporation of the system though CuAAC reaction with acetylene group of the sensor structure.

CHAPTER 6: EXPERIMENTAL METHODS

6.1 Fluorescent sensing system

6.1.1 Material and methods

Reagents and solvents were purchased from commercial suppliers and used without further purification. TLC analysis was performed on Merck silica gel 60 silica sheets. TLC plates were stained with the following stains: permanganate, ninhydrin, coumarin and bromocresol green. ^{1}H, and ^{13}C NMR spectra were obtained on Bruker AVIII300 or AVIII400 spectrometers. Chemical shifts (δ) are given in ppm and are relative to the residual solvent peak. Data was acquired using Bruker Topspin v3.2 and analysed with Mesternova v12.0.2-20910. IR spectroscopy was performed on dry samples with a Varian 660-IR FT-IR spectrometer. Silica gel column chromatography was carried out using Sigma-Aldrich 60 Å silica gel (35-70 μm). Mass spectra were obtained in Waters Xevo G2-XS using electrospray ionization mode. LC-MS chromatogram were conducted with a Shimadzu LCMS-IT-TOF instrument using Phenomenex Kinetex 5 μm XB-C18 100 A LC 250 x 4.6 mm column with a binary gradient water and AcCN or MeOH with 0.1 of TFA, according to methods previously discussed. Temperature of the column was fixed at 40 °C with a flow rate 0.9 mL/ min^{-1}. The MS was recorded in positive and negative ion mode. Preparative HPLC purification was performed on Agilent Technologies 1260 Infinity system using a Phenomenex Kinetex 5 μm EVC-C18 100 A LC 250 x 21.2 mm column. 5 ml of sample was injected with a run time of 45 minutes for each sample, at a flow rate of 3 mL/min. The UV/vis absorbance of each run was monitored at 290 nm and 350 nm. TFA was neutralized by basic resin, as described above. Collected fraction were then evaporated to dryness.

Resin preparation

Amberlite IRA-900 chloride form was purchased by sigma Aldrich and modified though ion basic exchange as shown in Figure 6.1. Amberlite IRA-900 chloride was washed with DCM to eliminate impurities. After washed with MeOH to remove DCM, and furtherly with water. A solution of 1M NaOH (5 mL) was added and left for 20 min. The resin was dried and used for further applications.

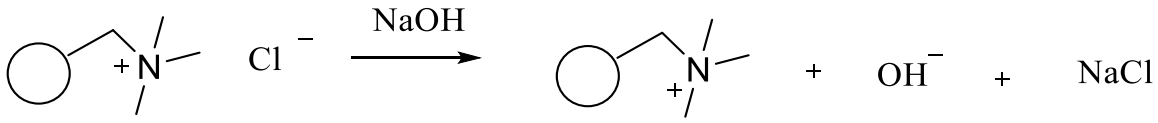
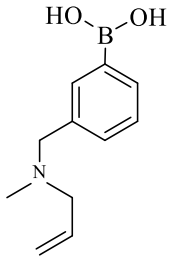


Figure 6.1. *Preparation of basic resin from Amberlite IRA-900 chloride was purchased.*

*Synthesis of (3-((allyl(methyl)amino)methyl)phenyl)boronic acid **1***

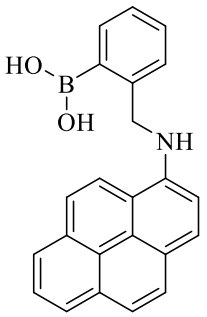


1

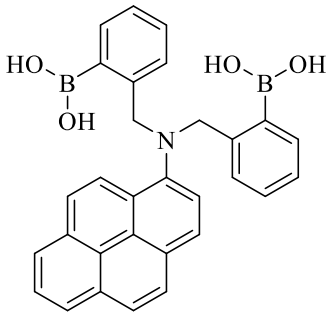
3-(Bromomethyl)phenylboronic acid **3** (500 mg, 2.33 mmol) was dissolved into 2.33 mL of DMSO and then deoxygenated. The N-allylmethylamine **4** (0.446 ml, 4.65 mmol) and triethylamine (Et_3N) (0.97 mL, 6.99 mmol) were added, and the reaction was heated to 60 °C for 45 minutes under agitation. After 45 min, TLC (Hex/EtOAc 1:1) was performed to monitor the reaction. The reaction was then precipitated in water and extracted with diethyl ether. The organic layer was dried with $MgSO_4$ and concentrated under reduced pressure. The final product **1** (365 mg; 77%).

was obtained after subjected under vacuum overnight. **^{1}H NMR** (300 MHz, DMSO-d_6) δ 7.70 (s, 1H), 7.66 (dd, J = 6.8, 1.4 Hz, 1H), 7.41 – 7.18 (m, 2H), 5.87 (dd, J = 16.5, 10.2, 6.3 Hz, 1H), 5.26 – 5.09 (m, 2H), 3.44 (s, 2H), 2.98 (d, J = 6.3 Hz, 2H), 2.07 (s, 3H). **^{13}C NMR** (101 MHz, DMSO-d_6) δ 137.6, 136.0, 134.7, 132.7, 130.5, 127.2, 117.3, 61.1, 59.8, 41.5. **MS (ES+)** Calcd for $C_{11}H_{17}BNO_2$ 206.13; Found 206.13 $[M+H]^+$; Calcd for $C_{12}H_{19}BNO_2$ 220.15; Found 220.15 $[M+Me]^+$

*Synthesis of (2-(((4,8-dihydropyren-2-yl) amino)methyl)phenyl)boronic acid **7** and (pyren-1-ylazanediyl)bis(methylene)) bis(2,1-phenylene))diboronic acid **12***



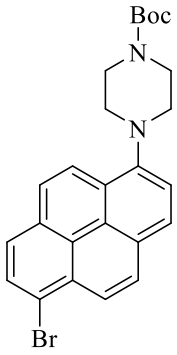
7



12

(2-(((4,8-dihydropyren-2-yl)amino)methyl)phenyl)boronic acid **7** was synthesised adapting a reported procedure.[191] To a solution of 1-aminopyrene **11** (107 mg; 0.493 mmol) and 2-bromomethyl)phenylboronic acid **3b** (70.7 mg, 0.329 mmol) in 5 mL of MeCN was added K_2CO_3 (102 mg, 0.740 mmol) in one portion. The resulting mixture was stirred overnight at room temperature. The reaction was filtered through a plug of celite using EtOAc as eluent and the filtrate was concentrated under reduced pressure. A product mixture of **7** and **12** was achieved. It was used as mixture for further experiments.

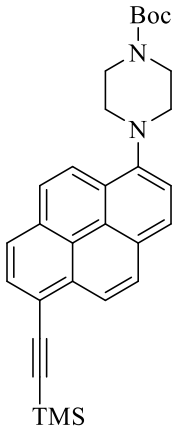
Synthesis of *tert-butyl 4-(6-bromopyren-1-yl) piperazine-1-carboxylate* **16**



16

Tert-butyl 4-(6-Bromopyren-1-yl) piperazine-1-carboxylate **16** was synthesised adapting a reported procedure.[259] 1,6-Dibromopyrene **15** (0.200 g, 0.556 mmol), NaO*t*Bu (56.3 mg, 0.586 mmol), $Pd(OAc)_2$ (6.58 mg, 29.3 μmol), BINAP (36.5 mg, 58.6 μmol) and toluene (30 mL) were placed in a 100-mL two-necked flask under nitrogen. After stirring for 15 minutes, the flask was heated to 100 °C. 1-Boc-piperazine **14b** (0.10914 g, 0.586 mmol) was then added to the solution and the resulting mixture was stirred for 12 h. Subsequently, it was quenched with water and extracted. The organic layer was washed with brine and was dried over $MgSO_4$. The reaction was verified by TLC and staining with ninhydrin. The crude product was purified by column chromatography DCM: Hex 25 % to obtain the product **16** (0.099 g, 46 %). **^{1}H NMR** (400 MHz, Chloroform-*d*) δ 8.34 (dd, *J* = 9, 9.2 Hz, 1H), 8.13 (dd, *J* = 14.4, 8.2 Hz, 2H), 8.00 (dd, *J* = 9.1, 9.2 Hz, 1H), 7.92 (d, *J* = 8.2 Hz, 2H), 7.70 (d, *J* = 8.1 Hz, 2H), 3.17 (s, 8H), 1.46 (s, 9H). **^{13}C NMR** (101 MHz, Chloroform-*d*) δ 154.92, 130.31, 130.02, 128.90, 126.01, 122.97, 117.76, 60.42, 53.47. **MS (ES$^+$)** Calcd for $C_{25}H_{25}BrN_2O_2$ 464.11; Found 465.11 $[M+H]^+$

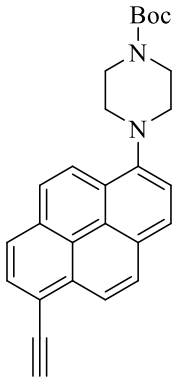
*Synthesis of tert-butyl 4-(6-((trimethylsilyl)ethynyl) pyren-1-yl) piperazine-1-carboxylate **18***



18

4-(6-((trimethylsilyl)ethynyl)pyren-1-yl)piperazine-1-carboxylate **18** was synthesised adapting a reported procedure.[260] To a degassed solution of **16** (98.6 mg, 0.270 mmol) in dry Et_3N (10 mL), Pd $(PPh_3)_2Cl_2$ (18.9 mg, 27.0 µmol), CuI (5.14 mg, 27.0 µmol) and ethynyl-trimethylsilane **17** (191 µL, 1.35 mmol) were added. The reaction mixture was stirred at 70 °C for 20 h. Afterwards, the solvent was evaporated under reduced pressure and the crude material was purified through silica gel column chromatography (DCM/Hex 7:1) to yield **18** (70.7 mg, 54 %). **^{1}H NMR** (300 MHz, Chloroform-*d*) δ 8.46 (d, *J* = 9.1 Hz, 1H), 8.08 (dd, *J* = 8, 6.0 Hz, 1H), 8.32 – 7.90 (m, 2H), 8.18 – 7.86 (m, 2H), 7.73 (d, *J* = 8.2 Hz, 2H), 3.61 (s, 8H), 1.52 (s, 9H), 0.89 (s, 9H). **MS (ES$^+$)** Calcd for $C_{30}H_{34}N_2O_2Si$ 482.24; Found 483.25 $[M+H]^+$

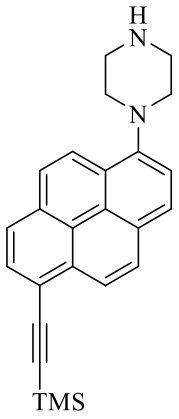
*Synthesis of tert-butyl 4-(6-ethynylpyren-1-yl)piperazine-1-carboxylate **19***



19

Tert-butyl 4-(6-ethynylpyren-1-yl)piperazine-1-carboxylate **19** was synthesized adapting a reported procedure.[200] A mixture of **24** (70.7 mg, 0.147 mmol) and tetrabutylammonium fluoride trihydrate (TBAF) (54.8 mg, 0.209 mmol) in 10 mL of THF. The mixture was stirred at room temperature for 1h. Afterwards, the solvent was evaporated under reduced pressure and the crude material was purified through silica gel column chromatography (DCM/Hex 5:1) to yield **25** (46.3 mg, 77 %). **^{1}H NMR** (300 MHz, Chloroform-*d*) δ 8.47 (dd, J = 9.1, 3.6 Hz, 1H), 8.30 – 8.13 (m, 2H), 8.10 (d, J = 14.4 Hz, 2H), 8.06 – 7.82 (m, 2H), 7.75 (d, J = 8.2 Hz, 1H), 3.37 (s, 1H), 3.25 (s, 4H), 2.90 (s, 4H), 1.52 (s, 9H). **MS (ES+)** Calcd for $C_{27}H_{26}N_2O_2$ 410.20; Found 411.21 $[M+H]^+$

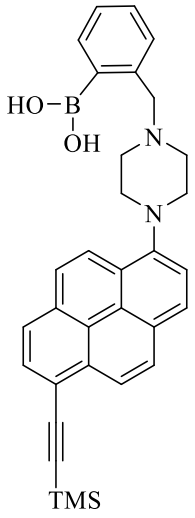
*Synthesis of 1-(6-(piperazin-1-yl)pyren-1-yl)ethan-1-one **18b***



18b

Deprotection of Boc group to achieve **18b** was achieved adapting a reported procedure.[219] 9 mL of Acetyl chloride solution (4M) in methanol was prepared in an ice bath, to generate hydrogen chloride in situ. **19** (0.216 g, 0.447 mmol) was dissolved in 9 ml of prepared solution. The mixture was stirred at room temperature. The reaction was monitored by TLC analysis until complete consummation of **19**. Afterwards the solvent was evaporated, and the crude product dissolved in water. A solution of K_2CO_3 was added until reach a pH 10-11 and extract with DCM. The solution was washed with water and brine and reduced to dryness. The crude was purified by the HPLC purification according to the condition described in section 4.3. Basic resins, prepared as described above, was added to the solution to neutralize trifluoroacetic acid TFA. The solvent was evaporated under reduce pressure to achieve **18b** as yellow solid (0.1086 g, 64 %). **^{1}H NMR** (300 MHz, Chloroform-*d*) δ 8.61 – 8.26 (dd, J = 9.1, 3.6 Hz, 1H), 8.25 – 8.15 (m, 2H), 8.10 – 7.99 (m, 2H), 7.76 (dd, J = 8.2, 2.6 Hz, 2H), 7.61 (d, J = 8.2 Hz, 1H), 3.25 (s, 2H), 2.90 (s, 2H), 1.26 (s, 1H), 0.39 (s, 9H). **MS (ES$^+$)** Calcd for $C_{25}H_{26}N_2Si$ 382.20; Found 383.19 $[M+H]^+$

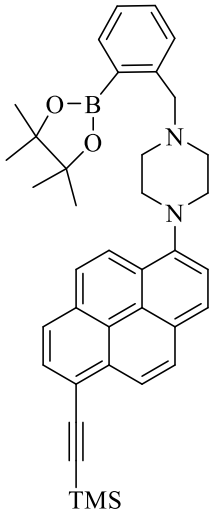
*Synthesis of (2-((4-(6-((trimethylsilyl)ethynyl)pyren-1-yl)piperazin-1-yl)methyl)phenyl)boronic acid **13b***



13b

Product **13b** was synthesised adapting a reported procedure.[146] **18b** (108.6 mg; 0.286 mmol) and 2-Bromomethyl) phenylboronic acid **3b** (60.8 mg; 0.286 mmol) were dissolved in dry MeCN (5 mL). Et_3N (80 µL; 0.572 mmol) was added in one portion and the resulting mixture was stirred at room temperature for 48h under argon. The reaction product was verified by TLC and visualized by curcumin stain. The crude product was purified by HPLC according to the condition reported in to achieve **13b** (44.3 mg, 30 %). The purity was calculated by LC-UV spectra (85%). **^{1}H NMR** (300 MHz, Chloroform-*d*) δ 8.82 (s, 1H), 9.03 – 8.20 (m, 2H), 8.95 (d, J = 9.4 Hz, 2H), 8.14 (s, 1H), 8.14 – 7.98 (m, 2H), 7.77 – 7.49 (m, 2H), 7.26 (s, 2H), 4.60 (d, J = 57.5 Hz, 2H), 3.82 (s, 2H), 3.31 (s, 4H), 2.98 – 2.42 (m, 4H), 0.41 (d, J = 8.0 Hz, 9H). **MS (ES$^+$)** Calc for $C_{32}H_{33}BN_2O_2$ 516.52; Found 517.25 $[M+H]^+$

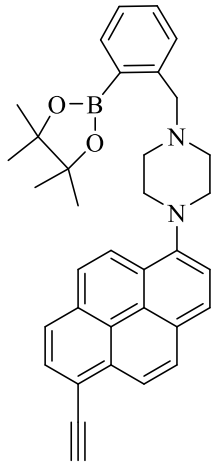
*Synthesis of 1-(2-(4,4,5,5-tetramethyl-1,3,2-dioxaborolan-2-yl) benzyl)-4-(6-((trimethylsilyl) ethynyl) pyren-1-yl) piperazine **23***



23

Product **23** was synthesised adapting a reported procedure.[146] **13b** (61.3 mg, 0.160 mmol) and 2-(2-(Bromomethyl) phenyl)-4,4,5,5-tetramethyl-1,3,2-dioxaborolane **3c** (47.5 mg, 0.160 mmol) were dissolved in dry MeCN (3 mL). K_2CO_3 (46.4 mg; 0.320 mmol) was added in one portion and the resulting mixture was stirred at room temperature for 48h under argon. The solvent was evaporated under reduce pressure and the crude material was used in next reaction, without purification. **MS (ES^+)** Calcd for $C_{38}H_{43}BN_2O_2Si$ 598.32; Found 599.33 $[M+H]^+$

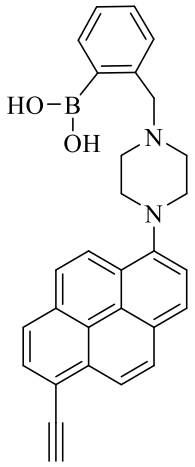
Synthesis of 1-(6-ethynylpyren-1-yl)-4-(2-(4,4,5,5-tetramethyl-1,3,2-dioxaborolan-2-yl) benzyl) piperazine ***23b***



23b

23 (74.3 mg, 0.141 mmol) was dissolved in a solution of THF and MeOH (1:1).[261] K_2CO_3 was added in excess (0.1167 g, 0.8454 mmol) and the mixture stirred for 1 hour at room temperature. The solvent was evaporated under reduce pressure and the crude material was used for the further reaction, without purification. **MS (ES$^+$)** Calcd for $C_{35}H_{35}BN_2O_2$ 526.28; Found 527.29 $[M+H]^+$

*Synthesis of (2-((4-(6-ethynylpyren-1-yl)piperazin-1-yl)methyl)phenyl)boronic acid **13***



13

(2-((4-(6-ethynylpyren-1-yl)piperazin-1-yl)methyl)phenyl)boronic acid ***13*** was synthesised adapting a reported procedure.[222] **23b** (8.26 mg, 15.5 μmol) and methylboronic acid (9.32 mg, 0.156 mmol) were dissolved in 0.2 M HCl (0.5 mL) and acetone (0.5 mL). The mixture was stirred overnight at room temperature. Afterwards, the solvent was evaporated under reduce pressure. The crude residue was dissolved in MeCN and deionized water and freeze dried. The purity was calculated by LC-UV (35%). **MS (ES$^+$)** Calcd for $C_{329}H_{25}BN_2O_2$ 444.20; Found 445.21 $[M+H]^+$

6.1.2 Optical Spectroscopy experiments

UV-Vis absorption measurements were performed using a Perkin-Elmer UV-Vis spectrometer Lambda 20, with cuvettes of a 10 mm path length. The machine was operated using UV Win lab software. Fluorescence experiments were conducted using Jasco FP-8500 Spectrofluorometer, both excitation and emission mode. The experiments were performed at 25 °C using aerated samples.

Solubilisation methods

Due to insolubility in water, methods for solubilisation needs to be implemented for anthracene and pyrene derivatives. It has been selected two solubilization methods (**A** and **B**). In method **A** the product was dissolved in DMSO/DMF and then diluted in a solution to reach desired concentration. In method **B** the product was dissolved in DCM, then concentrated under reduced pressure. The product was left to dry under vacuum overnight, then suspended in specific amount of a solution to reach desired concentration and gently stirred overnight.

*First sensing system: (3-(allyl(methyl) amino) methyl) phenyl) boronic acid 1 and of 9-azide anthracene **2***

All the fluorescence spectra were recorded from 400-550 nm under the excitation wavelength at 350 nm. A solution of 9-azide anthracene **2** (4 μM) was prepared in water, EtOH or sodium dodecyl sulphate (SDS) solution using method A (DMSO), then diluted to desired concentrations (between 0.02 to 2 μM). Fluorescence samples were prepared by mixing equal volumes of previous **2** solution (4 μM) and different aqueous solutions of (3-(allyl(methyl) amino) methyl)phenyl) boronic acid **1** (from 0.02 to 200 μM).

A 20 μM ethanolic solution of **2** and a set of solution of pyridinium chloride **5** at different concentration were prepared following literature.[262] Fluorescence samples were prepared by mixing equal volumes of previous **2** solution with different concentrations of **5** to give final concentrations of 50, 37.5; 25; 12.5; 2.5 mM

A solution of 2 μM of **2** in SDS (0.1 M) was prepared. Fluorescence samples were prepared by mixing equal volumes of previous **2** solution and different solution of **1** in SDS solution to give final concentrations of 12.5; 10; 7.5; 5; 2.5 mM.

*Second sensing system: pyrene-based sensor (sensor **6** and **7**) with coumarin probe*

*Sensor **6***

A solution of pyrene 1-boronic acid **6** (2 μM) in aqueous buffer (50 mM HEPES, 100 mM Na_2SO_3, 20 mM NaCl, pH 7.4) [263] was prepared using method **A** (DMSO). The pH of the aqueous buffer was further adjusted at pH 9 with NaOH aqueous solution. Stock solutions of D-Fructose **8** was prepared in both of previous buffer. Fluorescence samples were prepared by mixing equal volumes of 2 μM solution of **6** with different concentrations of D-Fructose **8** (2-20 mM), respectively for each aqueous buffer. Experiments were repeated according to the same procedure but substituting previous buffer with MeOH.

Solutions of dopamine **10** (2-20 mM) were prepared in same previous HEPES buffers. A set of solutions was prepared by mixing equal volumes of previous 2 μM solution of **6** with dopamine **10** solutions and analysed by fluorescence.

A 100 μM aqueous solution of coumarin **9** was prepared, then diluted to selected concentration (60; 90; 30 μM). A solution of **6** (3 μM) was prepared in water using method **A**. FRET experiments were performed with a solution of **6** (1 μM), a solution prepared mixing equal volumes of **6** (2 μM) and **9** (60 μM), and a solution prepared mixing equal volume of **6** (3 μM), **9** (90 μM) and **8** (30 mM).

*Compound **12***

A solution of **12** (2 μM) was prepared in previous HEPES buffer at pH 7.4 and 9 using method **B**, then diluted with respective buffer. Fluorescence samples were prepared by mixing equals volumes

of **12** (0.02 μM) solution with different concentrations of D-Fructose **8** (20 mM), respectively for each aqueous buffer.

Final sensing system: fluorescent sensing system based on pet-pyrene boronic acid sensor

All the fluorescence spectra were recorded from 400-550 nm under selected excitation wavelength. Phosphate buffer solution (PB) was prepared mixing 500 mL of K_2HPO_4 (50 mM) and 500 mL NaH_2PO_4 (50 mM) adjusting pH with HCl or NaOH aqueous solution. A solution of pyrene **13** (0.1 μM) in phosphate buffer was prepared using method **B**. Fluorescence samples were prepared by mixing equal volumes of previous **13** solution and different piperazine **14** aqueous solutions, concentrations ranging from 0 to 100 mM. The excitation wavelength was fixed at 344 nm.

Fluorescence titration (pH and sugars)

A stock solution of **13** or **13b** (5 mM) was prepared in DMF, then a diluted solution (10 μM) in PB. Fluorescence spectra of **13** and **13b** at different pHs in PB were recorded by adjusting the pH by addition of NaOH aqueous solution. Same procedure was repeated for solutions with same concentration of sensor plus D-Fructose (100 mM). Fluorescence spectra were conducted under excitation wavelength at 360 nm and 390 nm.

Saccharides (D-fructose, D-Sorbitol and D-Glucose) were dissolved in PB solution (pH 8) to obtain stock solutions (6.0 M). 0-200 μL of stock sugar solution were added into 2.8 mL of **13** (10 μM) buffer solution (50 mM, pH 8) to make final sugar concentrations 0-200 mM. Fluorescence spectra were conducted under excitation wavelength at 360 nm.

All the fluorescence spectra were corrected with a dilution factor and subjected to blank subtraction. Blanks were recorded for all PB solutions of different pHs used in pH titration and PB

solutions at pH 8 with different concentration of sugars. Binding constants were calculated using SigmaPlot software.

Calculation of quantum yield

A solution of 7-Diethylamino-4-methylcoumarin (5 mM) was prepared in DMF, then diluted in water to 10 μM. A solution of **13** (100 μM) was prepared following the same method **B**. Adsorption of 7-Diethylamino-4-methylcoumarin (10 μM) and **13** (100 μM) solution were recorded. Both fluorescence spectra were recorded under the same excitation wavelength at 380 nm and at same concentration (10 μM). Quantum yield of **13** was calculated according to equation 4-3.

FRET experiments

Solutions of **24**, **25** and **26** in PB solution (pH 8) were prepared following method **B** at different concentration. Fluorescence samples were prepared by mixing equal volumes of **24**, **25** (2; 1; 0.4 μM) or **26** (10; 4; 2 μM) PB solutions with a pyrene sensor **13** (20 μM) PB solution. Fluorescence samples involving D-Fructose were prepared by mixing equal volumes of **24**, **25** (3; 1.5; 0.6 μM) or **26** (15; 6; 3 μM) PB solutions, with same buffer solutions of **13** (30 μM) and D-Fructose (75; 30; 6 μM). Fluorescence spectra were recorded under excitation wavelength at 326 nm for experiment involving **24**, 296 nm for **25** and 360 nm for **26**.

6.2 Silica solid substrate

6.2.1 Materials and methods

Reagents and solvents were purchased from commercial suppliers and used without further purification. All silicon wafers are subjected to a thorough cleaning procedure with a piranha solution. It was prepared by adding 3 ml of hydrogen peroxide (H_2O_2) onto 7 mL of ice-cooled sulphuric acid (H_2SO_4) and leaving for 10 minutes. Silicon chips were immersed in the solution

for 8 minutes, then washed with Milli-Q water, ethanol (EtOH), and finally dried. The SAMs on silicon wafers have been formed with MPTMS and APTMS to have thiol and amino groups.[264-266] SAM Contact angle were obtained using Attension Theta contact angle meter from Biolin Scientific and images were analysed using the OneAttension software. SAM thickness was obtained by ellipsometry using Alpha-SE ellipsometer from J.A. Woollam and data was processed using CompleteEASE software. Dried silica nanospheres (250 mg, 80 nm) were purchased from nanoComposix and subjected to subjected to redispersion according with the procedure reported (10 mg for 1 mL).[267] Teflon vials (10 mL) and all the solvent were purchased from sigma Aldrich. Acetylene was degassed by argon. Particles sizes were measured with a Zetasizer Nano (Nano-S) particle-size analyser from Malvern Instruments Ltd (UK) for size and zeta potential measurement. NPs were dispersed in EtOH (10 mg/mL) and sonicated for 20 min before being analysed by DLS at 25 °C in a 3 mL disposable polystyrene cuvette. Attenuator position, measurement duration and number of runs were automatically chosen by the instrument. The values are reported as an average of 5 measurements. Zeta potentials measurements were performed by placing the sample in the special capillary cell with two electrodes. Thermogravimetry analysis was performed by Netzch TGA 209 F1, following a method reported in literature (Temperature 40 to 700 °C with a heat rate 10 K/min).[255] IR spectroscopy was performed on dry samples with a Varian 660-IR FT-IR spectrometer.

6.2.2 SAMs formation

Vapor deposition:[111] a vial with 0.2 mL of MPTMS or APTMS was put placed in the bottom of a sublimation chamber. Silicon chips, with a dimension of 1×1 cm, previously cleaned with piranha solution, were positioned in a support. The sublimation chamber was then subjected to reduced pressure and maintained under these conditions. The time under vacuum, the deposition time, and

the orientation of chips, up and down in the support, were changed during experiments. The silicon chips were then subjected to annealing at 100 ºC for 30 min and, after cooling down, were washed with MilliQ water, EtOH, and dried with argon.

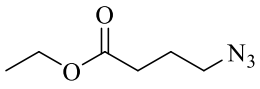
Liquid deposition: the silicon chips were immersed in a dry toluene solution of MPTMS or APTMS (1 mM: 1.5 mL) under argon condition. They were left under agitation overnight, washed with EtOH and milli-Q water, and placed in an oven for 2 hours.

6.2.3 Functionalization of silica nanoparticles

Synthesis of Amino-Grafted Silica Nanoparticles (NH_2-SiO_2 Np)

Amino-Grafted Silica Nanoparticles were prepared adapting a reported grafting procedure.[268] Silica nanoparticles (40 mg) were redispersed in 4 mL of dry MeCN in a Teflon vials. APTMS (494 mg, 2.7 mmol) was added to the homogeneous dispersion. The reaction mixture was stirred for 24 h at room temperature. Subsequently, the reaction mixture was centrifuged at 12 000 rpm for 30 min. The clear supernatant liquid was decanted from the solid deposit. The solid mass obtained was sonicated with ethanol for 20 min and then centrifuged three times. It was then dried at 50 °C under high vacuum for 6 h. Recovered mass: 20mg NPs were analysed by IR spectra.

*Synthesis of 4-azidobutanoate **30***

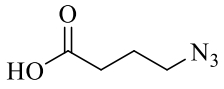


30

4-azidobutanoate **30** was synthesized according to a reported procedure.[269] Ethyl-4-bromobutyrate (1 g, 5.13 mmol) was mixed with sodium azide (0.50 g, 7.69 mmol) in DMSO (10 mL) and stirred overnight under argon at 55 ºC. The reaction mixture was diluted with water (7 mL) and extracted

in diethyl ether (3 x 7 mL), followed by washing with water and brine. The combined organic phases were dried over magnesium sulfate ($MgSO_4$), filtered, and concentrated by rotary evaporation to yield **30** (0.8 g, 97%). **^{1}H NMR** (300 MHz, Chloroform-*d*) δ 4.15 (q, J = 7.1 Hz, 2H), 3.35 (t, J = 6.7 Hz, 2H), 2.40 (t, J = 7.2 Hz, 2H), 1.98 – 1.82 (m, 2H), 1.26 (t, J = 7.1 Hz, 3H).

*Synthesis of 4-azidobutanoic acid **28***



28

4-azidobutanoic acid **28** was synthesized from **30** according to literature.[269] **30** (0.8 g**)** was dissolved in a mixture of 1 N NaOH (5 mL) and MeOH (5 mL). The solution was stirred at room temperature for 3 h, then reaction completion was checked by TLC, followed by removal of the MeOH by evaporating under reduce pressure. The pH of the aqueous phase was adjusted to 0 using 1 N HCl solution. The product was extracted into ethyl ether (3 x 5 mL), dried over $MgSO_4$, filtered, and concentrated to yield **28** (0.5 g, 75%). **^{1}H NMR** (300 MHz, Chloroform-d) δ 3.38 (t, J = 6.7 Hz, 2H), 2.47 (t, J = 7.2 Hz, 2H), 1.99 – 1.83 (m, 2H).

Synthesis of Azide-Grafted Silica Nanoparticles (N_3-SiO_2Np)

The synthesis of *N_3-SiO_2Np* was done though coupling reaction as reported in literature.[101] **28** (2.13 mg, 0.166 mmol), NHS (0.72 mg, 6.3 μmol), and EDC (3.85 mg, 20.0 μmol) were added to NH_2-SiO_2 Np (5 mg) in DMF (2 mL). The solution was stirred 24 hours under argon at 80 ºC. Particles were collected by centrifugation and washed with water and DMF. NPs were analysed by IR spectra.

CHAPTER 7: CONCLUSION AND FUTURE WORK

This work investigated the fluorescence capabilities of different boronic-acid-based sensing systems. The aim was to identify the system which provided the optimum signal upon sugar binding, and then immobilise this system onto a solid support. Boronic acids have been employed as receptor units due to their known ability to bind polyhydroxy compounds, such as saccharides. Fluorescence mechanisms including PET, ICT and FRET, or their combinations, were exploited to provide a significant response for saccharide detection. Although this work was focused on the research of simple saccharide molecular sensors, the ultimate aim of this research is to utilise this developed technology for the effective and efficient detection of glycans and their derivatives. Different strategies have been explored to achieve a working fluorescent system. The employment of boronic acid derivatives with a higher affinity towards sugars, alongside a high quantum yield probe, helped to enhance the final fluorescence signal. The two units constituting the molecular sensor could be independent of each other and be attached directly or through a linker or spacer. A suitable linker was demonstrated to strengthen the interaction of the units and the overall sensor performance. Moreover, the employment of solid substrates to confine the system within a given areas is believed to improve the performance further.

The first sensing system, described in chapter 3, involved phenylboronic acid as a receptor and an anthracene dye as a fluorophore. Both structures were modified to enable immobilisation onto the silicon surface. The fluorescence response upon saccharide binding was supposed to be modulated by PET mechanism. Fluorescent experiments recorded between the two units involved did not display a fluorescence decrease supposedly corresponding to the quenching of the fluorophore. It was proved that the first system did not show a PET mechanism and was hence deemed unsuitable

for the project's purpose. It was concluded that the fluorescent system's structure required changes to improve the interaction between the two units.

In chapter 3 the study of a different sensing system is described, involving a boronic acid-based pyrene and coumarin **9**, and their interaction to allow a FRET process. Sensor **6** provided a direct connection between boronic acid and pyrene. While sensor **7** employed an alkyl chain with an amino group as a linker. Sensor **6** displayed a fluorescence intensity increase upon saccharide binding. However, following the addition of coumarin **9** no change was observed in emission spectra, suggesting that FRET mechanism did not occur. Sensor **7** was designed with the expectation that a noticeable shift in the emission spectra following sugar-binding, caused by ICT mechanism, would be seen. Since the desired compound was unable to be attained, fluorescence experiments were performed with the di-substituted product **12**. Despite efforts, no noticeable shift in the emission spectra was observed. Yet, a higher fluorescence was observed in the latter sensor compared to that of sensor **6**, suggesting that the presence of a linker between the two units improved the interaction with saccharides and consequently the fluorescence. Further investigation regarding the structure of the linker to be employed in the sensing system was required.

The learnings afforded by the previous systems suggested that connection between units is needed and amino group is required to confer affinity to saccharides and promote the fluorescence mechanism. Thus, a modified system was developed. The final system described in chapter 4 involved a pyrene-based sensor with the boronic acid connected through the piperazine ring (sensor **13**). It acts both as a linker and a fluorescence quencher, ensuring a PET process is involved. The sensor was also functionalized with an acetylene group to allow immobilization onto the surface. Although few steps were necessary for the synthesis of sensor **13**, obtaining the desired product was challenging due to the formation of side products, such as methyl ketone **21** or phenol

22. The main issue was the presence of two distinct protective groups with different reactivities. Several iterations were needed to finally achieve an appropriate combination and sequence of reactions required to obtain sensor **13**. As a further complication, optimum purification conditions were not met and sensor **13** was yielded with low purity (35 %). Despite the low purity, the impurities were deemed unresponsive to saccharides, therefore the suitability of sensor **13** for saccharide detection could still be demonstrated by performing fluorescence experiments with D-Fructose. Previous experiments showed an enhancement of fluorescence intensity upon saccharide binding at pH 8, supporting the occurrence of a PET process. Results obtained by pH titration emission profile verified the binding abilities of the sensor at physiological pH (~ 7.4), translating to biological applications. Sensor **13** also had a higher selectivity for D-Fructose and D-Sorbitol, compared to D-Glucose.

Once the fluorescence intensity change produced by the saccharides binding was verified, the interaction with an alternative probe, attesting to a FRET process, could be tested. Fluorescence experiments performed with sensor **13** and the probes 1-ethynylpyrene (**24**) and 1-ethynylnaphathalene (**25**) demonstrated an interaction between **13** acting as acceptor, and **24** and **25** as donor probes.

The role of **13** as donor in the FRET process has not been verified, due to the missing interaction with a probe that acts as the acceptor, such as sulfonated coumarin dye (**26**). All the FRET systems investigated displayed a fluorescence response upon D-Fructose comparable to or higher than observed with sensor **13** on its own. It was therefore assumed that the fluorescence restoration following PET suppression did not enable a significant interaction with the probes investigated, due to the low quantum yield of sensor **13**.

The binding abilities of sensor **13** towards saccharides and its employment in sensing applications was demonstrated. However, it was believed that the sensing potential of **13** was affected by its low purity. Therefore, it was predicted that the actual sensitivity and the efficiency of the sensor would be improved with a higher purity compound. Moreover, a resulted higher quantum yield of the sensor was expected to enhance the FRET efficiency through a more successful interaction with the selected probes.

As the final step of the project involves the immobilisation of the system onto a surface, chapter 6 describes the investigation into the chosen silica substrates. Functionalization with MPTMS of silicon wafers was achieved successfully by SAM formation. However, ellipsometry and contact angle measurements attested to a poor homogeneity of deposition across wafers which resulted in poor reproducibility. Despite the formation of SAM, further evaluation to improve the homogeneity and the quality of monolayers is required. SiO_2 NP were selected as an alternative solid support for the fluorescence sensing system. The introduction of azide groups on the surface was achieved by a coupling reaction with amino functionalized SiO_2 NP. Azide groups will enable the next immobilisation of the system through click chemistry reaction with acetylene group of the sensor structure.

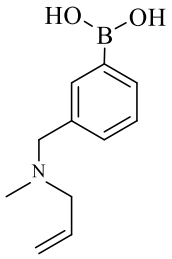
Future work will involve a deeper investigation of boronic acid based fluorescent systems described. In detail, the first analysed system, based on phenylboronic acid and anthracene units, should be examined also upon the incorporation of single unit into surface. Even if unbounded units showed not remarkable results, it would prove of interest evaluate the possible establishment of fluorescence mechanism desired afterward the incorporation of the units onto the surface. Moreover, a BA derivative with amino group in ortho position could be employed, to enhance the

performance of the system. About the systems based on FRET fluorescent sensing system, future work should continue researching an efficacious synthesis of sensor **6**, and thus, conduct experiments to evaluate the fluorescence performance of final system. Since promising results were achieved with sensor **13,** future work should continue optimising the synthesis and purification strategies to achieve sensor **13** with higher purity. It is also required more careful research about a probe with more suitable fluorescence properties, to be employed as acceptor or donor in FRET couple. Regarding silicon wafer as solid substrate, alternative strategies to improve homogeneity and the quality of monolayers must be considered. About silica nanoparticles, once complete the functionalization of azide group, different nanoparticle sizes and lengths of linker among the sensor should be evaluated to optimize the fluorescent platform. Designed sensor and the probe selected for FRET mechanism should then be immobilised onto silica nanoparticles. The incorporation of probes onto the surface through select linker will reduce the inter-probe distance and favour the orientation between their dipole, enhancing FRET. The concentration of dyes immobilised onto the surface will be investigated to identify the most suitable ratio between acceptor and donor. FRET antenna or surplus effect can then be used to further enhance the final performance of the system.

The work in this thesis and future work contributes to the research of high-sensitivity sensors for saccharide detection, exploiting the advantages of surface-confined sensors and the combination of the fluorescent mechanisms involved to modulate the signal.

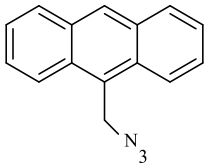
APPENDIX I: CHEMICAL STRUCTURES

1



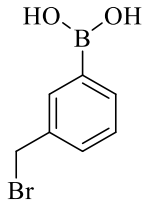
(3-((allyl(methyl)amino)methyl)phenyl)boronic acid

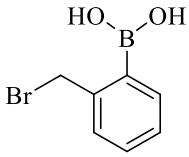
2

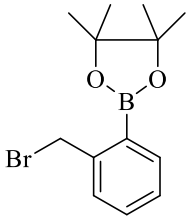


9-(azidomethyl)anthracene

3/ 3b /3c

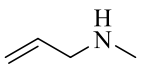






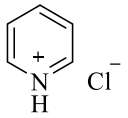
3)3-(bromomethyl)phenyl)boronic acid
3b) 2-(bromomethyl)phenyl)boronic acid
3c) 2-(2-(bromomethyl)phenyl)-4,4,5,5-tetramethyl-1,3,2-dioxaborolane

4



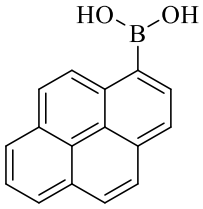
N-methylprop-2-en-1-amine

5



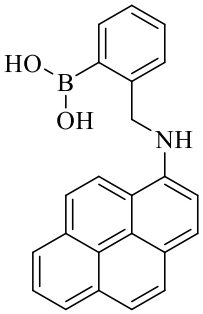
Pyridinium chloride

6



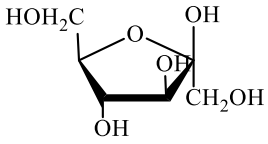
Pyren-1-yl-boronic acid

7



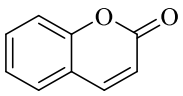
(2-((pyren-1-ylamino)methyl)phenyl)boronic acid

8



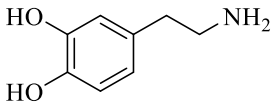
D-Fructose

9



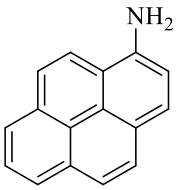
Coumarin

10



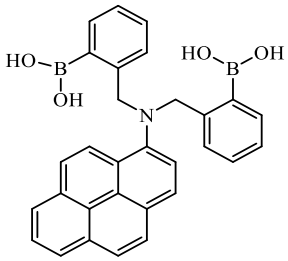
Dopamine

11



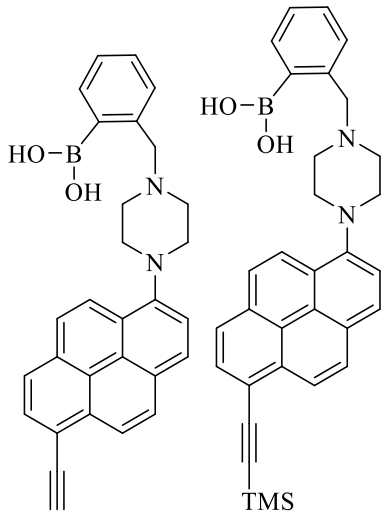
1-amino pyrene

12



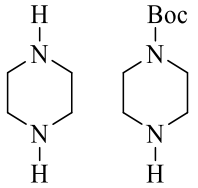
(((pyren-1-yl-azanediyl)bis(methylene))bis(2,1-phenylene))diboronic acid

13/13b



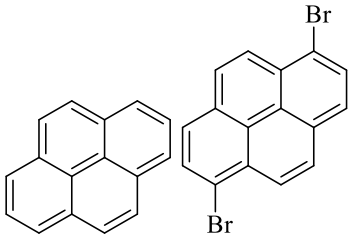
13) (2-((4-(6-ethynylpyren-1-yl)piperazin-1-yl)methyl)phenyl)boronic acid
13b) (2-((4-(6-((trimethylsilyl)ethynyl)pyren-1-yl)piperazin-1-yl)methyl)phenyl)boronic acid

14/ 14 b



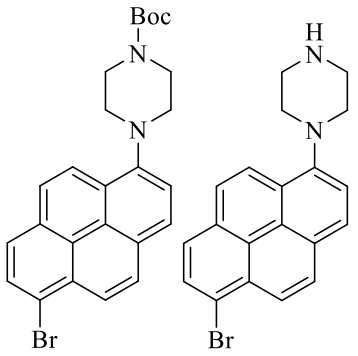
14) Piperazine
14b) Tert-butyl piperazine-1-carboxylate

15/ 15b



15) Pyrene
15b) 1,6-dibromopyrene

16 /16 b



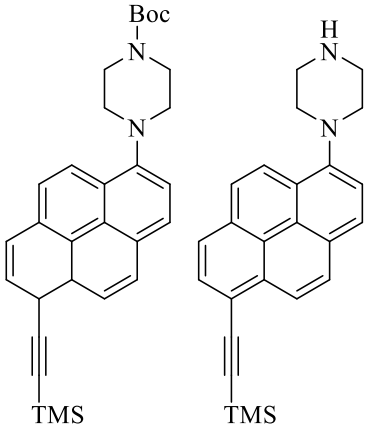
16) Tert-butyl 4-(6-bromopyren-1-yl)piperazine-1-carboxylate
16b) 4-(6-bromopyren-1-yl)piperazine

17



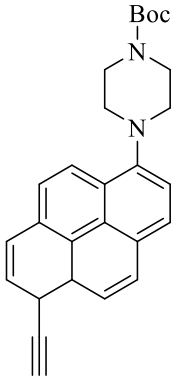
Ethynyltrimethylsilane

18/18b



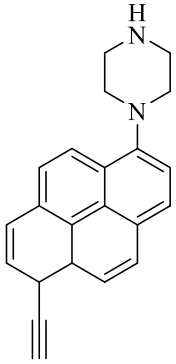
18) Tert-butyl 4-(6-((trimethylsilyl)ethynyl)pyren-1-yl)piperazine-1-carboxylate
18b) 1-(6-((trimethylsilyl)ethynyl)pyren-1-yl)piperazine

19



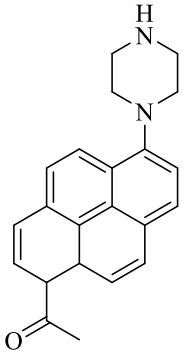
Tert-butyl 4-(6-ethynylpyren-1-yl)piperazine-1-carboxylate

20



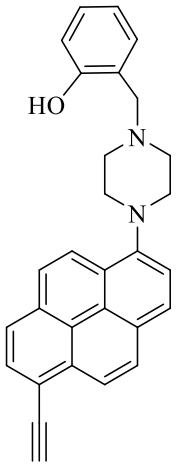
1-(6-ethynylpyren-1-yl)piperazine

21



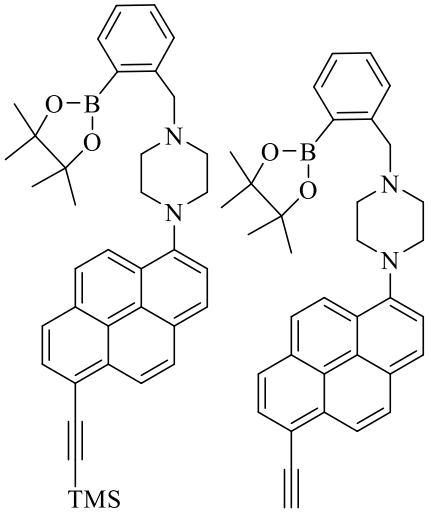
1-(6-(piperazin-1-yl)pyren-1-yl)ethan-1-one

22



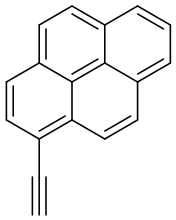
2-((4-(6-ethynylpyren-1-yl)piperazin-1-yl)methyl)phenol

23/23b



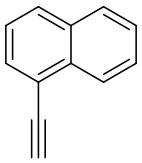
23) 1-(2-(4,4,5,5-tetramethyl-1,3,2-dioxaborolan-2-yl)benzyl)-4-(6-((trimethylsilyl)ethynyl)pyren-1-yl)piperazine
23b) 1-(6-ethynylpyren-1-yl)-4-(2-(4,4,5,5-tetramethyl-1,3,2-dioxaborolan-2-yl)benzyl)piperazine

24



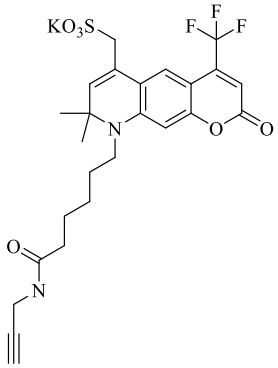
1-ethynylpyrene

25



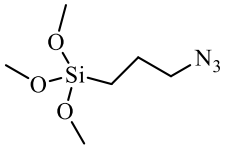
1-ethynylnaphthalene

26



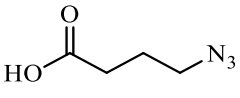
AF430) potassium (8,8-dimethyl-2-oxo-9-(6-oxo-6-(prop-2-yn-1-yl-l2-azaneyl)hexyl)-4-(trifluoromethyl)-8,9-dihydro-2H-pyrano[3,2-g]quinolin-6-yl)methanesulfonate

27



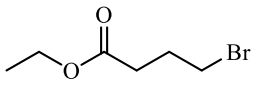
(3-azidopropyl)trimethoxysilane

28



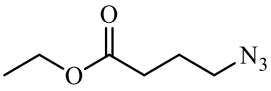
4-azidobutanoic acid

29



ethyl 4-bromobutanoate

30



ethyl 4-bromobutanoate

APPENDIX II: ELLIPSOMETRY & CONTACT ANGLE DATA

Table 1. *Ellipsometry results: thickness values of two or four chips analysed following conditions A-B-C-D shown in Table 5.1*

	Thickness values (nm)				Theoretical values (nm)
Chip	1°	2°	3°	4°	
A*	0.12 ± 0.06	0.37 ± 0.031	/	/	0.61 ± 0.07
B*	0.436 ± 0.353	0.977 ± 0.106	/	/	
C	0.16 ± 0.04	0.10 ± 0.025	0.16 ± 0.026	0.10 ± 0.015	
D	0.20 ± 0.01	0.25 ± 0.107	0.94 ± 0.144	0.01 ± 0.015	

Table 2. *Contact angle results: ADV and REC values of two or four chips analysed following conditions B-C-D shown in Table 5.1*

ADV values (◦)					
Chip	1°	2°	3°	4°	Blank
A*	61.0 ± 2.3	65.9 ± 1.7	/	/	42.1 ± 1.7
B*	71.4 ± 4.7	80.8 ± 5.4	/	/	48.25 ± 4.8
C	57.1 ± 1.58	56.7 ± 0.02	59.6 ± 2.26	54.9 ± 1.56	43.8 ± 10.5
D	64.6 ± 3.50	58.5 ± 2.84	67.2 ± 4.10	58.3 ± 2.96	46.6 ± 4.54
REC values (◦)					
Chip	1°	2°	3°	4°	
A*	49.1 ± 0.8	51.1 ± 1.0	/	/	22.15 ± 2.75
B*	59.7 ± 2.8	61.7 ± 10.8	/	/	31.95 ± 2.35
C	35.6 ± 3.07	37.5 ± 1.64	37.2 ± 0.77	34.8 ± 0.49	32 ± 1.98
D	43.5 ± 3.40	39.8 ± 0.14	45.6 ± 5.56	38.5 ± 0.18	31.25 ± 4.09

Table 3. *Ellipsometry results: thickness values of four chips analysed following conditions E-F-G-H shown in Table 5.2.*

	Thickness values (nm)				Theoretical values (nm)
Chip	1°	2°	3°	4°	
E	1.68 ± 0.06	1.52 ±0.03	1.63 ±0.07	1.54 ±0.02	0.61 ± 0.07
F	0.50 ±0.006	0.54 ±0.031	0.76 ±0.023	0.79 ±0.097	
F*	0.26 ±0	1.24 ±0.855	0.52 ±0.263	0.53 ±0.050	
G	2.17 ±0.15	2.78 ±0.83	0.45 ±0.03		
H	0.26 ± 0.11	0.23 ±0.03	0.27 ±0.01	0.38 ±0.06	

Table 4. *Contact angle results: ADV and REC values analysed following conditions E-F-G-H shown in Table 5.2.*

ADV values (◦)					
Chip	1°	2°	3°	4°	Blank
E	60.1 ± 2.07	55.4 ± 1.48	58.3 ± 0.54	56.6 ± 0.22	40.1 ± 0.02
F	78.8 ± 3.11	74.0 ± 1.69	68.4 ± 1.29	74.4 ± 0.79	40.6 ± 3.86
F*	57.8 ± 0.83	60.3 ± 4.74	80.8 ± 4.07	68.4 ± 1.08	39.1 ± 3.85
H	56.4 ± 0.80	60.4 ± 1.45	55.4 ± 2.57	55.1 ± 0.49	36.65 ± 166
REC values (◦)					
Chip	1°	2°	3°	4°	
E	40.6 ± 1.13	37.4 ± 1.60	39.9 ± 1.31	38.8 ± 0.45	21.6 ± 2.89
F	47.7 ± 2.60	51.2 ± 2.41	50.3 ± 4.90	50.3 ± 1.55	27.4 ± 3.50
F*	36.5 ± 1.84	42.0 ± 4.16	60.1 ± 4.85	44.8 ± 0.42	20.5 ± 1.59
H	36.0 ± 1.13	34.0 ± 1.99	34.5 ± 0.41	34.7 ± 0.22	18.8 ± 1.14

Table 5. *Ellipsometry results: thickness values of four chips analysed following conditions I–J shown in Table 5.3.*

	Thickness values (nm)				Theorical values (nm)
Chip	1°	2°	3°	4°	
I	0.46 ± 0.25	0.57 ± 0.5	0.9 ± 0.11	0.6 ± 0.28	0.58 ± 0.06
J	1.46 ± 0.06	1.64 ± 0.26	2.98 ± 0.023	2.24 ± 0.10	

Table 6. *Contact angle results: ADV and REC values analysed following conditions conditions I–J shown in* ***Table 5.3****.*

	ADV values (◦)			
Chip	1°	2°	3°	4°
I	77.5 ± 5.0	91.2 ± 3	71.3 ± 0.6	93.1 ± 17.6
J	64.7 ± 0.5	59.4 ± 0.5	67.3 ± 10.2	61.2 ± 1.7
	REC values (◦)			
Chip	1°	2°	3°	4°
I	53.4 ± 16.2	69.5 ± 8.2	55.5 ±4.2	70.8 ±16.1
J	43.9 ±7.3	39.6 ± 1.4	45 ±5.4	43.6 ±1

Table 7. *Ellipsometry results: thickness values of four chips analysed following liquid conditions.*

	Thickness values (nm)				Theorical values (nm)
Chip	1°	2°	3°	4°	
Liquid deposition	47.6 ± 6.7	14.1 ± 2.1	33.1 ± 2.0	28.2 ± 3.8	0.61 ± 0.07

Table 8. *Ellipsometry results: thickness values of different points (a-i) of one larger chip following conditions F-G shown in Table 5.2.*

Position	Experiment F2	Experiment G2
a	0.29 ±0.21	0.98 ±0.049
b	0.22 ±0.002	0.73 ±0.050
c	0.34±0.003	1.99±0.018
d	0.19 ±0.003	1.02 ±0.030
e	0.22 ±0.003	5.93 ±0.073
f	0.21 ±0.002	1.14 ±0.070
g	0.24 ±0.003	4.70 ±0.047
h	0.15 ±0.002	1.09 ±0.029
i	0.24±0.006	0.52±0.029
Theorical values (nm)	0.61± 0.07	

APPENDIX III: NMR, IR & MASS SPECTRA

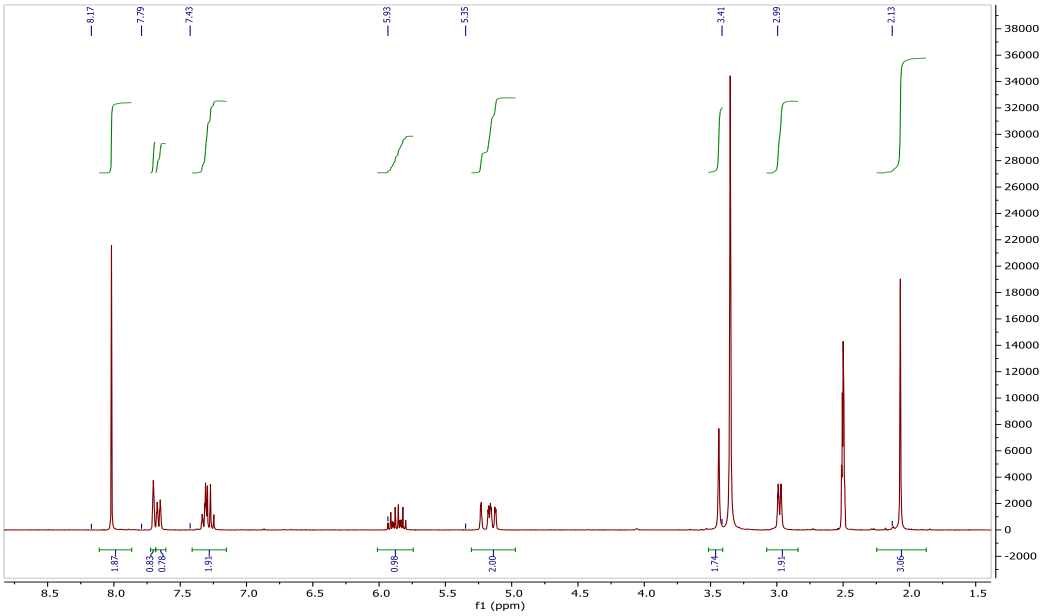


Figure 1. *Figure 7.1 ^{1}H NMR (DMSO-d6) of* ***1****.*

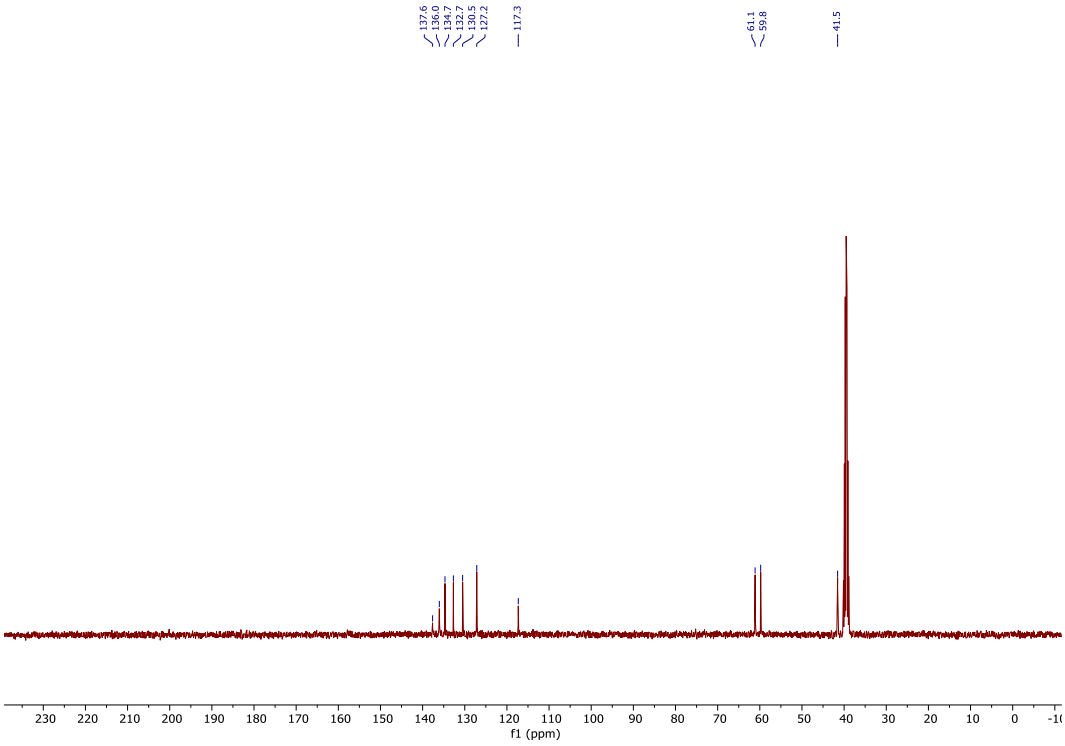


Figure 2. *^{13}C NMR (DMSO-d6) of* ***1****.*

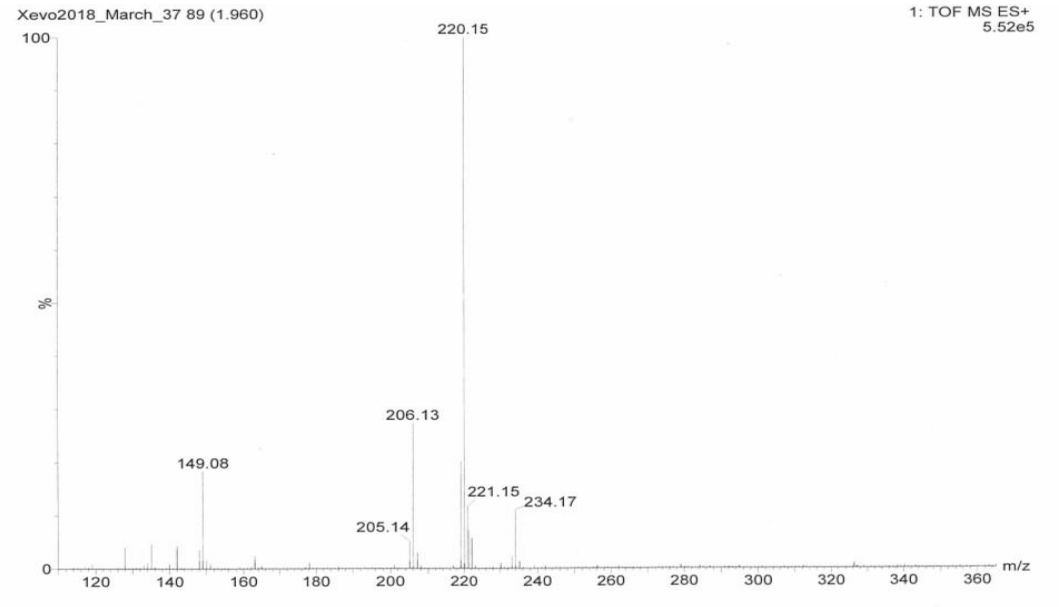


Figure 3. *Mass spectrum of* ***1****.*

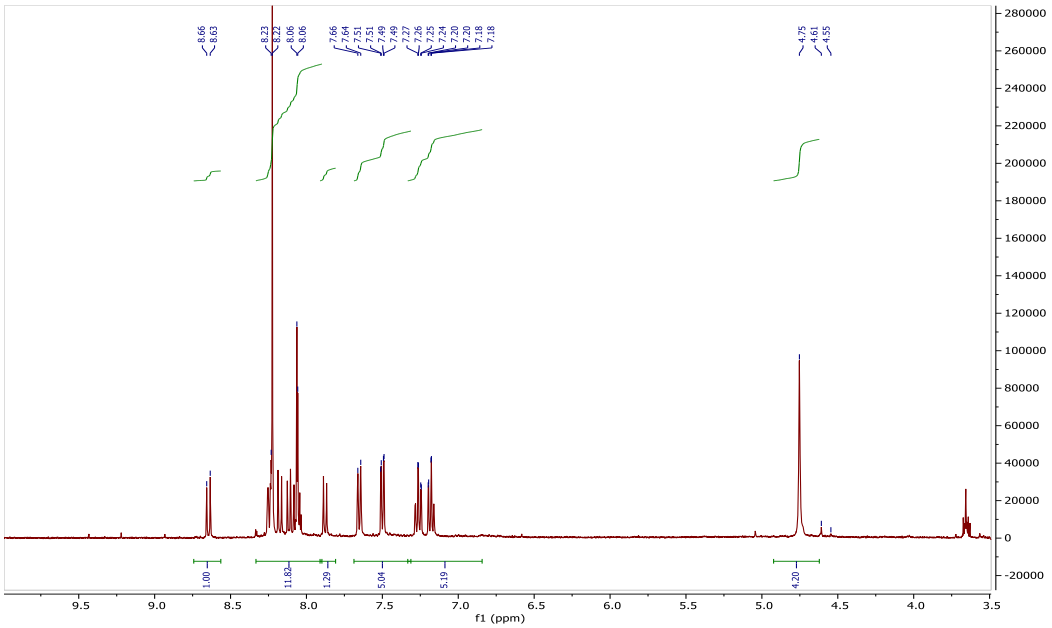


Figure 4 *^{1}H NMR (DMSO-d6) of* ***12.***

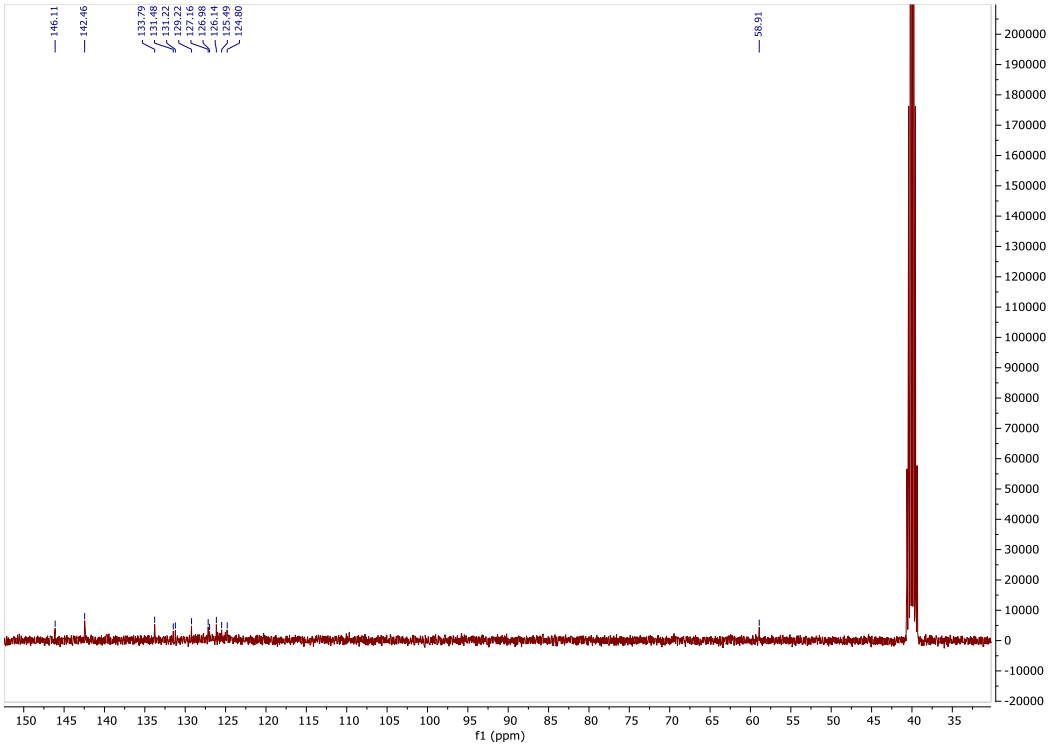


Figure 5. *^{13}C NMR (DMSO-d6) of* ***12.***

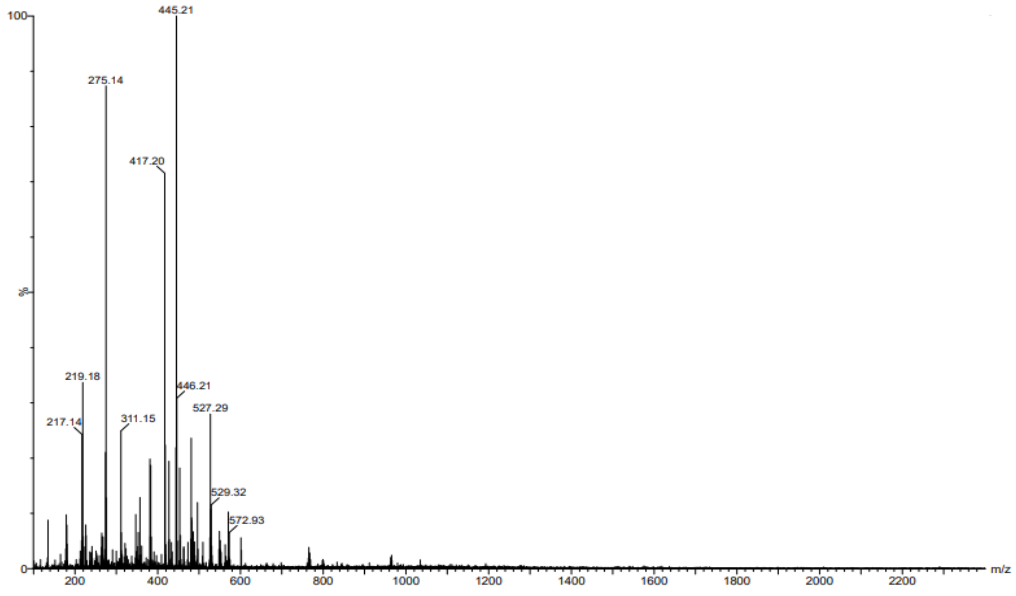


Figure 6. *Mass spectra of* ***13.***

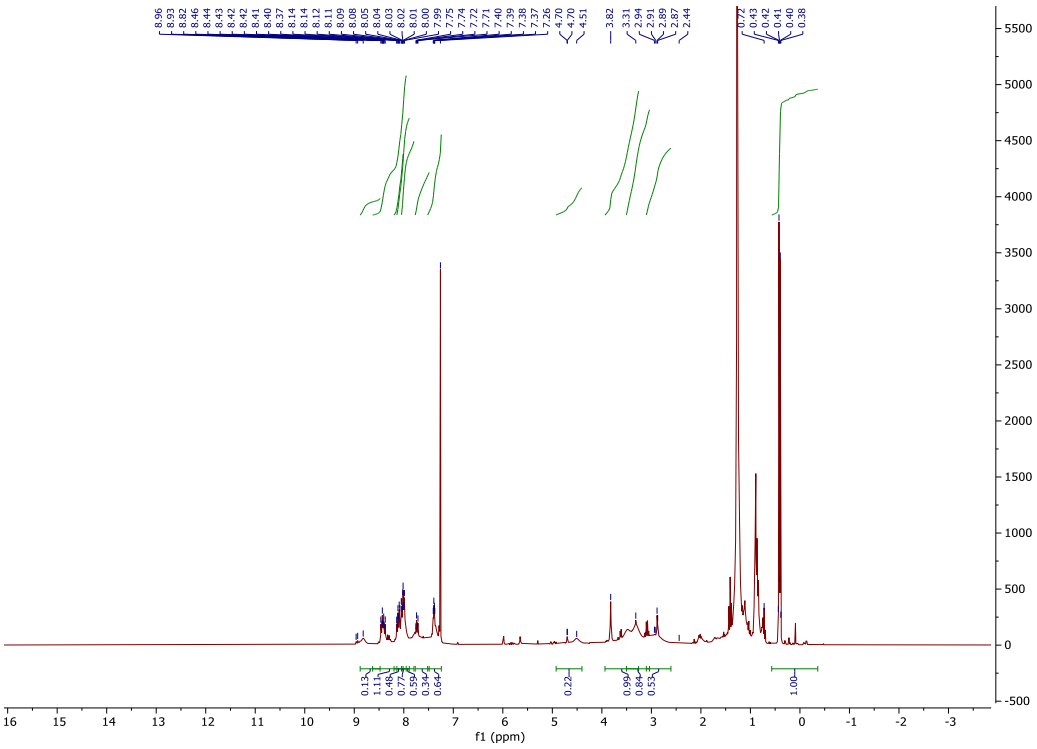


Figure 7. *^{1}H NMR ($CDCl_3$) of* ***13b.***

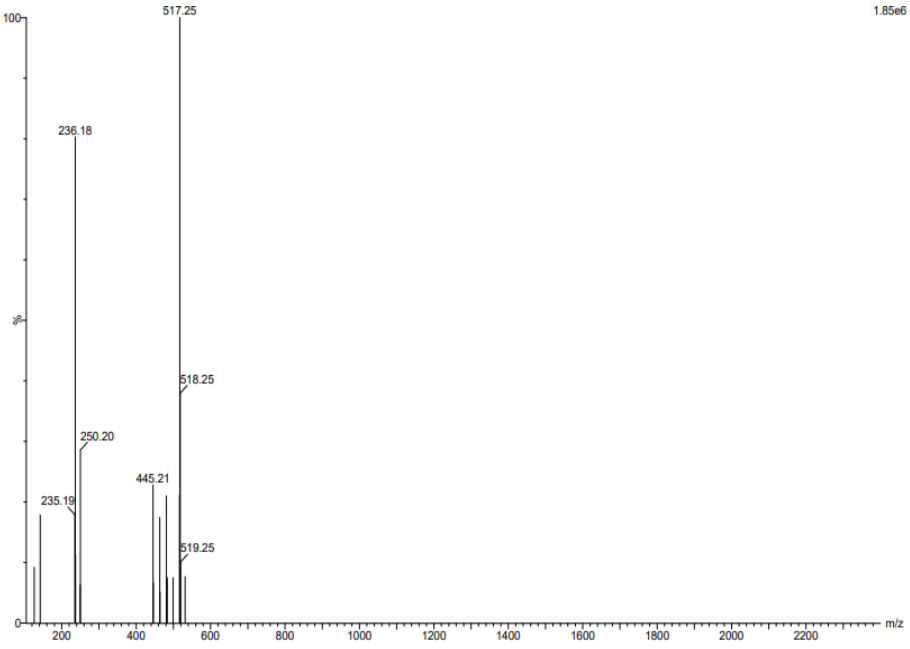


Figure 8. *Mass spectra of* ***13b****.*

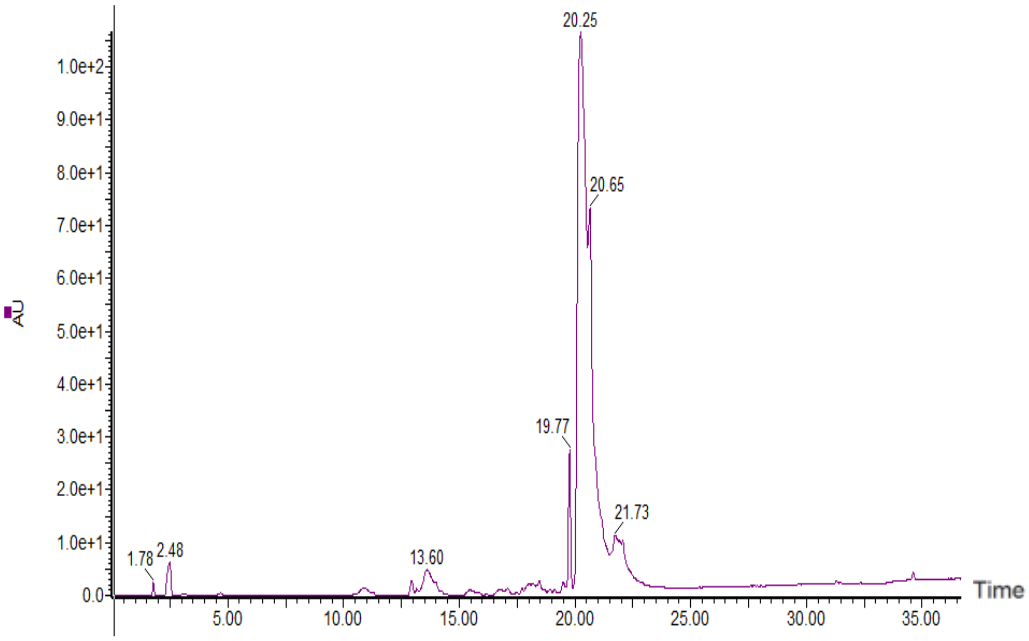


Figure 9. *Chromatogram of* ***13b.***

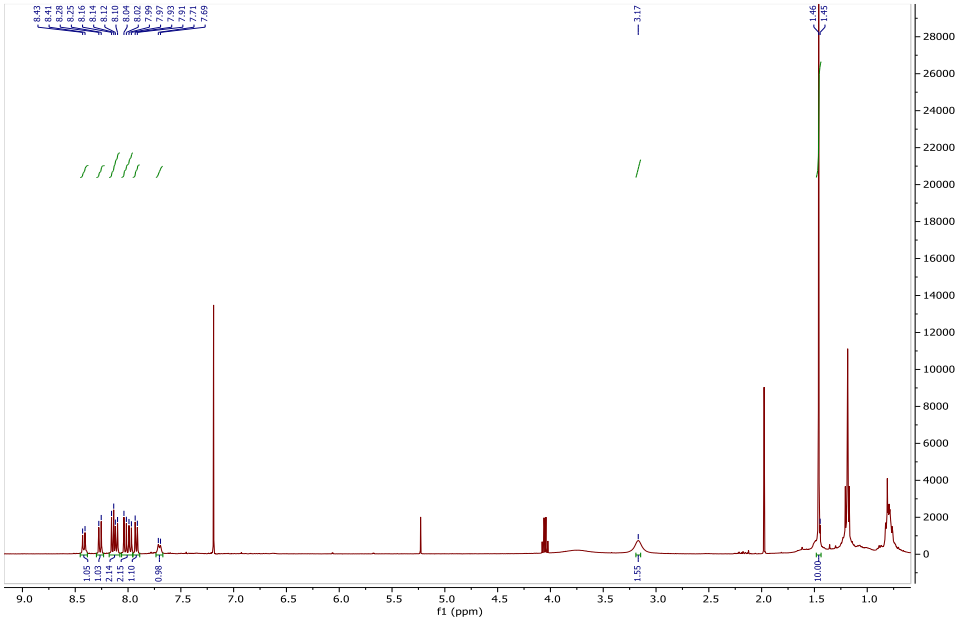


Figure 10. *^{1}H NMR ($CDCl_3$) of* ***16.***

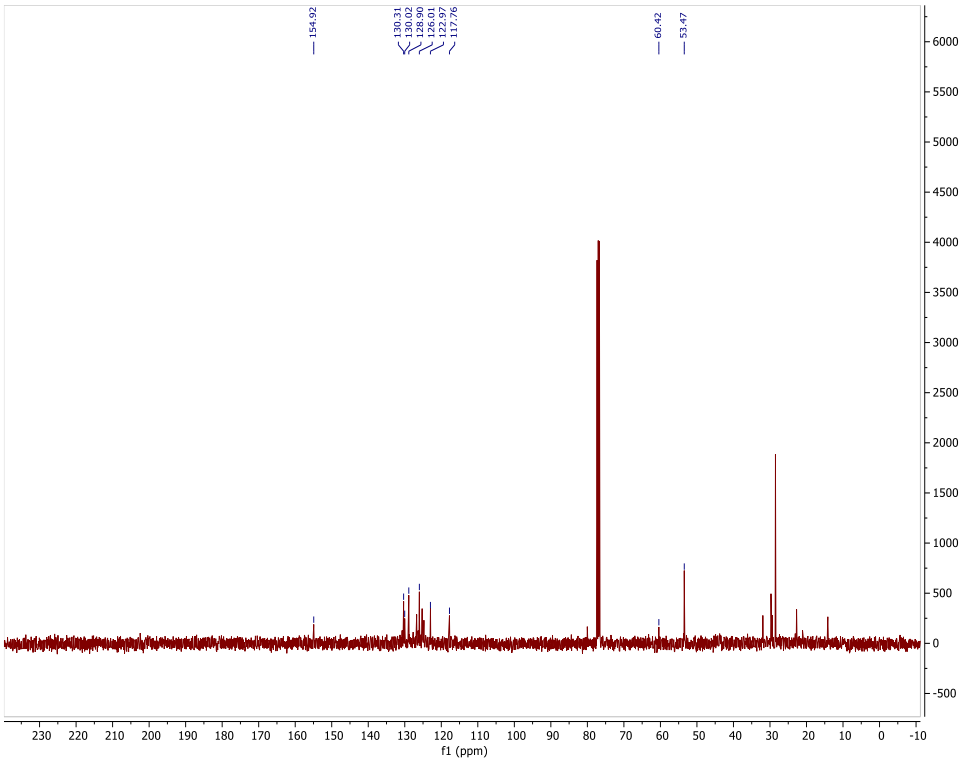


Figure 11. *^{13}C NMR ($CDCl_3$) of* ***16.***

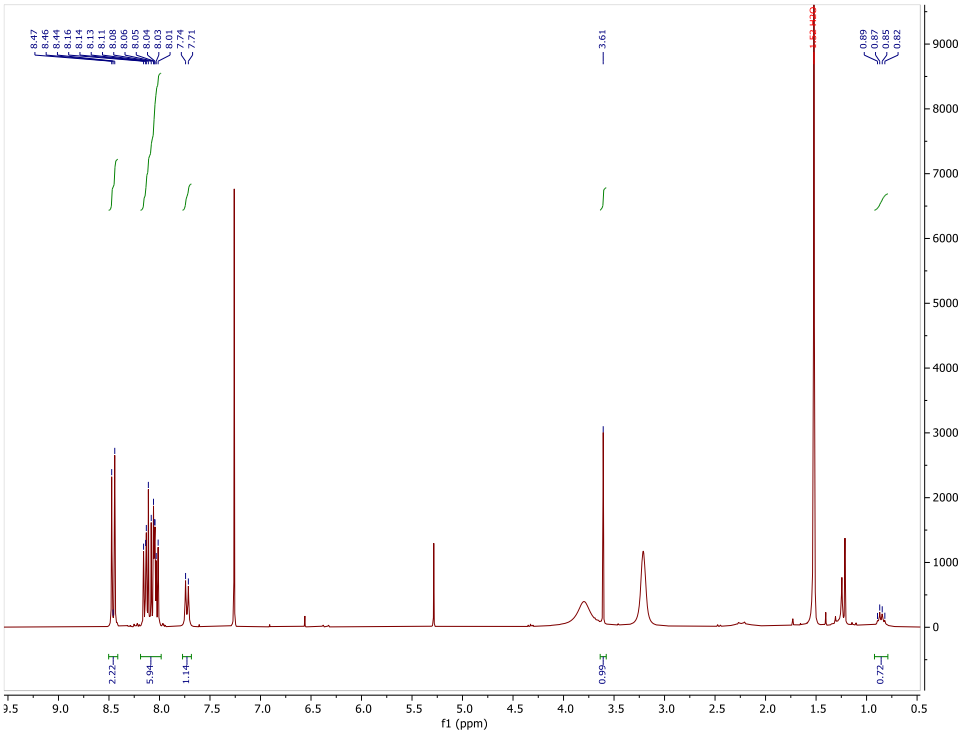


Figure 12. *^{1}H NMR (DMSO-d6) of* ***18.***

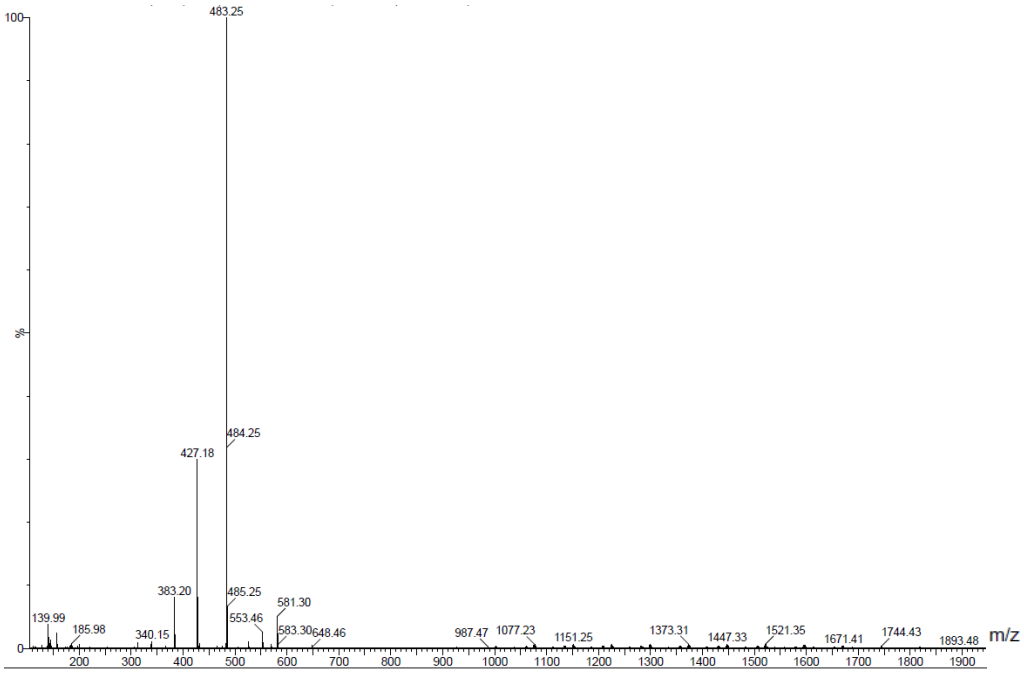


Figure 13. *Mass spectra of* ***18.***

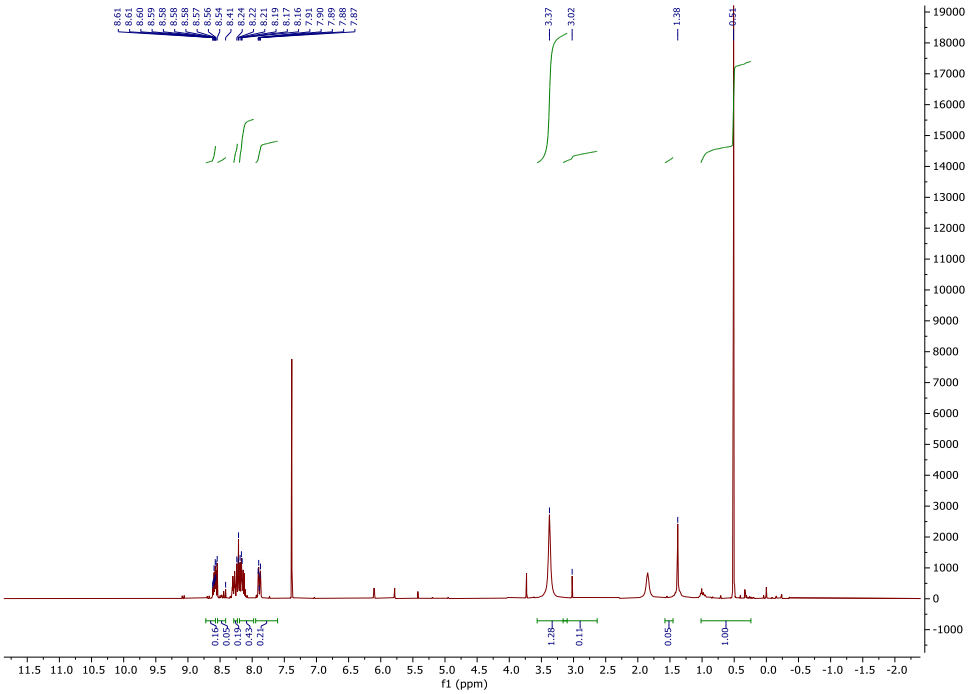


Figure 14. *^{1}H NMR ($CDCl_3$) of* ***18b.***

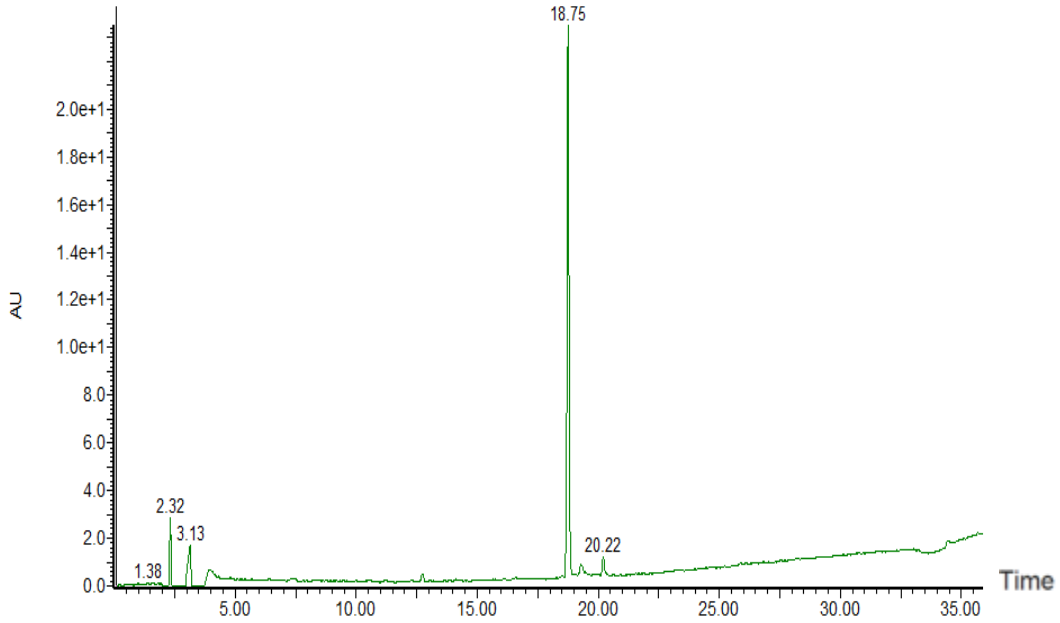


Figure 15. *Chromatogram of* ***18b****.*

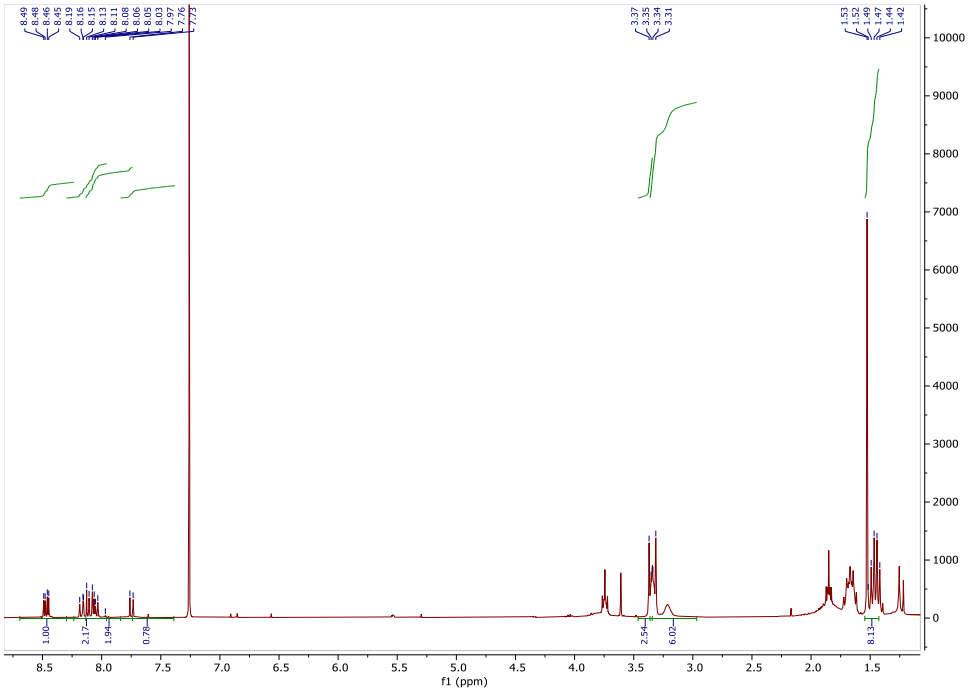


Figure 16. *^1H NMR ($CDCl_3$) of* ***19.***

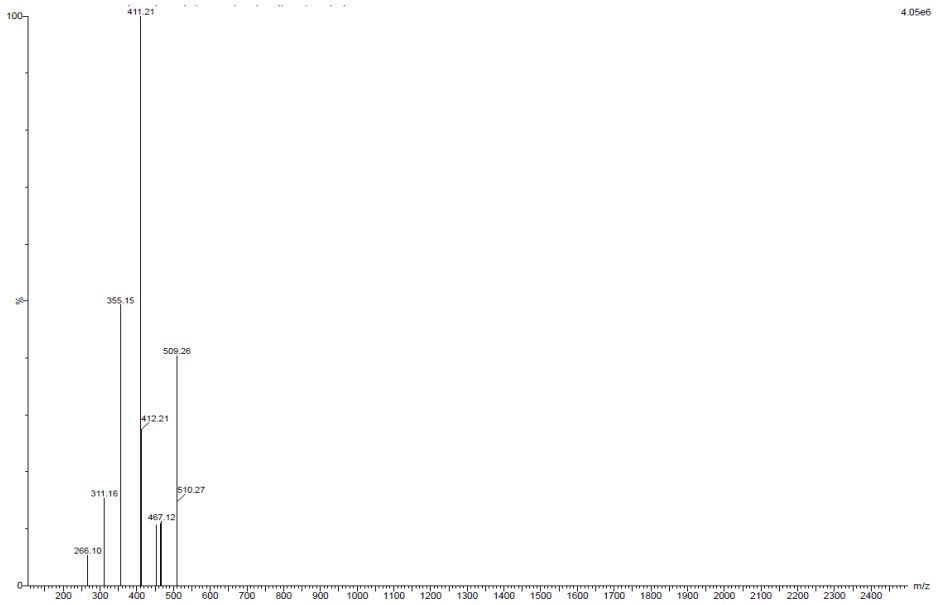


Figure 17. *Mass spectra of* ***19.***

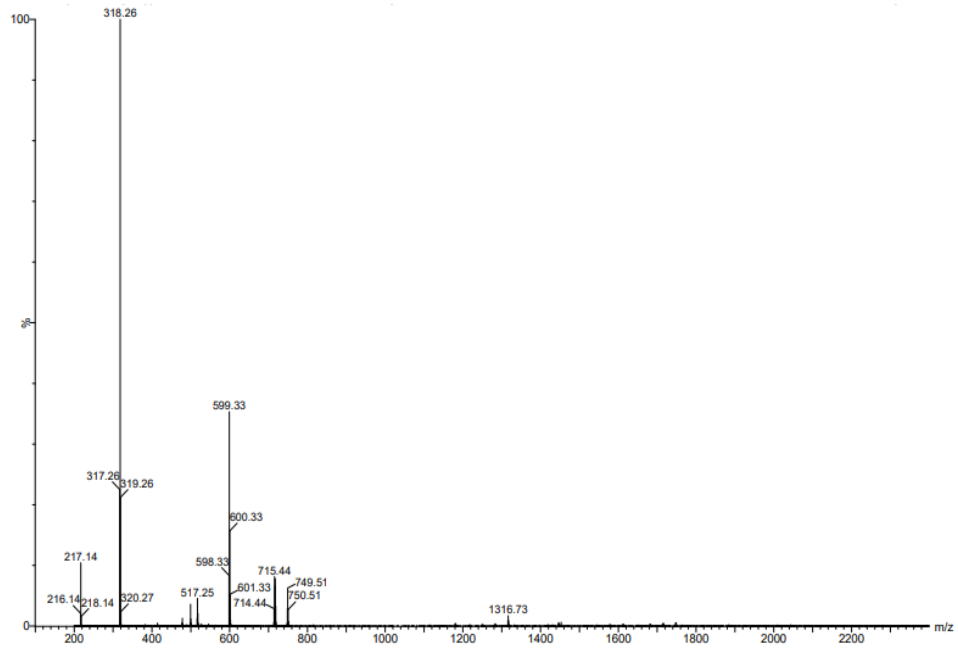


Figure 18. *Mass spectra of* ***23.***

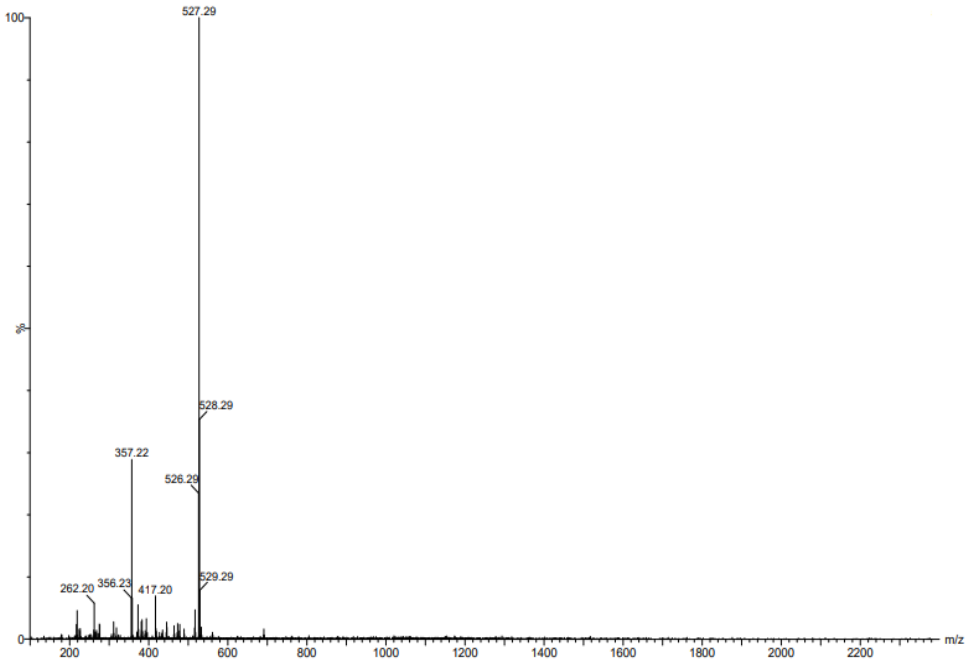


Figure 19. *Mass spectra of* ***23b.***

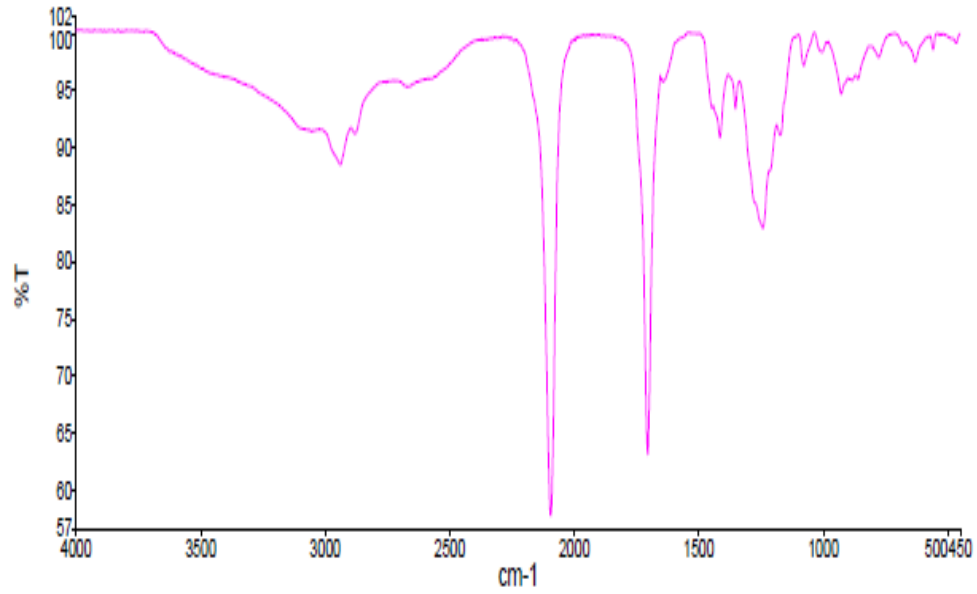


Figure 20. *3-Azidopropyltriethoxysilane* ***27.***

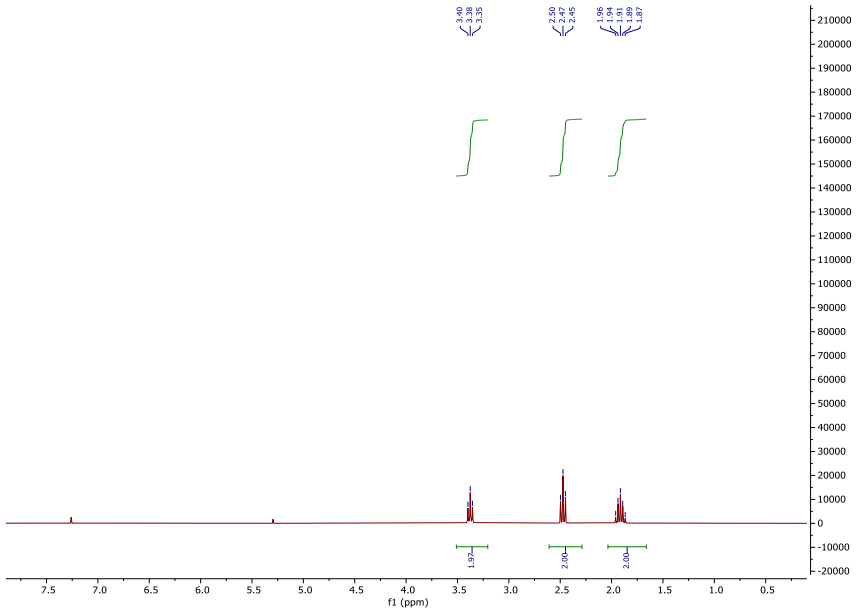


Figure 21. *^{1}H NMR ($CDCl_3$) of* ***28.***

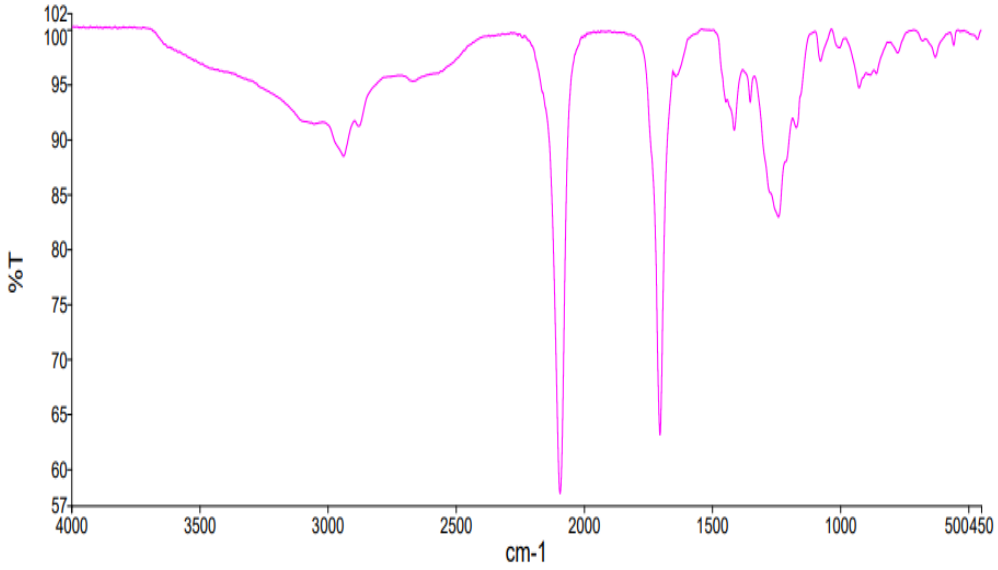


Figure 22. *IR spectra of* ***28.***

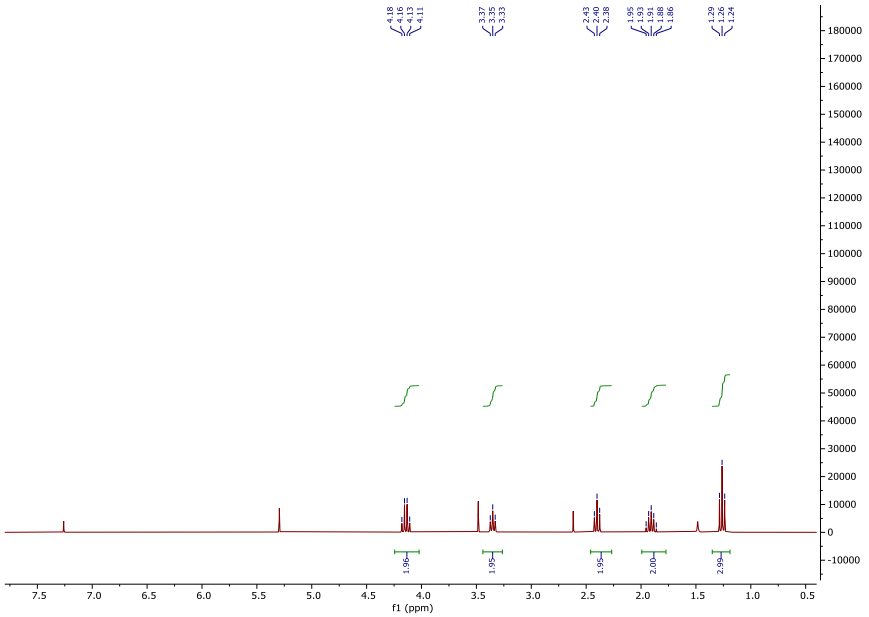


Figure 23. *^{1}H NMR ($CDCl_3$) of* ***30.***

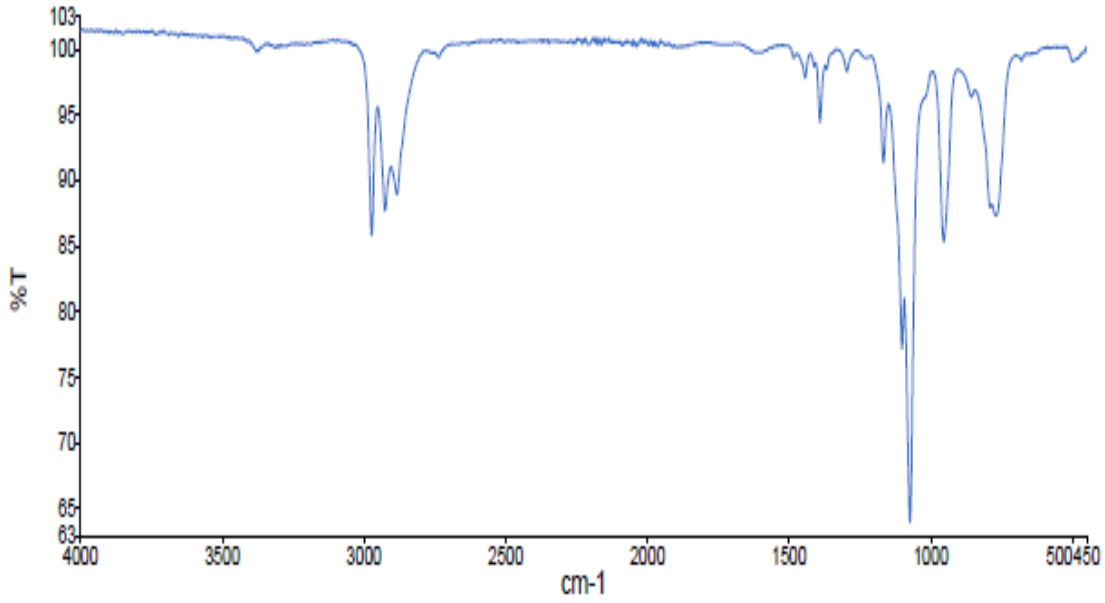


Figure 24. *IR spectra of AMPTS.*

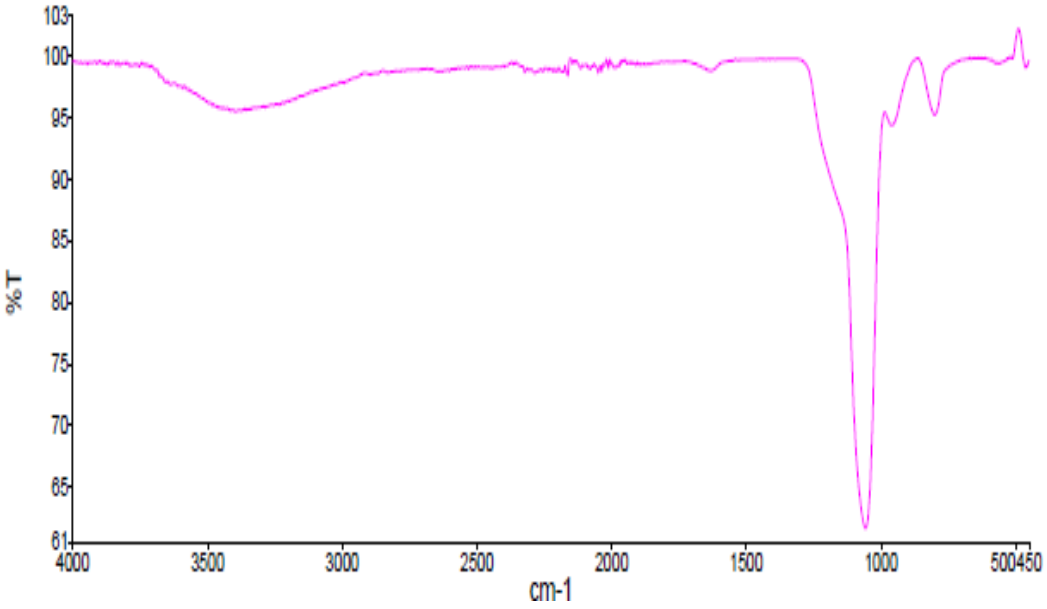


Figure 25. *IR spectra of SiO_2Np.*

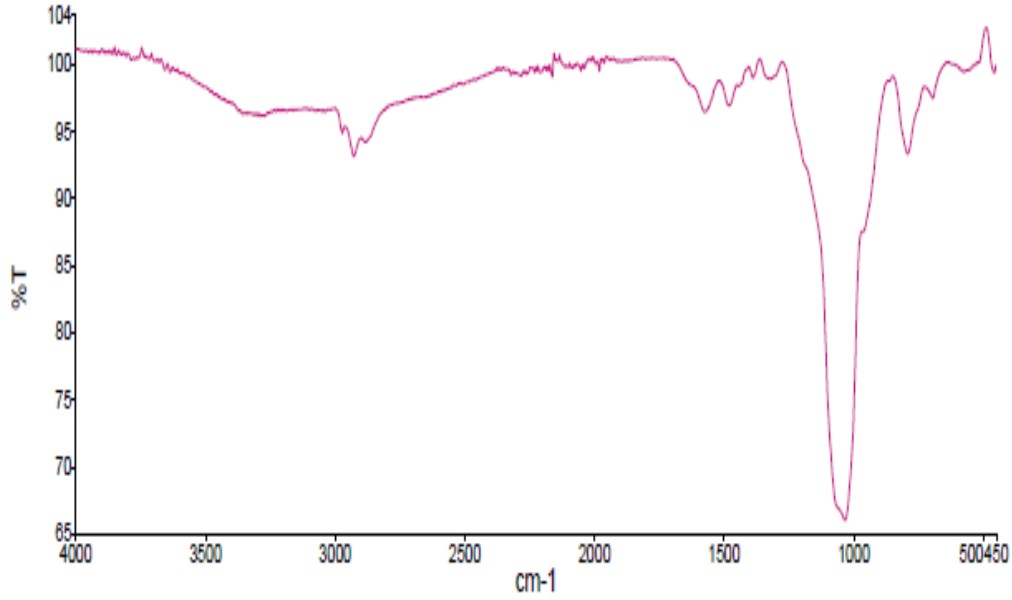


Figure 26. *IR spectra of NH_2-SiO_2Np.*

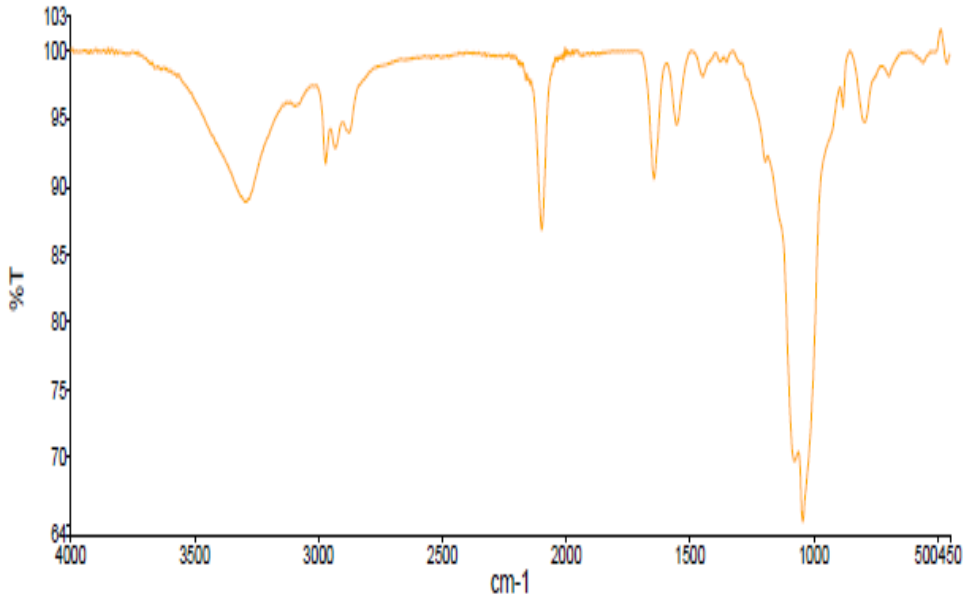


Figure 27. *IR spectra of N_3-SiO_2 Np.*

APPENDIX IV: FLUORESCENCE SPECTRA

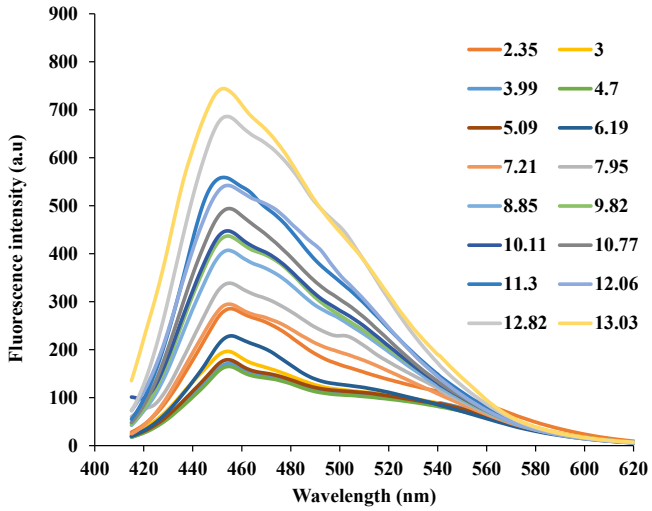


Figure 28. *Fluorescence intensity pH profiles of* ***13b*** *(10 µM) in 50 mM PB solution* λ_{ex} *390 nm.*

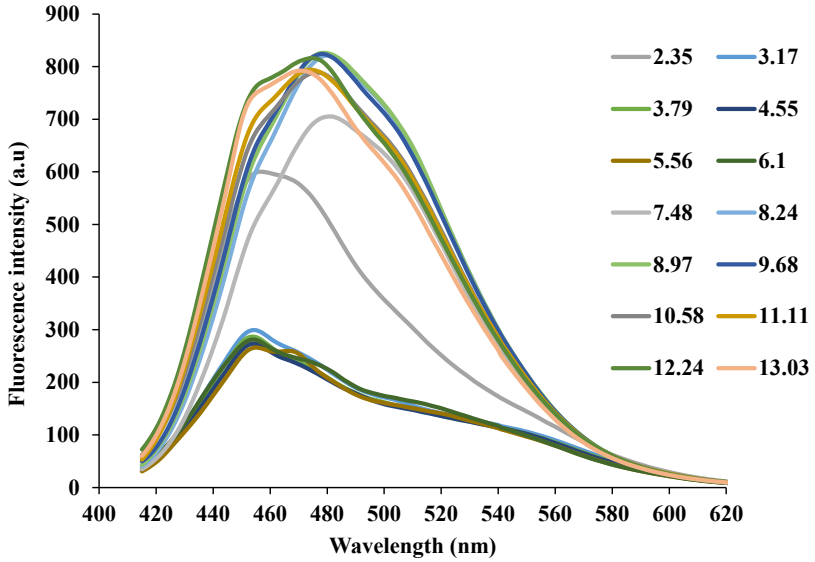


Figure 29. *Fluorescence intensity pH profiles of* ***13b*** *(10 µM) in 50 mM PB solution with D-Fructose (100 mM)* λ_{ex} *390nm.*

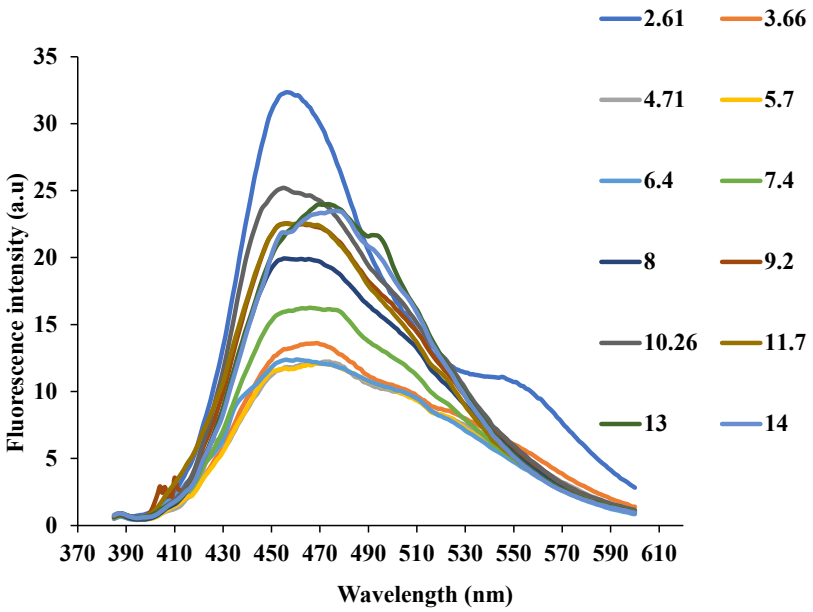


Figure 30. *Fluorescence intensity pH profiles of* ***13*** *(10 μM) in50 mM PB solution (100 mM)* λ_{ex} *360nm.*

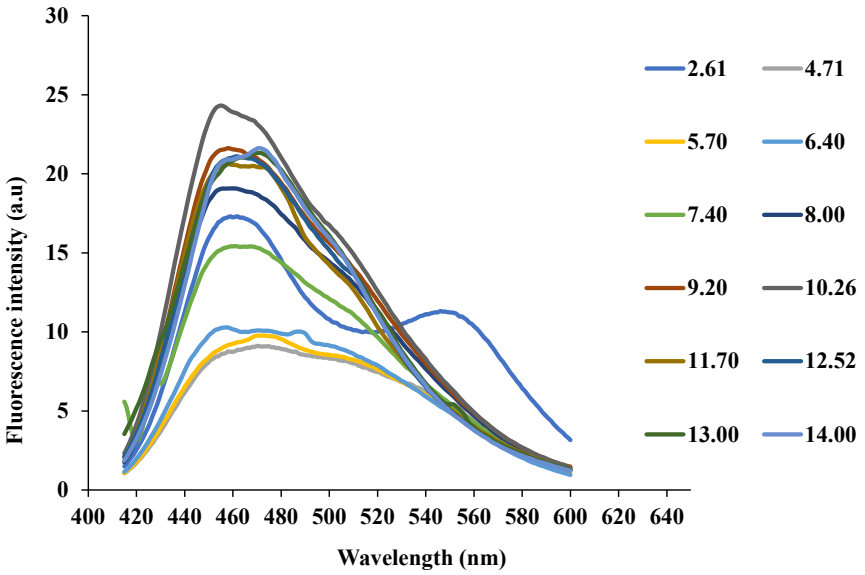


Figure 31. *Fluorescence intensity pH profile of* ***13*** *(10 μM) in50 mM PB solution* λ_{ex} *390nm.*

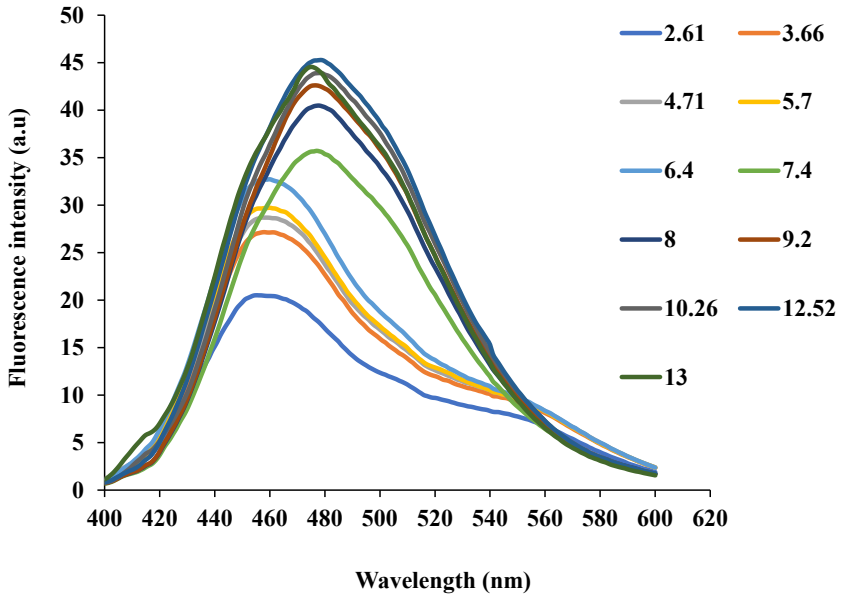


Figure 32. *Fluorescence intensity pH profile of* ***13*** *(10 μM) in 50 mM PB solution with D-Fructose* λ_{ex} *390nm*

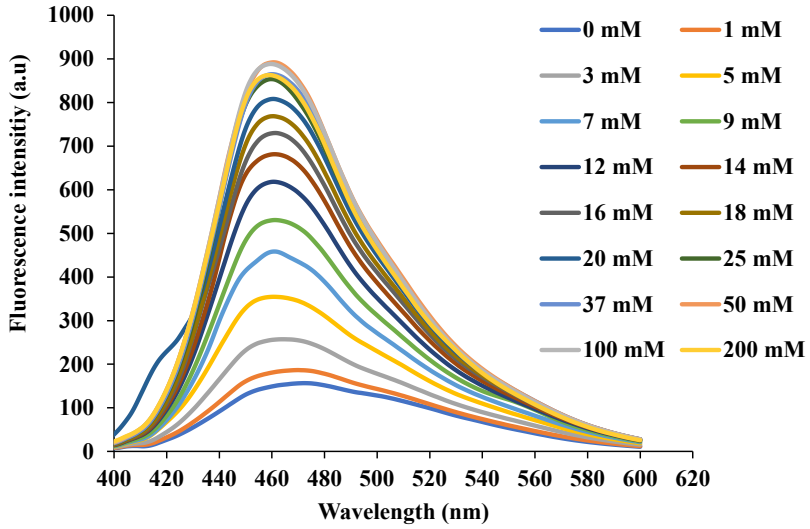


Figure 33. *Fluorescence titration of* ***13*** *with D-Sorbitol at different concentration (0-200 mM) at* λ_{ex} *360 nm.*

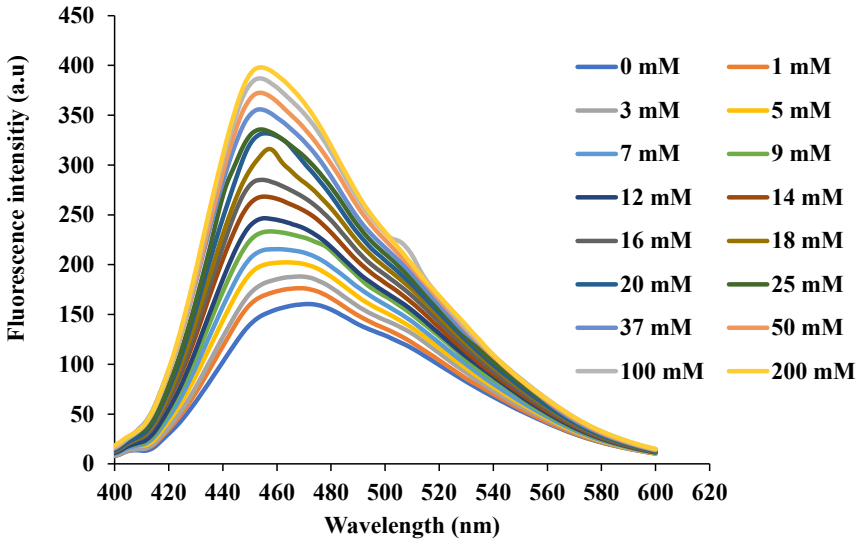


Figure 34. *Fluorescence titration of* ***13*** *with D-Glucose at different concentration (0-200 mM) at* λ_{ex} *360 nm.*

BIBLIOGRAPHY

1. Dwek, R. A., Glycobiology: Toward Understanding the Function of Sugars. *Chem Rev* **1996,** *96* (2), 683-720.

2. Robert V. Stick, S. W., *Carbohydrates: The Essential Molecules of Life*. Second Edition ed.; **2008**.

3. Williams, G. T.; Kedge, J. L.; Fossey, J. S., Molecular Boronic Acid-Based Saccharide Sensors. *ACS Sens* **2021,** *6* (4), 1508-1528.

4. Turnbull, J. E.; Field, R. A., Emerging glycomics technologies. *Nat Chem Biol* **2007,** *3* (2), 74-77.

5. Hu, M.; Lan, Y.; Lu, A.; Ma, X.; Zhang, L., Glycan-based biomarkers for diagnosis of cancers and other diseases: Past, present, and future. *Prog Mol Biol Transl Sci* **2019,** *162*, 1-24.

6. Yan, J.; Fang, H.; Wang, B., Boronolectins and fluorescent boronolectins: an examination of the detailed chemistry issues important for the design. *Med Res Rev* **2005,** *25* (5), 490-520.

7. Arnaud, J.; Audfray, A.; Imberty, A., Binding sugars: from natural lectins to synthetic receptors and engineered neolectins. *Chem Soc Rev* **2013,** *42* (11), 4798-4813.

8. Tommasone, S.; Allabush, F.; Tagger, Y. K.; Norman, J.; Kopf, M.; Tucker, J. H. R.; Mendes, P. M., The challenges of glycan recognition with natural and artificial receptors. *Chem Soc Rev* **2019,** *48* (22), 5488-5505.

9. Oliveira-Ferrer, L.; Legler, K.; Milde-Langosch, K., Role of protein glycosylation in cancer metastasis. *Semin Cancer Biol* **2017,** *44*, 141-152.

10. Rajamoorthi Kantian, C. M. H., 1 Thomas M. Harris, Jonathan P. Waltho,1 Nicholas J. Skelton,1 and Dudley H. Williams, Function of the Amino Sugar and N-Terminal Amino Acid of the Antibiotic Vancomycin in Its Complexation with Cell Wall Peptides. *J. Am. Chem. Soc.* **1988,** *110*, 2946-2953.

11. Council, N. R., *Transforming Glycoscience: A Roadmap for the Future*. The National Academies Press: Washington, DC, **2012**; p 208.

12. Tang, L., Versatile genome editing. *Nat Methods* **2021,** *18* (1), 27.

13. Oliver, N. S.; Toumazou, C.; Cass, A. E.; Johnston, D. G., Glucose sensors: a review of current and emerging technology. *Diabet Med* **2009,** *26* (3), 197-210.

14. Guemes, M.; Rahman, S. A.; Hussain, K., What is a normal blood glucose? *Arch Dis Child* **2016,** *101* (6), 569-574.

15. Kim, D. C.; Kang, D. J., Molecular Recognition and Specific Interactions for Biosensing Applications. *Sensors (Basel)* **2008,** *8* (10), 6605-6641.

16. Hulanicki, A.; Glab, S.; Ingman, F., Chemical Sensors Definitions and Classification. *Pure and Applied Chemistry* **1991,** *63* (9), 1247-1250.

17. Putzbach, W.; Ronkainen, N. J., Immobilization techniques in the fabrication of nanomaterial-based electrochemical biosensors: a review. *Sensors (Basel)* **2013,** *13* (4), 4811-4840.

18. Thompson, R. Q., Analytical Chemistry *Journal of Chemical Education* **2000,** *77* (4), 453-454.

19. Pomorski, A.; Kochanczyk, T.; Miloch, A.; Krezel, A., Method for accurate determination of dissociation constants of optical ratiometric systems: chemical probes, genetically encoded sensors, and interacting molecules. *Anal Chem* **2013,** *85* (23), 11479-11486.

20. Hirose, K., A Practical Guide for the Determination of Binding Constants. *Journal of Inclusion Phenomena and Macrocyclic Chemistry* **2001,** *39* (3/4), 193-209.

21. Roy, G. L.; Laferriere, A. L.; Edwards, J. O., A Comparative Study of Polyol Complexes of Arsenite, Borate, and Tellurate Ions. *J Inorg Nucl Chem* **1957,** *4* (2), 106-114.

22. Kuivila, H. G., Electrophilic Displacement Reactions. III. Kinetics of the Reaction between Hydrogen Peroxide and Benzeneboronic Acid. *J Am Chem Soc* **2002,** *76* (3), 870-874.

23. DeFrancesco, H.; Dudley, J.; Coca, A., Boron Chemistry: An Overview. In *Boron Reagents in Synthesis*, **2016**; pp 1-25.

24. Lopalco, A.; Lopedota, A. A.; Laquintana, V.; Denora, N.; Stella, V. J., Boric Acid, a Lewis Acid With Unique and Unusual Properties: Formulation Implications. *J Pharm Sci* **2020,** *109* (8), 2375-2386.

25. Hiller, N. D.; Silva, N. A. D. E.; Tavares, T. A.; Faria, R. X.; Eberlin, M. N.; Martins, D. D., Arylboronic Acids and their Myriad of Applications Beyond Organic Synthesis. *Eur J Org Chem* **2020,** *2020* (31), 4841-4877.

26. N.N. GreenWood, A. E., *Chemistry of the Elements*. Butterworth-Heinemann: **1997**.

27. Whyte, G. F.; Vilar, R.; Woscholski, R., Molecular recognition with boronic acids-applications in chemical biology. *J Chem Biol* **2013,** *6* (4), 161-174.

28. Werner, J. P.; Mitchell, J. M.; Taracila, M. A.; Bonomo, R. A.; Powers, R. A., Exploring the potential of boronic acids as inhibitors of OXA-24/40 beta-lactamase. *Protein Sci* **2017,** *26* (3), 515-526.

29. Stubelius, A.; Lee, S.; Almutairi, A., The Chemistry of Boronic Acids in Nanomaterials for Drug Delivery. *Acc Chem Res* **2019,** *52* (11), 3108-3119.

30. Galbraith, E.; James, T. D., Boron based anion receptors as sensors. *Chem Soc Rev* **2010,** *39* (10), 3831-3842.

31. Wang, X.; Xia, N.; Liu, L., Boronic Acid-based approach for separation and immobilization of glycoproteins and its application in sensing. *Int J Mol Sci* **2013,** *14* (10), 20890-20912.

32. Lacina, K.; Skladal, P.; James, T. D., Boronic acids for sensing and other applications - a mini-review of papers published in 2013. *Chem Cent J* **2014,** *8* (1), 60.

33. Bull, S. D.; Davidson, M. G.; van den Elsen, J. M.; Fossey, J. S.; Jenkins, A. T.; Jiang, Y. B.; Kubo, Y.; Marken, F.; Sakurai, K.; Zhao, J.; James, T. D., Exploiting the reversible covalent bonding of boronic acids: recognition, sensing, and assembly. *Acc Chem Res* **2013,** *46* (2), 312-326.

34. Jin, S.; Cheng, Y.; Reid, S.; Li, M.; Wang, B., Carbohydrate recognition by boronolectins, small molecules, and lectins. *Med Res Rev* **2010,** *30* (2), 171-257.

35. Tansil, N. C.; Gao, Z. Q., Nanoparticles in biomolecular detection. *Nano Today* **2006,** *1* (1), 28-37.

36. J.Böeseken, The use of Boric Acid for the Determination of the Configuration of Carbohydrates. *Advances in Carbohydrate Chemistry* **1949,** *Volume 4*, Pages 189-210.

37. Lampe, V.; Milobedzka, J., Studien über Curcumin. *Berichte der deutschen chemischen Gesellschaft* **2006,** *46* (2), 2235-2240.

38. Edwards, J. O.; Morrison, G. C.; Ross, V. F.; Schultz, J. W., The Structure of the Aqueous Borate Ion. *J Am Chem Soc* **1955,** *77* (2), 266-268.

39. Springsteen, G.; Wang, B. H., A detailed examination of boronic acid-diol complexation. *Tetrahedron* **2002,** *58* (26), 5291-5300.

40. Springsteen, G.; Wang, B., Alizarin Red S. as a general optical reporter for studying the binding of boronic acids with carbohydrates. *Chem Commun (Camb)* **2001,** (17), 1608-1609.

41. Bosch, L. I.; Fyles, T. M.; James, T. D., Binary and ternary phenylboronic acid complexes with saccharides and Lewis bases. *Tetrahedron* **2004,** *60* (49), 11175-11190.

42. Fang, G. Q.; Wang, H.; Bian, Z. C.; Sun, J.; Liu, A. Q.; Fang, H.; Liu, B.; Yao, Q. Q.; Wu, Z. Y., Recent development of boronic acid-based fluorescent sensors. *Rsc Advances* **2018,** *8* (51), 29400-29427.

43. Yan, J.; Springsteen, G.; Deeter, S.; Wang, B., The relationship among pKa, pH, and binding constants in the interactions between boronic acids and diols—it is not as simple as it appears. *Tetrahedron* **2004,** *60* (49), 11205-11209.

44. Berube, M.; Dowlut, M.; Hall, D. G., Benzoboroxoles as efficient glycopyranoside-binding agents in physiological conditions: structure and selectivity of complex formation. *J Org Chem* **2008,** *73* (17), 6471-6479.

45. Wulff, G., Selective binding to polymers via covalent bonds. The construction of chiral cavities as specific receptor sites. *Pure and Applied Chemistry* **1982,** *54* (11), 2093-2102.

46. Fowler, W. A., Experimental and Theoretical Nuclear Astrophysics - the Quest for the Origin of the Elements - Nobel Lecture. *Angew Chem Int Edit* **1984,** *23* (9), 645-671.

47. Wulff, G.; Lauer, M.; Bohnke, H., On the Chemistry of Binding-Sites .5. Rapid Proton-Transfer as Cause of an Unusually Large Neighboring Group Effect. *Angew Chem Int Edit* **1984,** *23* (9), 741-742.

48. Dowlut, M.; Hall, D. G., An improved class of sugar-binding boronic acids, soluble and capable of complexing glycosides in neutral water. *J Am Chem Soc* **2006,** *128* (13), 4226-4227.

49. Casado, J.; Rodriguez, I.; Ramil, M.; Cela, R., Selective determination of antimycotic drugs in environmental water samples by mixed-mode solid-phase extraction and liquid

chromatography quadrupole time-of-flight mass spectrometry. *J Chromatogr A* **2014,** *1339*, 42-49.

50. Kur, K.; Przybyt, M.; Miller, E., Study of 3-amino phenylboronic acid interactions with selected sugars by optical methods. *Journal of Luminescence* **2017,** *183*, 486-493.

51. Draffin, S. P.; Duggan, P. J.; Fallon, G. D., O^2,O^3:O^4,O^5-Bis(phenylboranediyl)-β-D-fructopyranose acetone solvate. *Acta Crystallographica Section E Structure Reports Online* **2004,** *60* (9), o1520-o1522.

52. Pizer, R.; Tihal, C., Equilibria and Reaction-Mechanism of the Complexation of Methylboronic Acid with Polyols. *Inorganic Chemistry* **1992,** *31* (15), 3243-3247.

53. van den Berg, R.; Peters, J. A.; van Bekkum, H., The structure and (local) stability constants of borate esters of mono- and di-saccharides as studied by 11B and 13C NMR spectroscopy. *Carbohydrate Research* **1994,** *253*, 1-12.

54. Zhang, X. T.; Liu, G. J.; Ning, Z. W.; Xing, G. W., Boronic acid-based chemical sensors for saccharides. *Carbohydr Res* **2017,** *452*, 129-148.

55. Badjic, J. D.; Nelson, A.; Cantrill, S. J.; Turnbull, W. B.; Stoddart, J. F., Multivalency and cooperativity in supramolecular chemistry. *Acc Chem Res* **2005,** *38* (9), 723-732.

56. Fasting, C.; Schalley, C. A.; Weber, M.; Seitz, O.; Hecht, S.; Koksch, B.; Dernedde, J.; Graf, C.; Knapp, E. W.; Haag, R., Multivalency as a chemical organization and action principle. *Angew Chem Int Ed Engl* **2012,** *51* (42), 10472-10498.

57. Comstock, M. J., Supramolecular Chemistry, Fluorescence, and Sensing. In *Fluorescent Chemosensors for Ion and Molecule Recognition*, **1993**; pp i-vi.

58. L.Prodi, M. M., N. Zaccheroni In *Luminescence Applied in Sensor Science*, Topics in Current Chemistry, Springer: 2011.

59. A. Lobnik, M. T., Š. K. Urek, Optical Chemical Sensors:Design and Applications. Wang, W., Ed. **2012**.

60. Markus Sauer, J. H., and Jörg Enderlein, *Handbook of Fluorescence Spectroscopy and Imaging From Single Molecules to Ensembles*. **2011**.

61. Demchenko, A. P., *Introduction to fluorescence sensing*. **2009**.

62. Lakowicz, J. R., *Principles of Fluorescence Spectroscopy*. **2006,**.

63. Levitus, M., Tutorial: measurement of fluorescence spectra and determination of relative fluorescence quantum yields of transparent samples. *Methods Appl Fluoresc* **2020,** *8* (3), 033001.

64. Ishida, H.; Tobita, S.; Hasegawa, Y.; Katoh, R.; Nozaki, K., Recent advances in instrumentation for absolute emission quantum yield measurements. *Coordination Chemistry Reviews* **2010,** *254* (21-22), 2449-2458.

65. Barradas, I.; Ferreira, J. A.; Thomaz, M. F., Intramolecular Heavy-Atom Effect and Intersystem-Crossing in Monohalogenated Pyrenes. *J. Chem. Soc., Faraday Trans. 2* **1973,** *69* (3), 388-394.

66. Valeur, B.; Berberan‐Santos, M. N., *Molecular Fluorescence*. Wiley-VCH: **2012**.

67. McCarroll, M. E.; Shi, Y.; Harris, S.; Puli, S.; Kimaru, I.; Xu, R.; Wang, L.; Dyer, D. J., Computational prediction and experimental evaluation of a photoinduced electron-transfer sensor. *J Phys Chem B* **2006,** *110* (46), 22991-22994.

68. Griesbeck, A. G.; Hoffmann, N.; Warzecha, K. D., Photoinduced-electron-transfer chemistry: from studies on PET processes to applications in natural product synthesis. *Acc Chem Res* **2007,** *40* (2), 128-140.

69. Escudero, D., Revising Intramolecular Photoinduced Electron Transfer (PET) from First-Principles. *Acc Chem Res* **2016,** *49* (9), 1816-1824.

70. Rosspeintner, A.; Kattnig, D. R.; Angulo, G.; Landgraf, S.; Grampp, G., The Rehm-Weller experiment in view of distant electron transfer. *Chemistry* **2008,** *14* (20), 6213-6221.

71. Dekhtyar, M.; Rettig, W.; Weigel, W., Mesomeric and twisted intramolecular-charge-transfer states as a key to polarity-dependent fluorescence of donor-acceptor-substituted aryl pyrenes. *Chem Phys* **2008,** *344* (3), 237-250.

72. Wang, C.; Chi, W.; Qiao, Q.; Tan, D.; Xu, Z.; Liu, X., Twisted intramolecular charge transfer (TICT) and twists beyond TICT: from mechanisms to rational designs of bright and sensitive fluorophores. *Chem Soc Rev* **2021,** *50* (22), 12656-12678.

73. Bigdeli, A.; Ghasemi, F.; Abbasi-Moayed, S.; Shahrajabian, M.; Fahimi-Kashani, N.; Jafarinejad, S.; Farahmand Nejad, M. A.; Hormozi-Nezhad, M. R., Ratiometric fluorescent nanoprobes for visual detection: Design principles and recent advances - A review. *Anal Chim Acta* **2019,** *1079*, 30-58.

74. Jiao, Y.; Zhu, B.; Chen, J.; Duan, X., Fluorescent sensing of fluoride in cellular system. *Theranostics* **2015,** *5* (2), 173-187.

75. Hochreiter, B.; Garcia, A. P.; Schmid, J. A., Fluorescent proteins as genetically encoded FRET biosensors in life sciences. *Sensors (Basel)* **2015,** *15* (10), 26281-26314.

76. Sahoo, H., Forster resonance energy transfer - A spectroscopic nanoruler: Principle and applications. *J Photoch Photobio C* **2011,** *12* (1), 20-30.

77. Syed Arshad Hussain*, D. D., Sekhar Chakraborty, Jaba Saha, Arpan Datta Roy, Santanu Chakraborty, Pintu Debnath, D. Bhattacharj, Fluorescence Resonance Energy Transfer (FRET) sensor. *J. Spectrosc. Dyn.* **2015,** *5: 7*.

78. Fabian, A. I.; Rente, T.; Szollosi, J.; Matyus, L.; Jenei, A., Strength in numbers: effects of acceptor abundance on FRET efficiency. *ChemPhysChem* **2010,** *11* (17), 3713-3721.

79. Bunt, G.; Wouters, F. S., FRET from single to multiplexed signaling events. *Biophys Rev* **2017,** *9* (2), 119-129.

80. Koushik, S. V.; Blank, P. S.; Vogel, S. S., Anomalous surplus energy transfer observed with multiple FRET acceptors. *PLoS One* **2009,** *4* (11), e8031.

81. Lakowicz, J. R., *Principles of fluorescence spectroscopy Third Edition*. **2006**.

82. Li, A. F.; Wang, J. H.; Wang, F.; Jiang, Y. B., Anion complexation and sensing using modified urea and thiourea-based receptors. *Chem Soc Rev* **2010,** *39* (10), 3729-3745.

83. Zheng, Y.; Orbulescu, J.; Ji, X.; Andreopoulos, F. M.; Pham, S. M.; Leblanc, R. M., Development of fluorescent film sensors for the detection of divalent copper. *J Am Chem Soc* **2003,** *125* (9), 2680-2686.

84. Yamakata, A.; Ishibashi, T.-a.; Onishi, H., Effects of Water Addition on the Methanol Oxidation on Pt/TiO_2 Photocatalyst Studied by Time-Resolved Infrared Absorption Spectroscopy. *J. Phys. Chem. B* **2003,** *107* (36), 9820-9823.

85. Burns, A.; Sengupta, P.; Zedayko, T.; Baird, B.; Wiesner, U., Core/Shell fluorescent silica nanoparticles for chemical sensing: towards single-particle laboratories. *Small* **2006,** *2* (6), 723-726.

86. Basabe-Desmonts, L.; Van der Baan, F.; Zimmerman, R. S.; Reinhoudt, D. N.; Crego-Calama, M., Cross-Reactive Sensor Array for Metal Ion Sensing Based on Fluorescent SAMs. *Sensors (Basel)* **2007,** *7* (9), 1731-1746.

87. Jun, B.-H., *Nanotechnology for Bioapplications*. Springer: **2021**.

88. Ding, L.; Fang, Y., Chemically assembled monolayers of fluorophores as chemical sensing materials. *Chem Soc Rev* **2010,** *39* (11), 4258-4273.

89. Herz, E.; Burns, A.; Bonner, D.; Wiesner, U., Large stokes-shift fluorescent silica nanoparticles with enhanced emission over free dye for single excitation multiplexing. *Macromol Rapid Commun* **2009,** *30* (22), 1907-1910.

90. Akhter, F.; Rao, A. A.; Abbasi, M. N.; Wahocho, S. A.; Mallah, M. A.; Anees-ur-Rehman, H.; Chandio, Z. A., A Comprehensive Review of Synthesis, Applications and Future Prospects for Silica Nanoparticles (SNPs). *Silicon* **2022,** *14* (14), 8295-8310.

91. Wang, L.; Wang, K.; Santra, S.; Zhao, X.; Hilliard, L. R.; Smith, J. E.; Wu, Y.; Tan, W., Watching Silica Nanoparticles Glow in the Biological World. *Anal Chem* **2006,** *78* (3), 646-654.

92. Wasserman, S. R.; Tao, Y. T.; Whitesides, G. M., Structure and Reactivity of Alkylsiloxane Monolayers Formed by Reaction of Alkyltrichlorosilanes on Silicon Substrates. *Langmuir* **1989,** *5* (4), 1074-1087.

93. Ulman, A., Formation and Structure of Self-Assembled Monolayers. *Chem Rev* **1996,** *96* (4), 1533-1554.

94. Gun, J.; Sagiv, J., On the formation and structure of self-assembling monolayers. *Journal of Colloid and Interface Science* **1986,** *112* (2), 457-472.

95. de Silva, A. P.; Eilers, J.; Zlokarnik, G., Emerging fluorescence sensing technologies: from photophysical principles to cellular applications. *Proc Natl Acad Sci U S A* **1999,** *96* (15), 8336-8337.

96. Combellas, C.; Kanoufi, F.; Pinson, J.; Podvorica, F. I., Sterically hindered diazonium salts for the grafting of a monolayer on metals. *J Am Chem Soc* **2008,** *130* (27), 8576-8577.

97. Wang, L.; Zhao, W. J.; Tan, W. H., Bioconjugated Silica Nanoparticles: Development and Applications. *Nano Res* **2008,** *1* (2), 99-115.

98. Shin, S. K.; Yoon, H. J.; Jung, Y. J.; Park, J. W., Nanoscale controlled self-assembled monolayers and quantum dots. *Curr Opin Chem Biol* **2006,** *10* (5), 423-429.

99. Adamkiewicz, M. Self-assembled monolayers on silicon: deposition and surface chemistry. University of St Andrews, **2013**.

100. Zhang, Y.; Tamijani, A. A.; Taylor, M. E.; Zhi, B.; Haynes, C. L.; Mason, S. E.; Hamers, R. J., Molecular Surface Functionalization of Carbon Materials via Radical-Induced Grafting of Terminal Alkenes. *J Am Chem Soc* **2019,** *141* (20), 8277-8288.

101. Li, W.; Xu, Y.; Zhou, Y.; Ma, W.; Wang, S.; Dai, Y., Silica nanoparticles functionalized via click chemistry and ATRP for enrichment of Pb(II) ion. *Nanoscale Res Lett* **2012,** *7* (1), 485.

102. Zhu, M.; Lerum, M. Z.; Chen, W., How to prepare reproducible, homogeneous, and hydrolytically stable aminosilane-derived layers on silica. *Langmuir* **2012,** *28* (1), 416-423.

103. Gooding, J. J.; Ciampi, S., The molecular level modification of surfaces: from self-assembled monolayers to complex molecular assemblies. *Chem Soc Rev* **2011,** *40* (5), 2704-2718.

104. Barness, Y.; Gershevitz, O.; Sekar, M.; Sukenik, C. N., Functionalized silanes for the preparation of siloxane-anchored monolayers. *Langmuir* **2000,** *16* (1), 247-251.

105. Herzer, N.; Haensch, C.; Hoeppener, S.; Schubert, U. S., Orthogonal functionalization of silicon substrates using self-assembled monolayers. *Langmuir* **2010,** *26* (11), 8358-8365.

106. Tian, R.; Seitz, O.; Li, M.; Hu, W. W.; Chabal, Y. J.; Gao, J., Infrared characterization of interfacial Si-O bond formation on silanized flat SiO_2/Si surfaces. *Langmuir* **2010,** *26* (7), 4563-4566.

107. Ito, Y.; Virkar, A. A.; Mannsfeld, S.; Oh, J. H.; Toney, M.; Locklin, J.; Bao, Z., Crystalline ultrasmooth self-assembled monolayers of alkylsilanes for organic field-effect transistors. *J Am Chem Soc* **2009,** *131* (26), 9396-9404.

108. Smith E, C. W., How to prevent the loss of surface functionality derived from aminosilanes. *Langmuir.* **2008,** *24(21)*, 12405–12409.

109. Bierbaum, K.; Kinzler, M.; Woll, C.; Grunze, M.; Hahner, G.; Heid, S.; Effenberger, F., A near-Edge X-Ray-Absorption Fine Structure Spectroscopy and X-Ray Photoelectron-Spectroscopy Study of the Film Properties of Self-Assembled Monolayers of Organosilanes on Oxidized Si(100). *Langmuir* **1995,** *11* (2), 512-518.

110. Hozumi, A.; Yokogawa, Y.; Kameyama, T.; Sugimura, H.; Hayashi, K.; Shirayama, H.; Takai, O., Amino-terminated self-assembled monolayer on a SiO_2 surface formed by chemical vapor deposition. *J Vac Sci Technol A* **2001,** *19* (4), 1812-1816.

111. Gubala, V.; Giovannini, G.; Kunc, F.; Monopoli, M. P.; Moore, C. J., Dye-doped silica nanoparticles: synthesis, surface chemistry and bioapplications. *Cancer Nanotechnol* **2020,** *11* (1).

112. Xiang, S.; Xing, G.; Xue, W.; Lu, C.; Lin, J. M., Comparison of two different deposition methods of 3-aminopropyltriethoxysilane on glass slides and their application in the ThinPrep cytologic test. *Analyst* **2012,** *137* (7), 1669-1673.

113. Santra, S.; Wang, K.; Tapec, R.; Tan, W., Development of novel dye-doped silica nanoparticles for biomarker application. *J Biomed Opt* **2001,** *6* (2), 160-166.

114. Dhir, A.; Datta, A., FRET on Surface of Silica Nanoparticle: Effect of Chromophore Concentration on Dynamics and Efficiency. *Journal of Physical Chemistry C* **2016,** *120* (36), 20125-20131.

115. James, T. D.; Phillips, M. D.; Shinkai, S., The Molecular Recognition of Saccharides. Complexation of Boronic Acids with Saccharides. Fluorescent Sensors. Modular Fluorescent Sensors. Other Types of Sensor. Other Systems for Saccharide Recognition. In *Boronic Acids in Saccharide Recognition*, **2007**; pp 3-176.

116. Wu, X.; Li, Z.; Chen, X. X.; Fossey, J. S.; James, T. D.; Jiang, Y. B., Selective sensing of saccharides using simple boronic acids and their aggregates. *Chem Soc Rev* **2013,** *42* (20), 8032-8048.

117. Arimori, S.; Bosch, L. I.; Ward, C. J.; James, T. D., Fluorescent internal charge transfer (ICT) saccharide sensor. *Tetrahedron Lett* **2001,** *42* (27), 4553-4555.

118. Yoon, J.; Czarnik, A. W., Fluorescent Chemosensors of Carbohydrates - a Means of Chemically Communicating the Binding of Polyols in Water Based on Chelation-Enhanced Quenching. *Journal of the American Chemical Society* **1992,** *114* (14), 5874-5875.

119. DiCesare, N.; Lakowicz, J. R., Charge transfer fluorescent probes using boronic acids for monosaccharide signaling. *J Biomed Opt* **2002,** *7* (4), 538-545.

120. Bosch, L. I.; Mahon, M. F.; James, T. D., The B-N bond controls the balance between locally excited (LE) and twisted internal charge transfer (TICT) states observed for aniline based fluorescent saccharide sensors. *Tetrahedron Lett* **2004,** *45* (13), 2859-2862.

121. James, T. D.; Sandanayake, K. R. A. S.; Shinkai, S., Novel Photoinduced Electron-Transfer Sensor for Saccharides Based on the Interaction of Boronic Acid and Amine. *J Chem Soc Chem Comm* **1994,** (4), 477-478.

122. Franzen, S.; Ni, W. J.; Wang, B. H., Study of the mechanism of electron-transfer quenching by boron-nitrogen adducts in fluorescent sensors. *J Phys Chem B* **2003,** *107* (47), 12942-12948.

123. Ni, W.; Kaur, G.; Springsteen, G.; Wang, B.; Franzen, S., Regulating the fluorescence intensity of an anthracene boronic acid system: a B-N bond or a hydrolysis mechanism? *Bioorg Chem* **2004,** *32* (6), 571-581.

124. Chapin, B. M.; Metola, P.; Vankayala, S. L.; Woodcock, H. L.; Mooibroek, T. J.; Lynch, V. M.; Larkin, J. D.; Anslyn, E. V., Disaggregation is a Mechanism for Emission Turn-On of ortho-Aminomethylphenylboronic Acid-Based Saccharide Sensors. *J Am Chem Soc* **2017,** *139* (15), 5568-5578.

125. Sun, X.; James, T. D.; Anslyn, E. V., Arresting "Loose Bolt" Internal Conversion from -B(OH)2 Groups is the Mechanism for Emission Turn-On in ortho-Aminomethylphenylboronic Acid-Based Saccharide Sensors. *J Am Chem Soc* **2018,** *140* (6), 2348-2354.

126. Cao, H.; Diaz, D. I.; DiCesare, N.; Lakowicz, J. R.; Heagy, M. D., Monoboronic acid sensor that displays anomalous fluorescence sensitivity to glucose. *Org Lett* **2002,** *4* (9), 1503-1505.

127. Liu, S. S.; Bai, H. Y.; Sun, Q.; Zhang, W. B.; Qian, J. H., Naphthalimide-based fluorescent photoinduced electron transfer sensors for saccharides. *RSC Advances* **2015,** *5* (4), 2837-2843.

128. Xiao, Y.; Qian, X. H., Novel highly efficient fluoroionophores with a peri-effect and strong electron-donating receptors: TICT-promoted PET and signaling response to transition metal cations with low background emission. *Tetrahedron Lett* **2003,** *44* (10), 2087-2091.

129. Bielecki, M.; Eggert, H.; Norrild, J. C., A fluorescent glucose sensor binding covalently to all five hydroxy groups of α-D-glucofuranose. A reinvestigation. *J. Chem. Soc., Perkin Trans. 2* **1999,** (3), 449-456.

130. Sandanayake, K. R. A. S.; James, T. D.; Shinkai, S., Two Dimensional Photoinduced Electron Transfer (PET) Fluorescence Sensor for Saccharides. *Chemistry Letters* **1995,** *24* (7), 503-504.

131. Arimori, S.; Frimat, K. A.; James, T. D.; Bell, M. L.; Oh, C. S., Modular fluorescence sensors for saccharides. *Chem. Commun* **2001,** (18), 1836-1837.

132. Arimori, S.; Bell, M. L.; Oh, C. S.; James, T. D., A modular fluorescence intramolecular energy transfer saccharide sensor. *Org Lett* **2002,** *4* (24), 4249-4251.

133. Chaicham, A.; Sahasithiwat, S.; Tuntulani, T.; Tomapatanaget, B., Highly effective discrimination of catecholamine derivatives via FRET-on/off processes induced by the intermolecular assembly with two fluorescence sensors. *Chem Commun* **2013,** *49* (81), 9287-9289.

134. Aung, Y. Y.; Kristanti, A. N.; Lee, H. V.; Fahmi, M. Z., Boronic-Acid-Modified Nanomaterials for Biomedical Applications. *ACS Omega* **2021,** *6* (28), 17750-17765.

135. Yum, K.; Ahn, J. H.; McNicholas, T. P.; Barone, P. W.; Mu, B.; Kim, J. H.; Jain, R. M.; Strano, M. S., Boronic acid library for selective, reversible near-infrared fluorescence

quenching of surfactant suspended single-walled carbon nanotubes in response to glucose. *ACS Nano* **2012,** *6* (1), 819-830.

136. Wang, Y.; Kotsuchibashi, Y.; Uto, K.; Ebara, M.; Aoyagi, T.; Liu, Y.; Narain, R., pH and glucose responsive nanofibers for the reversible capture and release of lectins. *Biomater Sci* **2015,** *3* (1), 152-162.

137. Gaur, M.; Misra, C.; Yadav, A. B.; Swaroop, S.; Maolmhuaidh, F. O.; Bechelany, M.; Barhoum, A., Biomedical Applications of Carbon Nanomaterials: Fullerenes, Quantum Dots, Nanotubes, Nanofibers, and Graphene. *Materials (Basel)* **2021,** *14* (20).

138. Hu, L.; Shu, T.; Wan, Y.; Fang, C.; Gao, F.; Serpe, M. J., Recent advances in stimuli-responsive polymers for sensing and actuation. *Mol. Syst. Des. Eng* **2021,** *6* (2), 108-121.

139. Cho, S.; Hwang, S. Y.; Oh, D. X.; Park, J., Recent progress in self-healing polymers and hydrogels based on reversible dynamic B–O bonds: boronic/boronate esters, borax, and benzoxaborole. *J. Mater. Chem. A* **2021,** *9* (26), 14630-14655.

140. Guan, Y.; Zhang, Y., Boronic acid-containing hydrogels: synthesis and their applications. *Chem Soc Rev* **2013,** *42* (20), 8106-8121.

141. Wei, J. R.; Ni, Y. L.; Zhang, W.; Zhang, Z. Q.; Zhang, J., Detection of glycoprotein through fluorescent boronic acid-based molecularly imprinted polymer. *Anal Chim Acta* **2017,** *960*, 110-116.

142. Lee, J.; Ko, J. H.; Mansfield, K. M.; Nauka, P. C.; Bat, E.; Maynard, H. D., Glucose-Responsive Trehalose Hydrogel for Insulin Stabilization and Delivery. *Macromol Biosci* **2018,** *18* (5), e1700372.

143. Zhang, S.; Cai, Y.; He, H.; Zhang, Y.; Liu, R.; Cao, H.; Wang, M.; Liu, J.; Zhang, G.; Li, Y.; Liu, H.; Li, B., Heteroatom doped graphdiyne as efficient metal-free electrocatalyst for oxygen reduction reaction in alkaline medium. *Journal of Materials Chemistry A* **2016,** *4* (13), 4738-4744.

144. Hsiao, H. Y.; Chen, M. L.; Wu, H. T.; Huang, L. D.; Chien, W. T.; Yu, C. C.; Jan, F. D.; Sahabuddin, S.; Chang, T. C.; Lin, C. C., Fabrication of carbohydrate microarrays through boronate formation. *Chem Commun (Camb)* **2011,** *47* (4), 1187-1189.

145. D'Hooge, F.; Elfeky, S. A.; Flower, S. E.; Pascu, S. I.; Jenkins, A. T. A.; van den Elsen, J. M. H.; James, T. D.; Fossey, J. S., Biotinylated boronic acid fluorophore conjugates: Quencher elimination strategy for imaging and saccharide detection. *Rsc Advances* **2012,** *2* (8), 3274-3280.

146. Qiao, Z. C.; Chen, Z. Y.; Zhang, S.; Cui, Z. P.; Xu, Z. R.; Zhang, W. B.; Qian, J. H., Naphthalimide-based fluorescent nanoprobes for the detection of saccharides. *New J Chem* **2018,** *42* (20), 16428-16435.

147. A. S. Spirin, L. P. G., Molecular Biology, Biochemistry, and Biophysics. In *Acta geneticae medicae et gemellologiae*, G. F. Springer, H. G. W., Ed. **2014**; Vol. 4, pp 116-117.

148. Crouch, S. D. H. F., *Principles of Instrumental Analysis*. Brooks Cole: **1980**.

149. V.S. Ramachandran, J. J. B., *Handbook of Analytical Techniques in Concrete Science and Technology*. William Andrew: **2001**.

150. Philip R. Bunker, P. J., *Molecular Symmetry and Spectroscopy*. Nrc Pubns: **1998**.

151. Peter Griffiths, J. A. D. H., *Fourier Transform Infrared Spectrometry*. Wiley-Interscience: **2007**.

152. Reynolds, W. F., Spectroscopic Methods in Organic Chemistry *J. Nat. Prod* **1998,** *61* (8), 1072-1073.

153. Wang, L.; Markley, J. L., Empirical correlation between protein backbone 15N and 13C secondary chemical shifts and its application to nitrogen chemical shift re-referencing. *J Biomol NMR* **2009,** *44* (2), 95-99.

154. Downard, K., *Mass Spectrometry : A Foundation Course*. Royal Society of Chemistry: **2004**; p X001-X004.

155. Fenn, J. B.; Mann, M.; Meng, C. K.; Wong, S. F.; Whitehouse, C. M., Electrospray ionization for mass spectrometry of large biomolecules. *Science* **1989,** *246* (4926), 64-71.

156. Harris, G. A.; Galhena, A. S.; Fernandez, F. M., Ambient sampling/ionization mass spectrometry: applications and current trends. *Anal Chem* **2011,** *83* (12), 4508-4538.

157. H J. Sherman and B.Fried, E., *Handbook of Thin-Layer Chromatography*. CRC Press: **1991.**

158. Lawrence, K.; Flower, S. E.; Kociok-Kohn, G.; Frost, C. G.; James, T. D., A simple and effective colorimetric technique for the detection of boronic acids and their derivatives. *Anal Methods-Uk* **2012,** *4* (8), 2215-2217.

159. Malviya R, B. V., Pal O.P. and Sharma P.K, High performance liquid chromatography: a short review. *Journal of Global Pharma Technology* **2010,** *2(5)*, 22-26.

160. Patel, K. N.; Patel, J. K.; Patel, M. P.; Rajput, G. C.; Patel, H. A., Introduction to hyphenated techniques and their applications in pharmacy. *Pharm Methods* **2010,** *1* (1), 2-13.

161. Pitt, J. J., Principles and Applications of Liquid Chromatography- Mass Spectrometry in Clinical BiochemistryJames. *Clin Biochem Rev* **2009,** *Vol 30*.

162. Sanogo, S.; Silimbani, P.; Gaggeri, R.; Masini, C., Development and validation of an HPLC-DAD method for the simultaneous identification and quantification of Topotecan, Irinotecan, Etoposide, Doxorubicin and Epirubicin. *Arabian Journal of Chemistry* **2021,** *14* (1).

163. Wang, S.; Jiang, L., Definition of superhydrophobic states. *Adv Mater* **2007,** *19* (21), 3423-3424.

164. A. Ulman, *An Introduction to Ultrathin Organic Films from Langmuir-Blodgett to Self-Assembly*. Academic Press: **1991**.

165. R. Förch, H. S., A. Tobias A. Jenkins, *Surface Design: Applications in Bioscience and Nanotechnology*. Wiley-VCH: **2009**.

166. Bass, M., *Handbook of Optics: Fundamentals, techniques, and design*. McGraw-Hill Professional: **1994**; p 1664.

167. Tompkins, H., *HANDBOOK OF ELLIPSOMETRY*. William Andrew: **2005**.

168. Pecora, R., *Dynamic Light Scattering: Applications of Photon Correlation Spectroscopy*. **1985**.

169. McNeil, S. E., *Characterization of Nanoparticles Intended for Drug Delivery*. Scott E. McNeil: **2011**.

170. Danaei, M.; Kalantari, M.; Raji, M.; Samareh Fekri, H.; Saber, R.; Asnani, G. P.; Mortazavi, S. M.; Mozafari, M. R.; Rasti, B.; Taheriazam, A., Probing nanoliposomes using single particle analytical techniques: effect of excipients, solvents, phase transition and zeta potential. *Heliyon* **2018,** *4* (12), e01088.

171. Menczel, J. D.; Prime, R. B., *Thermal analysis of polymers: Fundamentals and applications*. Wiley: **2009**; p 704.

172. Karaku, S. E., An anthracene based fluorescent probe for the selective and sensitive detection of Chromium (III) ions in an aqueous medium and its practical application. *Turk J Chem* **2020,** *44* (4), 941-949.

173. James, T. D.; Sandanayake, K. R. A. S.; Shinkai, S., Novel photoinduced electron-transfer sensor for saccharides based on the interaction of boronic acid and amine. *J. Chem. Soc., Chem. Commun.* **1994,** (4), 477-478.

174. Luvino, D.; Smietana, M.; Vasseur, J. J., Selective fluorescence-based detection of dihydrouridine with boronic acids. *Tetrahedron Lett* **2006,** *47* (52), 9253-9256.

175. Haldon, E.; Nicasio, M. C.; Perez, P. J., Copper-catalysed azide-alkyne cycloadditions (CuAAC): an update. *Org Biomol Chem* **2015,** *13* (37), 9528-9550.

176. Ulatowski, F.; Melaniuk, K., 1-(Methylamino)anthracene - An Accessible Building Block for Photoresponsive Compounds. *Eur J Org Chem* **2018,** *2018* (47), 6629-6633.

177. Förster, T., Excimers. *Angew. Chem. internat* **1969,** *8* (5), 333-343.

178. Pownall, H. J.; Smith, L. C., Fluorescence quenching of anthracene in charged micelles by pyridinium and iodide ions. *Biochemistry* **1974,** *13* (12), 2594-2597.

179. Barry, N. P. E.; Therrien, B., Pyrene: The Guest of Honor. In *Organic Nanoreactors*, **2016**; pp 421-461.

180. Schwarz, F. P.; Wasik, S. P., Fluorescence measurements of benzene, naphthalene, anthracene, pyrene, fluoranthene, and benzo(e)pyrene in water. *Anal Chem* **1976,** *48* (3), 524-528.

181. Hossain, M. A.; Mihara, H.; Ueno, A., Novel peptides bearing pyrene and coumarin units with or without beta-cyclodextrin in their side chains exhibit intramolecular fluorescence resonance energy transfer. *J Am Chem Soc* **2003,** *125* (37), 11178-11179.

182. Lee, Y. O.; Lee, J. Y.; Quang, D. T.; Lee, M. H.; Kim, J. S., Pyrene-coumarin based calix fluorophore emitting exciplex. *B Korean Chem Soc* **2006,** *27* (9), 1469-1472.

183. Suresh, M.; Mandal, A. K.; Suresh, E.; Das, A., First demonstration of two-step FRET in a synthetic supramolecular assembly. *Chem. Sci* **2013,** *4* (6), 2380–2386.

184. Akhter, F.; Rao, A. A.; Abbasi, M. N.; Wahocho, S. A.; Mallah, M. A.; Anees-ur-Rehman, H.; Chandio, Z. A., A Comprehensive Review of Synthesis, Applications and Future Prospects for Silica Nanoparticles (SNPs). *Silicon* **2022**.

185. Larkin, J. D.; Frimat, K. A.; Fyles, T. M.; Flower, S. E.; James, T. D., Boronic acid based photoinduced electron transfer (PET) fluorescence sensors for saccharides. *New J Chem* **2010,** *34* (12).

186. Fatima, S.; Mansha, A.; Asim, S.; Shahzad, A., Absorption spectra of coumarin and its derivatives. *Chemical Papers* **2022,** *76* (2), 627-638.

187. Suenaga, H.; Mikami, M.; Sandanayake, K. R. A. S.; Shinkai, S., Screening of fluorescent boronic acids for sugar sensing which show a large fluorescence change. *Tetrahedron Lett* **1995,** *36* (27), 4825-4828.

188. Stefansson, S.; Stefansson, L. A.; Chung, S.-w.; Ko, K.; Kwon, H. H.; Ahn, S. N., Evaluation of Aromatic Boronic Acids as Ligands for Measuring Diabetes Markers on Carbon Nanotube Field-Effect Transistors. *Journal of Nanotechnology* **2012,** *20121*, 1-6.

189. Huang, C.; Hao, Z.; Qi, T. X.; Pan, Y. L.; Zhao, X. Z., An integrated flexible and reusable graphene field effect transistor nanosensor for monitoring glucose. *Journal of Materiomics* **2020,** *6* (2), 308-314.

190. Shirbhate, M. E.; Kwon, S.; Song, A.; Kim, S.; Kim, D.; Huang, H.; Kim, Y.; Lee, H.; Kim, S. J.; Baik, M. H.; Yoon, J.; Kim, K. M., Optical and Fluorescent Dual Sensing of Aminoalcohols by in Situ Generation of BODIPY-like Chromophore. *J Am Chem Soc* **2020,** *142* (11), 4975-4979.

191. Low, D. W.; Pattison, G.; Wieczysty, M. D.; Churchill, G. H.; Lam, H. W., Enantioselective Rh(I)-catalyzed cyclization of arylboron compounds onto ketones. *Org Lett* **2012,** *14* (10), 2548-2551.

192. Friedman, M., Applications of the ninhydrin reaction for analysis of amino acids, peptides, and proteins to agricultural and biomedical sciences. *J Agric Food Chem* **2004,** *52* (3), 385-406.

193. Ondrisek, P.; Elie, M.; Pupier, M.; de Aguirre, A.; Poblador-Bahamonde, A. I.; Besnard, C.; Lacour, J., Acetylene Derivatives of Cationic Diazaoxatriangulenes and Diaza [4]Helicenes - Access to Red Emitters and Planar Chiral Stereochemical Traits. *Chemistry* **2022,** *28* (15), e202104405.

194. Kim, S. H.; Ryu, J. H.; Choi, H. J.; Kim, H. S., Electrochromic properties of new fluorophores containing triphenylamine moiety. *Dyes and Pigments* **2005,** *64* (3), 279-281.

195. Lei, Y. L.; Niu, Q. L.; Mi, H. Y.; Wang, Y. L.; Nurulla, I.; Shi, W., Carbazole-based conjugated polymer with tethered acetylene groups: Synthesis and characterization. *Dyes and Pigments* **2013,** *96* (1), 138-147.

196. Kim, K. W.; Kwon, S. H.; Lee, B. J.; Ahn, S. O.; Lee, J. H.; Choi, J. H., Synthesis and photophysical properties of fluorescent dyes based on triphenylamine, diphenylamine, diphenyl sulfone or triphenyltriazine derivatives containing an acetylene linkage group. *Dyes and Pigments* **2020,** *181*, 108617.

197. Fang, Q.; Xu, B.; Jiang, B.; Fu, H. T.; Zhu, W. Q.; Jiang, X. Y.; Zhang, Z. L., A novel fluorene derivative containing four triphenylamine groups: Highly thermostable blue emitter with hole-transporting ability for organic light-emitting diode (OLED). *Synthetic Metals* **2005,** *155* (1), 206-210.

198. Petreto, A.; Dos Santos, M. C.; Lefebvre, O.; Dos Santos, G. R.; Ponzellini, P.; Garoli, D.; De Angelis, F.; Ammar, M.; Hildebrandt, N., Optimizing FRET on Aluminum Surfaces via Controlled Attachment of Fluorescent Dyes. *Acs Omega* **2018,** *3* (12), 18867-18876.

199. Gayrard, C.; Borghi, N., FRET-based Molecular Tension Microscopy. *Methods* **2016,** *94*, 33-42.

200. Keller, S.; Yi, C.; Li, C.; Liu, S. X.; Blum, C.; Frei, G.; Sereda, O.; Neels, A.; Wandlowski, T.; Decurtins, S., Synthesis, structures, redox and photophysical properties of benzodifuran-functionalised pyrene and anthracene fluorophores. *Org Biomol Chem* **2011,** *9* (18), 6410-6416.

201. Voronin, V. V.; Ledovskaya, M. S.; Bogachenkov, A. S.; Rodygin, K. S.; Ananikov, V. P., Acetylene in Organic Synthesis: Recent Progress and New Uses. *Molecules* **2018,** *23* (10).

202. Aguilar-Martínez, M.; Antonio Bautista-Martínez, J.; Rivera, E., Thermal, Optical, Electrochemical Properties and Conductivity of Pyrene Monomers. *Designed Monomers and Polymers* **2012,** *11* (2), 173-186.

203. Talele, T. T., Acetylene Group, Friend or Foe in Medicinal Chemistry. *J Med Chem* **2020,** *63* (11), 5625-5663.

204. Shah, A.; Shah, A. H.; Parveen, N.; Rehman, Z. U.; Khan, S. Z.; Rana, U. A.; Khan, S. U. D.; Nisar, J.; Lashin, A.; Qureshi, R., Synthesis and electrochemical investigations of piperazines. *Electrochim Acta* **2016,** *220*, 705-711.

205. Montejano, H. A.; Cosa, J. J.; Garrera, H. A.; Previtali, C. M., Solvent Effects on the Photoinduced Electron-Transfer Reaction between Excited Singlet Pyrene and Indole. *J Photoch Photobio A* **1995,** *86* (1-3), 115-120.

206. Zweig, A.; Maurer, A. H.; Roberts, B. G., Oxidation Reduction and Electrochemiluminescence of Donor-Substituted Polycyclic Aromatic Hydrocarbons. *J Org Chem* **1967,** *32* (5), 1322-1329.

207. M. Montalti, A. C., L Prodi, M. T. Gandolfi, Photophysics of Organic Molecules in Solution. In *Handbook of photochemistry*, Dekker, M., Ed. **2006**; p 48.

208. Hatanaka, Y.; Hiyama, T., Cross-coupling of organosilanes with organic halides mediated by a palladium catalyst and tris(diethylamino)sulfonium difluorotrimethylsilicate. *J. Org. Chem* **2002,** *53* (4), 918-920.

209. George, N.; Ofori, S.; Parkin, S.; Awuah, S. G., Mild deprotection of the N-tert-butyloxycarbonyl (N-Boc) group using oxalyl chloride. *RSC Adv* **2020,** *10* (40), 24017-24026.

210. Ashworth, I. W.; Cox, B. G.; Meyrick, B., Kinetics and mechanism of N-Boc cleavage: evidence of a second-order dependence upon acid concentration. *J Org Chem* **2010,** *75* (23), 8117-8125.

211. Benfodda, Z.; Fritz, V.; Henriquet, C.; Fattorusso, C.; Torrejon, G. C.; Persico, M.; Dato, A. D.; Menna, M.; Blancou, H.; Fajas, L., Synthesis, Anticancer Activity and Computational SAR Analysis of Acylsulfonylpiperazines Derivatives. *Medicinal Chemistry* **2017,** *07* (09), 257-267.

212. Chen, Z. W.; Luo, M. T.; Ye, D. N., TFA-Mediated Alkyne Hydration Reaction to Synthesize Methyl Ketones. *Asian J. Chem* **2014,** *26* (19), 6528-6530.

213. Khalili, F.; Henni, A.; East, A. L. L., pKaValues of Some Piperazines at (298, 303, 313, and 323) K. *J. Chem. Eng* **2009,** *54* (10), 2914-2917.

214. Routier, S.; Saugé, L.; Ayerbe, N.; Coudert, G.; Mérour, J.-Y., A mild and selective method for N-Boc deprotection. *Tetrahedron Lett* **2002,** *43* (4), 589-591.

215. Choy, J.; Jaime-Figueroa, S.; Jiang, L.; Wagner, P., Novel Practical Deprotection of N-Boc Compounds Using Fluorinated Alcohols. *Synthetic Commun* **2008,** *38* (21), 3840-3853.

216. Repine, J. T.; Johnson, D. S.; White, A. D.; Favor, D. A.; Stier, M. A.; Yip, J.; Rankin, T.; Ding, Q.; Maiti, S. N., Synthesis of monofluorinated 1-(naphthalen-1-yl)piperazines. *Tetrahedron Lett* **2007,** *48* (31), 5539-5541.

217. Han, G.; Tamaki, M.; Hruby, V. J., Fast, efficient and selective deprotection of the tert-butoxycarbonyl (Boc) group using HCl/dioxane (4 m). *J Pept Res* **2001,** *58* (4), 338-341.

218. Hall, D. G., *Boronic Acids Preparations, applications in organuc synthesis and medicine*. Wiley VCH: **2005**; p 571.

219. Nudelman, A.; Bechor, Y.; Falb, E.; Fischer, B.; Wexler, B. A.; Nudelman, A., Acetyl Chloride-Methanol as a Convenient Reagent for: A) Quantitative Formation of Amine Hydrochlorides B) Carboxylate Ester Formation C) Mild Removal of N-t-Boc-Protective Group. *Synthetic Commun* **1998,** *28* (3), 471-474.

220. Fischer, F. C.; Havinga, E., Thermal and photoinduced deboronations of some pyridine- and benzeneboronate anions. *Recueil des Travaux Chimiques des Pays-Bas* **2010,** *93* (1), 21-24.

221. Sun, J.; Perfetti, M. T.; Santos, W. L., A method for the deprotection of alkylpinacolyl boronate esters. *J Org Chem* **2011,** *76* (9), 3571-3575.

222. Hinkes, S. P. A.; Klein, C. D. P., Virtues of Volatility: A Facile Transesterification Approach to Boronic Acids. *Org Lett* **2019,** *21* (9), 3048-3052.

223. Dowlut, M.; Hall, D. G., An improved class of sugar-binding boronic acids, soluble and capable of complexing glycosides in neutral water. *J Am Chem Soc* **2006,** *128* (13), 4226-4227.

224. Seraj, S.; Rouhani, S.; Faridbod, F., Naphthalimide-based optical turn-on sensor for monosaccharide recognition using boronic acid receptor. *RSC Adv* **2019,** *9* (31), 17933-17940.

225. Xiang, D. S.; Zhou, G. H.; Luo, M.; Ji, X. H.; He, Z. K., Dual color fluorescence quantitative detection of specific single-stranded DNA with molecular beacons and nucleic acid dye SYBR Green I. *Analyst* **2012,** *137* (16), 3787-3793.

226. James, T. D.; Sandanayake, K. R. A. S.; Shinkai, S., Novel Photoinduced Electron-Transfer Sensor for Saccharides Based on the Interaction of Boronic Acid and Amine. *J. Am. Chem. Soc* **1994,** (117), 8982-8987.

227. Demchenko, A. P., *Introduction to Fluorescence Sensing*. Springer Cham: **2015**.

228. Zhai, J.; Pan, T.; Zhu, J.; Xu, Y.; Chen, J.; Xie, Y.; Qin, Y., Boronic acid functionalized boron dipyrromethene fluorescent probes: preparation, characterization, and saccharides sensing applications. *Anal Chem* **2012,** *84* (23), 10214-10220.

229. Cheng, Y.; Ni, N.; Yang, W.; Wang, B., A new class of fluorescent boronic acids that have extraordinarily high affinities for diols in aqueous solution at physiological pH. *Chemistry* **2010,** *16* (45), 13528-13538.

230. D. Kuntz, J., F. P. Gasparro, M. D. Johnston, Jr., and R. P. Taylor, Molecular Interactions and the Benesi-Hildebrand Equation. *J. Am. Chem. Soc* **1968,** *90* (18), 4778–4781

231. Poor, M.; Zand, A.; Szente, L.; Lemli, B.; Kunsagi-Mate, S., Interaction of alpha- and beta-zearalenols with beta-cyclodextrins. *Molecules* **2017,** *22* (11).

232. Trupp, S.; Schweitzer, A.; Mohr, G. J., A fluorescent water-soluble naphthalimide-based receptor for saccharides with highest sensitivity in the physiological pH range. *Org Biomol Chem* **2006,** *4* (15), 2965-2968.

233. Kandi, D.; Mansingh, S.; Behera, A.; Parida, K., Calculation of relative fluorescence quantum yield and Urbach energy of colloidal CdS QDs in various easily accessible solvents. *Journal of Luminescence* **2021,** *231*, 117792.

234. Jones, G.; Jackson, W. R.; Choi, C. Y.; Bergmark, W. R., Solvent effects on emission yield and lifetime for coumarin laser dyes. Requirements for a rotatory decay mechanism. *J. Phys. Chem* **1985,** *89* (2), 294-300.

235. Lemmens, A. K.; Rap, D. B.; Thunnissen, J. M. M.; Willemsen, B.; Rijs, A. M., Polycyclic aromatic hydrocarbon formation chemistry in a plasma jet revealed by IR-UV action spectroscopy. *Nat Commun* **2020,** *11* (1), 269.

236. Hebestreit, M.-L.; Henrichs, C.; Schäfer, J.; Martini, J.; Auerswald, J.; Fischer, I.; Krueger, A.; Schmitt, M., Structural changes of 1-(phenylethynyl)naphthalene upon electronic excitation from Franck–Condon fits of several fluorescence emission spectra. *Journal of Molecular Structure* **2022,** *1250*.

237. Carpentier, Y.; Pino, T.; Brechignac, P., R2PI spectroscopy of aromatic molecules produced in an ethylene-rich flame. *J Phys Chem A* **2013,** *117* (39), 10092-10104.

238. Judkins, E. C.; Zeller, M.; Ren, T., Synthesis and Characterizations of Macrocyclic Cr(III) and Co(III) 1-Ethynyl Naphthalene and 9-Ethynyl Anthracene Complexes: An Investigation of Structural and Spectroscopic Properties. *Inorg Chem* **2018,** *57* (4), 2249-2259.

239. Vega, B.; Wondraczek, H.; Bretschneider, L.; Nareoja, T.; Fardim, P.; Heinze, T., Preparation of reactive fibre interfaces using multifunctional cellulose derivatives. *Carbohydr Polym* **2015,** *132*, 261-273.

240. Masuko, M.; Ohuchi, S.; Sode, K.; Ohtani, H.; Shimadzu, A., Fluorescence resonance energy transfer from pyrene to perylene labels for nucleic acid hybridization assays under homogeneous solution conditions. *Nucleic Acids Res* **2000,** *28* (8), E34.

241. Saha, J.; Dey, D.; Roy, A. D.; Bhattacharjee, D.; Hussain, S. A., Multi step FRET among three laser dyes Pyrene, Acriflavine and Rhodamine B. *Journal of Luminescence* **2016,** *172*, 168-174.

242. Sahana, A.; Banerjee, A.; Lohar, S.; Banik, A.; Mukhopadhyay, S. K.; Safin, D. A.; Babashkina, M. G.; Bolte, M.; Garcia, Y.; Das, D., FRET based tri-color emissive rhodamine-pyrene conjugate as an Al3+ selective colorimetric and fluorescence sensor for living cell imaging. *Dalton Trans* **2013,** *42* (37), 13311-13314.

243. Kashida, H.; Takatsu, T.; Sekiguchi, K.; Asanuma, H., An efficient fluorescence resonance energy transfer (FRET) between pyrene and perylene assembled in a DNA duplex and its potential for discriminating single-base changes. *Chemistry* **2010,** *16* (8), 2479-2486.

244. Batsis, J. A.; Boateng, G. G.; Seo, L. M.; Petersen, C. L.; Fortuna, K. L.; Wechsler, E. V.; Peterson, R. J.; Cook, S. B.; Pidgeon, D.; Dokko, R. S.; Halter, R. J.; Kotz, D. F., Development and Usability Assessment of a Connected Resistance Exercise Band Application for Strength-Monitoring. *World Acad Sci Eng Technol* **2019,** *13* (5), 340-348.

245. Kern, W., The Evolution of Silicon-Wafer Cleaning Technology. *J. Electrochem. Soc* **1990,** *137* (6), 1887-1892.

246. Booth, B. D.; Vilt, S. G.; McCabe, C.; Jennings, G. K., Tribology of monolayer films: comparison between n-alkanethiols on gold and n-alkyl trichlorosilanes on silicon. *Langmuir* **2009,** *25* (17), 9995-10001.

247. Song, X.; Zhai, J.; Wang, Y.; Jiang, L., Self-assembly of amino-functionalized monolayers on silicon surfaces and preparation of superhydrophobic surfaces based on alkanoic acid dual layers and surface roughening. *J Colloid Interface Sci* **2006,** *298* (1), 267-273.

248. Li, H.; Chen, X.; Shen, D.; Wu, F.; Pleixats, R.; Pan, J., Functionalized silica nanoparticles: classification, synthetic approaches and recent advances in adsorption applications. *Nanoscale* **2021,** *13* (38), 15998-16016.

249. Mohammadi Ziarani, G.; Hassanzadeh, Z.; Gholamzadeh, P.; Asadi, S.; Badiei, A., Advances in click chemistry for silica-based material construction. *RSC Advances* **2016,** *6* (26), 21979-22006.

250. Svechkarev, D.; Mohs, A. M., Organic Fluorescent Dye-based Nanomaterials: Advances in the Rational Design for Imaging and Sensing Applications. *Curr Med Chem* **2019,** *26* (21), 4042-4064.

251. Rosiuk, V.; Runser, A.; Klymchenko, A.; Reisch, A., Controlling Size and Fluorescence of Dye-Loaded Polymer Nanoparticles through Polymer Design. *Langmuir* **2019,** *35* (21), 7009-7017.

252. Sikora, A.; Shard, A. G.; Minelli, C., Size and zeta-Potential Measurement of Silica Nanoparticles in Serum Using Tunable Resistive Pulse Sensing. *Langmuir* **2016,** *32* (9), 2216-2224.

253. Petreanu, I.; Niculescu, V.-C.; Enache, S.; Iacob, C.; Teodorescu, M., Structural Characterization of Silica and Amino-Silica Nanoparticles by Fourier Transform Infrared (FTIR) and Raman Spectroscopy. *Analytical Letters* **2022**, 1-14.

254. Lieber, E.; Rao, C. N. R.; Chao, T. S.; Hoffman, C. W. W., Infrared Spectra of Organic Azides. *Anal Chem* **1957,** *29* (6), 916-918.

255. Ranjan, R.; Brittain, W. J., Combination of living radical polymerization and click chemistry for surface modification. *Macromolecules* **2007,** *40* (17), 6217-6223.

256. Nakazawa, J.; Smith, B. J.; Stack, T. D., Discrete complexes immobilized onto click-SBA-15 silica: controllable loadings and the impact of surface coverage on catalysis. *J Am Chem Soc* **2012,** *134* (5), 2750-2759.

257. Hermanson, G. T., Microparticles and Nanoparticles. In *Bioconjugate Techniques*, Academic Press: **2013**; pp 549-587.

258. Grabarek, Z.; Gergely, J., Zero-Length Crosslinking Procedure with the Use of Active Esters. *Anal Biochem* **1990,** *185* (1), 131-135.

259. Niko, Y.; Cho, Y.; Kawauchi, S.; Konishi, G.-i., Pyrene-based D–π–A dyes that exhibit solvatochromism and high fluorescence brightness in apolar solvents and water. *RSC Advances* **2014,** *4* (69), 36480–36484.

260. Rocard, L.; Berezin, A.; De Leo, F.; Bonifazi, D., Templated Chromophore Assembly by Dynamic Covalent Bonds. *Angew Chem Int Ed Engl* **2015,** *54* (52), 15739-15743.

261. Jester, S. S.; Schmitz, D.; Eberhagen, F.; Hoger, S., Self-assembled monolayers of clamped oligo(phenylene-ethynylene-butadiynylene)s. *Chem Commun (Camb)* **2011,** *47* (31), 8838-8840.

262. Robins, M. J.; Wilson, J. S.; Hansske, F., Nucleic-Acid Related-Compounds .42. A General Procedure for the Efficient Deoxygenation of Secondary Alcohols - Regiospecific and Stereoselective Conversion of Ribonucleosides to 2'-Deoxynucleosides. *J Am Chem Soc* **1983,** *105* (12), 4059-4065.

263. Chaicham, A.; Sahasithiwat, S.; Tuntulani, T.; Tomapatanaget, B., Highly effective discrimination of catecholamine derivatives via FRET-on/off processes induced by the intermolecular assembly with two fluorescence sensors. *Chem Commun (Camb)* **2013,** *49* (81), 9287-9289.

264. Samanta, D.; Sarkar, A., Immobilization of bio-macromolecules on self-assembled monolayers: methods and sensor applications. *Chem Soc Rev* **2011,** *40* (5), 2567-2592.

265. Lenigk, R.; Carles, M.; Ip, N. Y.; Sucher, N. J., Surface characterization of a silicon-chip-based DNA microarray. *Langmuir* **2001,** *17* (8), 2497-2501.

266. Aswal, D. K.; Lenfant, S.; Guerin, D.; Yakhmi, J. V.; Vuillaume, D., A tunnel current in self-assembled monolayers of 3-mercaptopropyltrimethoxysilane. *Small* **2005,** *1* (7), 725-729.

267. Nanocomposix NanoComposix_Storage_and_Handling https://nanocomposix.com 2022.

268. Kar, M.; Vijayakumar, P. S.; Prasad, B. L.; Sen Gupta, S., Synthesis and characterization of poly-L-lysine-grafted silica nanoparticles synthesized via NCA polymerization and click chemistry. *Langmuir* **2010,** *26* (8), 5772-5781.

269. Huang, M.; Deng, Z.; Tian, J.; Liu, T., Synthesis and biological evaluation of salinomycin triazole analogues as anticancer agents. *Eur J Med Chem* **2017,** *127*, 900-908.